

**Investigation of SAFit2 as a potential treatment option  
for nerve injury- and chemotherapy-induced  
neuropathic pain**

Dissertation

zur Erlangung des akademischen Grades

Doctor rerum naturalium (Dr. rer. nat.)

genehmigt vom Fachbereich Biologie  
der Technischen Universität Darmstadt  
in Darmstadt

von

Saskia Wedel

Erstgutachter: Prof. Dr. Gerhard Thiel  
Zweitgutachter: PD Dr. Marco Sisignano

Darmstadt 2023

**Autor:** M.Sc. Saskia Wedel

**Titel:** Investigation of SAFit2 as a potential treatment option for nerve injury- and chemotherapy-induced neuropathic pain

**Tag der Einreichung:** 24.08.2023

**Tag der mündlichen Prüfung:** 31.10.2023

**Ort:** Darmstadt, Technische Universität Darmstadt

**Jahr der Veröffentlichung der Dissertation auf TUprints:** 2023

**Veröffentlicht unter CC BY-SA 4.0 International**

<https://creativecommons.org/licenses>

---

## Zusammenfassung

---

Neuropathische Schmerzen beschreiben einen pathologischen und oft chronischen Schmerzzustand, der bis zu 10% der Weltbevölkerung betrifft. Hervorgerufen wird der neuropathische Schmerz durch Nervenschäden, die durch verschiedene Auslöser wie Krankheiten, medizinische Eingriffe und Vorfälle verursacht werden. Jedoch weisen derzeitige empfohlenen Behandlungsstrategien eine geringe Wirksamkeit sowie ein hohes Risiko für Nebenwirkungen auf. Folglich gibt es einen großen Bedarf an neuen Zielstrukturen sowie neuen Medikamenten für die Therapie von neuropathischen Schmerzen. Basierend darauf wurde in dieser Arbeit der selektive FKBP51 Inhibitor und potentielle Arzneimittelvorläufer SAFit2 im Kontext neuropathischer Schmerzen untersucht, die durch Nervenverletzung oder Chemotherapie verursacht werden.

Im ersten Teil dieser Arbeit wurde der Einfluss von SAFit2 auf neuropathische Schmerzen nach Nervenverletzungen und die zugrundeliegenden Mechanismen in einem Mausmodell untersucht. Hierbei linderte SAFit2 die mechanische Hypersensitivität von Mäusen durch Verminderung der exzessiven Nervenentzündung. Mechanistisch betrachtet, wirkte SAFit2 einer verstärkten NF- $\kappa$ B Aktivierung entgegen und verringerte dadurch die Infiltration von Immunzellen sowie die Konzentration von proinflammatorischen Zytokinen und Chemokinen in den Spinalganglien und im Rückenmark. SAFit2 beeinträchtigte jedoch nicht die Auflösung der Entzündung an der Verletzungsstelle, dem Ischiasnerv. Außerdem desensibilisierte SAFit2 den schmerzvermittelnden Ionenkanal TRPV1 in primären sensorischen Neuronen, indem SAFit2 die Aktivität der Phosphatase Calcineurin verstärkte, was zu einer Verringerung des TRPV1 vermittelten Calciuminfluxes führte. Infolgedessen verringerte SAFit2 die Freisetzung des proinflammatorischen Neuropeptids *calcitonin gene-related peptide* (CGRP), wodurch die Schmerzübertragung nach Nervenverletzung verringert und eine neurogene Entzündung gemindert wurde.

Im zweiten Teil dieser Arbeit wurde die Wirkung von SAFit2 auf das Lipidprofil in neuronalen Geweben untersucht, da Lipide wichtige Schmerzmediatoren darstellen. Interessanterweise stellte eine SAFit2 Behandlung basale Lipidkonzentrationen nach Nervenverletzung wieder her, insbesondere die des C16 Dihydroceramids in den Spinalganglien. Die Charakterisierung des C16 Dihydroceramids zeigte in primären sensorischen Neuronen, dass das Lipid den

---

schmerzvermittelnden TRPV1 Kanal ebenfalls desensibilisieren und die CGRP-Freisetzung von sensorischen Neuronen verringern kann. Weiterhin linderte das C16 Dihydroceramid die akute thermische Hypersensitivität in einem Capsaicin Mausmodell, was auf dessen anti-nozizeptive Eigenschaften hinweist.

Im dritten Teil dieser Arbeit wurde die Wirkung von SAFit2 auf neuropathische Schmerzen nach Chemotherapie, insbesondere durch Paclitaxel induzierte neuropathische Schmerzen, in einem Mausmodell untersucht. Hierbei konnte gezeigt werden, dass SAFit2 die durch Paclitaxel verursachte mechanische Hypersensitivität wirksam lindern konnte. Darüber hinaus wirkte SAFit2 der Paclitaxel induzierten Spinalgliose entgegen, da es die Aktivierung von Astrozyten und Mikroglia sowie die Konzentration schmerzvermittelnder Chemokine im dorsalen Rückenmark reduzieren konnte. Neben der immunologischen Komponente ergab die Analyse des Lipidprofils, dass SAFit2 die Spiegel von entzündungshemmenden und -auflösenden Oxylipinen nach Paclitaxel Behandlung in den Spinalganglien und im Rückenmark erhöhen konnte. Diese Ergebnisse erweitern das mechanistische Verständnis entscheidend und identifizieren, inwiefern SAFit2 Paclitaxel induzierte neuropathische Schmerzen lindern und schmerzverursachende Prozesse verringern kann.

Zusammenfassend zeigen diese Erkenntnisse vielversprechende analgetische Eigenschaften von SAFit2 im Kontext von Nervenverletzung und durch Paclitaxel hervorgerufener neuropathischer Schmerzen. SAFit2 linderte neuropathische Schmerzen, indem es durch Nervenverletzung veränderte Lipidspiegel wiederherstellte und mehrere zugrunde liegende neuroinflammatorische Mechanismen regulierte. Hingegen ist eine Verbesserung der Bioverfügbarkeit und Selektivität des Wirkstoffs SAFit2 für eine präklinische und klinische Anwendung notwendig. Auf dieser Grundlage stellt SAFit2 eine neue und vielversprechende Leitstruktur sowie einen möglichen Arzneimittelvorläufer für die Behandlung von Nervenverletzungen und Paclitaxel induzierten neuropathischen Schmerzen dar.

---

## Summary

---

Neuropathic pain describes a pathological and often chronic pain state that affects around 10% of the world population. The pathological pain arises after nerve lesions which are caused by diverse etiologies, encompassing diseases, medical conditions, and interventions. However, current and recommended treatment strategies carry a high risk of adverse effects and are inefficient in many cases. Consequently, the demand of novel targets and drug candidates for neuropathic pain emerges. In line with this, the focus of this thesis is set on the investigation of SAFit2, a selective FKBP51 inhibitor, as novel treatment option for nerve injury- and chemotherapy-induced neuropathic pain.

In the first part of this thesis, the influence of SAFit2 on nerve injury-induced neuropathic pain and the underlying mechanisms was assessed in a spared nerve injury mouse model. The results showed that SAFit2 ameliorates mechanical hypersensitivity as it diminishes excessive neuroinflammation after nerve injury. More specifically, SAFit2 counteracted an enhanced NF- $\kappa$ B activation and thereby reduced immune cell infiltration as well as pro-inflammatory cytokine and chemokine levels in dorsal root ganglia and spinal cord of nerve injured mice. However, SAFit2 did not impair the immune cell distribution and resolution of inflammation at the site of injury, the sciatic nerve. Besides this, SAFit2 desensitized the pain-mediating ion channel TRPV1 in primary sensory neurons by enhancing the activity of calcineurin, resulting in a reduction of TRPV1-mediated calcium transients. In consequence, SAFit2 decreased the release of the pro-inflammatory neuropeptide calcitonin gene-related peptide (CGRP) as downstream event, leading to a reduction of exacerbated pain transmission and neuroinflammation after nerve injury.

In the second part of this thesis, the impact of SAFit2 on lipid distribution was assessed in a spared nerve injury mouse model, since lipids represent crucial mediators in pain. Interestingly, SAFit2 restored lipid levels after nerve injury, especially levels of the C16 dihydroceramide in dorsal root ganglia. Like SAFit2, C16 dihydroceramide desensitized the pain-mediating ion channel TRPV1 in primary sensory neurons as well as reduced the CGRP release from primary sensory neurons. In line with this, C16 dihydroceramide alleviated acute thermal hypersensitivity in a capsaicin mouse model, indicating its anti-nociceptive properties.

---

In the third part of this thesis, the effect of SAFit2 on chemotherapy-induced neuropathic pain, especially paclitaxel-induced neuropathic pain, was evaluated in a multiple low dose mouse model. The data demonstrated that SAFit2 efficiently ameliorates paclitaxel-induced mechanical hypersensitivity. Moreover, SAFit2 counteracted paclitaxel-mediated spinal cord gliosis since it reduced the activation of astrocytes and microglia, as well as the levels of pain-mediating chemokines in the spinal cord. Beside the immunological component, the analysis of lipids revealed that SAFit2 increases anti-inflammatory and pro-resolving oxylipin levels in dorsal root ganglia and spinal cord after paclitaxel treatment. These results crucially expand our mechanistic understandings as well as identify how SAFit2 alleviates paclitaxel-induced neuropathic pain and decreases pain contributing processes.

In summary, these insights reveal promising analgesic properties of SAFit2 in the context of nerve injury- and paclitaxel-induced neuropathic pain. Furthermore, SAFit2 mediated a neuropathic pain relief by restoring injury-altered lipid levels and addressing several underlying neuroinflammatory mechanisms. However, the bioavailability and selectivity of SAFit2 has to be improved for preclinical and clinical usage. Based on this, SAFit2 constitutes as novel and promising lead compound and drug precursor for the treatment of nerve injury- and paclitaxel-induced neuropathic pain.

---

## Table of content

---

Zusammenfassung	I
Summary	III
Table of content	V
1 General Introduction	1
1.1 Nociception and physiological pain	1
1.2 Pathological nociceptive pain	3
1.3 The role of TRP channels in the context of pain	4
1.3.1 TRPV1 as member of the TRPV family	5
1.3.2 TRPA1 as member of the TRPA family	8
1.4 Peripheral and central sensitization	10
1.5 Lipid mediators in pain	12
1.5.1 Sphingolipids in the context of pain	12
1.5.2 PUFAs in the context of pain	13
1.5.3 Oxidized PUFA mediators in pain	15
1.6 Neuropathic pain	19
1.6.1 Nerve injury-induced neuropathic pain	20
1.6.2 Chemotherapy-induced neuropathic pain	23
1.6.3 Therapeutic options for neuropathic pain	26
1.7 FKBP51 as potential target for neuropathic pain	28
1.7.1 FKBP51 structure and its main function as co-chaperone	28
1.7.2 FKBP51 in the context of pain	30
1.7.3 SAFit2 as selective FKBP51 inhibitor	31
1.8 Aim of this thesis	33
2 Publication 1	35
<b>SAFit2 reduces neuroinflammation and ameliorates nerve injury- induced neuropathic pain</b>	
2.1 Author contributions	35
2.2 Manuscript	36
2.3 Supplemental file	57

3	Publication 2	86
	<b>The FKBP51 Inhibitor SAFit2 Restores the Pain-Relieving C16 Dihydroceramide after Nerve Injury</b>	
3.1	Author contributions	86
3.2	Manuscript	87
3.3	Supplemental file	106
4	Publication 3	123
	<b>SAFit2 ameliorates paclitaxel-induced neuropathic pain by reducing spinal gliosis and elevating pro-resolving lipid mediators</b>	
4.1	Author contributions	123
4.2	Manuscript	124
4.3	Supplemental file	145
5	General discussion	156
5.1	SAFit2-mediated effects in nerve injury- and chemotherapy-induced neuropathic pain in relation to the glucocorticoid receptor signaling	156
5.2	The influence of SAFit2 on TRPV1 sensitization and the phosphatase calcineurin	162
5.3	Risks and advantages of targeting FKBP51	164
5.4	SAFit2 as novel treatment option for pathological disorders especially neuropathic pain?	170
5.5	Future perspectives and conclusion	174
	References	176
	List of figures	210
	Abbreviation list	214
	Declaration - Ehrenwörtliche Erklärung	I
	Acknowledgement	II
	Curriculum Vitae	III



---

# 1 General Introduction

---

## 1.1 Nociception and physiological pain

Pain is classified by the international association for the study of pain (IASP) as an unpleasant sensory perception of the nervous system that is influenced by many biological, psychological, and social factors (1). Even though it is experienced as an unpleasant sensation, pain in its physiological form serves as warning system in which nociception protects the body from potential tissue damage. Furthermore, it enables a well-working interaction of the body with its surrounding environment (2).

Nociception is caused by noxious thermal (hot or cold), mechanical or chemical stimuli, which are detected by a population of terminal nerve fibers, called nociceptors (3). To transduce such noxious stimuli, nociceptors express a variety of ion channels such as transient receptor potential (TRP) channels at their membrane to convert noxious stimuli into electric activity (4). To activate such ligand-gated and voltage-gated ion channels under physiological conditions, a stimulus has to reach a high-threshold in a noxious range (5). Once those ion channels are activated, intracellular calcium levels increase which subsequently alter the membrane potential and in turn open voltage-gated ion channels. This finally results in the generation of an action potential which is transmitted to the dorsal root ganglia (DRGs), the cell bodies of nociceptors. From the DRGs, the electrical signal is subsequently transmitted to the laminae I and II of the spinal cord, where the signal is firstly processed and conveyed in a synaptic connection. After this first synaptic transduction, the signal is further transmitted through the spinothalamic tract and the thalamus to the somatosensory cortex. In the brain, the noxious stimulus signal is processed, and a withdrawal information is sent through descending pathways into the periphery (Figure 1) (2, 3, 6, 7).

Nociceptors are pseudounipolar nerve fibers which means that they have axonal branches into both ascending and descending directions which enables them to additionally innervate the surrounding organs such as muscles and skin but also internal organs (8). Nociceptors in general describe a highly heterogeneous group which was loosely classified and categorized upon its conducting and molecular properties (9). Based on the conducting properties, nociceptors can be mainly classified into two classes. The first class consists of

myelinated medium diameter nociceptors that are called A $\delta$  fibers and transduce stimuli rapidly to the central nervous system, resulting in a fast and well-localized pain sensation. In contrast, the second class of nociceptors comprises unmyelinated nerve fibers with small diameter that conduct pain slower than A $\delta$  fibers. Accordingly, these nerve fibers transmit the “second slow” or more diffuse pain and are termed C fibers. In addition, C fibers can be further subdivided into two classes: the “peptidergic” and “non-peptidergic” sensory neurons. Peptidergic nerve fibers release neuropeptides such as neuropeptide P and calcitonin gene-related peptide (CGRP) upon activation, whereas non-peptidergic nerve fibers do not (2).

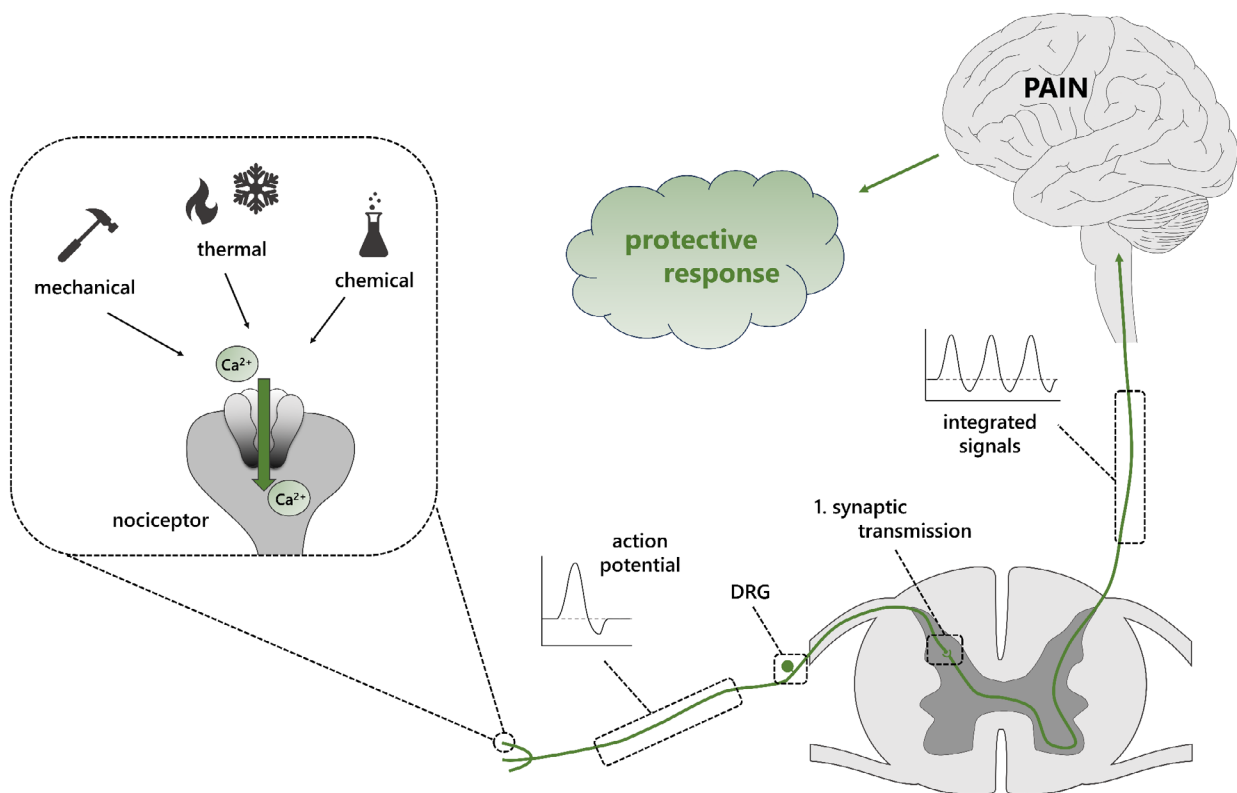


**Figure 1: Nociception in physiological pain.** Noxious stimuli (thermal, mechanical, or chemical) are recognized by nociceptors at terminal endings of sensory neurons. The respective nociceptors transduce high-threshold stimuli into electric signals via the influx of cationic ions such as calcium. Next, the electric signal is conveyed via the cell bodies of sensory neurons, located in the dorsal root ganglia (DRGs), to the dorsal horn of the spinal cord. In the spinal cord, the signal reaches the first synaptic transmission and is processed. Afterwards, the signal is further transduced via ascending fibers into the brain to the somatosensory cortex. In the somatosensory cortex, the signal is finally processed and converted into a protective response which is then send via descending pathways to the executing organ. The illustration was created with images from motifolio.

---

## 1.2 Pathological nociceptive pain

The second type of pain is termed pathological nociceptive or inflammatory pain and serves as protective function of the body like physiological pain. However, inflammatory pain is defined as a pathophysiological type of pain since it occurs after tissue damage and the subsequent resulting inflammation (10). Nevertheless, the primary function of inflammatory pain is to prevent further tissue damage and to enable a successful tissue healing. Therefore, the sensory system undergoes changes regarding its responsiveness towards external stimuli (11). In line with this, an increased responsiveness leads to an enhanced and prolonged perception of noxious stimuli and to the sensation of pain after innocuous stimuli. These changes in pain perception are termed hyperalgesia and allodynia respectively and describe typical symptoms of inflammatory pain (12). More specifically, hyperalgesia is described as signal amplification of painful stimuli, leading to an increased sensation of pain after a painful stimulus. Whereas allodynia is described as a more severe form of hypersensitivity, since it is defined as the sensation of pain after non-nociceptive stimuli like light touches (12).

Usually, symptoms of inflammatory pain such as an altered pain perception are locally restricted to the site of inflammation and do not affect the non-inflamed surrounding tissue. Furthermore, the altered pain perception is mainly caused by pro-inflammatory mediators which are secreted from the inflamed tissue (13). In turn, further immune cells are recruited to the site of inflammation and pro-inflammatory mediators are released, generating an "inflammatory soup" (3). This inflammatory soup can directly affect and increase the responsiveness of nociceptors which is called peripheral sensitization (Figure 2) (14).

Under physiological circumstances, the altered pain perception typically resolves after tissue healing and resolution of inflammation. Thereby, sensitizing mechanisms are reverted and mechanisms of physiological pain restored (15). However, inflammatory pain can become chronic in disorders such as rheumatic arthritis. In these cases, the inflammatory pain persists as long as the inflammation is active and mechanisms of central sensitization become more relevant (16, 17). Central sensitization is defined as changes in the ascending pathways like the dorsal horn of the spinal cord, resulting in a prolonged and spatially non-restricted perception of pain (18). The mechanisms of both peripheral and central sensitization are described in detail in a separate following chapter.

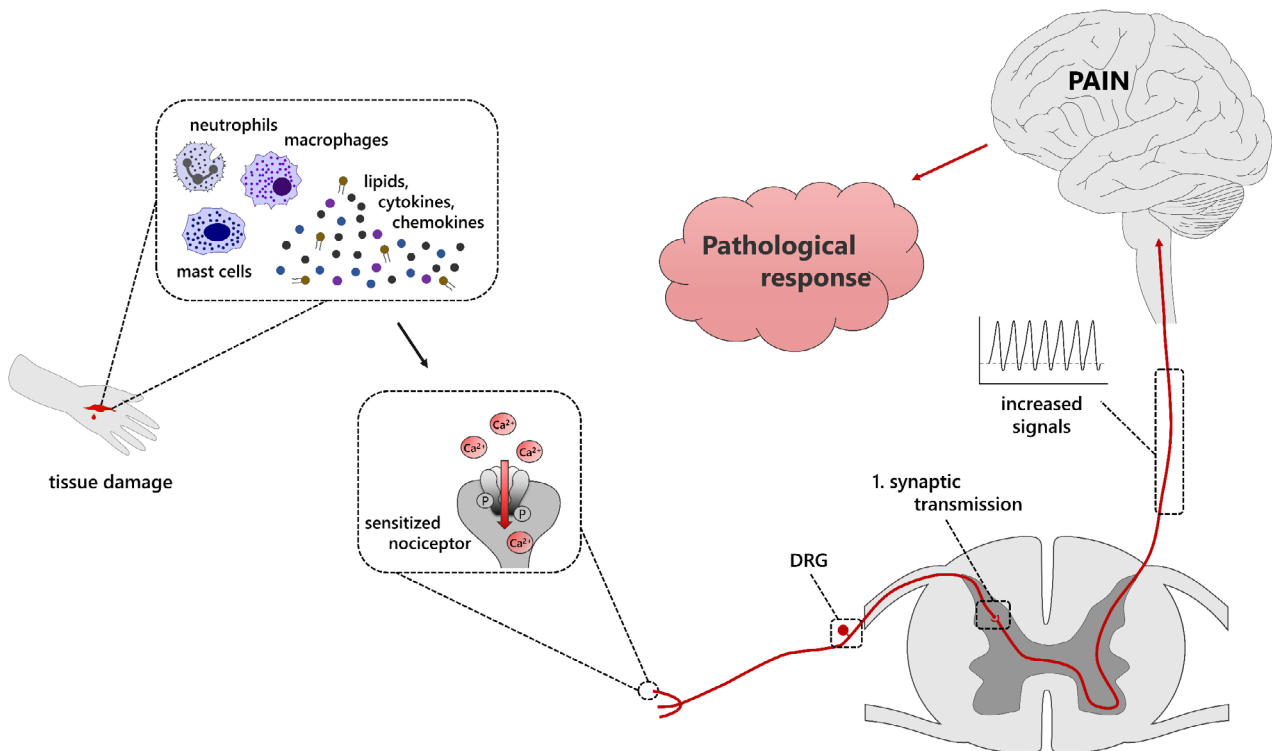


**Figure 2: Pain transmission in pathological nociceptive pain.** Upon tissue damage, sensitization processes such as peripheral sensitization are established to prevent the body from further tissue damage and to enable a successful wound healing. Therefore, resident immune cells like mast cells and macrophages release pro-inflammatory mediators. These in turn recruit immune cells which release further mediators such as cytokines, chemokines, and nerve growth factors. Beside immune cells, sensory neurons additionally release mediators such as lipids and neuropeptides that contribute to the inflammatory soup and mediate a crosstalk between neurons and immune cells. The inflammatory soup leads to the sensitization of nociceptors and an increased calcium response upon stimuli, resulting in an enhanced action potential firing and a pathologically increased pain response. The illustration was created with images from motifolio.

### 1.3 The role of TRP channels in the context of pain

TRP channels represent a major class of nociceptive signal transducers and are polymodally expressed in nociceptors throughout the body (19). Furthermore, the large ion channel superfamily encompasses the capability to detect a broad variety of physical and chemical noxious stimuli (20). Although the family comprises many functional differences, TRP channels have been characterized as non-selective cation channels, which are permeable even to large calcium ions (21). In total, the TRP channel superfamily consists of 28 members. The superfamily can be subdivided into six subfamilies that are classified as canonical (TRPC), vanilloid (TRPV), ankyrin (TRPA), melastin (TRPM), polycystin (TRPP) and mucolipin (TRPML) (22).

---

Structurally, TRP channels are composed of four subunits forming a tetramer, with each subunit consisting of six transmembrane domains (23). Furthermore, the transmembrane domains five and six of each subunit build up together a hydrophilic loop that functions as ion conducting pore (24). The amino acid residues within this pore determine the cation selectivity of the respective ion channel (25). The most structural variation between TRP families occurs at the cytosolic amino and carboxy terminal end. However, the TRPC, TRPV, and TRPM family share a motif at the carboxy terminal which consists of a six amino acid sequence and is termed as TRP box (24). In addition, the TRPC and TRPV family have a conserved ankyrin repeat sequence at their amino terminal end which mostly consists of three to six repeats. In contrast, the amino terminal of the TRPA family consists of 14 repeats (26). Beside those conserved structures, many other structural elements as the calcium binding EF-hand domain, PDZ domain, coiled-coil domain, kinase domain and other domains characterize different TRP channels (27).

In the context of pain, especially members of the TRPV, TRPA and TRPM family like the TRPV1, TRPA1 and TRPM8 have been shown to be key players in the transmission of pain (28). The latter one is primarily activated by thermal changes, transducing noxious cold stimuli (29). Nevertheless, it can also be activated by its ligands icilin, menthol, several lysophosphatidylcholines and poly unsaturated fatty acids (PUFAs) (24, 30). However, the TRPM8 channel is only expressed in a small subpopulation of DRG neurons which corresponds to 5-10% of all DRG neurons. Based on that, TRPM8 is expressed to a lesser extent than TRPV1 and TRPA1 in sensory neurons (31). Hence, only the two other key nociceptive TRP channels, TRPA1 and TRPV1, are described in the following.

### **1.3.1 TRPV1 as member of the TRPV family**

The TRPV1 channel is the most well-characterized TRP channel of the TRPV family (26). It is predominantly and widely expressed in the peripheral nervous system (PNS), albeit its expression has additionally been observed in the central nervous system (CNS) but to a lesser extent (32). In the PNS, TRPV1 is mainly expressed by small and medium sized nociceptive nerve fibers such as peptidergic and non-peptidergic C fibers as well as in a lower amount by A $\delta$  fibers. Based on that, the expression of TRPV1 was confirmed in the associated ganglia such as the dorsal root ganglia, the trigeminal ganglion, the nodal ganglion, and the sympathetic ganglion (33, 34). Furthermore, some studies confirmed the expression of

---

TRPV1 in other nerve fibers of the PNS, in which TRPV1 covers other functions than the sensation of noxious stimuli such as the sensing of irritants in the lung and airways, innervating the bladder or contributing to hearing processes in the cochlea (35). In the CNS, TRPV1 is primarily expressed pre-synaptically in dorsal horn neurons of laminae I and II, where it regulates the synaptic transmission of nociceptive signals (24, 27, 36). However, some groups also suggested the involvement of TRPV1 in the hippocampal synaptic transmission and described its expression in the caudal hypothalamus (37).

Structurally, TRPV1 is set up like all TRP channels with six transmembrane domains and a conducting pore between domain five and six. Furthermore, TRPV1 comprises a TRP box at the carboxy terminal end and six ankyrin repeats at the amino terminal end (Figure 3) (38, 39). While TRPV1 is a non-selective cation channel such as the other TRP channels, it has a preference for calcium ions upon activation (40). It gets polymodally activated by heat ( $> 43\text{ }^{\circ}\text{C}$ ), chemical ligands such as vanilloid capsaicin, and protons ( $\text{pH} < 5.9$ ) (Figure 3) (41). Moreover, several other TRPV1 agonists have already been identified such as resiniferatoxin, eicosanoids, endocannabinoid lipids like anandamide or oxidized lipid mediators like 9-hydroxyoctadecadienoic acid (9-HODE) and 13-HODE (41-44).

Since TRPV1 can be activated polymodally, activation of TRPV1 by different agonists can affect its responsiveness, respectively. For instance, an extracellular acidification to a pH around 6.5 lowers the thermal activation threshold of TRPV1 to a range of 35 to 37  $^{\circ}\text{C}$ , reflecting a temperature range already below body temperature (27, 45). This cross-regulation of TRPV1 becomes particularly relevant in pain states that cover acidosis such as cancer or injury-induced inflammation (33, 46). Beside those various direct activating mechanisms, TRPV1 can also be sensitized by endogenous mechanisms mediated by pro-inflammatory and proalgesic mediators. These mediators in turn initiate intracellular signaling cascades via their receptors, leading to the activation of kinases and phosphatases. These activated kinases, on the one hand, phosphorylate TRPV1 at serine and threonine residues, lowering the activation threshold, or, on the other hand, increase the trafficking and incorporation of TRPV1 into the plasma membrane (27).

However, the particular phosphorylation site determines the affected functional properties of TRPV1. The phosphorylation of TRPV1 by protein kinase A (PKA) and PKC increases the proton sensitivity of TRPV1, shifting its activation threshold into a physiological pH range. In

contrast, the phosphorylation by the calcium calmodulin-dependent kinase II (CaMKII) affects the TRPV1 vanilloid binding site, influencing the activation of TRPV1 by its ligands (31, 47-49). Nevertheless, the activation of all the respective kinases as well as the activation of the mitogen-activated protein kinase (MAPK) lead to an increased expression of TRPV1, which enables a maintenance of sensitization (50). Furthermore, previous studies showed that the activation of those kinases can contribute to the trafficking of TRPV1 to the plasma membrane (51). In addition, its activation triggers the release of neuropeptides like CGRP and substance P that are capable to contribute to the development of neurogenic inflammation (52). The counterpart of TRPV1 sensitization displays TRPV1 desensitization. Thereby, either TRPV1 channels are internalized or the phosphorylation state of TRPV1 is reduced by the phosphatase calcineurin (PP2B) (53). This phosphatase is primarily expressed in neurons and is activated among other mechanisms by the calcium calmodulin complex, which is formed upon increasing intracellular calcium concentrations (54, 55).

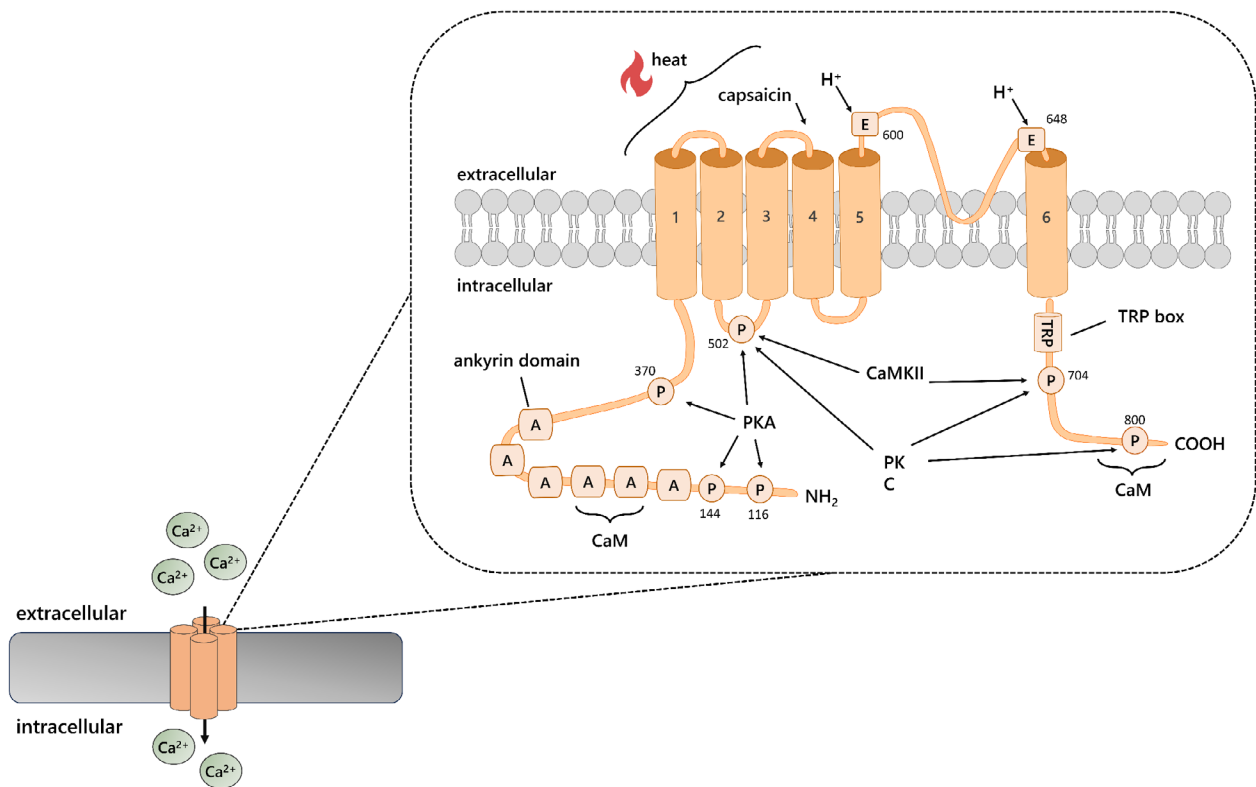


**Figure 3: Structure of the TRPV1 channel.** The TRPV1 channel is composed of four subunits building a tetramer as all members of the TRP channel family (bottom left). One subunit of the homotetramer consists of six transmembrane domains from which domains five and six build up the conducting pore with the respective domains of the other subunits (top right). Both the amino and carboxy terminal of the channel are located intracellularly and comprise six ankyrin repeat domains and a TRP box domain, respectively. Furthermore,

---

several phosphorylation sites, consisting of serine and threonine, are located along both terminal ends that can in turn be phosphorylated by protein kinase A and C or CaMKII. In addition, each terminal end provides a calmodulin (CaM) binding site. The TRPV1 channel can be activated by noxious heat stimuli, protons that act on glutamic acid residues (indicated at the extracellular loops) and capsaicin that was proposed to bind close to the fourth transmembrane domain. The illustration was created with images from motifolio.

Based on the involvement of TRPV1 in the development and maintenance of various pain states, it was highlighted as a potential target for the treatment of pain (56-60). Furthermore, it has been suggested that targeting TRPV1 has a low probability of central side effects, since it is predominantly expressed in sensory neurons. However, targeting TRPV1 with first generation antagonists resulted in hyperthermia in clinical trial patients. This severe side effect was induced since the first generation of antagonists interfered in the TRPV1-mediated body temperature regulation (61). Nevertheless, the second generation of antagonists, which is currently tested in clinical trials, seems to comprise analgesic properties without impairing the body temperature regulation (62).

### **1.3.2 TRPA1 as member of the TRPA family**

The TRPA1 channel is the only member of the TRPA family, and it is named ankyrin TRP channel as its amino terminal domain comprises 14 (mouse) or 16 (human) ankyrin repeats (Figure 4). Furthermore, the TRPA1 amino terminal domain displays the largest part of the channel as it represents 64% of the entire protein and contains a cysteine rich domain (63). However, TRPA1 lacks the typical TRP box at the carboxy terminal (26). Furthermore, TRPA1 is mainly expressed in small diameter neurons of the dorsal root ganglia, trigeminal ganglia and nodose ganglia (63, 64). Beside the PNS, TRPA1 was also found to be expressed in various other tissues like the brain, hair, skin, and in different cell types such as myocytes and renal tubular cells (26). Nevertheless, the function of TRPA1 in those tissues is poorly understood until now.

Comparable to TRPV1, TRPA1 can be polymodally activated by a wide range of chemicals. Hence, TRPA1 is mainly known as a chemosensor, although its involvement in cold and mechanical sensation has been broadly discussed (65, 66). The respective chemical agonists can be loosely subdivided into electrophilic agonists which covalently modify TRPA1 and non-electrophilic agonists that activate TRPA1 non-covalently (67). Based on the variety of chemical agonists, studies show that electrophilic agonists such as isothiocyanate and allyl



isothiocyanate (AITC) which are found in wasabi, mustard, and mustard oil, in common interact with the cysteine rich domain at the amino terminal (Figure 4) (31, 68). Beside isothiocyanate and AITC, lipids such as prostaglandins, mediators of oxidative stress, cytokines, and chemokines are also identified as endogenous electrophilic agonists (69, 70). In addition, there are also non-electrophilic agonists known such as menthol, cannabinoids, carvacrol, thymol, and gingerol that activate the TRPA1 channel (71, 72). However, the binding mechanism of these agonists is largely unknown, except for the suggestion that some of them might bind to some kind of binding pocket located in close proximity to the fifth transmembrane domain (Figure 4). Nevertheless, this was only indicated for menthol and is assumed for other non-electrophilic agonists (63).

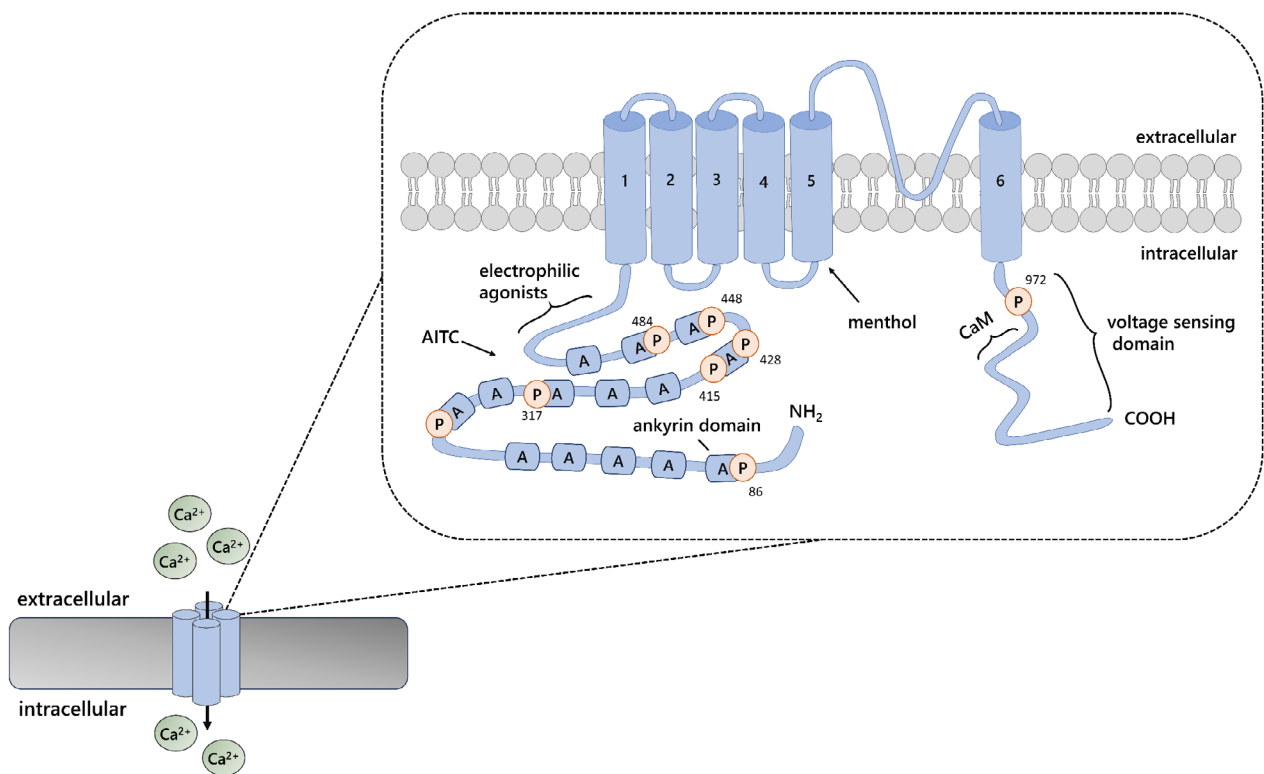


**Figure 4: Structure of the murine TRPA1 channel.** The TRPA1 channel is composed of four subunits that build a tetramer (bottom left). One subunit comprises six transmembrane domains from which domains five and six build up the conducting pore with the respective domains of the other subunits (top right). The amino terminal of the murine TRPA1 channel consists of 14 ankyrin repeat domains and several phosphorylation sites. Furthermore, the amino terminal comprises a suggested binding region for electrophilic agonists. In contrast menthol was predicted to bind near the fifth transmembrane domain. The carboxy terminal comprises predominantly a large voltage sensitive domain and provides a calmodulin (CaM) binding site. The illustration was created with images from motifolio.

---

In the context of pain, TRPA1 also displays an interesting target, since it is known as the “gatekeeper of inflammation” (11). Several studies have already shown that the pharmacological inhibition or deletion of TRPA1 led to a reduction of cold and mechanical hypersensitivity in inflammatory pain models (70). Furthermore, TRPA1 was shown to be involved in the mediation of persistent pain states such as neuropathic pain after nerve injuries or chemotherapy (70). Based on the emerging evidence of TRPA1 being involved in pain development and maintenance, its role as potential target in pain treatment increases more and more (70, 73, 74).

#### **1.4 Peripheral and central sensitization**

Peripheral sensitization describes a mechanism which occurs after any kind of lesion and increases the excitability of nociceptors. Thereby peripheral sensitization establishes a pain state in which innocuous stimuli are experienced as pain and noxious stimuli are sensed exaggerated, as described previously. These symptoms can either be caused by a direct activation of nociceptors or a reduction of the nociceptor threshold. In the case of a direct activation, ion channels such as TRP channels are activated by mediators secreted from injured cells or mediators from the inflammatory soup (3, 75). Mediators such as adenosine triphosphate (ATP) and protons are immediately released from damaged cells after injury (76). Both ATP and protons can directly activate ion channels which are expressed on the peripheral membrane of nociceptors. ATP activates the purinic receptor P2X3 and protons activate TRPV1, leading to a calcium influx, alterations in the membrane potential, depolarization as well as subsequently to the generation of an action potential (38, 77).

In the case of a nociceptor threshold reduction, mediators from the pro-inflammatory soup like cytokines, growth factors as nerve growth factor (NGF), kinins as bradykinin, purines, amines as histamine, lipids as prostaglandins, and other mediators indirectly affect the activity of nociceptors (46, 78). Those mediators bind to G protein coupled receptors (GPCRs) and tyrosine kinase receptors which are subsequently activated and in turn internally activate protein kinases of the family A and C (79). Upon their activation, protein kinases phosphorylate TRP channels at serine and threonine residues which is termed as sensitization (80). Based on the sensitization, the threshold of those ion channels is reduced and the open probability increased, leading to a pathologically increased pain perception. Furthermore, the persistent activation of nociceptors can lead to transcriptional changes in

---

terminal nerve fibers like the enhanced expression of ion channels and neuropeptides such as substance P and CGRP. Afterwards, these neuropeptides are released upon the activation of nociceptors and act on immune cells as well as on other sensory neurons, contributing to the maintenance of peripheral sensitization (6, 76).

In contrast to peripheral sensitization, central sensitization describes a state which involves the first synaptic connection at the dorsal horn of the spinal cord (18). Furthermore, central sensitization contributes to an enhanced and prolonged pain perception as well as a spatially extended sensation of peripheral stimuli, leading to increased pain perception in non-inflamed surrounding tissue (81). The amplification of peripheral signals occurs due to structural and functional changes in synaptic connections which are induced by various mechanisms (82). Firstly, an increased excitability of primary afferents leads to an enhanced excitement of postsynaptic neurons (83). Furthermore, an enhanced primary afferent activity leads to the release of neurotransmitters such as bone derived neurotrophic factor (BDNF), glutamate, and neuropeptides such as substance P and CGRP, which bind to postsynaptic dorsal horn neurons (84). Upon the binding of those mediators, various mechanisms are initiated in dorsal horn neurons: (1) phosphorylation and subsequent sensitization of ion channels, (2) activation of amino-3-hydroxy-5-methylisoxazole-4-propionic acid (AMPA) and N-methyl-D-aspartate (NMDA) receptors, and (3) translocation of ionotropic AMPA receptors to the post-synaptic membrane (85, 86). Moreover, under physiological conditions, the activation of NMDA receptors is blocked by a magnesium ion located in the pore of the receptor. However, due to an increased excitability and a constantly depolarized membrane potential, the magnesium blockage is removed and NMDA receptors get activated by glutamate, which further depolarizes post-synaptic neurons in the dorsal horn (87). In addition, functional modulation such as sensitization of NMDA receptors through second messengers like kinases would even intensify the external signal amplification (88). Thereby, innocuous stimuli like light touches would be experienced as unpleasant pain.

In later phases of central sensitization, transcriptional changes arise due to the activation of transcription factors such as nuclear factor 'kappa-light-chain-enhancer' of activated B-cells (NF- $\kappa$ B) (79). Thereby, inflammatory genes are induced and repressors such as downstream regulatory element antagonist modulator (DREAM) are removed, initiating further intracellular cascades that contribute to the maintenance of sensitization (3, 89). Beside those transcriptional changes, alterations additionally occur at gap junctions as well as in the

---

interaction between neurons, astrocytes, microglia or even invading immune cells (90, 91). These interactions play an essential part in central sensitization mechanisms and neuroinflammation, which occurs especially in neuropathic pain states and is described in the neuropathic pain chapter.

Furthermore, lipid mediators and lipid oxidizing enzymes have been proposed to contribute to sensitized states. More specifically, oxidized lipid mediators can modulate the sensitivity of pain-mediating ion channels and thereby influence pain transmission (92). Especially the enhanced activity of the cyclooxygenase 2 leads to the production of prostaglandin E2 which represses the inhibitory function of glycine receptors and enhances the activity of terminal afferents (93). Accordingly, the function of further lipid mediators is described in the following chapter. In summary, peripheral sensitization is described as accumulation of mechanisms that amplify external stimuli in the periphery and central sensitization is characterized by mechanisms that lead to central signal amplification and induce long lasting changes in neuronal plasticity (82).

## **1.5 Lipid mediators in pain**

Lipids in general describe a loosely defined group that covers a broad variety of hydrophobic molecules (94). Based on the high group diversity, there are also several subgroups existing such as fatty acids, phospholipids, sterol lipids, sphingolipids, and glycerolipids among others that affect various processes in the body and properties of compartments (94-97). In the context of pain, lipid mediators function as important signaling mediators in paracrine signaling and interaction of neurons and glial cells (98, 99). More specific, mainly mediators from the endocannabinoid system, the group of fatty acids and the group of sphingolipids have been identified as mediators in the context of pain (98, 100, 101). However, the relevance of lipids emerges in the context of pain with the increase of described endogenous lipid mediators and characterized pain-mediating TRP channel modulators (92, 102, 103).

### **1.5.1 Sphingolipids in the context of pain**

From the group of sphingolipids predominantly ceramides and the ceramide/sphingosine pathway were shown to contribute to pain transmission (104). Ceramides are active metabolites of sphingosines that are known to regulate and modulate various cellular mechanisms such as cell cycle arrest, apoptosis, and inflammation (105, 106). In detail,

---

ceramides can act as second messengers themselves, activating transcription factors like NF- $\kappa$ B or kinases like MAPKs. These in turn induce or enhance the expression of pro-inflammatory cytokines among other pro-inflammatory mediators (107). In addition, ceramides serve as precursors for other mediators in pain such as the sphingosine-1-phosphate (S1P). Especially S1P emerged as an important mediator in pain as it was shown to contribute to peripheral and central sensitization (107-109). However, targeting the ceramide/sphingosine pathway with therapeutics led to exacerbating pain states as well (110). Based on this, the ceramide/sphingosine pathway contributes to pathological pain states but cannot be targeted easily because of the pleiotropic effects of sphingolipids.

### **1.5.2 PUFAs in the context of pain**

In contrast to sphingolipids in pain, the influence of polyunsaturated fatty acids (PUFAs) and their metabolites on pain transmission has been described in several studies (111, 112). PUFAs in general can be further categorized upon their degree and position of unsaturation (113). Thereby, eicosapentaenoic acid (EPA) and docosahexaenoic acid (DHA) belong to the group of omega-3 fatty acids, whereas linoleic acid (LA) and arachidonic acid (AA) belong to the group of omega-6 fatty acids (Figure 5). Both PUFA groups are also known to comprise essential fatty acids that cannot be synthesized by the body itself and have to be taken up by nutrition (111, 114). Once taken up, these PUFAs are either directly metabolized and oxidized, or processed and esterified into phospholipids which get incorporated into cell membranes. In turn, PUFAs can be released from the cell membrane through the activation of the phospholipase A II (PLA<sub>2</sub>) pathway (Figure 5) (115).

In mammals the PLA<sub>2</sub> superfamily comprises more than 50 enzymes. Despite the variety of PLA<sub>2</sub> enzymes, only cPLA<sub>2</sub>, iPLA<sub>2</sub>, and sPLA<sub>2</sub> were shown to play an important role in the context of inflammation and pain (116-118). Although the expression of the respective phospholipases is confirmed in CNS and PNS, their activation is not fully understood yet (116). There is evidence in literature that the activation of cPLA<sub>2</sub> and sPLA<sub>2</sub> requires increased intracellular calcium conditions, whereas the activation of iPLA<sub>2</sub> does not (119, 120). In addition, it was shown that cPLA<sub>2</sub> can be activated by extracellular stimuli like ATP and colony-stimulating factor 1 (CSF1) or under neuroinflammatory conditions by the activated CaMKII pathway (121, 122). In contrast, the iPLA<sub>2</sub> activity has been shown to be regulated by ATP binding, calmodulin, or caspase cleavage (123). Nevertheless, the respective PLA<sub>2</sub>

enzymes have in common that they hydrolyze the second ester bond of phospholipids upon their activation and thereby release a lysophospholipid and a PUFA (123).

From the cell membrane released PUFAs consist of different chain lengths and unsaturated double bonds. Usually, they are rapidly processed into their metabolites after their release, but they can also serve as antioxidants, scavenging reactive oxygen species (124). In general, fatty acids such as AA and LA are associated with pro-inflammatory properties and fatty acids such as EPA and DHA with anti-inflammatory properties, although the respective groups can also comprise metabolites with opposing properties (113, 125). Nevertheless, previous studies showed that long chain PUFAs such as DHA are capable to directly activate the chemosensor TRPA1, leading to a desensitization of TRPA1 in the long term. Based on such results, analgesic properties are ascribed to long chain PUFAs such as DHA (126).

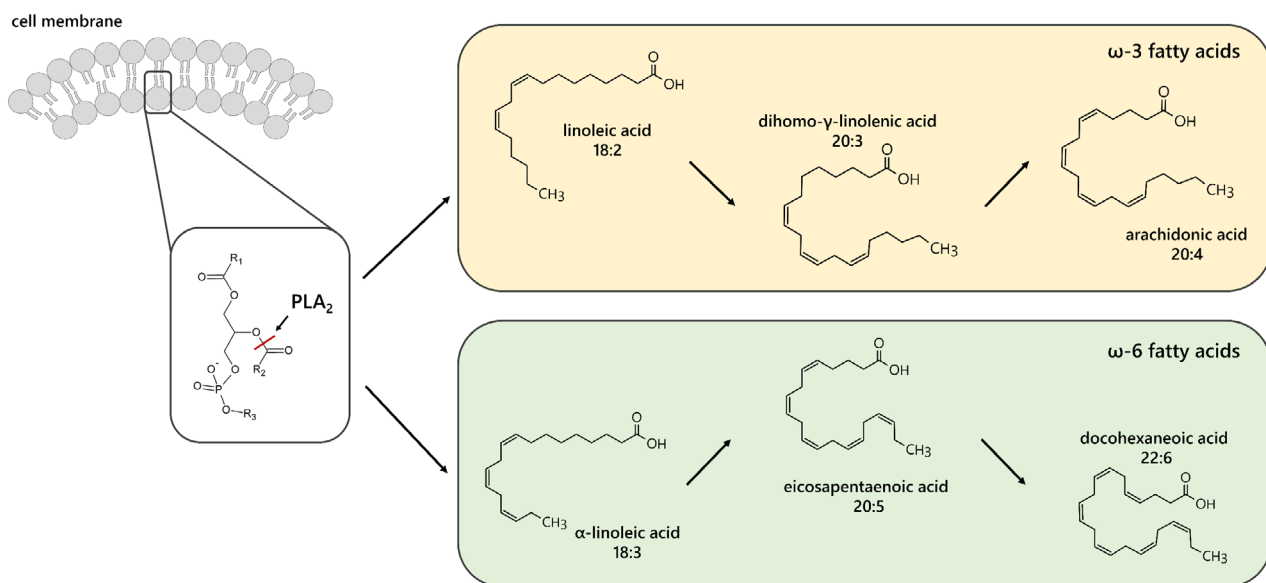


**Figure 5: PUFA release by the phospholipase A<sub>2</sub> from cellular membrane.** Polyunsaturated fatty acids (PUFAs) can be released by the phospholipase A<sub>2</sub> from the cellular membrane. Thereby, phospholipase A<sub>2</sub> hydrolyses the second ester bond of glycerophospholipids, liberating a lysophospholipid and a PUFA. Furthermore, PUFAs can be converted into other PUFAs upon elongation and desaturation processes. However, the depicted direction of PUFA conversion serves only for explanatory purposes and does not implicate that e.g. arachidonic and docosahexaenoic acid cannot be incorporated into cell membranes. The molecular structures were drawn with ChemSketch and the lipid bilayer was modified and originates from motifolio.

---

### 1.5.3 Oxidized PUFA mediators in pain

In general, oxidized PUFA mediators are produced by cyclooxygenases, lipoxygenases and cytochrome-P<sub>450</sub>-epoxygenases and -hydroxylases that rapidly metabolize PUFAs into their oxidized metabolites (127-129). In detail, cyclooxygenases predominantly generate under incorporation of oxygen molecules bicyclic hydroperoxides that get subsequently peroxidized (128, 130, 131). Lipoxygenases catalyze the incorporation of one oxygen molecule in dependency of iron ions, creating a hydroperoxyl fatty acid, and cytochrome-P<sub>450</sub>-epoxygenases attach either an epoxide group or a terminal hydroxyl to the molecule also in dependency of iron ions (Figure 6) (127, 132). Thereby, many different lipid mediators can be generated, which are named oxylipins and comprise various properties and functions. In the following, the resulting fatty acid metabolites are described and sorted by the originating fatty acid, starting with the metabolites of arachidonic acid which belong to the group of eicosanoids.

The PUFA arachidonic acid gets processed by cyclooxygenases (COX) into prostaglandins and thromboxanes, by lipoxygenases (LOX) into leukotrienes and predominantly hydroxyeicosatetraenoic acids (HETEs), and by cytochrome-P<sub>450</sub>-epoxygenases (CYP) into various epoxy, hydroxy and dihydroxy metabolites (133, 134). The first group of metabolites, prostaglandins and thromboxanes, consists of pro-inflammatory mediators that contribute to inflammation and enhance inflammatory pain (135, 136). Furthermore, various non-steroidal anti-inflammatory drugs (NSAIDs) target the synthesis of prostaglandins and thromboxanes by inhibiting non-selectively COX enzymes, indicating the relevance of those mediators in inflammation (137-139). Beside COX metabolites, the group of leukotrienes is also involved in the mediation of inflammatory processes, however their major function encompasses the mediation of allergic reactions (140). In contrast, other LOX enzyme mediators such as HETEs have already been described in the context of pain (92, 141). However, HETEs are not directly generated by lipoxygenases. For the oxidation of AA into HETEs, arachidonic acid firstly gets processed via LOX enzymes into hydroperoxyeicosatetraenoic acids (HPETEs) and then subsequently reduced into HETEs by the glutathione peroxidase system (142). Nevertheless, both mediator classes were previously shown to comprise pro-inflammatory and proalgesic properties. In particular, the

---

mediators 5-,12- and 15-HETE were shown to function as direct agonists of the pain-mediating TRPV1 channel or at least to increase pain sensation (101, 143-145).

The latter group of AA oxylipins describes a heterogenous group of mediators since CYP enzymes can either generate HETEs or epoxyeicosatrienoic acids (EETs) (100). Although they generate other HETEs like 19-HETE and 20-HETE than LOX enzymes, their properties such as activating the pain-mediating TRPV1 channel are similar (146-148). In contrast to HETEs, EETs, also termed as EpETrEs, have been shown to comprise anti-inflammatory properties and to ameliorate neurodegenerative diseases as they reduce microglial activation and immune cell infiltration (125, 129). However, 5,6-EET has also been described as TRPA1 agonist (149). In summary, the PUFA arachidonic acid is predominantly metabolized into pro-inflammatory mediators except for some epoxy metabolites, which possess more anti-inflammatory properties.

The PUFA linoleic acid can be metabolized into hydroxyotadecadienoic acids (HODEs) and epoxyoctadecenoid acids (EpOMEs) which can be further processed into dihydroxyoctadecenoic acid (DiHOMEs) (150, 151). However, the generation of the respective metabolites and the required enzymes are not fully identified. Nevertheless, emerging evidence indicates that HPODE, the HODE precursors, can be generated by LOX enzymes (92, 152). Afterwards, HPODEs get subsequently processed into the stable metabolites like 9-HODE and 13-HODE by the glutathione peroxidase (92, 153). In addition, both metabolites were shown to sensitize the TRPV1 channel in primary sensory neurons and to induce spontaneous pain and thermal hypersensitivity after administration *in vivo* (154, 155). Furthermore, both mediators can activate the TRPA1 channel in a heterologous expression system, revealing proalgesic properties of both (156). In line with this, chemotherapeutically treated mice that developed neuropathic pain symptoms, showed elevated 9-HODE levels in neuronal tissues such as sciatic nerve and DRGs (157).

Beside HODEs, EpOMEs such as 9,10- and 12,13-EpOME represent another group of LA metabolites. These are mainly generated by CYP enzymes and can be further metabolized by the soluble epoxide hydrolase (sEH) into their corresponding diols 9,10- and 12,13- DiHOME (158). In addition, EpOMEs and DiHOMEs, are predominantly attributed with pro-inflammatory and proalgesic properties (151). In particular, the mediators 9,10-EpOME and 12,13-DiHOME sensitized the pain-mediating TRPV1 channel in primary sensory



---

neurons and 12,13-DiHOME induced a thermal hyperalgesia *in vivo* (141, 159). In line with this, another study postulated that all four oxidative LA metabolites activate TRPV1 and TRPA1 and contributed to thermal hyperalgesia *in vivo* (160). In addition to the described proalgesic properties, EpOMEs are known to be especially synthesized by leucocytes in inflammatory diseases in which they contribute to inflammation (92). Furthermore, DiHOMEs directly activate neutrophils, indicating that oxidated LA metabolites contribute to inflammation and increase pain perception in inflammatory and chronic pain states (92, 161).

Beside these oxidized linoleic acid metabolites, LA can be metabolized into dihomo-gamma-linolenic acid (DGLA) which itself gives rise to either hydroxyeicosatrienoic acids (HETrEs) via LOX enzymes or prostaglandins via COX enzymes (162). HETrEs and especially 15-HETrE was shown to comprise a more anti-inflammatory profile as it inhibits the production of leukotrienes in immune cells via inhibiting the lipoxygenase 5 (163). Beside the omega-6 fatty acid DGLA, there is another linolenic acid called alpha-linolenic acid ( $\alpha$ -LA). However,  $\alpha$ -LA is classified as an omega-3 fatty acid and is known to comprise anti-inflammatory properties (164, 165). The  $\alpha$ -LA in turn can be metabolized by LOX enzymes into hydroxyoctadecatrienoic acids (HOTrEs) which also encompass anti-inflammatory properties (166, 167). Although less is known about HOTrEs in the context of pain, their anti-inflammatory properties indicate that they might be beneficial for the reduction or resolution of neurogenic inflammation in pathological pain states.

Other omega-3 PUFAs like EPA or DHA can be generated by the desaturation and elongation of  $\alpha$ -LA (168). Both comprise anti-inflammatory properties as  $\alpha$ -LA and give rise to anti-inflammatory metabolites (15, 165, 169-172). Moreover, both PUFAs can be metabolized into less potent prostaglandins and thromboxanes, thereby preventing the prostaglandin synthesis from arachidonic acid as they compete directly as substrate with AA (173). Beside repressing the prostaglandins synthesis, EPA and DHA can be metabolized into resolvins and DHA additionally into maresins and protectins. These metabolites belong to the group of specialized pro-resolving mediators (SPMs) (95, 174-176). Moreover, these SPMs were shown to encompass essential regulatory functions in the context of pain and to be involved in the active resolution of inflammation (169, 177, 178). However, the synthesis of SPMs is not elucidated in detail and their occurrence controversially discussed in literature as SPMs are difficult to detect even with sensitive methods such as tandem mass spectrometry. Nevertheless, the generation of their precursors such as hydroxyeicosapentaenoic acids

(HEPEs) and hydroxydocosahexaenoic acids (HDHAs) is characterized and their detection well established (179-184). HDHAs originate from DHA and are produced in the same way as HEPEs via LOX enzymes and the glutathione peroxidase. Furthermore, DHA can be processed into epoxydocosapentaenoic acids (EDPs) and dihydroxydocosapentaenoic acids (DiHDPAs) by CYP enzymes as well as into hydroxydocosahexaenoic acids (HDoHEs) by LOX enzymes (179, 185). In addition, CYP enzymes give rise to epoxyeicosatetraenoic acids (EEQs) by metabolizing EPA (179).

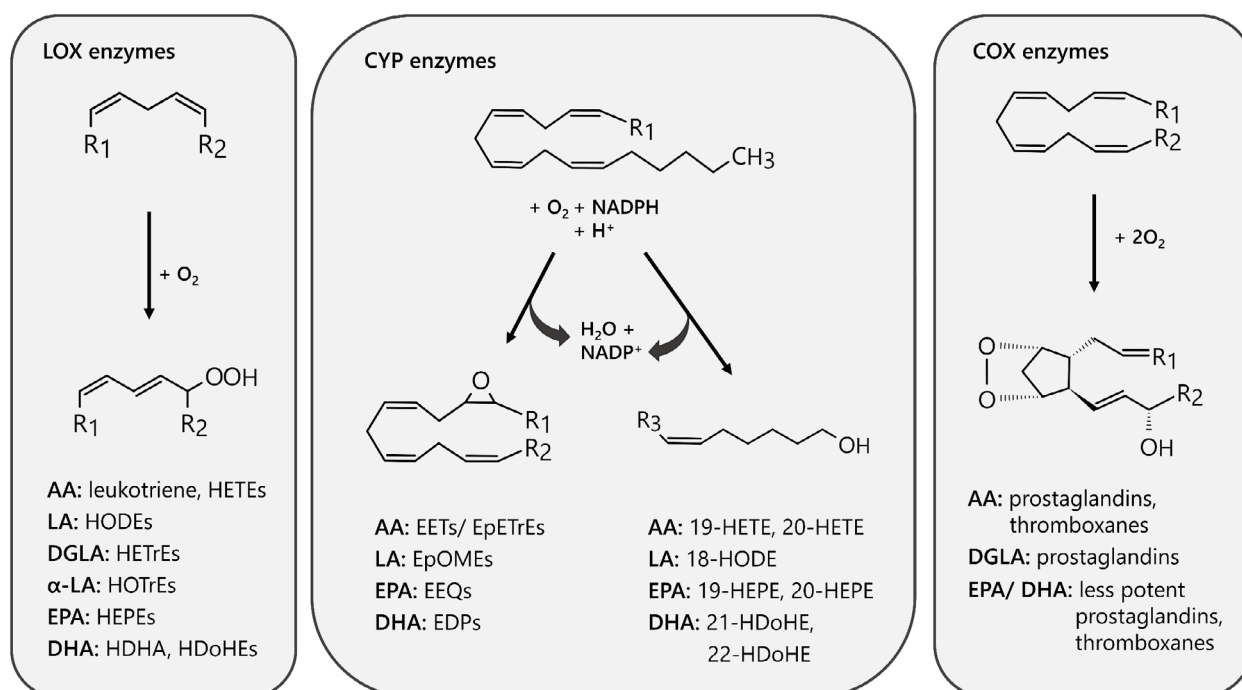


**Figure 6: Enzymatic reactions catalyzed by LOX, CYP and COX enzymes.** The iron containing lipoxygenases (LOX enzymes) generate hydroperoxyl fatty acids under incorporation of one oxygen molecule. Cytochrome-P<sub>450</sub>-epoxygenases (CYP enzymes) catalyze epoxygenase and hydroxylase activities in dependency of iron ions, attaching either an epoxide group, preferentially to the double bond closest to the amino group, or a terminal hydroxyl group, respectively. Cyclooxygenases (COX enzymes) catalyze the generation of predominantly bicyclic hydroperoxides under the incorporation of two oxygen molecules. The oxidized metabolites generated from the respective PUFA are depicted per enzyme. The molecular structures were drawn with ChemSketch.

In summary, oxidized PUFA mediators, which are also termed as oxylipins, play an essential and very divers role in the regulation of various inflammatory diseases and pain states. Nevertheless, many underlying mechanisms are not elucidated yet and have to be further investigated. However, the extremely low endogenous level of lipids as well as their short half times make the investigation of lipids challenging.

---

## 1.6 Neuropathic pain

The third type of pain, beside physiological and inflammatory pain, is termed neuropathic pain. Neuropathic pain is characterized as a pain state which arises after a lesion or disease of the somatosensory nervous system (186). Although pain serves as protective function of the body, neuropathic pain is commonly defined as maladaptive pain response and persistent pain state (187). Furthermore, this maladaptive pain state is not only provoked by the nerve damage itself but also by an imbalanced inflammatory response, the subsequent initiated mechanisms, and resulting disorders (188, 189).

The initial nerve damage can be induced by a variety of causes like metabolic diseases such as diabetes mellitus, nervous diseases such as herpes zoster and multiple sclerosis, infectious diseases like HIV, surgical interventions like amputations, medical conditions like stroke, nerve traumas and nerve injuries or even by neurotoxic substances like chemotherapeutics (190). Based on the high variety of elicitors, neuropathic pain is defined by a broad symptom scope which includes several phenotypes of abnormal pain perception. In detail, neuropathic pain patients experience hypersensitivities, allodynia, and hyperalgesia but also paresthesia and spontaneous pain which feels like an electroshock or burning pain (191, 192). Unfortunately, the latter described symptoms occur stimuli-independent, demanding neuropathic pain patients even more (193). Based on the severity and persistency of symptoms, neuropathic pain is classified as one of the most difficult pain forms to treat, which leads to a high burden for pain patients. Furthermore, neuropathic pain can even become incurable and life long lasting (193).

Such harsh symptoms are mediated by a variety of underlying mechanisms, which are partially understood and differ depending on the type of neuropathic pain. However, mechanisms such as peripheral and central sensitization as well as events like ectopic discharges were shown to contribute to the most frequent neuropathic pain symptoms (194). In addition, independent from the initial elicitor, all nerve lesions lead at first to an inflammation at the site of injury. This specific type of inflammation is termed neuroinflammation since it describes a neuroimmune interaction (195). Furthermore, it is characterized by the activation of glial cells like astrocytes and microglia, the infiltration of immune cells into PNS and CNS compartments like DRGs or spinal cord, respectively, and the synthesis of inflammatory mediators (196). Nevertheless, the intensity of

---

neuroinflammation is diverse in different types of neuropathic pain. Among the different neuropathic pain types, predominantly nerve injury-induced neuropathic pain is characterized by a strong ongoing neuroinflammation. In contrast, other forms of neuropathic pain such as the chemotherapy-induced neuropathic pain comprise a weaker neuroinflammation (197, 198). Both forms of neuropathic pain (nerve injury- and chemotherapy-induced) and their underlying mechanisms such as neuroinflammation are described in the following in detail since these two neuropathic pain models were used to firstly investigate the effects of SAFit2 on neuropathic pain.

### **1.6.1 Nerve injury-induced neuropathic pain**

Nerve injury-induced neuropathic pain describes a specific type of neuropathic pain, which arises after nerve injuries like nerve transections or nerve stretches and crushes that can occur during events such as surgeries or even amputations (199-203). As previously described, this type of nerve lesion induces a strong neurogenic inflammation which characterizes this type of neuropathic pain. Immediately after lesion, resident glial and immune cells such as Schwann cells or macrophages and mast cells, respectively, get activated in the surrounding tissue (198). Upon their activation, Schwann cells dedifferentiate and start to degrade the myelin sheath at the site of nerve injury to prepare the site of injury for regeneration (204). In addition, resident immune cells such as mast cells release pro-inflammatory mediators such as cytokines, growth factors and histamine among others. These recruit further immune cells and firstly sensitize nociceptors as explained in the peripheral sensitization chapter. Beside peripheral sensitization, those mediators also recruit further immune cells to the site of injury (198, 205, 206). However, the resulting immune cell infiltration occurs in a distinct time response. Firstly, neutrophils are infiltrating within hours followed by macrophages within days (196). Furthermore, the differentiation of monocytes into macrophages is initiated as well as the polarization of macrophages into a pro-inflammatory phenotype is established (207). Lastly, T cells infiltrate in the inflamed region within days and weeks (196). In summary, all these infiltrating immune cells further release pro-inflammatory mediators, building up the so-called inflammatory soup which further mediates the development of inflammation as well as modulates nociceptor sensitization (208).

---

The complex interaction of immune cells and mediators is usually strictly regulated and balanced to facilitate the resolution of neuroinflammation and nerve injury (209). Unfortunately, in the case of arising neuropathic pain, this beneficial regulation is out of balance and the local neurogenic inflammation cannot be resolved. This in turn promotes the appearance of central mechanisms like central sensitization and enhanced glial activation (90, 210). Nevertheless, the respective central mechanisms can also arise even faster when nerve lesions occur directly in compartments of the CNS (211). Especially the activation of glial cells such as microglia and astrocytes displays a key mechanism of neuroinflammation and is described in the following (212, 213). The underlying neuronal mechanisms of central sensitization are not explained in detail in the following as they have been described in a previous chapter.

The activation of glial cells is induced by either mediators of the inflammatory soup or by mediators like ATP, chemokines, CSF1 or CGRP released from primary nerve terminals after spontaneous discharges (196, 214, 215). Furthermore, glial cells can respectively influence their activation by the secretion of distinct mediators (207). Upon glial activation, glial cells like microglia and astrocytes change their phenotype from a controlling resting state into an effector state (216, 217). Though, the activation of astrocytes and microglia takes places in a time dependent manner, in which microglia get activated immediately after nerve injuries and astrocytes within days (212).

Microglia start to rapidly proliferate, change their morphology, and start to express several markers like chemokine receptors and the ionized calcium-binding adaptor molecule-1 (IBA1) upon their activation (218-220). Furthermore, they facilitate other responses such as antigen presentation, migration, phagocytosis, as well as production of inflammatory mediators (221). Mechanistically, the generation of pro-inflammatory mediators is induced through external stimuli, which activate further signaling cascades including MAPK or initiate the NF- $\kappa$ B pathway (222). Thereby, the activated microglia release mediators like tumor necrosis factor  $\alpha$  (TNF $\alpha$ ), interleukin 1 $\beta$  (IL-1 $\beta$ ), IL-6, C-C motif ligand 5 (CCL5) and BDNF, acting paracrine on neurons and astrocytes (223, 224). Thereby, effector microglia also actively contribute to the development and maintenance of sensitization and neuroinflammation.

---

Beside microglia, astrocytes are also activated upon noxious stimuli as well as subsequently undergo morphological changes, proliferate, and express several markers such as the glial fibrillary acidic protein (GFAP) (212, 225). Although astrocytes are activated later than microglia, their activation is more persistent and can last for months (226). In contrast to microglia, astrocytes are connected via gap junctions in a network and form contacts with synapses through which they have a direct influence on signal transduction (212, 227). This is of particular interest, since activated astrocytes release D-serine as gliotransmitter into synaptic gaps. D-serine itself is characterized as an endogenous co-agonist of NMDA receptors and can thereby directly modulate synaptic transmission as well as interfere in the regulation of synaptic plasticity (193, 228).

Beside the neuron-glia interaction, glial cells can also crosstalk with other glial cells through the secretion of glial mediators. These glial mediators can therefore, on the one hand amplify the activation of other glial cells, or on the other hand resolve it, depending on their properties (207). In the case of astrocytes, pro-inflammatory gliomediators are predominantly chemokines such as CCL2, CCL5, CCL7 and chemokine C-X-C motif ligand 10 (CXCL10) among others that are secreted upon the activation of MAPK and the NF- $\kappa$ B signaling pathway (207, 229, 230). Furthermore, these chemokines play an important role in the transmission of pain as they enhance or sustain the activation of microglia (231).

Nevertheless, those secreted chemokines also contribute to the sensitization of neurons. In particular, CCL2 displays a prominent chemokine candidate in pain transmission as it directly binds to the C-C motif chemokine receptor 2 (CCR2) on neurons. Thereby, CCL2 induces an increase of AMPA and NMDA mediated currents, resulting in an amplification of amplitude and frequency of post synaptic currents (212). In summary, the orchestrated release of mediators by neurons and glial cells as well as the possible interactions between neurons and glial cells in neuroinflammatory conditions result in multi-combinatorial possibilities of effects. Nevertheless, the prevention of both astrogliosis and microgliosis as well as the neutralization of glial mediators was shown to attenuate chronic pain states after nerve injury, highlighting both as target in chronic and especially neuropathic pain states (232-235). However, due to the multitude of interactions and influences, the underlying mechanism of nerve injury-induced neuropathic pain are only superficially elucidated and have to be studied further in depth.

---

## 1.6.2 Chemotherapy-induced neuropathic pain

Another prominent type of neuropathic pain is described as chemotherapy-induced peripheral neuropathy (CIPN) and arises during or after chemotherapy. Unfortunately, CIPN affects up to 80% of all cancer patients and appears as a dose dependent and severe side effect of chemotherapy (197, 236). CIPN can already occur immediately after the first cytostatic treatment, multiple treatment cycles or even after the end of chemotherapy (197, 237). The latter described event is especially challenging for oncologists as they cannot respond anymore in order to modulate chemotherapy and to reduce CIPN. During chemotherapy, CIPN is firstly recognized by altered sensory perceptions of patients, starting in hands and feet. In the progression of CIPN, these altered sensory perceptions such as numbness, paresthesia, and hypersensitivities spread throughout the limbs to more central regions (236-238). Thereby, CIPN limits and impedes an effective cancer treatment in many cases as chemotherapy has to be interrupted or reduced in frequency and dose after the occurrence of CIPN (239, 240).

The commonly used cytostatics that can cause CIPN can be classified into taxanes such as paclitaxel, platinum compounds like cisplatin and oxaliplatin, and vinca alkaloids such as vincristine. In addition, newer cytostatic classes include protease inhibitors like bortezomib and immunomodulatory compounds like thalidomide (238, 241, 242). Although these cytostatics are used to preferentially target and kill proliferating malignant cells, they also affect non-malignant and non-proliferating cells. Thereby, cytostatics often affect the somatosensory system since it is well susceptible due to a low nerve-blood barrier (243). The most affected parts of the PNS are distal nerve fiber endings, cell bodies of sensory neurons and their axonal components such as myelin, mitochondria, and microtubules among others. Furthermore, cytostatics also affect glial cells like astrocytes and microglia (244). However, the underlying mechanisms vary between the different chemotherapeutics as they target different structures, leading to different lesions and symptoms.

In this work, the focus is further set on the cytostatic paclitaxel and the underlying mechanisms of paclitaxel-mediated neuropathic pain. Paclitaxel was chosen for a chemotherapeutic model since it is efficiently and widely used for the treatment of solid tumors such as lung, prostate, or ovarian cancer (245, 246). Moreover, paclitaxel is used as a first-line chemotherapy for breast cancer which affects one out of eight women in their life

---

time based on the current Robert Koch incidence rates (247, 248). In addition, paclitaxel is used for the treatment of malignancies which are previously refractory for other cytostatics such as small cell lung cancer or bladder cancer (249-251). However, although paclitaxel is known as one of the most successful natural cytostatics, unfortunately up to 87% of paclitaxel patients develop neuropathic pain after their treatment (244, 252). Furthermore, some patients even experience an acute pain syndrome immediately after paclitaxel treatment, reaching its peak 3-4 days after treatment (197, 253). In summary, the high efficiency of paclitaxel and frequency of side effects display a high need of therapeutics for paclitaxel-mediated neuropathic pain.

Paclitaxel itself belongs to the group of taxanes and is described as a microtubule stabilizing agent (254). Under physiological conditions, microtubules are characterized as dynamic cytoskeletal polymers that polymerize and depolymerize. However, upon the binding of paclitaxel to  $\beta$ -tubulin, the microtubule lattice is stabilized and the depolymerization repressed. Thereby, paclitaxel efficiently arrests cell cycle between metaphase and anaphase and disrupts cell proliferation. Moreover, those arrested cells, predominantly rapid proliferating cancer cells, undergo apoptosis over time (255). Unfortunately, the stabilizing of microtubule affects also other cytoskeleton-related mechanisms beside proliferation. In particular, paclitaxel impairs the axonal transport in neurons, leading to axonal degeneration and a phenomenon termed as axonal dying back pattern. This in turn can lead to demyelination processes and a complete loss of sensory nerve action potentials (236). Furthermore, the disruptions of microtubule-related functions can even lead to the complete loss of intraepidermal nerve fibers, which are predominantly pain-mediating C-fibers and A $\delta$ -fibers, resulting in a loss-of-function symptoms like numbness (256, 257).

The impaired axonal transport further affects mitochondria, since they are primary localized in axons and rely on the rapid trafficking of mRNA and nutrients (258, 259). In addition, they play a crucial role in the excitability of neurons as they provide a lot of energy, which is required for the regeneration of ion gradients and membrane potentials (260). In addition to the impaired supply of mitochondria, paclitaxel altered the morphology of mitochondria. After paclitaxel treatment, mitochondria were shown to be swollen up, start to vacuolize and show fragmentation of cristae (236, 261). This effect is presumably caused by an increased permeability of the mitochondrial permeability transition pore (mPTP), leading to alterations in the calcium flux in mitochondria (262). Furthermore, a sustained opening of mPTP leads



---

to the disruption of the electrochemical gradient and the respiratory chain which finally results in ATP deficiencies and the leakage of pro-apoptotic mediators (263).

Beside the ATP deficiency, the paclitaxel-mediated disruption of mitochondria causes the generation of reactive oxygen species (ROS) and oxidative stress (197). However, ROS and oxidative stress themselves were shown to affect mitochondria as they induce mitochondrial membrane potential loss, revealing two closely dependent and regulating systems (264). Furthermore, accumulating ROS induce the expression of matrix-metalloproteinases, which enables the infiltration of immune cells into neuronal tissue (236). Nevertheless, paclitaxel-mediated oxidative stress and mitochondrial dysfunction were shown to be reduced by antioxidants and other compounds that counteract an enhanced ROS production or promote an endogenous antioxidant cascade (265, 266). Taken together, the diverse effects of paclitaxel on axonal transport and mitochondria are closely related, dependent on each other and lead to the experience of neuropathic pain in variable intensities.

Beside those oxidative stress and axonal transport effects of paclitaxel, paclitaxel itself is described as ligand of toll-like receptor 4 (TLR4) (265). This receptor is expressed by sensory neurons, glial cells, and other immune cells such as macrophages (267-269). TLR4 is a transmembrane receptor which is coupled to two adaptor proteins: myeloid differentiation primary response 88 (MyD88), and TIR domain-containing adaptor inducing IFN- $\beta$  (TRIF) (270). Upon its activation, the respective adaptor proteins promote signal transduction and activate intracellular signaling cascades. These downstream signaling cascades then result in the activation of transcription factors like NF- $\kappa$ B, activator protein 1 (AP-1) and cyclic adenosine monophosphate (cAMP) response element-binding protein (CREB) (271, 272). Thereby, paclitaxel induces the expression of several pro-inflammatory cytokines and chemokines that contribute to sensitization processes and recruit further immune cells (265). Moreover, paclitaxel directly activates resident immune cells as well as initiates the degranulation of mast cells through the TLR4 mediated signaling (265). Based on these downstream effects, paclitaxel itself generates a pro-inflammatory environment and contributes to the development of neuroinflammation.

Despite to the paclitaxel-mediated expression of cytokines and activation of immune cells, paclitaxel was additionally shown to enhance the expression of several factors, contributing to the development of neuropathic pain. For instance, paclitaxel increased the expression of

---

chemokine receptors (273). This expressional upregulation plays an important role in the maintenance of paclitaxel-induced neuropathic pain as chemokines are strongly involved in the mediation of neuroinflammation and pain transmission (274-277). Furthermore, the blockage of chemokines such as CCL2 was shown to prevent paclitaxel-induced hypersensitivity (278). Beside the inflammation-related expression, paclitaxel increased the expression of TRPV1 in sensory neurons (279, 280). In addition, it enhanced the expression of neuropeptides like substance P which play an essential role in sensitization processes (265, 281, 282). Moreover, paclitaxel was shown to induce a glutamate release from sensory neurons and to disrupt glutamate homeostasis in the dorsal horn which further contributes to paclitaxel-induced neuropathic pain (274, 283). In summary, paclitaxel is used as a potent antineoplastic agent for the treatment of various cancer types. However, it additionally affects multiple other processes than proliferation, resulting in many cases to the development of neuropathic pain.

### **1.6.3 Therapeutic options for neuropathic pain**

Although neuropathic pain affects up to 10% of the world population, the treatment strategies for neuropathic pain are limited due to either severe side effects or a low efficacy of the available therapeutics. Nevertheless, the pharmacological guidelines for neuropathic pain recommend gabapentinoids like gabapentin or pregabalin, tricyclic antidepressants such as amitriptyline as well as serotonin-noradrenaline reuptake inhibitors (SNRIs) such as duloxetine as first-line treatments (284). Gabapentin and pregabalin bind both to subunits of voltage-dependent calcium channels and thereby reduce calcium influxes and the calcium-mediated release of excitatory neurotransmitters (285, 286). Although this mechanism of action seems to be beneficial for many neuropathic pain types, the treatment with gabapentinoids showed no amelioration in a clinical phase III study with CIPN patients (284, 287, 288). Furthermore, such channel blockers lead to adverse effects like vertigo, lethargy, obesity and peripheral swelling (288, 289). Tricyclic antidepressants were found to be efficient in nerve injury-induced neuropathic pain patients among others (284). However, they are contraindicated for patients with cardiovascular diseases as they could lead to a reduced blood flow and have an inhibitory influence on choline, adrenalin, and histamine receptors (290, 291). Based on this, tricyclic antidepressants can induce arrhythmia, walking difficulties, and cognitive impairment, which could lead to an accidental overdosing and an

---

increased suicide risk (288). SNRIs were shown to be beneficial in diverging types of pain like nerve injury-induced and chemotherapy-induced neuropathic pain (197, 284). Those SNRIs such as duloxetine are beneficial for the treatment of neuropathic pain as they balance neurotransmitter concentrations by inhibiting the reuptake of serotonin and noradrenaline (292). Nevertheless, the treatment with SNRIs should be closely surveilled as those agents increase the blood pressure which can lead to vertigo, nausea, hypertension, and ataxia (284).

As second-line treatments, topical agents like lidocaine and capsaicin as TRPV1 agonist were used to locally reduce and prevent spontaneous discharges (293). These treatments were shown to be quite analgesic in cases of post-operative pain but failed to mediate an efficient pain relief in more systemic neuropathic pain forms (284, 294). Beside the topical treatments, opioids such as tramadol and tapentadol are recommended as second-line treatment for more systemic forms of neuropathic pain such as diabetic neuropathy (295). These weak  $\mu$ -opioid receptor agonists also act on neurotransmitter balances as they additionally function as SNRIs (197, 296). Although these opioids are recommended as second-line treatments, since they comprise a low potential of abuse, the risk of addiction and other adverse effects such as confusion should not be underestimated. Third-line treatments include more potent opioids like morphine and oxycodone as well as neurotoxins like botulinum toxin (284, 288). Nevertheless, strong opioids were used less in the treatment of neuropathic pain as they carry a high risk of misuse and are not adequate for long-term treatments (297). Botulinum toxin is recommended as last choice for the treatment of refractory cases. It inhibits neural transmission and therefore can efficiently reduce peripheral neuropathic pain states, however it inhibits also the transmission of any other neuronal signal (298).

In addition to the limited choice of unsuitable drugs, several of which are used off-label to treat neuropathic pain, many patients develop resistance or tolerance to their therapeutics. In these cases, alternative therapies such as spinal cord stimulation, transcranial and epidural stimulation, or deep brain stimulation can be considered (288, 299). These therapy options try to address pathological pain transmission with electrical or magnetic signals. However, these techniques are characterized as invasive treatment options and carry potential risks (300-302). In summary, neuropathic pain patients have to deal with a limited and often inadequate choice of treatments, highlighting an emerging need for novel therapeutics to cope with different types of neuropathic pain.

---

## 1.7 FKBP51 as potential target for neuropathic pain

### 1.7.1 FKBP51 structure and its main function as co-chaperone

The FK506 binding protein 51 (FKBP51) is encoded by the gene *FKBP5* and belongs to the family of immunophilins (303). Immunophilins are characterized by the ability to bind immunosuppressing agents such as FK506 and rapamycin (304). Within the family of immunophilins FKBP51 is homologous to FKBP52, sharing 60% sequence identity and a similarity of 75% (305). Structurally, FKBP51 consists of three domains. The amino terminal constitutes the FK1 domain, followed by the FK2 domain in the center and the tetratricopeptide repeat (TRP) domain at the carboxy end (Figure 7) (306). The best characterized domain of FKBP51 is the FK1 domain which comprises five antiparallel beta strands, surrounding a central alpha helix (306). Furthermore, it possesses a catalytic pocket that facilitates a prolyl-peptidyl-isomerase (PPIase) activity and binds ligands such as FK506 (306, 307). The function and structure of the FK2 domain is less characterized compared to FK1. However, FK2 is assumed to comprise scaffold functions since it displays neither an enzymatic function nor the ability to bind immunosuppressing agents, although it shares almost the same structure with FK1 except for some residues (308). The TRP domain at the carboxy terminal comprises three TRP repeats that are folded into seven alpha helices (309). In addition, it serves as further binding site for protein-protein interactions especially for the chaperone heat shock protein 90 (HSP90) (310, 311).

Based on the binding affinity of the TRP domain to HSP90, FKBP51 and other immunophilins are described as co-chaperones and are involved in the mediation of protein folding and stabilization (306, 312, 313). Although the regulatory function of FKBP51 as co-chaperone is barely understood in many pathways, it was shown to be involved in the regulation of steroid hormone receptors (SHR) (314-317). The family of SHRs includes the androgen receptor (AR), the estrogen receptor (ER), the mineralcorticoid receptor (MR), the progesterone receptor (PR), as well as the glucocorticoid receptor (GR) (308, 318). However, FKBP51 was shown to be most sensitive to the glucocorticoid receptor and to negatively regulates its activity (308). In contrast, FKBP52 potentiates the signal transduction of GR, although FKBP51 and FKBP52 share almost the same structure (319, 320). These contrary effects are suggested to be mediated by conformational differences since the relative orientation of FK1 and FK2 was described to be twisted in FKBP52 compared to FKBP51 (305).

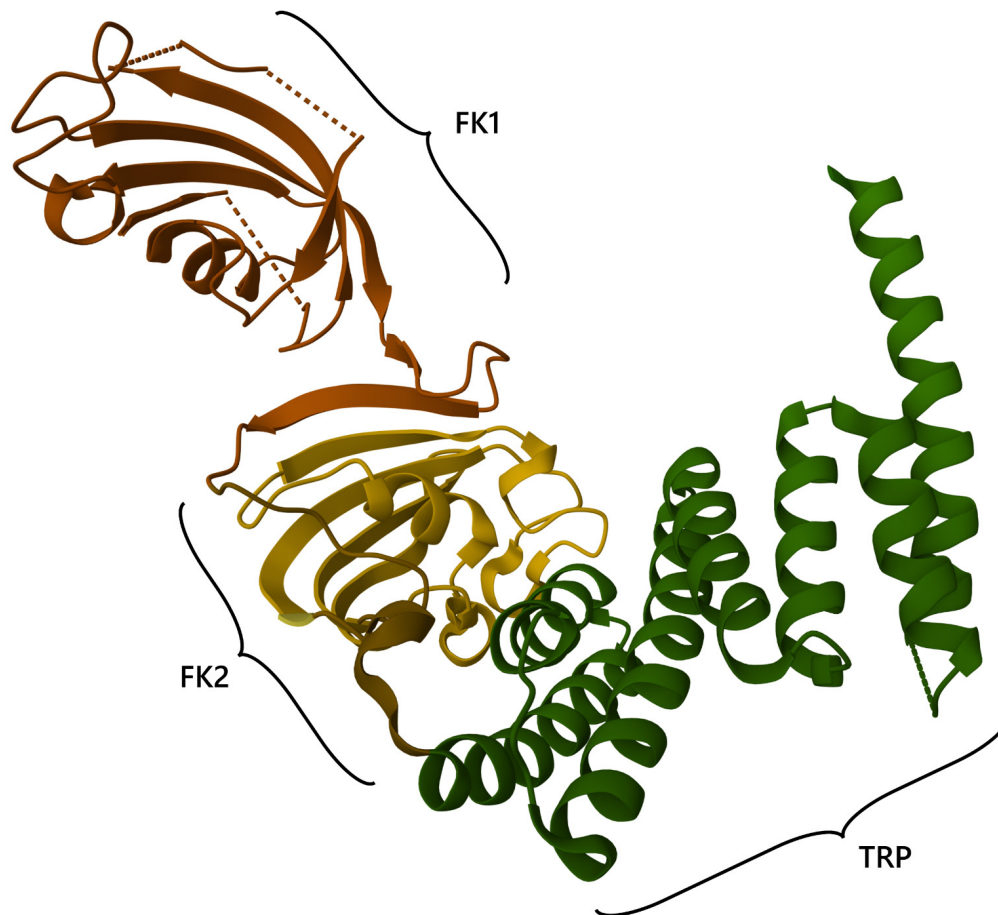


**Figure 7: Structure of FKBP51.** FKBP51 comprises a FK1 domain at the amino terminal (brown), an FK2 domain at the center (yellow) and a TRP domain at the carboxy terminal (green). The crystallographic structure was taken from the RSCB database (PDB-ID: 1KT0) and colored as well as labeled individually (306).

The GR activity is closely regulated by the binding of FKBP51 or FKBP52 to the heterocomplex including the GR itself, HSP90 and other co-chaperones (321). While glucocorticoid concentrations are low in the cytosol, predominantly FKBP51 was shown to occupy the binding site of the heterocomplex. However, upon glucocorticoid binding, the heterocomplex undergoes a conformational change and FKBP51 is exchanged to FKBP52 (322, 323). FKBP52 in turn recruits the dynein-dynactin motor complex which allows the translocation of the heterocomplex into the nucleus (324). Next, the expression of GR targets such as FKBP51 is enhanced (325). This subsequently leads to increased FKBP51 levels in the cytosol that counterbalance the FKBP51/FKBP52 homeostasis and reduce the transcriptional activity of GRs. Based on that, the GR-FKBP51 regulation functions as an ultrashort negative feedback loop and can lead to a glucocorticoid resistance and a lack of negative feedback signaling towards the hypothalamic–pituitary–adrenal (HPA) axis (326, 327). Thereby, the diminished negative feedback towards the HPA axis results in a prolonged stress response

---

and the development of stress-related diseases and mood disorders such as depression (321, 323).

In line with the development of stress-related diseases, human genetic studies revealed a correlation of *FKBP5* gene variants with a higher risk of psychiatric disorders. In particular, *FKBP5* single nucleotide polymorphisms (SNPs) are associated with either a dysregulation of the FKBP51-GR system, enhanced levels of FKBP51 or both, leading to various types of disorders (328-333). Thereby, patients, carrying such *FKBP5* SNPs, have been found to be prone to develop depressive disorders, a post-traumatic stress disorder, bipolar disorders, a psychosis, or to show suicidality (334-338). Beside psychiatric disorders, FKBP51 has also been linked to metabolic diseases since studies identified increased FKBP51 levels in diabetes type II patients. Furthermore, several studies implicated a FKBP51-mediated glucose intolerance in obesity, and an insulin resistance in type II diabetes (339, 340). In summary, various animal and human studies showed that increased FKBP51 levels are related to many disorders that can be improved by the deficiency or reduction of FKBP51.

### **1.7.2 FKBP51 in the context of pain**

While FKBP51 is quite well known as target for stress disorders, the understanding of its role is rather limited and is currently increasing in the context of pain. Based on the role of *FKBP5* in neuropsychiatric disorders, it was firstly associated with being involved in the development of post-traumatic chronic musculoskeletal pain (MSP) (341, 342). Although the development of MSP is poorly understood, genetic studies identified *FKBP5* gene variants as predictor for the severity of MSP (341). Besides MSP, FKBP51 deficiency was shown to reduce mechanical hypersensitivity in an inflammatory joint mouse model (343). However, a FKBP51 deficiency did not impair acute nociceptive pain, which is quite important for the protective function of nociception (343). Based on this data, FKBP51 was firstly revealed to be involved in the mediation of pathological pain. Furthermore, the deficiency of FKBP51 ameliorated inflammatory pain in both male and female mice (344). This is of particular interest, as other studies suggested sex specifies in inflammatory pain mechanisms. Based on this, targets postulated from earlier studies were less efficient in either male or female mice in the inflammatory context (345-351), highlighting FKBP51 as potential target for both sexes.

---

Previous studies also investigated the involvement of FKBP51 in the establishment of chronic pain states such as neuropathic pain (344). Thereby, FKBP51 was identified as central mediator of chronic and especially neuropathic pain, and as pharmacological target for neuropathic pain. This conclusion was based on data which shows that FKBP51 deficient mice experienced less nerve injury-induced neuropathic pain than wild type animals (344). Furthermore, the treatment of nerve injured wild type mice with an FKBP51 silencing RNA resulted in comparably low pain behavior (344). Beside the nerve injury-induced neuropathic pain, FKBP51 was also shown to play an essential role in chemotherapy-induced neuropathic pain states, since FKBP51 deficient mice showed less hypersensitivity after cytostatic treatment (344). In addition, Maiaru et al. confirmed elevated FKBP51 levels in the dorsal horn of wild type mice after nerve injury. The increase of FKBP51 was suggested to induce a disbalance in the FKBP51-GR regulation and to lead to chronic pain states. However, these chronic pain states could be counteracted by pharmacologically targeting FKBP51 (344).

Beside the *in vivo* data, FKBP51 has additionally been described as regulator of the NF- $\kappa$ B signaling pathway (308). Although the influence of FKBP51 on the NF- $\kappa$ B signaling pathway is controversially discussed in literature, there is emerging evidence that FKBP51 seems to promote the activation of the NF- $\kappa$ B signaling pathway (352-357). This is of particular relevance in the context of pain as NF- $\kappa$ B induces the expression of various cytokines and chemokines, which play an essential role in the development of neuroinflammation (189, 222, 358-360). In addition, the NF- $\kappa$ B signaling pathway was associated with FKBP51-mediated cell migration, indicating its involvement in metastasis (361, 362). However, the underlying mechanism of FKBP51-mediated NF- $\kappa$ B regulation are poorly elucidated. Nevertheless, a reduction of FKBP51 levels was shown to be beneficial in many chronic inflammatory disorders (342-344, 363, 364).

### **1.7.3 SAFit2 as selective FKBP51 inhibitor**

Since FKBP51 was revealed as potential target for neuropsychiatric disorders, metabolic diseases and chronic pain states, the development of an FKBP51 specific inhibitor gained interest. However, the structural resemblance of other FKBP5s, especially FKBP52 to FKBP51, hampered the development of a FKBP51 specific inhibitor for a long time (365, 366). Nevertheless, Gaali et al. firstly developed two FKBP51 selective ligands by an induced fit mechanism (367). Based on this, the FKBP51 inhibitors were termed SAFit (selective

antagonist of FKBP51 by an induced fit mechanism) (367). From these two FKBP51 ligands, SAFit1 showed the highest affinity with 4 nM, however SAFit2 was shown to be more CNS permeable, while comprising an affinity of 6 nM towards FKBP51 (367, 368). Based on these results, the selective FKBP51 inhibitor SAFit2 was used for further animal studies (369-371).

The selectivity of SAFit2 to FKBP51 is mainly facilitated by a conformational change, which is induced at the FK1 domain of FKBP51 upon its binding (367). Mechanistically, the phenylalanine (Phe) 67 of FK1 is displaced towards lysine (Lys) 58 and Lys60, due to the C $\alpha$  of SAFit2, and gets stabilized by Phe129 (Figure 8) (367). In contrast, FKBP52 is unsusceptible to undergo such conformational changes as the respective residues (threonine 58, tryptophan 60 and valine 129) are too bulky therefore (367). Nevertheless, FKBP52 could undergo such conformational changes but the resulting conformation is very strained and unlikely. Based on that, SAFit2 comprises a 10,000 fold selectivity for FKBP51 over FKBP52 (367).

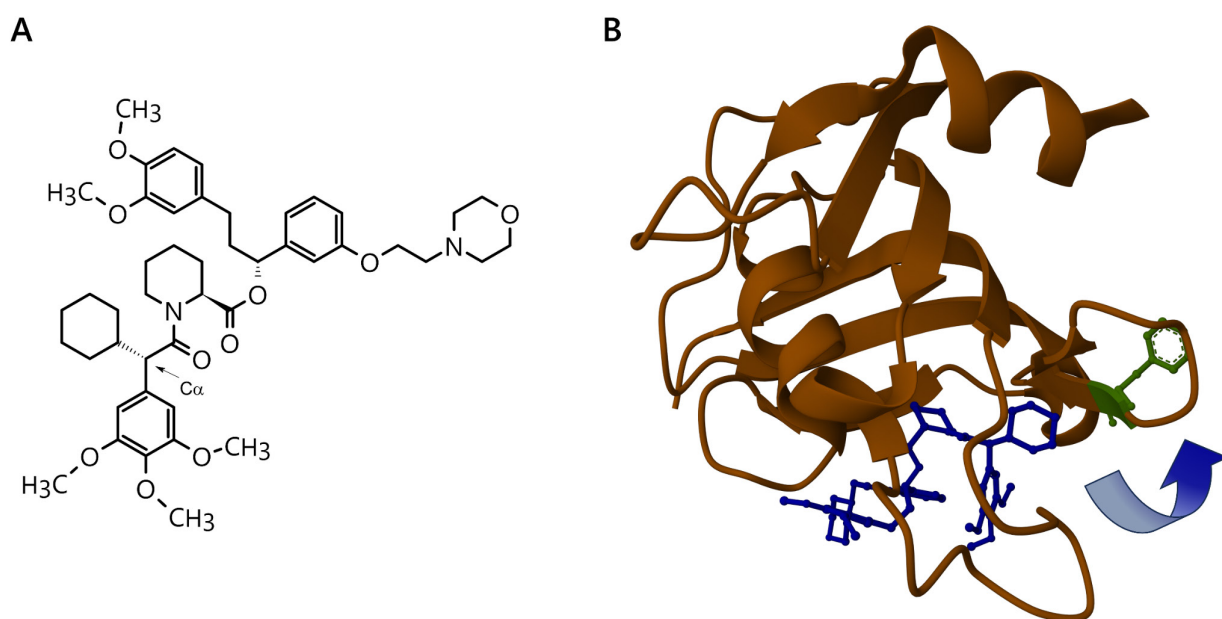


**Figure 8: Structure of SAFit2 and SAFit2 bound to FK1 of FKBP51. (A)** Molecular structure of SAFit2 with indicated C $\alpha$  which facilitates the conformational change in FKBP51. **(B)** Crystallographic structure of the FK1 domain of FKBP51 bound to SAFit2. The FK1 domain is colored in brown and SAFit2 in blue. The arrow indicates the displacement of phenylalanine 67 (green) due to the binding of SAFit2. The molecular structure was drawn with ChemSketch and the crystallographic structure was taken from the RSCB database (PDB-ID: 6txx) (372).



## 1.8 Aim of this thesis

Based on the high demand of neuropathic pain therapeutics and the limited and inadequate options for neuropathic pain treatment, the need of novel therapeutical drug candidates emerges. Interestingly, previous studies revealed a significant pain relieve of nerve injury- and chemotherapy-induced neuropathic pain in FKBP51 deficient mice, highlighting FKBP51 as potential target for these types of neuropathic pain. However, the pharmacological targeting of FKBP51 was hampered for years due to the lack of a selective FKBP51 inhibitor. Nevertheless, the development of SAFit2 as specific and highly potent FKBP51 inhibitor enabled the opportunity to target FKBP51 pharmacologically *in vitro* and *in vivo* (Figure 9).

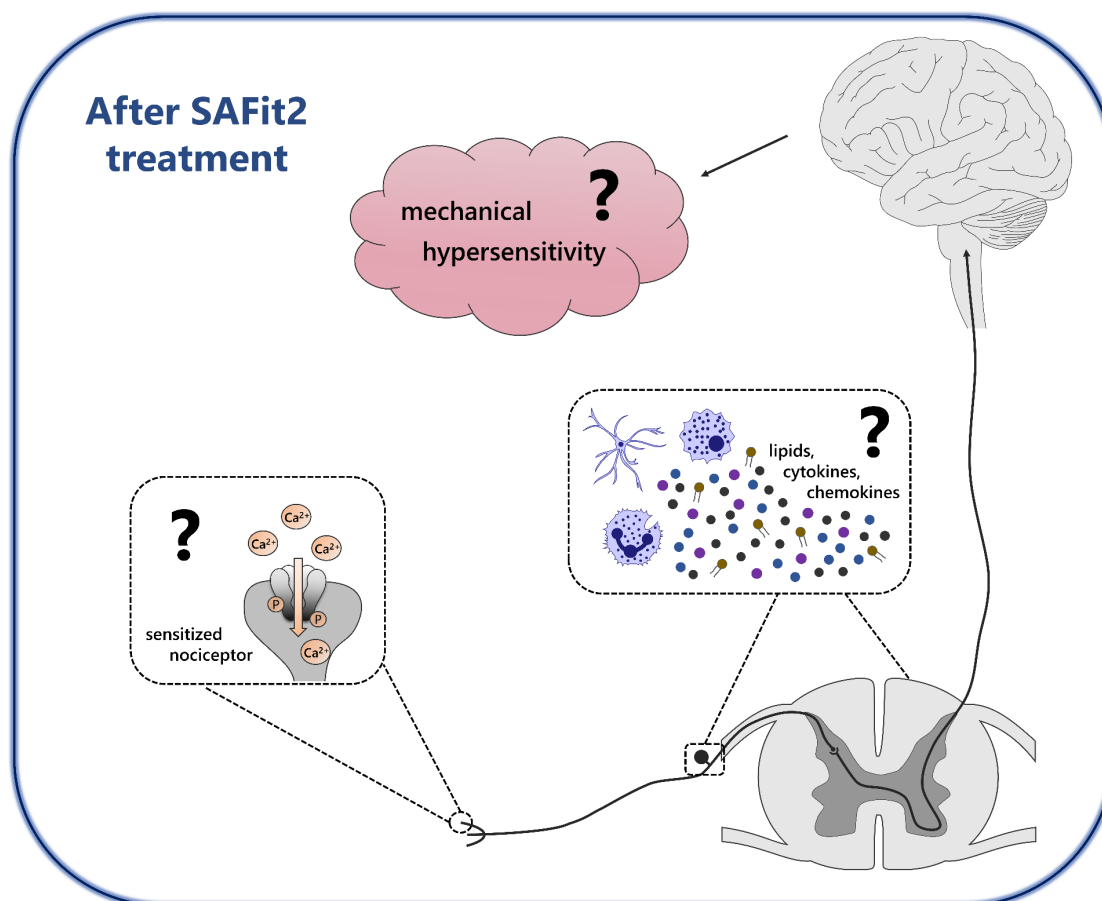


**Figure 9: Illustration of aims scheduled within this thesis.** To address the central question whether SAFit2 constitutes as potential novel treatment option for nerve injury- and paclitaxel-induced neuropathic pain, we firstly measured the mechanical hypersensitivity of mice as neuropathic pain behavior in both neuropathic pain models after SAFit2 treatment. Furthermore, lipid levels, cytokine and chemokine levels, the number of invading immune cells and the activation of glial cells was analyzed in dorsal root ganglia and spinal cord samples. In addition, we investigated the sensitization state of different pain-mediating TRP channels after SAFit2

---

treatment via calcium transients in primary sensory neurons and assessed related underlying mechanisms. The illustration was created with images from motifolio.

Hence, the overall objective of this thesis was to address and assess the hypothesis that SAFit2 constitutes as novel treatment option for nerve injury- and chemotherapy-induced neuropathic pain. In line with this, the **first aim** of this thesis was to investigate whether inhibiting FKBP51 with SAFit2 ameliorates nerve injury-induced and chemotherapy-induced neuropathic pain *in vivo* like the deficiency of FKBP51 does. The **second aim** encompassed the description of endogenous mediators such as lipids, chemokines, and cytokines in spinal cord and dorsal root ganglia of nerve injured and paclitaxel treated mice. Furthermore, the direct influence of SAFit2 on the excitability of primary sensory neurons and migration of primary macrophages was investigated. The **third aim** was to identify which impact changes of mediator profiles, sensory neuron excitability and macrophage migration might have on mechanisms occurring in neuropathic pain. In addition, first approaches should be made to understand how these changes are mediated after SAFit2 treatment.

---

## 2 Publication 1

---

### SAFit2 reduces neuroinflammation and ameliorates nerve injury-induced neuropathic pain

Saskia Wedel<sup>1</sup>, Praveen Mathoor<sup>2</sup>, Oliver Rauh<sup>3</sup>, Tim Heymann<sup>4</sup>, Cosmin I. Ciotu<sup>5</sup>, Dominik C. Fuhrmann<sup>2</sup>, Michael J. M. Fischer<sup>5</sup>, Andreas Weigert<sup>2</sup>, Natasja de Bruin<sup>6</sup>, Felix Hausch<sup>4</sup>, Gerd Geisslinger<sup>1,6</sup> and Marco Sisignano<sup>1,6</sup>

<sup>1</sup> Institute of Clinical Pharmacology, Pharmazentrum frankfurt/ZAFES, University Hospital, Goethe-University, 60590 Frankfurt am Main, Germany

<sup>2</sup> Institute of Biochemistry I, Faculty of Medicine, Goethe-University Frankfurt, 60590 Frankfurt am Main, Germany.

<sup>3</sup> Membrane Biophysics, Department of Biology, Technical University of Darmstadt, 64287 Darmstadt, Germany.

<sup>4</sup> Department of Chemistry, Technical University of Darmstadt, 64287 Darmstadt, Germany.

<sup>5</sup> Center of Physiology and Pharmacology, Medical University of Vienna, 1090 Vienna, Austria.

<sup>6</sup> Fraunhofer Institute for Translational Medicine and Pharmacology ITMP and Fraunhofer Cluster of Excellence for Immune Mediated Diseases CIMD, 60596 Frankfurt am Main, Germany.

#### 2.1 Author contributions

Conceptualization: FH, MS and GG conceptualized the project.

Funding acquisition: MS, FH, OR, NdB and MF acquired the funding.

Experimental design: **SW**, OR, AW, NdB, and MS designed the experiments.

Data acquisition: **SW** performed the multiplex assays, qPCRs, Western Blots, transwell assays, calcium imaging experiments, CGRP assay, calcineurin assay, WST assay and prepared all primary cells and tissue samples for measurements. PM performed the FACS measurements. OR performed the electrophysiological experiments. TH synthesized ddSAFit2. CC performed the SAFit2 screening in HEK cells. DF performed the seahorse run.

Data analysis: **SW** analyzed all the data. AW helped with the FACS analysis and OR performed the analysis of the electrophysiological measurements.

Data curation: **SW** performed the data curation.

Original draft preparation: **SW** and MS wrote and revised the manuscript.

All authors approved the final manuscript.

RESEARCH

Open Access



# SAFit2 reduces neuroinflammation and ameliorates nerve injury-induced neuropathic pain

Saskia Wedel<sup>1</sup>, Praveen Mathoor<sup>2</sup>, Oliver Rauh<sup>3</sup>, Tim Heymann<sup>4</sup>, Cosmin I. Ciotu<sup>5</sup>, Dominik C. Fuhrmann<sup>2</sup>, Michael J. M. Fischer<sup>5</sup>, Andreas Weigert<sup>2</sup>, Natasja de Bruin<sup>5</sup>, Felix Hausch<sup>4</sup>, Gerd Geisslinger<sup>1,6</sup> and Marco Sisignano<sup>1,6\*</sup>

### Abstract

**Background:** Neuropathic pain is experienced worldwide by patients suffering from nerve injuries, infectious or metabolic diseases or chemotherapy. However, the treatment options are still limited because of low efficacy and sometimes severe side effects. Recently, the deficiency of FKBP51 was shown to relieve chronic pain, revealing FKBP51 as a potential therapeutic target. However, a specific and potent FKBP51 inhibitor was not available until recently which hampered targeting of FKBP51.

**Methods:** In this study, we used the well-established and robust spared nerve injury model to analyze the effect of SAFit2 on nerve injury-induced neuropathic pain and to elucidate its pharmacodynamics profile. Therefore, the mice were treated with 10 mg/kg SAFit2 after surgery, the mice behavior was assessed over 21 days and biochemical analysis were performed after 14 and 21 days. Furthermore, the impact of SAFit2 on sensory neurons and macrophages was investigated in vitro.

**Results:** Here, we show that the FKBP51 inhibitor SAFit2 ameliorates nerve injury-induced neuropathic pain in vivo by reducing neuroinflammation. SAFit2 reduces the infiltration of immune cells into neuronal tissue and counteracts the increased NF- $\kappa$ B pathway activation which leads to reduced cytokine and chemokine levels in the DRGs and spinal cord. In addition, SAFit2 desensitizes the pain-relevant TRPV1 channel and subsequently reduces the release of pro-inflammatory neuropeptides from sensory neurons.

**Conclusions:** SAFit2 ameliorates neuroinflammation and counteracts enhanced neuronal activity after nerve injury leading to an amelioration of nerve injury-induced neuropathic pain. Based on these findings, SAFit2 constitutes as a novel and promising drug candidate for the treatment of nerve injury-induced neuropathic pain.

**Keywords:** SAFit2, FKBP51, Neuropathic pain, Neuroinflammation, Sensory neurons

### Background

Neuropathic pain is defined as lesion or disease of the somatosensory system [8]. It is a pathological pain state experienced worldwide by patients suffering from nerve injuries, diseases such as diabetes or chemotherapy [50]. However, the therapeutic options for neuropathic pain are very limited due to low treatment responses and severe side effects of available drugs [12]. Nerve

\*Correspondence: [Marco.Sisignano@med.uni-frankfurt.de](mailto:Marco.Sisignano@med.uni-frankfurt.de)

<sup>1</sup>Institute of Clinical Pharmacology, Pharmazentrum Frankfurt/ZAFES, University Hospital, Goethe-University, 60590 Frankfurt am Main, Germany  
Full list of author information is available at the end of the article



© The Author(s) 2022. **Open Access** This article is licensed under a Creative Commons Attribution 4.0 International License, which permits use, sharing, adaptation, distribution and reproduction in any medium or format, as long as you give appropriate credit to the original author(s) and the source, provide a link to the Creative Commons licence, and indicate if changes were made. The images or other third party material in this article are included in the article's Creative Commons licence, unless indicated otherwise in a credit line to the material. If material is not included in the article's Creative Commons licence and your intended use is not permitted by statutory regulation or exceeds the permitted use, you will need to obtain permission directly from the copyright holder. To view a copy of this licence, visit <http://creativecommons.org/licenses/by/4.0/>. The Creative Commons Public Domain Dedication waiver (<http://creativecommons.org/publicdomain/zero/1.0/>) applies to the data made available in this article, unless otherwise stated in a credit line to the data.

injury-induced neuropathic pain comprises several types of symptoms such as mechanical hypersensitivity which is defined as the reduction of the mechanical pain threshold, and painful sensations that can be mediated by innocuous stimuli [60].

The pain state itself arises by an increased activity of damaged nerve fibers, often in combination with an inflammatory response of the organism, which results in a pathological neuroinflammation [11]. Neuroinflammation is characterized as the infiltration of immune cells into neuronal tissue and the secretion of pro-inflammatory and proalgesic mediators such as cytokines, chemokines and neuropeptides that directly affect sensory neurons [22]. Moreover, the activation and sensitization of pain-mediating transient receptor potential (TRP) ion channels lead to the release of neuroinflammation-promoting neuropeptides [23].

During nerve injury-induced neuropathic pain, the release of pro-inflammatory and proalgesic mediators changes the microenvironment of sensory neurons which enhances neuronal activity. This can lead to peripheral and central sensitization and can subsequently to an increased pain perception [22]. The multitude of responsible mediators and the variety of different immune cell types, involved in their orchestrated synthesis and release, makes it difficult to target neuroinflammation at a large scale. Unfortunately, inhibiting individual cytokines, such as the tumor necrosis factor alpha, interleukin 6 or blocking their respective receptors does not significantly ameliorate neuropathic pain in patients [27, 58].

However, neuroinflammation can also be initiated by neurons themselves. More specifically, enhanced neuronal activity caused, for example, by increased activity of ion channels and depolarization can lead to an augmented downstream release of pro-inflammatory neuropeptides, such as calcitonin gene-related peptide (CGRP). These neuropeptides can cause vasodilation and recruitment of T cells and initiate neuroinflammation via their G protein-coupled receptors [3, 15, 56]. These studies indicate that a broader approach is required to target neuroinflammation-mediated persistent pain in patients.

Interestingly, previous studies revealed the FK506 binding protein 51 (FKBP51, encoded by the FKBP5 gene) as a novel potential therapeutic target for relieving neuropathic pain since its deficiency led to a significant amelioration of inflammatory and neuropathic pain [30, 31]. Initially, FKBP51 was discovered as a potential target for treating stress endocrinology [52] and glucocorticoid signaling related diseases [17]. Nevertheless, its strong upregulation, exclusively in sensory neurons of the dorsal horn after an ankle joint inflammation, indicated its involvement in the pathophysiological progress leading

to chronic pain [31]. However, the pharmacological targeting of FKBP51 inhibitor was not possible for a long time due to low specificity of synthesized inhibitors and cross-interactions with other related proteins.

Nevertheless, these challenges were overcome, exploiting an FKBP51-specific conformation [20], to generate an highly potent FKBP51 inhibitor called SAFit2 (selective antagonist of FKBP51 by induced fit) [2, 13]. In addition, a good pharmacokinetic availability and an improved blood–brain barrier permeability of SAFit2 compared to SAFit1 was already confirmed in previous pharmacokinetic studies for the dose of 10 mg/kg SAFit2 injected intraperitoneally [13, 14]. However, the underlying analgesic and anti-hyperalgesic mechanisms have not been identified yet. Here, we used the well-established and robust spared nerve injury (SNI) mouse model to analyze the effect of SAFit2 on nerve injury-induced neuropathic pain. Further, we investigated the neuronal and neuro-inflammatory effects of a SAFit2 treatment in vivo and in vitro to elucidate its pharmacodynamics profile.

## Materials and methods

### Animals, spared nerve injury surgery and SAFit2 treatment

In all experiments, wild-type mice (male C57Bl/6N mice, age from 8 to 12 weeks at the start of the study) were purchased from commercial breeding companies (Janvier and Charles River). For inducing neuropathic pain in mice, a spared nerve injury (SNI) surgery was performed under anesthesia to establish neuroinflammation. During the surgery, the sciatic nerve was exposed by a blunt dissection on the level of the knee joint. Then, two of the three sciatic nerve branches, common peroneal and tibial branch, were ligated with 6/0 non-sterile silk thread and cut distally from the ligature, leaving the sural nerve branch intact. Contact with the sural nerve branch was avoided to prevent stretching or harming. Afterwards, muscle and skin were closed in two layers [9].

For assessing the impact of SAFit2 on neuropathic pain behavior and neuroinflammation, animals were treated intraperitoneally with either 10 mg/kg SAFit2 or vehicle (PBS supplemented with 5% PEG400, 5% Tween and 0.7% ethanol) two times daily on six consecutive days starting on day five after surgery.

### Behavioral experiments

During all behavioral experiments, the experimenter was blinded. The motoric function of all animals was verified via rotarod before treatment. All animals were transferred into respective test cages for at least one hour before the measurement to allow habituation. For the determination of the mechanical withdrawal threshold, a dynamic plantar test was performed, using a Dynamic Plantar Aesthesiometer (Ugo Basile) as described

previously. Briefly, a steel rod was pushed against the mid-plantar area of the hind paw with linear ascending force up to 5 g over 10 s and a holding force of 5 g until a withdrawal response occurred. For behavioral experiments a cut-off time of 20 s was set [49].

#### Tissue isolation

For tissue isolation, mice were euthanized by isoflurane, cardio puncture and cranial dislocation either on day 14 or on day 21 after surgery covering different time points in neuroinflammation. The sciatic nerve, lumbar (L4–L6) dorsal root ganglia (DRGs) and the respective segments of the spinal cord were dissected from injured (ipsilateral) and unimpaired (contralateral) sites, followed by freezing tissue samples in liquid nitrogen for either RNA isolation, Western blot or multiplex assay. For flow cytometry analysis, the tissue was dissected and stored in 500  $\mu$ l ice-cooled PBS at 4 °C until further processing.

#### Quantitative real-time PCR

Total RNA was isolated from L4–L6 DRGs and the respective segments of spinal cord using the mirVana miRNA Isolation Kit (Applied Biosystems) according to the manufacturer's instructions. Afterwards, RNA concentrations were quantified with a NanoDrop ND-1000 spectrophotometer (NanoDrop Technologies) and a cDNA synthesis was performed with 200 ng RNA from DRGs and 400 ng RNA from spinal cord. The reverse transcription was performed with the First Strand cDNA Synthesis Kit (Thermo Fisher Scientific) according to the manufacturer's recommendations. The quantitative real-time PCR was conducted with QuantStudio™ Design & Analysis Software v 1.4.3 (Thermo Fisher Scientific) in a TaqMan® Gene Expression Assay System (Table 1, Thermo Fisher Scientific) according to the manufacturer's instructions. The raw data were

evaluated using the  $\Delta\Delta C(T)$  method, as described previously [29, 47].

#### Multiplex assay

For performing the ProcartaPlex multiplex immunoassay (Thermo Fisher), proteins were isolated with a manufacturer recommended cell lysis buffer, which was further supplemented with a phosphatase inhibitor cocktail (PhosSTOP, Roche) and a protease inhibitor cocktail (cComplete, Roche). DRG samples were suspended in 100  $\mu$ l and spinal cord samples in 200  $\mu$ l of cell lysis buffer. The spinal cord samples were further processed by a cell grinder. Afterwards, the tissue was homogenized two times per sample using a Sonopuls Sonicator (Bandelin) with the setting  $6 \times 10\%$ . During sonication, the samples were cooled in an ice bath, preventing proteins from degradation. Finally, the samples were centrifuged with  $16,000 \times g$  at 4 °C for 10 min, followed by collecting the supernatant for a protein concentration determination via Bradford.

The ProcartaPlex multiplex immunoassay was performed according to the manufacturer's recommendations. Briefly, a dark wall 96-well plate was prepared by several washing steps and coating steps with respective magnetic beads. Afterwards, standards were prepared in a serial dilution (1:4, (v/v)) and added to the plate, followed by further washing steps. Lastly, the samples were diluted (1:2, (v/v)) and added to the plate, which was sealed and incubated for 40 min with 500 rpm on an orbital shaker at room temperature, overnight at 4 °C and further 50 min with 500 rpm at room temperature. On the next day, the detection antibody mixture was added after a washing step and the plate was further incubated on an orbital shaker for 30 min at room temperature. Again, the plate was washed and streptavidin phycoerythrin was added to the plate and incubated for 30 min as described above. After the last washing step, the plate

**Table 1** List of used TaqMan® gene expression assays

Target	Gene	Article number	Company
ATF3	Activating transcription factor 3	Mm00476033_m1	Thermo Fisher
cFOS	FBJ osteosarcoma oncogene	Mm00487425_m1	Thermo Fisher
GAPDH	Glyceraldehyde-3-phosphate dehydrogenase	Mm99999915_g1	Thermo Fisher
iNOS	Inducible nitric oxide synthase 2	Mm00440502_m1	Thermo Fisher
MMP9	Matrix metalloproteinase 9	Mm00442991_m1	Thermo Fisher
NFATc3	Nuclear factor of activated T cells, calcineurin dependent 3	Mm01249200_m1	Thermo Fisher
NFATc4	Nuclear factor of activated T cells, calcineurin dependent 4	Mm00452375_m1	Thermo Fisher
NOX2	NADPH oxidase 2	Mm01287743_m1	Thermo Fisher
NOX4	NADPH oxidase 4	Mm00479246_m1	Thermo Fisher
XDH	Xanthine dehydrogenase	Mm00442110_m1	Thermo Fisher

was prepared with reading buffer, incubated for 5 min with 500 rpm on an orbital shaker, and measured with the Luminex 200 system (Bio-Rad).

#### Western blot

For Western blot purposes, the tissue of five animals was pooled and proteins isolated from the respective tissue samples. Therefore, 300  $\mu$ l of cell lysis buffer, which was described in part 2.5, were added to spinal cord samples and 100  $\mu$ l to DRG samples. The tissue samples were homogenized as previously described and the protein amount was determined by a Bradford assay.

Afterwards, 30  $\mu$ g tissue lysate was loaded and separated by SDS-polyacrylamide gel electrophoresis (4% stacking gel, 12% running gel) and transferred on a nitrocellulose membrane with the Trans-Blot<sup>®</sup>Turbo<sup>™</sup> Transfer System (BioRad). For total protein detection, the membrane was blocked with TBST buffer (20 mM Tris, 150 mM NaCl and 0.1% Tween20) containing 5% skimmed milk powder at room temperature for two hours, followed by an incubation overnight with primary antibodies at 4 °C: p65 1:500 (8242S, cell signaling technology), IKB $\alpha$  1:500 (4812S, cell signaling technology) and IKK $\beta$  1:250 (2370S, cell signaling technology). For phosphorylated protein detection, the membranes were blocked with TBST buffer containing 5% BSA at room temperature for 2 h, followed by an incubation for at least 48 h with primary antibodies at 4 °C: p-p65 1:500 (3033, cell signaling technology) and p-IKB $\alpha$  1:250 (2859S, cell signaling technology). Beta-actin 1:1000 (ab8229, abcam) was used as a loading control. For labeling targets, the fluorescent-labeled secondary antibodies anti-rabbit labeled with IRDye680ED from donkey (Licor), and anti-goat labeled with IRDye800CW from donkey (Licor) were used in 1:5000 dilutions for one hour at room temperature. The antibody detection was performed with an Odyssey CLx device from Licor, followed by a quantification with Image Studio Software.

#### Flow cytometry analysis

For creating single-cell suspensions, sciatic nerves were sliced with a tissue scissor and spinal cords were briefly pottered with a tissue grinder at first. Afterwards, all tissue samples (DRGs, sciatic nerve and spinal cord) were incubated in 500  $\mu$ l Dulbecco's modified Eagle medium (DMEM, Gibco) supplemented with 3 mg/mL collagenase and 1  $\mu$ l/mL DNase for 30 min at 37 °C. Then, the enzymatic reaction was stopped by further adding 500  $\mu$ l DMEM supplemented with 10% FCS. To obtain a single-cell suspension, the samples were filtered through a 70- $\mu$ m cell strainer and centrifuged at 400 g for 5 min. The supernatant was discarded and the cell pellet washed with 500  $\mu$ l PBS supplemented with 0.5% BSA, followed

by a further centrifugation step. Lastly, the cell pellet was suspended in 500  $\mu$ l PBS supplemented with 0.5% BSA and 1 mM EDTA to prevent cells from aggregating until and during flow cytometry analysis. The flow cytometry analysis was performed essentially as described previously [37]. Single-cell suspensions were blocked with FcR blocking reagent (Miltenyi Biotec) in 0.5% PBS-BSA for 20 min, stained with fluorochrome-conjugated antibodies (Table 2) and analyzed on a FACSymphony A5 flow cytometer (BD Biosciences). The data were analyzed using FlowJo VX (TreeStar). All antibodies and secondary reagents were titrated to determine optimal concentrations. Comp-Beads (BD Biosciences) were used for single-color compensation to create multicolor compensation matrices. For gating, fluorescence minus one control were used. The instrument calibration was controlled daily using Cytometer Setup and Tracking beads (BD Biosciences). For characterization of immune cell subsets, the antibodies in Table 2 were used.

#### Isolation and purification of dorsal root ganglia (DRGs)

For methods using sensory neurons in cell culture, DRGs were dissected and transferred into ice-cold HBSS with CaCl<sub>2</sub> and MgCl<sub>2</sub> (Gibco) directly after dissection. Afterwards, DRGs were treated with a collagenase/dispase solution, 500 U/mL collagenase and 2.5 U/mL dispase diluted in neurobasal medium (Gibco), at 37 °C for 75 min. The collagenase/dispase solution was removed by centrifuging and discarding the supernatant, the

**Table 2** List of antibodies used for flow cytometry analysis

Target	Dye	Cell type	Identifier	Source
CD11b	BV605	Monocytes, eosinophils, neutrophils	AB_2737951	Biolegend
CD11c	BV711	AMs	AB_2734778	BD Biosciences
CD19	APC-H7	B cells	AB_1645234	BD Biosciences
CD3	APC-Cy7	T cells	AB_1727461	BD Biosciences
CD326	BV711	Epithelial cells	AB_2738022	BD Biosciences
CD4	BV711	CD4 + T cells	AB_2737973	BD Biosciences
CD45	VioBlue	All leukocytes	AB_2659925	Miltenyi
CD8a	BV650	CD8 + T cells	AB_2563056	Biolegend
CD90	PE	Lymphocytes	AB_2659874	Miltenyi
F4/80	PE-Cy7	Macrophages	AB_893478	Biolegend
GITR	FITC	Tregs	AB_1089125	Biolegend
Ly6C	PerCP-Cy5.5	Monocytes	AB_1727558	BD Biosciences
Ly6G	APC-Cy7	Neutrophils	AB_10640819	Biolegend
MHCII	APC	cDCs, IMs	AB_313329	Miltenyi
NK1.1	BV510	NK cells	AB_2738002	Biosciences
SiglecF	PE	Eosinophils	AB_394341	Biolegend
$\gamma\delta$ TCR	APC	$\gamma\delta$ T cells	AB_1731813	Biolegend

Capsaicin, SAFit2 and RuR supplemented bath solutions were prepared directly before the measurements by adding the appropriate volume of stock solutions to the external solution. Bath solution exchange was performed using a gravity flow perfusion system. Whole-cell currents were elicited by repetitively applying 500 ms voltage pulses from  $-120$  mV to  $+80$  mV (20 mV increments) from a holding potential of  $-40$  mV and 500 ms voltage ramps from  $-60$  mV to  $+60$  mV from a holding potential of  $-60$  mV. Currents were recorded with a 10 kHz low-pass filter and sampled with a frequency of 50 kHz. Data were memorized with Patchmaster (HEKA Elektronik) and analyzed with Fitmaster (HEKA Elektronik). To account for the different sizes of the measured cells, whole-cell currents were normalized to the cell membrane capacity.

#### Calcitonin gene-related peptide assay

For measuring the effect of SAFit2 on calcitonin gene-related peptide (CGRP) secretion, DRGs were isolated as previously described (part 2.8) and stimulated with the respective compound the next day. Therefore, the cells were washed with HBSS and incubated with 250  $\mu$ l of the respective compound, diluted in HBSS to their final concentration, and 1  $\mu$ M capsaicin for 15 min at 37 °C. The respective volume of the vehicle was used as a negative control, and 1  $\mu$ M capsaicin alone as positive control. The CGRP quantification was performed with an ELISA kit from Bertin Bioreagent, which was used according to the manufacturer's recommendations. The final detection was performed measuring the absorption at 405 nm. The raw data were evaluated using linear regression according to the manufacturer's recommendation.

#### Calcineurin assay

The calcineurin activation was measured with a cellular calcineurin phosphatase activity assay kit from abcam, which was used according to the manufacturer's instructions. The enzyme calcineurin was isolated from HEK-293 cells using 1 mL of TBS buffer containing 20 mM Tris and 150 mM NaCl (adjusted to pH 7.3) for a 90% confluent T75 flask. The cell lysate was further purified according to the kit protocol. To measure the impact of the respective compounds on the activity of calcineurin, the purified cellular extract with calcineurin was supplemented with the respective compound and added to the prepared assay plate. Afterwards, the plate was incubated for 30 min at 30 °C to stimulate the activity of the enzyme for a distinct period of time. Finally, the reaction was terminated by adding the assay reagent to the plate and the absorption was detected after 20 to 30 min at 620 nm. The raw data were evaluated using linear regression according to the manufacturer's instructions.

#### Differentiation of bone marrow-derived macrophages (BMDM)

For bone marrow isolation, mice were killed and hind legs were dissected and transferred into ice-cold PBS. The bones were cleaned from muscle tissue, cut open and transferred into 0.5-mL Eppendorf tubes with holes at their peak end. To isolate the bone marrow via centrifugation (1300 rpm, 1 min, RT), the tubes were placed into 1.5-mL Eppendorf tubes, containing 50  $\mu$ L of BMDM medium (RPMI + GlutaMAX (Thermo Fisher Scientific) supplemented with 10% FCS (Sigma-Aldrich), 100 U/mL penicillin + 100  $\mu$ g/mL streptomycin (Thermo Fisher Scientific) and 20 ng/mL M-CSF (PeproTech). After centrifugation, the bone marrow pellet was resuspended in BMDM medium and distributed equally into a 6-well plate. For macrophage differentiation, cells were incubated overnight at 37 °C, followed by a change of BMDM medium the next day. At day four of differentiation, fresh growth factors were provided by adding the same amount of BMDM medium to the differentiating cells. After 7 days, the cells were fully differentiated and used for further experiments [57].

#### Human macrophage isolation and purification

For isolating buffy coats from whole bloods samples, 50-mL Leucosep tubes were equilibrated with 15 mL lymphocyte separation medium, which was passed through the membrane by centrifuging at  $1000 \times g$  for 5 min. Afterwards, 40 mL whole blood was transferred into a tube, which was then filled up to 50 mL with PBS containing 2 mM EDTA. The samples were centrifuged at  $440 \times g$  for 35 min at room temperature without break to enable a clear separation of fractions comprising a plasma fraction at the top, the buffy coat in the middle and an erythrocyte and granulocyte fraction at the bottom. The plasma was discarded and the buffy coat transferred into a fresh 50-mL tube, which was then again filled up to 50 mL with PBS containing 2 mM EDTA for purification. The suspension was again centrifuged at  $500 \times g$  at room temperature for 5 min and the purification step was repeated until the supernatant was almost clear. Afterwards, the cell pellet was resuspended in 50 mL RPMI medium supplemented with 1% P/S and the cell solution was plated with 1 mL/ well into 6-well plates. The cells were incubated for one hour at 37 °C, followed by a medium change with 2 mL RPMI supplemented with 1% P/S and 3.3% human plasma for differentiation purpose. The medium was changed every 2–3 days until day seven of differentiation. Monocytes were now fully differentiated into macrophages and can be used for further experiments [43].



sensory neurons were washed twice with neurobasal medium containing 10% FCS, followed by an incubation with 0.05% trypsin (v/v) (Gibco) for another 10 min. The washing steps were repeated, and the cells were mechanically dissociated in neurobasal medium (Gibco) supplemented with L-glutamine (2 mM; Gibco), penicillin (100 U/mL; Gibco), streptomycin (100 µg/mL; Gibco), B-27 (Gibco) and gentamicin (50 µg/mL; Gibco). Afterwards, the cell solution was plated on poly-L-lysine-coated cover slips or 48-well plates. After two hours of incubation, 2 mL of neurobasal medium was added and the cells were incubated overnight at 37 °C. For further investigations, the cultured DRGs were further used and treated as described in part 2.9 and 2.13.

#### Calcium imaging

For calcium imaging, the cultured sensory neurons were stained with fura-2-AM (Thermo Fisher) for at least 60 min at 37 °C and washed afterwards twice with Ringer's solution. This was set up freshly with 145 mM NaCl, 1.25 mM CaCl<sub>2</sub> × 2H<sub>2</sub>O, 1 mM MgCl<sub>2</sub> × 6 H<sub>2</sub>O, 5 mM KCl, 10 mM D-glucose and 10 mM HEPES and adjusted to a pH of 7.3. During the experiments, Ringer's solution was also used for baseline measurements and for washing out agonists and compounds between stimulations. For investigating the effect of SAFit2 on different TRP channels, the sensory neurons were pre-incubated with the respective compound for 2 min and stimulated with respective agonists afterwards: 100 nM capsaicin for 30 s (TRPV1 agonist) and 100 mM allyl isothiocyanate for 45 s (TRPA1 agonist). Control experiments were performed with the respective volume of the corresponding vehicle. All stimulating compounds were dissolved in Ringer's solution to their final concentration. The measurements were performed using a DMI4000 B Microscope, the compact light source CTR550 HS (Leica) and the ValveBank II system (AutoMate Scientific).

#### Flexstation method

Cells were grown in 96-well black-walled plates. Human TRPV1 was transiently expressed in HEK-293t cells using jetPEI transfection reagent (Polyplus Transfection). Cells were loaded with Calcium 6 for two hours (Calcium 6 Kit; Molecular devices, San Jose, CA), in an extracellular solution containing 145 mM NaCl, 5 mM KCl, 10 mM glucose, 10 mM HEPES, 1.25 mM CaCl<sub>2</sub>, and 1 mM MgCl<sub>2</sub>, buffered to pH 7.4 with NaOH. According to the manufacturer's protocol, cells are not washed, but extracellular dye is chemically quenched. Calcium 6 fluorescence excited at 488 nm every 2.5 s served as an index of intracellular calcium. Assays were performed at 25 °C. A volume of 50 µL of each applied solution was pipetted automatically according to a preset protocol into 100 µL

of extracellular solution in the wells. Fluorescence change was measured by a Flexstation3 (Molecular devices) and is reported relative to baseline fluorescence.

#### Transfection of HEK-293 cells

For functional expression of green fluorescent protein (GFP) flanked TRPV1, HEK-293 cells were transfected 16–24 h before the start of patch-clamp experiments using TransfeX™ Transfection Reagent (LGC Standards GmbH) according to the manufacturer's instructions. HEK-293 cells (German Collection of Microorganisms and cell cultures) were grown at 37 °C in a humidified 95% air/ 5% CO<sub>2</sub> incubator in Dulbecco's modified Eagle medium (DMEM; Gibco) supplemented with 10% v/v heat-inactivated fetal bovine serum, 100 U/mL penicillin G, 100 µg/mL streptomycin sulfate and 2 mM L-glutamine (all from Invitrogen). After reaching approximately 80% confluence HEK-293 cells were transfected in a 35-mm petri dish with 1 µg of hTRPV1\_GFP (NM\_080705, RG217713, OrgiGene) plasmid DNA.

#### Electrophysiology

On the day of experiment, transfected HEK-293 cells were separated by trypsinization, seeded at low density on coverslips (15 mm in diameter), and then incubated for 2 to 4 h to allow adhering of cells on the glass surface. For patch-clamp experiments, coverslips were transferred to a perfusion chamber filled with bath solution and placed on the stage of an inverted microscope. Transfected cells were identified by the fluorescence of the GFP fused to the C-terminus of TRPV1. Patch-clamp experiments were performed in the whole-cell configuration with an EPC-10 patch-clamp amplifier (HEKA Elektronik) at room temperature (20–25 °C). Patch-pipettes were pulled from borosilicate capillaries (DWK Life Sciences) using a single stage glass microelectrode puller (PP-830) resulting in pipettes with 1.5–3 MΩ resistances. The capillaries were coated with Sigmacote® (Merck KGaA) and baked after pulling at 65 °C for 45 min. The pipette solution contained: 140 mM CsCl, 1.93 mM CaCl<sub>2</sub>, 2 mM MgCl<sub>2</sub>, 5 mM 4-(2-hydroxyethyl)-1-piperazineethanesulfonic acid (HEPES), 5 mM ethylene glycol-bis (β-aminoethyl ether)-N,N,N',N'-tetraacetic acid (EGTA), and 2 mM MgATP. pH and osmolarity were adjusted to 7.2 with 1 M CsOH and 320 mOsmol/kg with D-mannitol, respectively. The bath solution contained: 140 mM NaCl, 5 mM KCl, 2 mM CaCl<sub>2</sub>, 1 mM MgCl<sub>2</sub>, 10 mM HEPES and 10 mM D-glucose. pH and osmolarity were adjusted to 7.4 with 1 M NaOH and 320 mOsmol/kg with D-mannitol, respectively. Capsaicin (M2028, Sigma Aldrich), SAFit2 and Ruthenium Red (RuR) (557,450, Sigma Aldrich) stock solutions were prepared by dissolving 10 mM, 2.5 mM and 10 mM in DMSO, respectively.

### Transwell assay

For investigating the migration of macrophages, cultivated macrophages were starved overnight and harvested the next day by incubating them 10 min with 600  $\mu$ l accutase/well (Sigma-Aldrich) at 37 °C and using a cell scraper. The reaction was terminated using 1% (w/v) BSA solution for murine macrophages. Afterwards, the macrophages were centrifuged at 1000 rpm for 5 min and the cell pellet was resuspended in 1 mL of the respective starving medium. The cell concentration was determined, using a Neubauer counting chamber and the cell concentration adjusted to  $10^6$  cells/mL. Transwell inserts (Greiner) were placed into 24-well plates, which contain 500  $\mu$ l medium/well with either 10% FCS as chemoattractant for murine cells or 3.3% human plasma for human cells and the respective compound. The cells were seeded by adding 300  $\mu$ l cell solution per insert. After incubating the setup for two hours at 37 °C, the inserts were rinsed with PBS and cells were fixed with 2% PFA for two minutes, followed by further washing steps and a further fixation and permeabilization step with 100% ice-cooled methanol for 20 min. Lastly, the membranes were stained with DAPI in a final concentration of 0.2 ng/mL in the dark for two minutes and embedded on slides with mounting media for quantification purposes. Five images were taken per membrane with the fluorescence microscope Observer.Z1 (Carl Zeiss) and quantified with ImageJ software.

### Cytotoxicity assay with WST-1

Primary murine macrophages were isolated and differentiated as previously described (part 2.15). The cells were harvested the same way as described in part 2.17. Afterwards, the cell concentration was adjusted to  $3.6 \times 10^5$  cells/mL and cells were seeded with 1 mL/well into 24-well plates, followed by an incubation for further 48 h at 37 °C. For analyzing the compound's cytotoxicity, DMEM medium was supplemented with 10% (v/v) WST-1 and either the compound of interest or the according volume of the dissolvent. The cells were treated with 300  $\mu$ l of prepared medium for two hours at 37 °C and the absorption wavelength was measured at 450 nm and 600 nm afterwards.

### Seahorse bioanalyzer

For measuring the metabolic parameters with the Seahorse bioanalyzer device, primary murine macrophages were isolated and differentiated as previously described (part 2.15). The macrophages were harvested in the same way as described in the part 2.17, seeded ( $25 \times 10^3$  cells/well) into Seahorse 96-well cell culture plates and incubated overnight. On the day of measurement, the media was replaced by XF RPMI medium supplemented with

10 mM glucose and 2 mM glutamine (all from Agilent). The plate was equilibrated for 30 min in a non-CO<sub>2</sub> incubator at 37 °C. Metabolic parameters were measured on a Seahorse XFe 96 extracellular flux analyzer (Agilent). To analyze the ATP production rate, 2.5  $\mu$ M oligomycin and 500 nM rotenone together with antimycin A were sequentially added to the cells. All chemicals were purchased from Cayman chemicals. Data were processed using Wave Desktop (Version 2.6.0.31) and ATP rates were calculated using the Seahorse Analytics online tool (Version from February 2022).

### Data analysis and statistics

All data are presented as mean  $\pm$  SEM. Normal distribution was confirmed using the Shapiro–Wilk test. For in vitro experiments comparing only two groups, an unpaired and heteroskedastic Student's *t* test was conducted with Welch's correction. When comparing more than two groups, a one-way analysis of variance (ANOVA) was used and for the comparison of more than three groups a two-way ANOVA was conducted. For statistical analysis of behavioral experiments, an ANOVA was performed, followed by Bonferroni's post hoc correction. For all statistical analysis the software GraphPad Prism 9 was used. A *p* value of  $< 0.05$  was considered statistically significant.

## Results

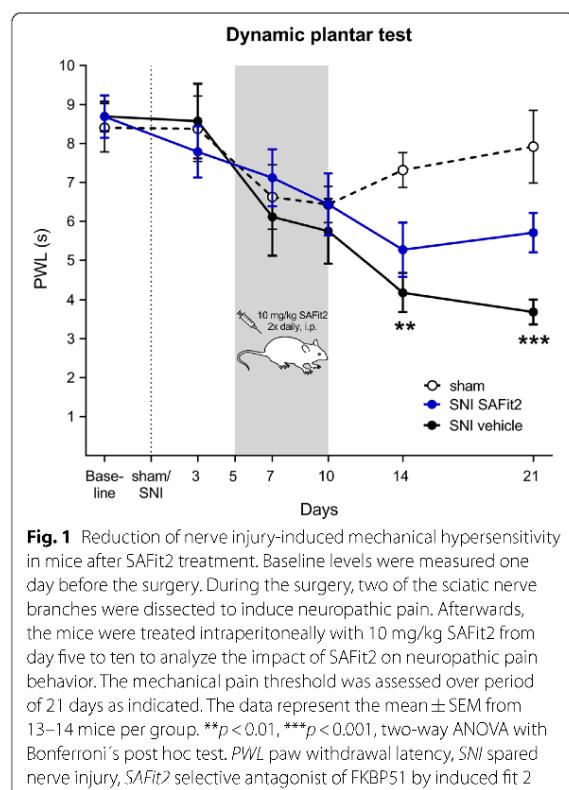
### SAFit2 ameliorates nerve injury-induced mechanical hypersensitivity

Our initial goal was to investigate whether SAFit2 has an influence on nerve injury-induced neuropathic pain. Therefore, we chose the robust and well described spared nerve injury (SNI) model to generate neuropathic pain in mice [9] and treated the mice intraperitoneally either with 10 mg/kg SAFit2 or vehicle from day five to ten after the surgery.

To analyze neuropathic pain, we determined the mechanical pain threshold of mice paws in a dynamic plantar test over 21 days (Fig. 1). After the surgery, the vehicle-treated SNI animals developed a significant mechanical hypersensitivity over time as compared to the sham-treated animals. In contrast, the SAFit2-treated SNI animals showed less mechanical hypersensitivity than the vehicle-treated animals (Fig. 1).

### SAFit2 reduces cytokine and chemokine levels in dorsal root ganglia and spinal cord after nerve injury

Since we detected that SAFit2 reduces the mechanical hypersensitivity in nerve-injured mice, we isolated lumbar dorsal root ganglia (DRGs) and spinal cord (SC) at day 21 after the surgery to investigate how amelioration of mechanical hypersensitivity is mediated. Therefore,



we analyzed at first the expression of neuronal stress markers (activating transcription factor 3, matrix metalloproteinase 9, cFOS) and oxidative stress markers (xanthine dehydrogenase, NADPH oxidase 2 and 4, inducible nitric oxide synthase) but did not detect any significant differences between vehicle and SAFit2-treated animals (Additional file 1: Fig. S1). Since we did not observe any changes in the expression of common stress markers, we next analyzed the concentrations of inflammatory and proalgesic mediators in DRGs and spinal cord. We therefore performed a multiplex immunoassay to detect alterations in inflammatory and pain-mediating cytokines and chemokines after SAFit2 treatment (Figs. 2, 3, Additional file 1: Fig. S2).

All cytokines and chemokines were significantly upregulated in lumbar DRGs of vehicle-treated SNI animals (Fig. 2A–G, I–P) as compared to sham-treated animals, except for interleukin (IL)-18 (Fig. 2H). However, DRGs of SAFit2-treated SNI mice showed quite similar cytokine and chemokine levels as the DRGs of sham-treated mice (Fig. 2A–P). Moreover, we detected significant differences between vehicle and SAFit2-treated mice for both pro-inflammatory cytokines as IL-1 $\beta$ , IL-6, IL-18, IL-23 (Fig. 2 A, D, H, J) and anti-inflammatory

cytokines as IL-4, IL-5, IL-13, IL-22 (Fig. 2B, C, E, I). Also, significant differences were observed for pain-mediating chemokines as C-C motif ligand (CCL) 2, CCL3, CCL4 and C-X-C ligand 2 (Fig. 2K, L, M, P). In DRGs SAFit2 overall reduced cytokine and chemokine levels after nerve injury, which were thereby largely similar to levels in sham operated animals.

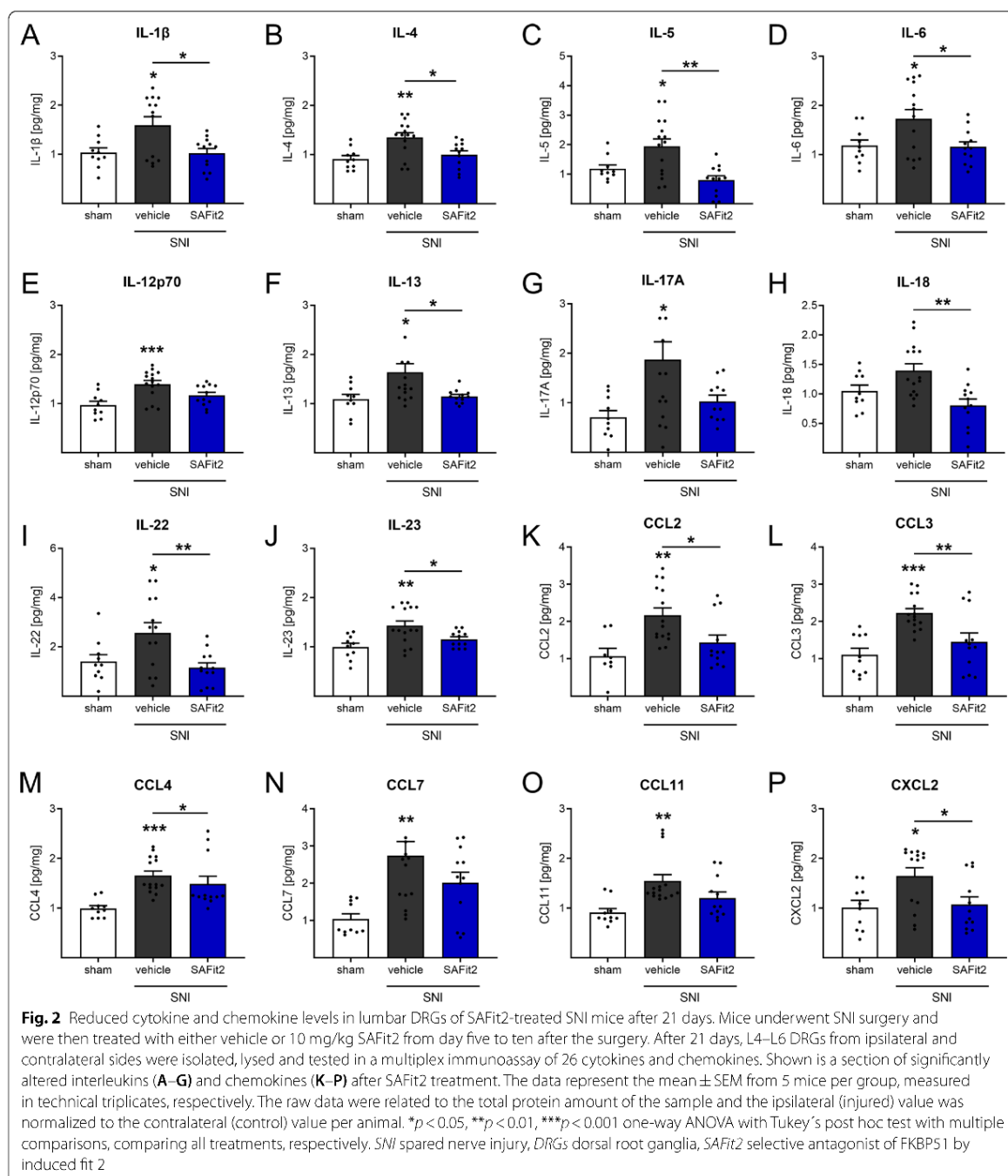
We next analyzed the concentrations of cytokines and chemokines in the dorsal spinal cord (Fig. 3). Interestingly, the analysis of spinal cord samples revealed similar trends for SAFit2 treatment as shown in the DRG measurements, including an increase of mediators after vehicle treatment which was blunted after SAFit2 treatment. However, SAFit2 reduced pain-mediating chemokines CCL2, CCL3, CCL4, CCL7, CCL11 and C-X-C ligand 2 (Fig. 3I–N) more substantially in the spinal cord than in DRG samples. In addition, we observed significant differences in the cytokines IL-2, IL-4, IL-10 and IL-18 (Fig. 3B, C, E, G) for vehicle and SAFit2-treated animals. Overall, SAFit2 treatment had a major effect on chemokine levels in the spinal cord and on cytokine levels in DRGs. In summary, these results indicate that SAFit2 significantly reduces inflammation and pain-mediating cytokine and chemokine secretion after nerve injury.

#### SAFit2 in vivo treatment reduces NF- $\kappa$ B pathway activation after SNI

Based on the significant reduction of cytokines and chemokines in lumbar DRGs and spinal cord after SAFit2 treatment, we hypothesized that SAFit2 has an impact on the NF- $\kappa$ B signaling pathway and its activation, since NF- $\kappa$ B is one of the most relevant transcription factors being involved in the regulation of cytokine and chemokine expression. Moreover, FKBP51 has repeatedly been implicated in the NF- $\kappa$ B signaling pathway [17].

To investigate this hypothesis, we again performed an SNI mouse model and treated mice with either vehicle or 10 mg/kg SAFit2 (i.p.) over the same period of time as in the previous experiment. For examining the underlying mechanisms, we isolated lumbar DRGs and the respective parts of the spinal cord at day 14 after SNI surgery. This timepoint represents a phase of acute to chronic neuropathic pain with an established neuroinflammation [9, 44], being appropriate to analyze the ongoing inflammation on its peak.

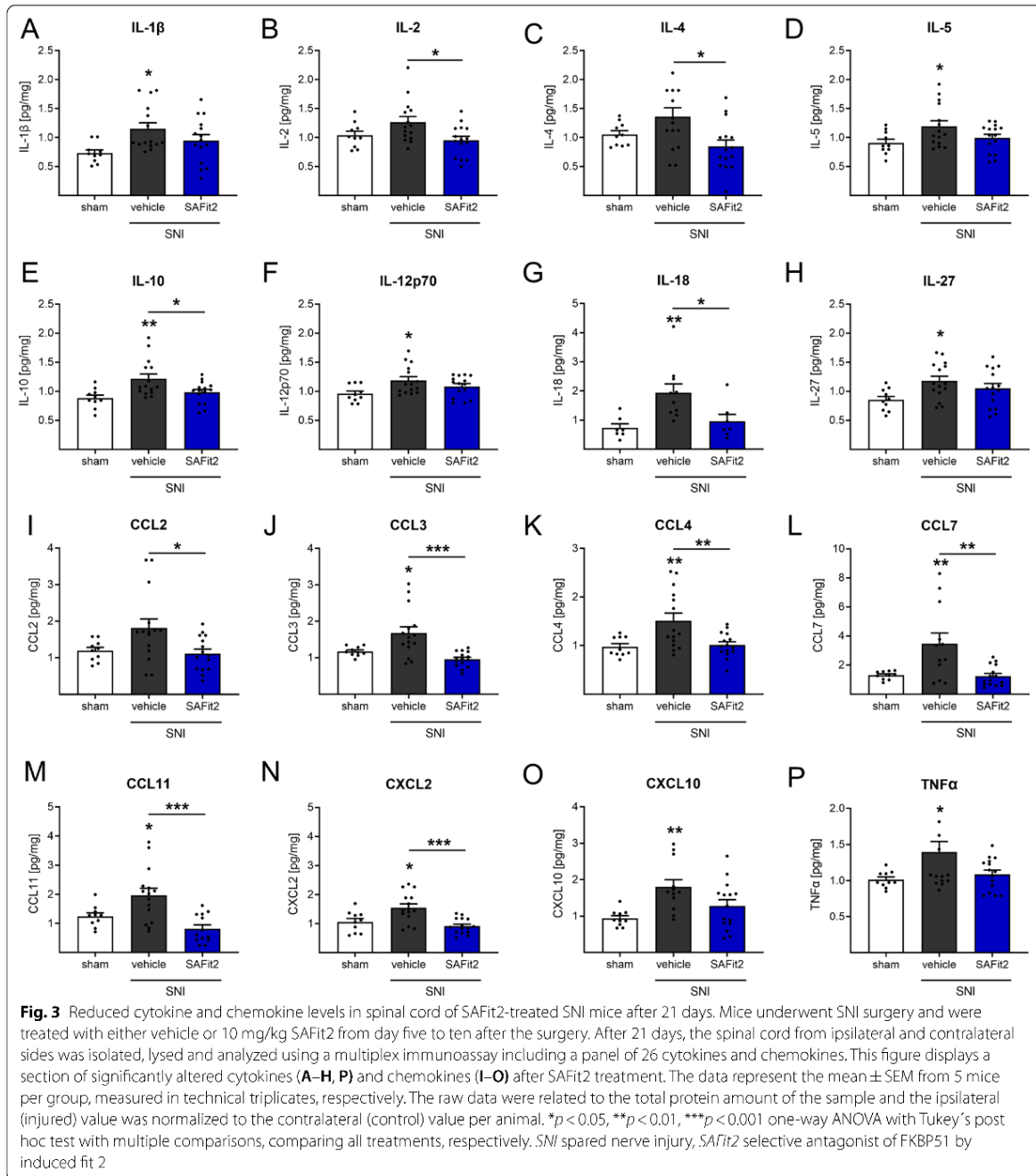
We performed Western blots with respective tissue lysates, in which we analyzed the total and the phosphorylated amount of three crucial protein members of the NF- $\kappa$ B signaling pathway: the inhibitor complex alpha (I $\kappa$ B $\alpha$ ), p65 itself and the upstream I $\kappa$ B $\alpha$  kinase beta (IKK $\beta$ ). These factors were analyzed in both DRGs and spinal cord, respectively (Fig. 4), observing that SAFit2



treatment has no influence on the total protein amount of I $\kappa$ B $\alpha$  (Fig. 4B), p65 (Fig. 4C) and IKK $\beta$  (Fig. 4D).

However, SAFit2 significantly affects the phosphorylation state of the respective factors (Fig. 4E–G). We

observed that SAFit2 treatment leads to a significant decrease of I $\kappa$ B $\alpha$  phosphorylation (Fig. 4F) and p65 phosphorylation (Fig. 4G) in lumbar DRGs and spinal cord of nerve-injured mice. Based on this, we concluded



that SAFit2 does not change the basal expression of the respective factors, but strongly reduces the NF- $\kappa$ B pathway activation. Besides the NF- $\kappa$ B pathway, the transcription factor NFAT might also have an influence

on cytokine and chemokine regulation. However, we detected no alterations in the regulation of NFAT after SAFit2 treatment (Additional file 1: Fig. S1), indicating the NF- $\kappa$ B pathway as primary pathway for cytokine and chemokine production after nerve injury.

### SAFit2 treatment reduces immune cell infiltration into dorsal root ganglia and spinal cord after nerve injury

Since modulation of the NF- $\kappa$ B signaling pathway activation can influence immune cell migration [19, 28, 39], we next investigated the influence of SAFit2 on the immune cell distribution in neuronal tissue after nerve injury. We hypothesized that a reduced immune cell infiltration would additionally explain reduced cytokine and chemokine levels. Therefore, we performed the same *in vivo* experiment, an SNI surgery followed by SAFit2 treatment, and collected lumbar DRGs, the respective parts of the spinal cord and both sciatic nerves 14 days after surgery. The tissue was gently homogenized, and the subset of immune cells determined in the respective tissues using a flow cytometry analysis (Fig. 5).

Interestingly, we detected a significant reduction of all immune cells in the DRGs (CD45<sup>+</sup>, Fig. 5A) which was not the case for the inflamed sciatic nerve which is the core of inflammation (Fig. 5K). Moreover, we observed a significant reduction of dendritic cells (Fig. 5D), regulatory T cells (Fig. 5H), memory T cells (Fig. 5I) and gamma delta T cells (Fig. 5J) in the DRGs after SAFit2 treatment, which we could not observe in the sciatic nerve samples. Instead, a slight upregulation of the respective immune cells was measured in the sciatic nerve samples (Fig. 5N, R, S, T). A significant decrease of monocytes (Fig. 5B) and eosinophils (Fig. 5E) was detected in the spinal cord after SAFit2 treatment. In contrast, these immune cell types were unaltered in the sciatic nerve samples comparing vehicle and SAFit2-treated animals (Fig. 5L and O). Also, the total amount of immune cells was not altered by SAFit2 treatment in the sciatic nerve samples (CD45<sup>+</sup>, Fig. 5K). In summary, SAFit2 treatment *in vivo* leads to a reduced infiltration of immune cells into DRGs and spinal cord, but it does not affect the number nor the distribution of immune cells at the sciatic nerve.

### SAFit2 reduces the migration of primary murine and human macrophages

As we have seen significant changes in the number of immune cells in neuronal tissue after SAFit2 treatment and the counteracting effect of the compound on the pro-migratory NF- $\kappa$ B pathway, we next assessed whether SAFit2 has a direct effect on the migratory behavior of

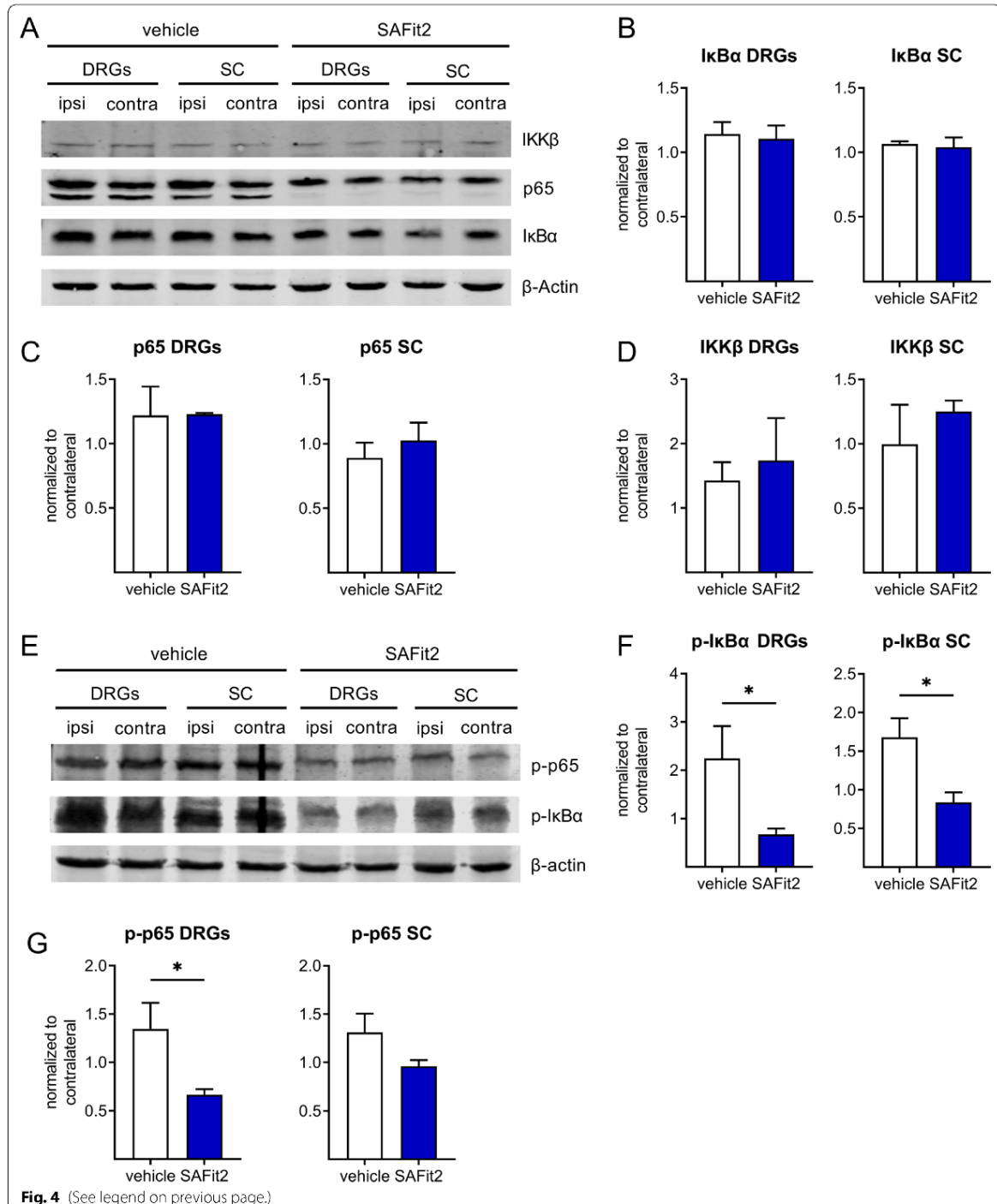
antigen presenting cells. In particular, we focused on analyzing the impact of SAFit2 on macrophage migration since macrophages constitute an essential role in neuroinflammation and central sensitization [62]. In addition, the target FKBP51 was previously suggested to be involved in promoting cell migration [32, 54].

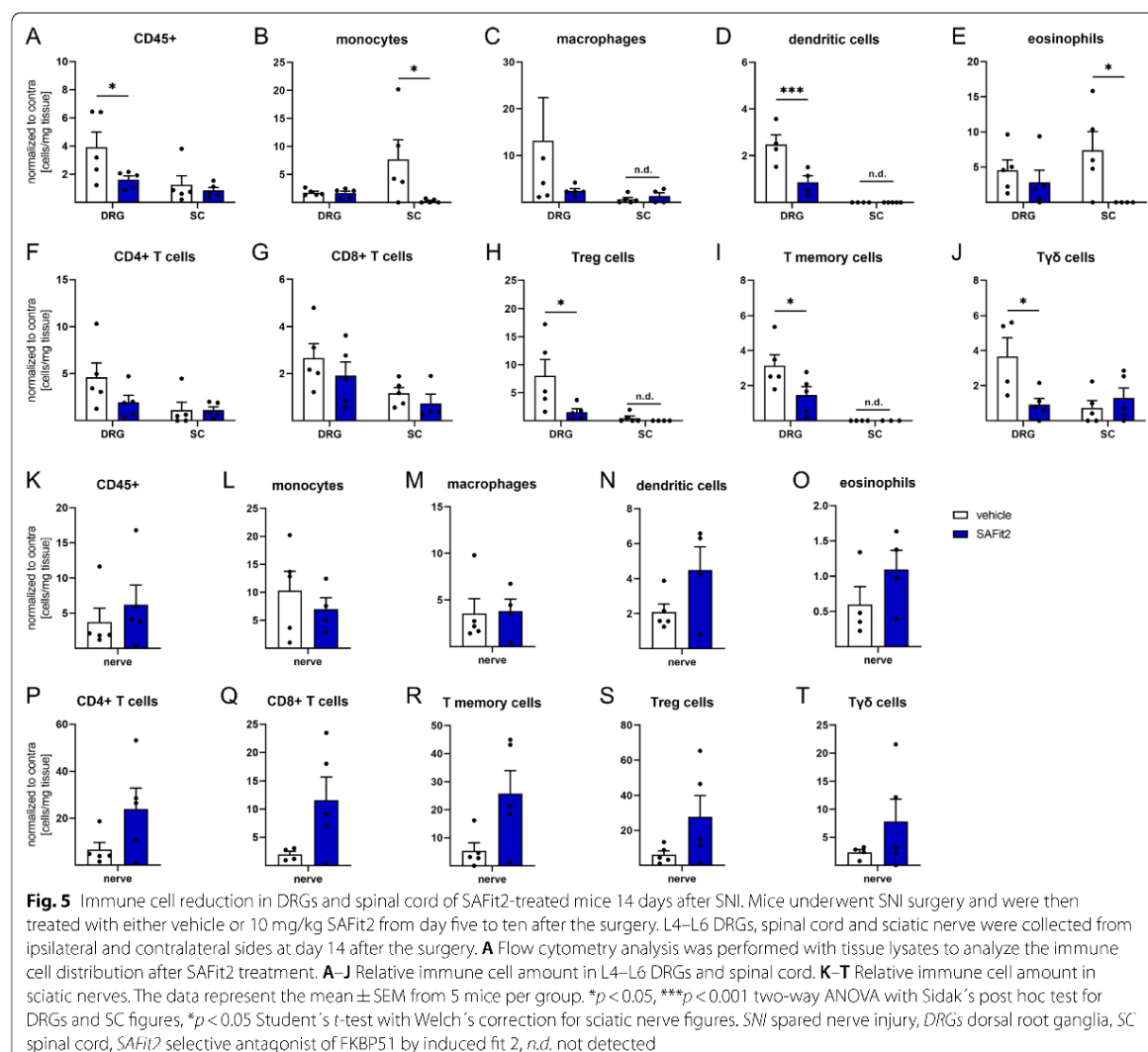
For investigating the migration of primary macrophages, we isolated monocytes either from murine bone marrow or from human blood donations and differentiated the monocytes into primary macrophages in cell culture. Afterwards, their migratory behavior was assessed in Transwell assays during the treatment with SAFit2 (Fig. 6). Interestingly, SAFit2 significantly reduced the migration of both murine (Fig. 6B) and human macrophages (Fig. 6C) in a concentration dependent manner. However, ddSAFit2 (Additional file 1: Fig. S3), which corresponds almost to the structure of SAFit2 as chiral analogue and is instead biologically inactive, does not affect the migration of murine and human macrophages (Fig. 6B, C). As a control experiment, we analyzed the impact of SAFit2 on murine macrophage viability and metabolism to exclude any cytotoxic effect which could also reduce the total amount of migrated macrophages (Additional file 1: Fig. S4). However, SAFit2 has neither a detectable influence on cell viability nor on oxidative phosphorylation, adenosine triphosphate (ATP) synthesis and mitochondrial oxygen consumption rate (Additional file 1: Fig. S4).

As we discovered that SAFit2 reduces macrophage migration, we wanted to further investigate whether this effect is on target (i.e., mediate by FKBP51) or a potential off-target effect of the compound (Fig. 6D, E). Therefore, we again performed Transwell assays with primary murine macrophages, however pretreating the cells this time with two FKBP inhibitors from a different chemical series [26, 41]. The concentration and treatment duration for a successful inhibition were chosen based on previous intracellular FKBP51 occupancy studies [16]. These FKBP inhibitors also reduced the murine macrophage migration at low concentrations (Fig. 6D) and in a non-additive manner to SAFit2 (Fig. 6E), strongly suggesting an FKBP as relevant target for the reduction of macrophage migration. Likewise, SAFit2 shows similar effects in low micromolar concentrations after two hours of treatment.

(See figure on next page.)

**Fig. 4** SAFit2 treatment reduces NF- $\kappa$ B pathway activation in SNI-treated mice after 14 days. Mice underwent SNI surgery and were then treated with either vehicle or 10 mg/kg SAFit2 from day five to ten after the surgery. Lumbar L4–L6 DRGs and spinal cord were collected from ipsilateral and contralateral sides at day 14. **A** Representative Western blot of the total protein expression of the factors IKK $\beta$ , p65 and I $\kappa$ B $\alpha$  after vehicle and SAFit2 treatment. **B–D** Quantification of the total protein expression of I $\kappa$ B $\alpha$  (**B**), p65 (**C**) and IKK $\beta$  (**D**). **E** Representative Western blot of phosphorylated I $\kappa$ B $\alpha$  and p65 after vehicle and SAFit2 treatment. **F, G** Quantification of phosphorylated I $\kappa$ B $\alpha$  (**F**) and phosphorylated p65 (**G**) levels in DRGs and spinal cord. The data represent the mean  $\pm$  SEM of 3–5 Western blots measured with the tissue pooled from 5 mice per group. \* $p < 0.05$  Student's t-test with Welch's correction. SNI spared nerve injury, DRGs dorsal root ganglia, SC spinal cord, SAFit2 selective antagonist of FKBP51 by induced fit 2, I $\kappa$ B $\alpha$  NF- $\kappa$ B inhibitor alpha, IKK $\beta$  I $\kappa$ B kinase beta





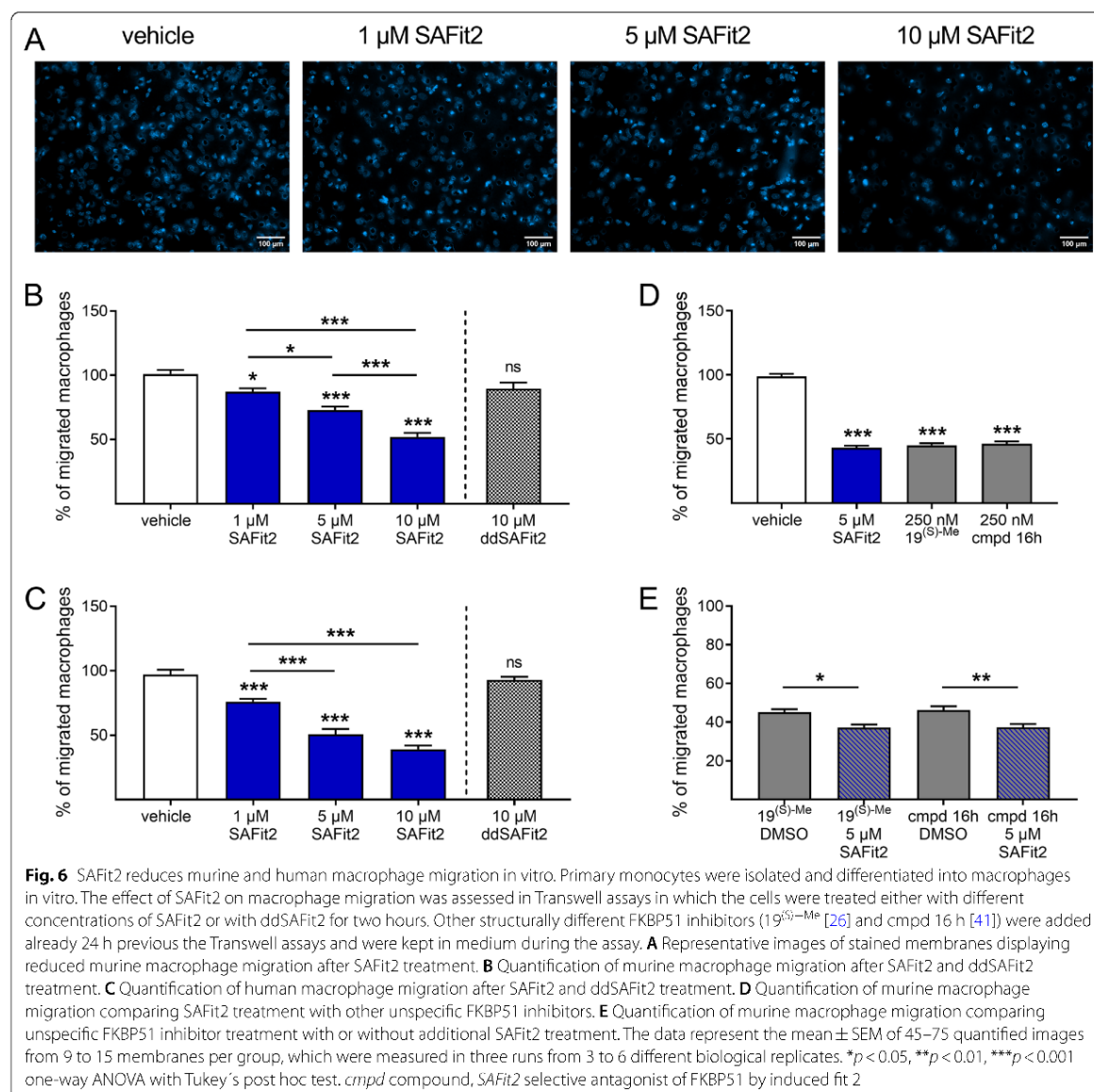
#### SAFit2 causes a calcineurin-dependent desensitization of the TRPV1 channel in sensory neurons which reduces the secretion of CGRP

We observed a beneficial role of SAFit2 in nerve injury-induced neuroinflammation. Neuroinflammation is on the one hand mediated by immune cells, but also on the other by an increased activity of sensory neurons and the subsequent release of pro-inflammatory mediators [6, 7]. We therefore hypothesized that SAFit2 may also have an effect on the activity of sensory neurons and subsequently on the downstream signaling that may involve processes which initiate neuroinflammation. More specifically, sensory neurons express ion channels such as the transient receptor potential cation channel

subfamily V member 1 (TRPV1) which plays an important role in the development of neuropathic pain. States of hypersensitivity, as in the SNI experiments, can be associated with TRPV1 modulation. To test whether SAFit2 alters the activity of TRPV1, we dissected DRGs from naïve mice and measured the TRPV1 activity via calcium imaging.

For examining the impact of SAFit2 on TRPV1-mediated calcium flux, we established a protocol in which we stimulated TRPV1 twice: at first with capsaicin alone and second after a preincubation with SAFit2 to determine whether SAFit2 alters the channel-mediated calcium influx. The effect of the compound was verified by comparing the calcium fluxes of both stimuli.





Indeed, SAFit2 treatment concentration dependently reduced the second capsaicin induced calcium influx, at 5 μM to less than half of the vehicle response (Fig. 7A, B). In contrast, the chiral analogue ddSAFit2 did not affect the capsaicin induced calcium influx (Fig. 7C, D).

To further investigate this effect of SAFit2, we performed additional control calcium imaging experiments with FKBP inhibitors from a different chemical series to verify whether this effect is FKBP dependent (Fig. 7E, F). However, none of the structurally unrelated FKBP inhibitors was capable of reducing the TRPV1

channel-mediated calcium fluxes (Fig. 7F). Since the structurally unrelated FKBP inhibitors were shown to potentially occupy FKBP51 in human cells [16], we concluded that SAFit2 reduces the activity of TRPV1 in an FKBP51-independent manner.

As the TRPA1 channel is closely related to the TRPV1 channel and co-expressed in a subset of TRPV1 expressing neurons, we also examined the influence of SAFit2 on the TRPA1 channel. However, we did not observe any effect of SAFit2 on the activity of the TRPA1 channel (Additional file 1: Fig. S5).

To examine the impact of SAFit2 on the downstream signaling of TRPV1, we performed a calcitonin gene-related peptide (CGRP) assay. CGRP is a neuropeptide that is released from sensory neurons upon increasing intracellular calcium concentrations and is involved in pain mediation (Fig. 7G). Furthermore, the activation of its receptors can cause vasodilation and neurogenic inflammation [3, 15, 56]. Interestingly, we detected that SAFit2 reduces the CGRP concentrations in the supernatant of capsaicin-treated sensory neurons when they were co-treated with SAFit2 during stimulation (Fig. 7H). Based on these results, we conclude that the influence of SAFit2 on the TRPV1 channel activity also affects the downstream signaling events such as the secretion of CGRP.

Next, we wanted to determine whether SAFit2 antagonizes the TRPV1 directly. This might be problematic since TRPV1 antagonists led to severe side effects when they were tested in human volunteers [59]. Therefore, we assessed the influence of SAFit2 in a heterologous expression system using calcium imaging on TRPV1 transfected HEK-293t cells. There was no indication for TRPV1 inhibition over the large concentration range of 0.15 to 15  $\mu\text{M}$  SAFit2 (Additional file 1: Fig. S6). In addition, we analyzed specifically whether SAFit2 has a direct impact on the channel activity of TRPV1 using whole-cell patch-clamp recordings. In these measurements, we demonstrated that 5  $\mu\text{M}$  SAFit2 alone does not alter the amplitude of capsaicin-activated TRPV1 currents or the kinetics of the channel when added either to the intracellular or extracellular solution (Additional file 1: Fig. S7), ruling out a direct effect of SAFit2 on TRPV1 activity. In summary, SAFit2 does not inhibit the TRPV1 channel but desensitizes TRPV1 by affecting another factor that changes TRPV1 activity in sensory neurons.

As a next step, we tried to examine how the desensitization of TRPV1 is mediated. Since the TRPV1 channel's open probability is also strongly affected by phosphorylation [34], we suggested that SAFit2 probably has an impact on the most relevant phosphatase in sensory neurons which is the protein phosphatase 3 (PP3/calcineurin). Based on this, we hypothesized that SAFit2 enhances the calcineurin-mediated dephosphorylation

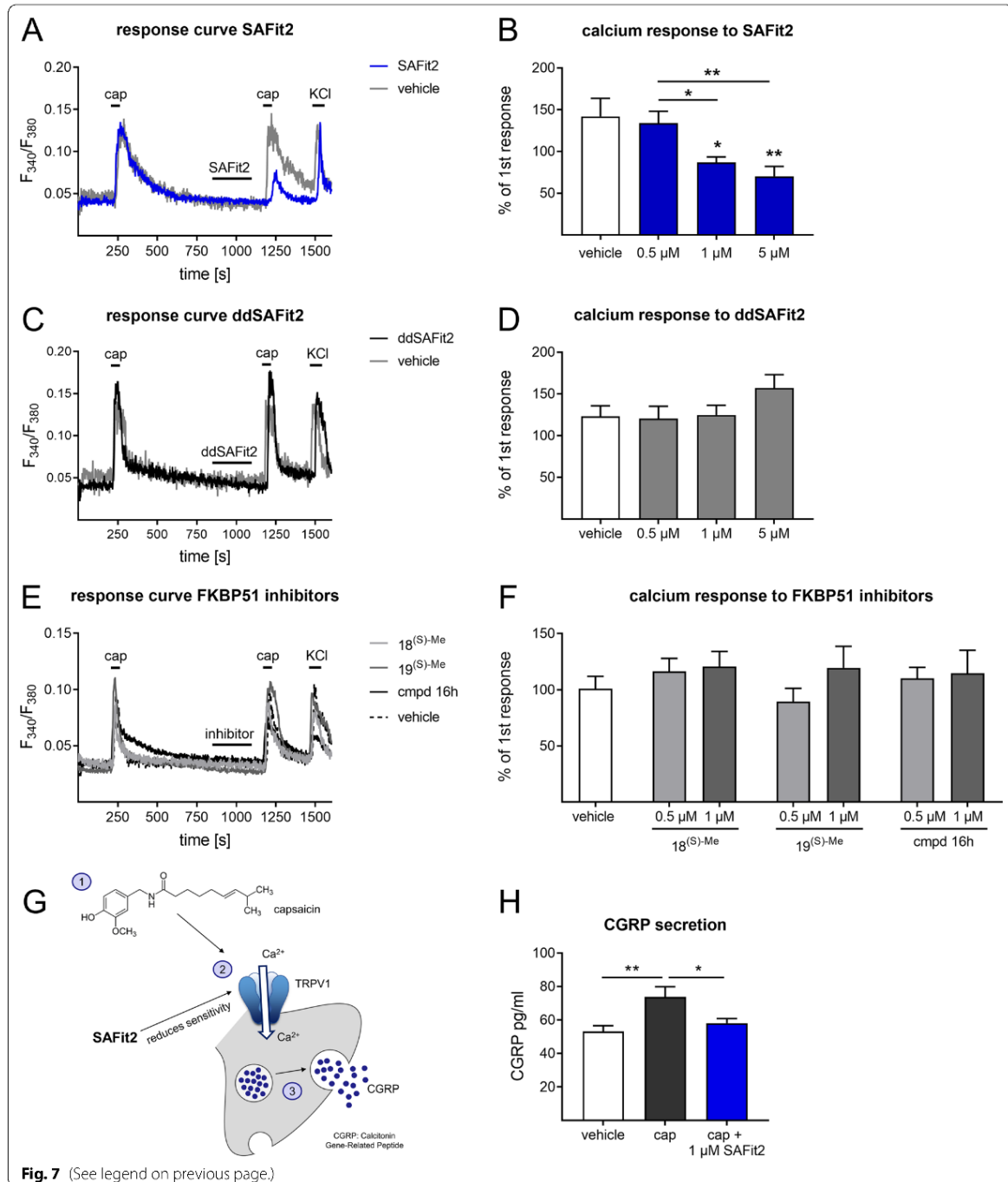
of TRPV1 which further leads to a reduced open probability and a reduced calcium influx. To investigate the effect of SAFit2 on calcineurin, we performed calcium imaging with sensory neurons in which we inhibited calcineurin with cyclosporine while treating the cells with SAFit2 (Fig. 8A). Interestingly, we detected that an additional cyclosporine treatment restored calcium flux to vehicle level (Fig. 8B), indicating that SAFit2 may have an effect on the phosphatase activity of calcineurin. Finally, we explored this effect in a calcineurin activation assay in which we measured the phosphate release by calcineurin in the presence of different SAFit2 concentrations. Indeed, we observed an increased phosphate release by calcineurin with increasing SAFit2 concentrations (Fig. 8D). In contrast, the inactive analogue ddSAFit2 as well as structurally unrelated FKBP inhibitor did not enhance the phosphate release by calcineurin (Fig. 8D). Based on these results, we assumed that SAFit2 desensitizes the TRPV1 channel in a calcineurin-dependent manner, which is not mediated by FKBP51, and thereby is probably capable to counteract the increased activity of sensory neurons in neuroinflammation.

## Discussion

SAFit2 has previously been shown to pass the blood-brain barrier [13]. Based on these results, it is quite likely that SAFit2 can also pass the blood spinal cord barrier and may partly mediate its analgesic effect in the central nervous system. As depicted in Fig. 9, we detected that SAFit2 reduces nerve injury-induced mechanical hypersensitivity *in vivo* by reducing neuroinflammation in neuronal tissue after SNI. On the one hand, SAFit2 has a direct effect on sensory neurons, particularly on the pain-mediating TRPV1 channel, on the other hand it reduces inflammatory processes. Thereby, SAFit2 diminishes enhanced neuronal activity and excessive neuroinflammation that can lead to central sensitization and to enhanced mechanical hypersensitivity. In detail, we showed that SAFit2 enhances the activity of the most relevant phosphatase in sensory neurons which is calcineurin. As a consequence, the phosphorylation state of the pain-mediating TRPV1 channel is decreased, and its open probability reduced. This in turn decreases the

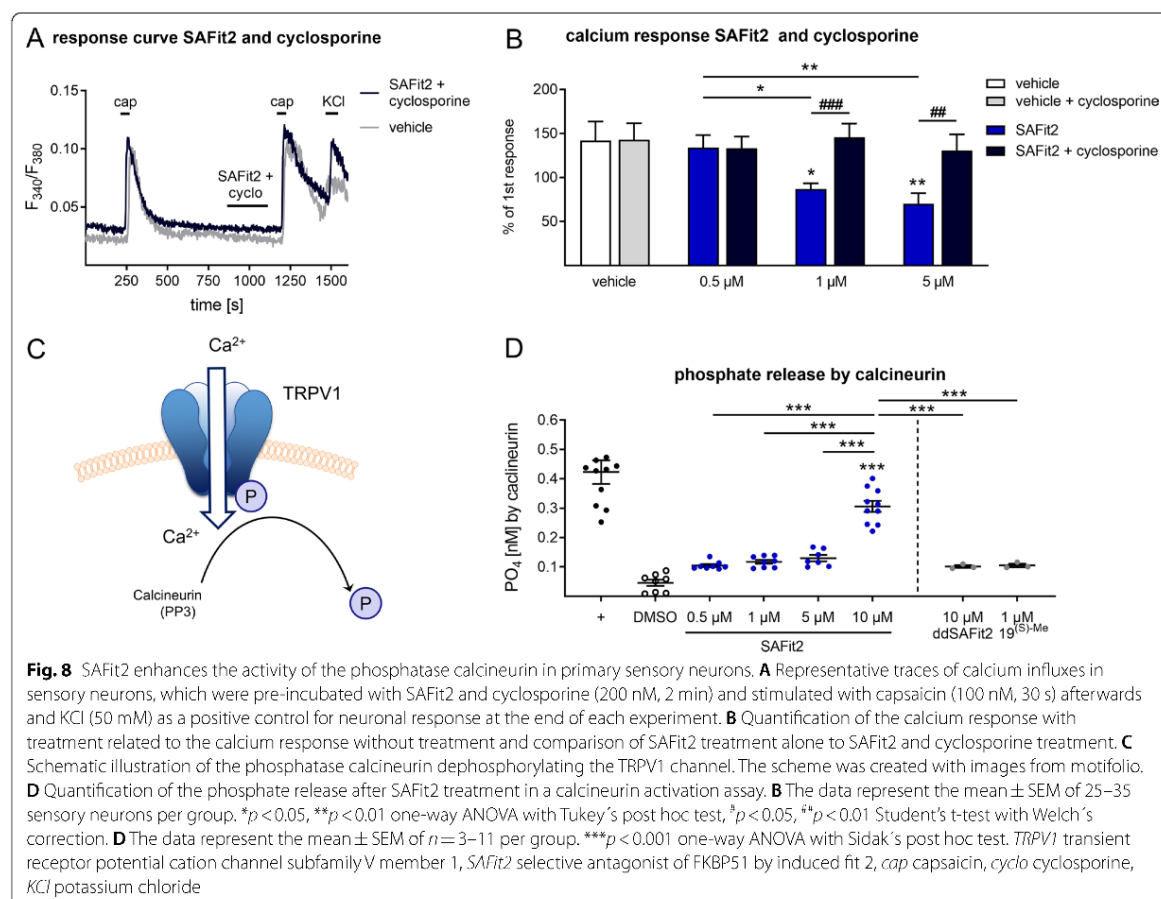
(See figure on next page.)

**Fig. 7** SAFit2 desensitizes the TRPV1 channel and reduces the CGRP secretion in primary sensory neurons. Primary sensory neurons were isolated from mice and the effect of SAFit2 on the TRPV1 channel activity was assessed in calcium imaging experiments. **A, C, E** Representative traces of calcium influxes in sensory neurons, which were pre-incubated with 5  $\mu\text{M}$  SAFit2 (**A**), 1  $\mu\text{M}$  ddSAFit2 (**C**) or 1  $\mu\text{M}$  structurally unrelated FKBP inhibitors (**E**) for 2 min and stimulated with capsaicin (100 nM, 30 s) afterwards and KCl (50 mM) as a positive control for neuronal response at the end of each experiment. **B, D, F** Quantification of the treated calcium response related to the untreated calcium response. **G** Schematic illustration of the release of CGRP from sensory neurons after capsaicin treatment. The scheme was created with images from motifolio. **H** Quantification of the amount of CGRP in the supernatant of treated DRG cultures. **B, D, F** The data represent the mean  $\pm$  SEM of 25–49 sensory neurons per group. **H** The data represent the mean  $\pm$  SEM of  $n = 4–5$  per group \* $p < 0.05$ , \*\* $p < 0.01$ , one-way ANOVA with Tukey's post hoc test. TRPV1 transient receptor potential cation channel subfamily V member 1, CGRP calcitonin gene-related peptide, SAFit2: selective antagonist of FKBP51 by induced fit 2, *cap* capsaicin, KCl potassium chloride



calcium influx and subsequently the transmitter release, including the release of the pro-inflammatory neuropeptide CGRP, leading to a reduction of exacerbated pain transmission (Fig. 9).

Moreover, we observed that SAFit2 ameliorates neuroinflammation in nerve-injured mice by reducing the infiltration of immune cells into neuronal tissue without affecting the inflammation resolution at the site of



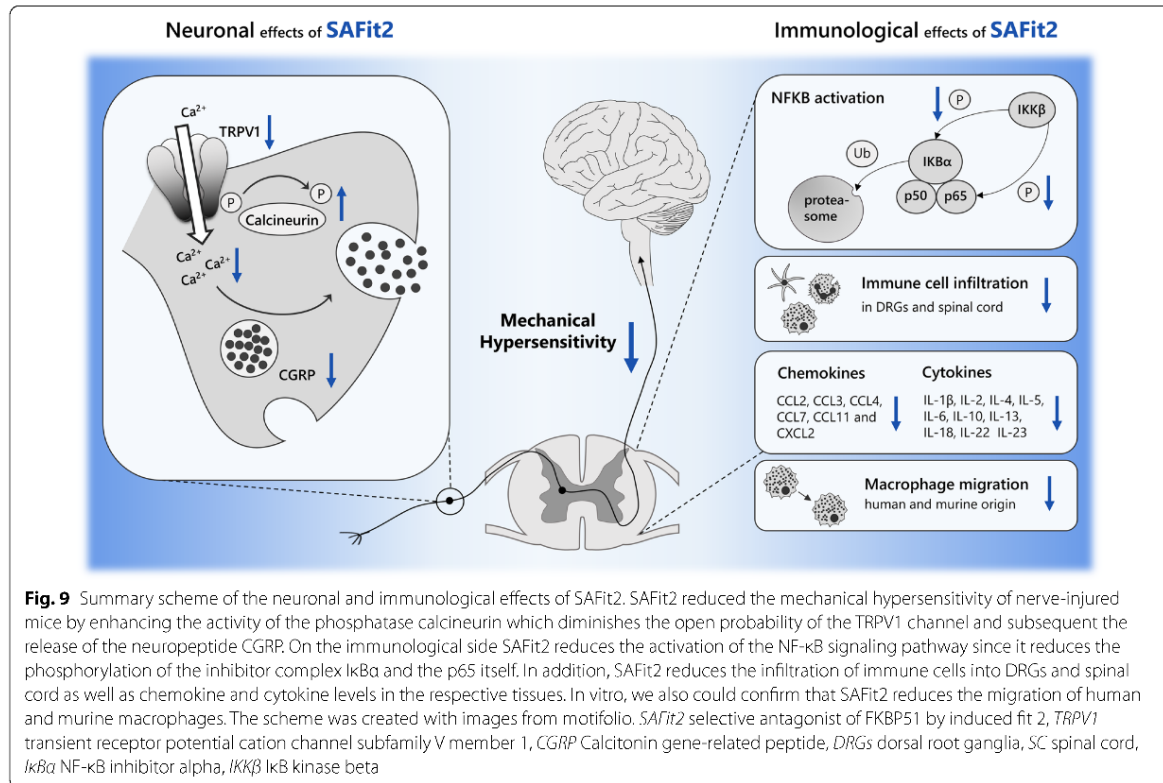
injury. This effect was further confirmed by the reduction of murine and human macrophage migration in vitro, pointing out translational potential to the human disease state. In addition, we detected that SAFit2 reduces the activation of the NF- $\kappa$ B signaling pathway. Both effects of SAFit2 reduced cytokine and chemokine levels in DRGs and spinal cord that contribute to neurogenic inflammation and pain transmission. In summary, SAFit2 reduces neuroinflammation and ameliorates nerve injury-induced mechanical hypersensitivity (Fig. 9).

Interestingly, we observed that SAFit2 showed its anti-hyperalgesic effects after the treatment phase. We therefore assume that SAFit2 interferes rather in the maintenance of neuropathic pain than in its onset, and that it takes a certain time until its cellular and molecular effects are reflected in behavioral changes.

This raises the question whether SAFit2 may serve as preventative or protective therapy for nerve injury-induced neuropathic pain. Mechanistically, we would argue that SAFit2 is a treatment option after injury rather

than a protective/preventative therapeutic, because for the observed effects of SAFit2 (reduction of nociceptive input and reduction of immune cell migration and mediator secretion) a previous injury is required for their initiation. It seems that SAFit2 reduces these effects, but does not completely stop them. Therefore, we presume that SAFit2 can reduce these injury-related effects but might not be able to prevent them. However, this is speculation and should be addressed by future studies.

Neuroinflammation comprises the activation of resident immune cells, such as microglia and astrocytes, as well as migration of neutrophils, macrophages and T cells. Moreover, the secretion of pro-inflammatory mediators is a hallmark of neuroinflammation. These mediators can be cytokines, chemokines and growth factors and lead to central sensitization and an increased activity of peripheral sensory neurons, attributing these mechanisms an essential role in the onset and maintenance of neuropathic pain [21]. In this study, we detected that SAFit2 treatment can reduce the number of immune



cells in the peripheral nervous system and at the interface between the peripheral and central nervous system. Likewise, the concentrations of pro-inflammatory and proalgesic mediators is reduced in the respective tissues compared to tissues from vehicle-treated mice. SAFit2 treatment also caused a reduction of anti-inflammatory cytokines (IL-4, IL-5, IL-13, IL-22) in DRGs and the spinal cord. These anti-inflammatory cytokines are mainly produced by T helper cells, such as Th2 and Th17 cells [10]. Although we did not directly measure the amount of Th cells by FACS, we see reduced amounts of other T cell species especially in the DRGs following SAFit2 treatment (Treg, Tm, Tγδ). Based on these data, we presume that T-cell migration to the DRGs is reduced after SAFit2 treatment, including Th2 and Th17 cells which leads to the observed decrease of IL-4, IL-5, IL-13 and IL-22 concentrations. According to our observations, this is mediated by a reduced activation of the NF-κB signaling pathway in SAFit2-treated mice. The interaction between FKBP51 and the NF-κB pathway has previously been suggested in the context of steroid-refractory inflammation and cancer biology [24, 45] which is in line with our observations. In more detail, we mainly see strong influences of SAFit2 treatment on the phosphorylation state

of p65 and IκBα, which are both central components of the NF-κB pathway.

We started the SAFit2 treatment 5 days after the SNI surgery, a time point when glial cell activation and neuroinflammation have already been initiated [53]. This might be the reason why the mechanical hypersensitivity of the SNI-treated animals is not completely restored to baseline levels and can explain why we still observe immune cells in DRGs and spinal cord, although significantly lower in the DRGs of SAFit2-treated animals. In addition, the difference of immune cell quantity is particularly strong between DRGs from vehicle and SAFit2-treated animals. We also observe a strong reduction of dendritic cells in DRG tissue after SAFit2 treatment. Recently, it was shown that dendritic cells release chemokines which cause an increased activity of peripheral sensory neurons via the activation of the C-C chemokine receptor 4 [48]. This is in line with our observation that SAFit2-treated animals show fewer dendritic cells and reduced levels of proalgesic mediators in DRGs.

In the spinal cord, the total number of immune cells is similar in SAFit2 and vehicle-treated mice, probably because the activated microglia and astrocytes in the spinal cord are resident immune cells, whereas infiltration

of migrating immune cells occurs much stronger in the DRGs during persistent pain [42, 62]. However, we detected less eosinophils infiltrating into the spinal cord after SAFit2 treatment. Eosinophils are well known to induce several diseases like eosinophilia, eosinophilic vasculitis and many others when they are infiltrating into tissues [5, 35, 55]. Moreover, these cells were also associated with peripheral neuropathy and have been attributed effects on sensory nerve branching [36].

Apart from the immune cell component, neuroinflammation can also be initiated by increased neuronal activity and the subsequent release of neuropeptides, such as calcitonin gene-related peptide (CGRP) which serves as chemoattractant for immune cells [6, 7]. While most anti-inflammatory agents can target the immune cell component of neuroinflammation, they are generally not capable of addressing the neuronal component. However, we observed that SAFit2 causes a desensitization of the neuronal TRPV1 channel that seems to be mediated by a calcineurin-dependent dephosphorylation.

While TRPV1 represents an interesting target in persistent pain, its complex regulatory functions and its requirement for normal maintenance of the body temperature has made it difficult to target and even more than 20 years after its initial discovery, there is still no TRPV1 antagonist available for clinical use [23, 25, 59]. It may thus be more promising to keep TRPV1 activity in the physiological range and reduce its sensitization that occurs in pathophysiological pain states. In this regard, the desensitizing effect of SAFit2 could be an additional beneficial effect of the compound to ameliorate persistent pain. Subsequently, the release of the neuropeptide CGRP triggered by an enhanced TRPV1 channel activation can also be diminished by SAFit2 in cultured sensory neurons, which shows that SAFit2 can reduce neuroinflammation both at the immune cell level, but also at the level of sensory neurons and neuropeptide release.

A limitation of this study is the lack of female mice in the behavioral assays. Previously, it was reported that sex differences occur in development and maintenance of neuropathic pain in vivo [33, 51]. Although the contribution of FKBP51 to neuropathic pain has been found to be sex independent [30], it is conceivable that the effects of SAFit2 during neuropathic pain and in neuroinflammation differ between male and female mice.

Besides the influences of the drug target FKBP51 in the peripheral nervous system, it was previously also revealed as a target for central nervous system (CNS) indications and psychological disorders [46]. In particular, a strong genetic association was validated for FKBP51 in stress-related and endocrinologic mediated diseases as depression, type two diabetes and obesity [46]. Moreover, inhibiting FKBP51 recently revealed an

improvement of anxiety related [18] as well as of stress-related disorders [40].

In the context of chronic pain, the target FKBP51 was already shown to be upregulated in spinal cord and DRGs, whereas the knockout of FKBP51 was shown to relieve pain in a chronic ankle joint inflammation model [31]. Moreover, the knockdown of FKBP51 was also shown to ameliorate neuropathic pain after chronic constriction injury [61], revealing FKBP51 as a promising therapeutically target for a broad range of disorders ranging from psychological disorders to chronic pain. However, the development of a possible drug candidate was hampered in the past, due to the lack of a specific and potent FKBP51 inhibitor, highlighting SAFit2 as a novel and promising treatment option for neuropathic pain.

#### Abbreviations

BMDM: Bone marrow-derived macrophages; CCL: C-C motif ligand; CGRP: Calcitonin gene-related peptide; CXCL: C-X-C motif ligand; DRGs: Dorsal root ganglia; FKBP51: FK506-binding protein 51; I $\kappa$ B $\alpha$ : NF- $\kappa$ B inhibitor alpha; IKK $\beta$ : IKK $\beta$  kinase beta; IL: Interleukin; SAFit2: Selective antagonist of FKBP51 by induced fit; SC: Spinal cord; SNI: Spared nerve injury; TRP: Transient receptor potential; TRPV1: Transient receptor potential cation channel subfamily V member 1.

#### Supplementary Information

The online version contains supplementary material available at <https://doi.org/10.1186/s12974-022-02615-7>.

**Additional file 1: Figure S1.** Gene expression of neuronal stress and oxidative stress markers in lumbar DRGs and spinal cord of SAFit2 treated mice 21 days after SNI. **Figure S2.** Cytokine and chemokine levels in lumbar DRGs and spinal cord of SAFit2 treated SNI mice after 21 days. **Figure S3.** Synthesis of ddSAFit2 and competitive fluorescence assay (IPA) of SAFit2 and ddSAFit2. **Figure S4.** Cytotoxic and metabolic influence of SAFit2 on primary bone marrow derived macrophages. **Figure S5.** SAFit2 has no impact on the TRPA1 activity in primary sensory neurons. **Figure S6.** SAFit2 has no direct impact on the human hTRPV1 channel in HEK-293T cells. **Figure S7.** Extracellularly or intracellularly administered SAFit2 has no effect on the amplitude and kinetics of capsaicin activated TRPV1 currents in HEK-293 cells. **Figure S8.** Uncropped Western Blot images for NF- $\kappa$ B signaling pathway.

#### Acknowledgements

We thank Michael Bauder for preliminary synthetic work on ddSAFit2 and Wisely Oki Sugiarto for affinity measurements.

#### Author contributions

SW, OR, DF, MF, AW, NdB, GG, FH and MS designed the experiments. SW, PM, OR, CC, TH and DF performed the experiments. SW, OR, CC, DF, AW, NdB and MS analyzed the data. SW and MS wrote the manuscript. All authors reviewed and edited the manuscript. All authors read and approved the final manuscript.

#### Funding

Open Access funding enabled and organized by Projekt DEAL. This work was supported by grants 51 laValP of the Federal German Ministry of Education and Research (BMBWF) and SFB1039 A09 and Z01 of the Deutsche Forschungsgemeinschaft (German Research Foundation). It was also supported by the Fraunhofer Foundation Project: Neuropathic Pain as well as the Fraunhofer Cluster of Excellence for Immune Mediated Diseases (CMD). Additional

funding was received by the European Research Council (ERC; 2015 Advanced Grant 495 (AdG) n. 6950/8 noMAGIC).

#### Availability of data and materials

All data generated or analyzed during this study are included in this published article and its supplementary information files.

#### Declarations

##### Ethics approval and consent to participate

All experiments involving animals were approved by the local Ethics Committee for Animal Research (Darmstadt) under the permit number T152/1021. Furthermore, all animal experiments were performed according to the recommendations of the Preclinical Pain Research Consortium for Investigating Safety and Efficacy (PPRECISE) Working Group [1], according to the updated ARRIVE guidelines for reporting animal research [38] and guidelines as defined by European Quality In Preclinical Data (EQIPD) [4]. All efforts were made to minimize animal suffering.

##### Consent for publication

Not applicable.

##### Competing interests

The authors declare that they have no competing interests.

##### Author details

<sup>1</sup>Institute of Clinical Pharmacology, Pharmazentrum Frankfurt/ZAFES, University Hospital, Goethe-University, 60590 Frankfurt am Main, Germany. <sup>2</sup>Institute of Biochemistry I, Faculty of Medicine, Goethe-University Frankfurt, 60590 Frankfurt am Main, Germany. <sup>3</sup>Membrane Biophysics, Department of Biology, Technical University of Darmstadt, 64287 Darmstadt, Germany. <sup>4</sup>Department of Chemistry, Technical University of Darmstadt, 64287 Darmstadt, Germany. <sup>5</sup>Center of Physiology and Pharmacology, Medical University of Vienna, 1090 Vienna, Austria. <sup>6</sup>Fraunhofer Institute for Translational Medicine and Pharmacology ITPP and Fraunhofer Cluster of Excellence for Immune Mediated Diseases CIMD, 60596 Frankfurt am Main, Germany.

Received: 11 August 2022 Accepted: 4 October 2022

Published online: 10 October 2022

#### References

- Andrews NA, Latremoliere A, Basbaum AI, Mogil JS, Porreca F, Rice ASC, Woolf CJ, Currie GL, Dworkin RH, Fisenach JC, Evans S, Gewandter JS, Gover TD, Handwerker H, Huang W, Iyengar S, Jensen MP, Kennedy JD, Lee N, Levine J, Lidster K, Machin I, McDermott MP, McMahon SB, Price TJ, Ross SE, Scherrer G, Seal RP, Sena ES, Silva E, Stone L, Svensson CI, Turk DC, Whiteside G. Ensuring transparency and minimization of methodologic bias in preclinical pain research: PPRECISE considerations. *Pain*. 2016;157:901–9.
- Bauder M, Meyners C, Purder PL, Merz S, Sugiarto WO, Voll AM, Heymann T, Hausch F. Structure-based design of high-affinity macrocyclic FKBP51 inhibitors. *J Med Chem*. 2021;64:3320–49.
- Benarroch EE. CGRP: sensory neuropeptide with multiple neurologic implications. *Neurology*. 2011;77:281–7.
- Bespalov A, Bernard B, Gillis A, Gerlach B, Guillen J, Castagne V, Iefevre IA, Ducrey F, Monk L, Bongiovanni S, Altevogt B, Arroyo-Araujo M, Bikovski L, de Bruin N, Castanos-Velez E, Dityatev A, Emmerich CH, Fares R, Ferland-Beckham C, Froger-Colleaux C, Gailus-Durner V, Holter SM, Hofmann MC, Kabitzke P, Kas MJ, Kurreck C, Moser P, Pietraszek M, Popik P, Potschka H, et al. Introduction to the FOIPD quality system. *Flife*. 2021. <https://doi.org/10.554/ei.fc.63294>.
- Chao C-C, Hsieh S-T, Shun S-T. Skin Denervation and Cutaneous Vasculitis in Eosinophilia-Associated Neuropathy. *Arch Neurol*. 2007. <https://doi.org/10.1001/archneur.64.7.959>.
- Chiu IM, Heesters BA, Ghasemlou N, von Hehn CA, Zhao F, Tran J, Wainger B, Strominger A, Muralidharan S, Iorwill AR, Wardenburg JB, Ilwag SW, Carroll MC, Woolf CJ. Bacteria activate sensory neurons that modulate pain and inflammation. *Nature*. 2013. <https://doi.org/10.1038/nature12479>.
- Chu C, Artis D, Chiu IM. Neuro-immune interactions in the tissues. *Immunity*. 2020;52:464–74.
- Colloca L, Ludman T, Bouhassira D, Baron R, Dickenson AH, Yarnitsky D, Freeman R, Truini A, Aital N, Finnerup NB, Eccleston C, Kalso E, Bennett DL, Dworkin RH, Raja SN. Neuropathic pain. *Nat Rev Dis Primers*. 2017;3:17002.
- Decosterd I, Woolf CJ. Spared nerve injury: an animal model of persistent peripheral neuropathic pain. *Pain*. 2000. [https://doi.org/10.1016/S0304-3959\(00\)00276-1](https://doi.org/10.1016/S0304-3959(00)00276-1).
- Dong C. Cytokine regulation and function in T cells. *Annu Rev Immunol*. 2021;39:51–76.
- Ellis A, Bennett DL. Neuroinflammation and the generation of neuropathic pain. *Br J Anaesth*. 2013;111:26–37.
- Finnerup NB, Attal N, Haroutounian S, McNicol E, Baron R, Dworkin RH, Gilron I, Haanpää M, Hansson P, Jensen TS, Kamerman PR, Lund K, Moore A, Raja SN, Rice ASC, Rowbotham M, Sena F, Siddall P, Smith BH, Wallace M. Pharmacotherapy for neuropathic pain in adults: a systematic review and meta-analysis. *The Lancet Neurology*. 2015;14:162–73.
- Gaali S, Kirschner A, Cuboni S, Hartmann J, Kozary C, Balsevich G, Namendorf C, Fernandez-Vizcarra P, Sippel C, Zannas AS, Draenert R, Binder EB, Almeida OF, Ruhter G, Uhr M, Schmidt MV, Touma C, Bracher A, Hausch F. Selective inhibitors of the FK506-binding protein 51 by induced fit. *Nat Chem Biol*. 2015;11:33–7.
- Gabani BB, Sulochana SP, Siddesh AHA, Kiran V, Saini NK, Samanta SK, Hallur MS, Rajagopal S, Mullangi R. Validated LC-MS/MS method for simultaneous quantitation of SAIT-1 and SAIT-2 in mice plasma: application to a pharmacokinetic study. *Drug Res (Stuttg)*. 2020;70:325–32.
- Geppetti P, Capone JG, Irevisani M, Nicoletti P, Zagli G, Iola MR. CGRP and migraine: neurogenic inflammation revisited. *J Headache Pain*. 2005;6:61–70.
- Gnatzy MT, Geiger TM, Kuehn A, Gutfreund N, Walz M, Kolos JM, Hausch F. Development of NanoBRET binding assays for FKBP ligand profiling in living cells. *ChemBioChem*. 2021;22:2257–61.
- Hähle A, Merz S, Meyners C, Hausch F. The many faces of FKBP51. *Biomolecules*. 2019. <https://doi.org/10.3390/biom9010035>.
- Hartmann J, Wagner KV, Gaali S, Kirschner A, Kozary C, Ruhter G, Dedic N, Hausl AS, Hocjmakers L, Westerholz S, Namendorf C, Gerlach T, Uhr M, Chen A, Deussing JM, Holsboer F, Hausch F, Schmidt MV. Pharmacological inhibition of the psychiatric risk factor FKBP51 has anxiolytic properties. *J Neurosci*. 2015;35:9007–16.
- Helbig G, Christopherson KW, Bhat-Nakshatri P, Kumar S, Kishimoto I, Miller KD, Broxmeyer IIC, Nakshatri I. NF- $\kappa$ B promotes breast cancer cell migration and metastasis by inducing the expression of the chemokine receptor CXCR4. *J Biol Chem*. 2003;278:21631–8.
- Jagtap PKA, Asami S, Sippel C, Kaila VRI, Hausch F, Sattler M. Selective inhibitors of FKBP51 employ conformational selection of dynamic invisible states. *Angew Chem Int Ed Engl*. 2019;58:9479–33.
- Ji RR, Nacklely A, Huh Y, Terrando N, Maixner W. Neuroinflammation and central sensitization in chronic and widespread pain. *Anesthesiology*. 2018. <https://doi.org/10.1097/ALN.0000000000002130>.
- Ji RR, Xu ZZ, Gao YJ. Emerging targets in neuroinflammation-driven chronic pain. *Nat Rev Drug Discov*. 2014;13:533–48.
- Julius D. TRP channels and pain. *Annu Rev Cell Dev Biol*. 2013;29:355–84.
- Kastle M, Kistler B, Lamla T, Bretschneider T, Lamb D, Nicklin P, Wyatt D. FKBP51 modulates steroid sensitivity and NF- $\kappa$ B signalling: a novel anti-inflammatory drug target. *Eur J Immunol*. 2018;48:1904–14.
- Koivisto AP, Belvisi MG, Gaudet R, Szallasi A. Advances in TRP channel drug discovery: from target validation to clinical studies. *Nat Rev Drug Discov*. 2021. <https://doi.org/10.1038/s41573-021-00268-4>.
- Kolos JM, Pomplun S, Jung S, Riess B, Purder PL, Voll AM, Merz S, Gnatzy M, Geiger TM, Quist-Lokken I, Jatzlau J, Knaus P, Holien I, Bracher A, Meyners C, Czodrowski P, Krewald V, Hausch F. Picomolar FKBP inhibitors enabled by a single water-displacing methyl group in bicyclic [4.3.1] azamides. *Chem Sci*. 2021;12:14758–65.
- Leung L, Cahill CM. TNF alpha and neuropathic pain—a review. *J Neuroinflammation*. 2010;7:27.
- Liu T, Zhang L, Joo D, Sun SC. NF- $\kappa$ B signaling in inflammation. *Signal Transduct Target Ther*. 2017. <https://doi.org/10.1038/sigtrans.2017.23>.

29. Livak KJ, Schmittgen TD. Analysis of relative gene expression data using real-time quantitative PCR and the  $2^{-\Delta\Delta CT}$  method. *Methods*. 2001;25:402–8.
30. Maiaru M, Morgan OB, Mao T, Breitsamer M, Bamber H, Pohlmann M, Schmidt MV, Winter G, Hausch F, Geranton SM. The stress regulator FKBP51: a novel and promising druggable target for the treatment of persistent pain states across sexes. *Pain*. 2018;159:1224–34.
31. Maiaru M, Tochiki KK, Cox MB, Annan LV, Bell CG, Feng X, Hausch F, Geranton SM. The stress regulator FKBP51 drives chronic pain by modulating spinal glucocorticoid signaling. *Sci Transl Med*. 2016;8:325ra19.
32. Mao S, Zhang D, Chen L, Ian J, Chu Y, Huang S, Zhou W, Qin H, Xia Q, Zhao Y, Li R, Qin S, Wei M. FKBP51 promotes invasion and migration by increasing the autophagic degradation of TIMP3 in clear cell renal cell carcinoma. *Cell Death Dis*. 2021;12:899.
33. Mogil JS. Qualitative sex differences in pain processing: emerging evidence of a biased literature. *Nat Rev Neurosci*. 2020;21:353–65.
34. Mohapatra DP, Nau C. Regulation of  $Ca^{2+}$ -dependent desensitization in the vanilloid receptor TRPV1 by calcineurin and cAMP-dependent protein kinase. *J Biol Chem*. 2005;280:13424–32.
35. Na SJ, Lee KO, Ko JH. Eosinophilic vasculitis of the spinal cord associated with Churg–Strauss syndrome. *J Neurol Sci*. 2010;295:107–9.
36. Nassenstein C, Krasteva-Christ G, Renz H. New aspects of neuroinflammation and neuroimmune crosstalk in the airways. *J Allergy Clin Immunol*. 2018;142:1415–22.
37. Olesch C, Brunn D, Aktay-Cetin O, Sirait-Fischer L, Pullamsetti SS, Grimming F, Seeger W, Brune B, Weigert A, Savai R. Picturing of the lung tumor cellular composition by multispectral flow cytometry. *Front Immunol*. 2022;13: 827719.
38. Percie du Sert N, Hurst V, Ahluwalia A, Alam S, Avey MT, Baker M, Browne WJ, Clark A, Cuthill IC, Dirnagl U, Emerson M, et al. The ARRIVE guidelines 2.0: Updated guidelines for reporting animal research. *PLoS Biol*. 18, e3000410.
39. Pires BR, Menclha AI, Ferreira GM, de Souza WF, Morgado-Diaz JA, Maia AM, Correa S, Abdolhay FS. NF- $\kappa$ B is involved in the regulation of EMT genes in breast cancer cells. *PLoS ONE*. 2017;12: e0169622.
40. Pohlmann M, Hausl AS, Harbich D, Balsevich G, Engelhardt C, Feng X, Breitsamer M, Hausch F, Winter G, Schmidt MV. Pharmacological modulation of the psychiatric risk factor FKBP51 alters efficiency of common antidepressant drugs. *Front Behav Neurosci*. 2018;12:262.
41. Pomplun S, Sippel C, Hahle A, Tay D, Shima K, Klages A, Unal CM, Riess B, Toh HT, Hansen G, Yoon HS, Bracher A, Preiser P, Rupp J, Steinert M, Hausch F. Chemogenomic profiling of human and microbial FK506-binding proteins. *J Med Chem*. 2018;61:3660–73.
42. Raouf R, Willemen IJLDM, Cijkkelkamp N. Divergent roles of immune cells and their mediators in pain. *Rheumatology*. 2018;57:429–40.
43. Raue R, Frank AC, Fuhrmann DC, De la Cruz-Ojeda P, Rosser S, Bauer R, Cardamone G, Weigert A, Syed SN, Schmid I, Brune B. MicroRNA-200c attenuates the tumor-infiltrating capacity of macrophages. *Biology (Basel)*. 2022. <https://doi.org/10.3390/biology11030349>.
44. Richner M, Bjerrum OJ, Nykjaer A, Vægter CB. The spared nerve injury (SNI) model of induced mechanical allodynia in mice. *J Vis Exp*. 2011. <https://doi.org/10.3791/3092>.
45. Romano S, Mallardo M, Romano MF. FKBP51 and the NF- $\kappa$ B regulatory pathway in cancer. *Curr Opin Pharmacol*. 2011;11:288–93.
46. Schmidt MV, Paez-Pereda M, Holsboer F, Hausch F. The prospect of FKBP51 as a drug target. *ChemMedChem*. 2012;7:1351–9.
47. Schmittgen TD, Livak KJ. Analyzing real-time PCR data by the comparative  $C_T$  method. *Nat Protoc*. 2008;3:1101–8.
48. Silva JR, Iltinca M, Fernandes Gomes FI, Segal JP, Smith OMA, Bannerman CA, Silva Mendes A, Defaye M, Robinson MLC, Gilron I, Cunha TM, Altier C, Ghasemlou N. Skin-resident dendritic cells mediate postoperative pain via CCR4 on sensory neurons. *Proc Natl Acad Sci U S A*. 2022. <https://doi.org/10.1073/pnas.2118238119>.
49. Sisignano M, Angioni C, Ferreiros N, Schuh CD, Suo J, Schreiber Y, Dawes JM, Antunes Martins A, Bennett DJ, McMahon SB, Geisslinger G, Scholich K. Synthesis of lipid mediators during UVB-induced inflammatory hyperalgesia in rats and mice. *PLoS ONE*. 2013;8: e81228.
50. Sisignano M, Lotsch J, Parnham MJ, Geisslinger G. Potential biomarkers for persistent and neuropathic pain therapy. *Pharmacol Ther*. 2019;199:16–29.
51. Sorge RF, Mapplebeck JC, Rosen S, Beggs S, Taves S, Alexander JK, Martin IJ, Austin JS, Sotocinal SG, Chen D, Yang M, Shi XQ, Huang H, Pillion NJ, Bilan PJ, Tu Y, Klip A, Ji RR, Zhang J, Salter MW, Mogil JS. Different immune cells mediate mechanical pain hypersensitivity in male and female mice. *Nat Neurosci*. 2015;18:1081–3.
52. Storer CL, Dickey CA, Galigniana MD, Rein T, Cox MB. FKBP51 and FKBP52 in signaling and disease. *Trends Endocrinol Metab*. 2011;22:481–90.
53. Suter MR, Wen YR, Decosterd I, Ji RR. Do glial cells control pain? *Neuron Glia Biol*. 2007;3:255–68.
54. Takaoka M, Ito S, Miki Y, Nakanishi A. FKBP51 regulates cell motility and invasion via RhoA signaling. *Cancer Sci*. 2017;108:380–9.
55. Vaglio A, Buzio C, Zwerina J. Eosinophilic granulomatosis with polyangiitis (Churg–Strauss): state of the art. *Allergy*. 2013;68:261–73.
56. Walsh DA, Mapp PJ, Kelly S. Calcitonin gene-related peptide in the joint: contributions to pain and inflammation. *Br J Clin Pharmacol*. 2015;80:965–78.
57. Wedel S, Osthuus T, Zimmer B, Angioni C, Geisslinger G, Sisignano M. Oxidized linoleic acid metabolites maintain mechanical and thermal hypersensitivity during sub-chronic inflammatory pain. *Biochem Pharmacol*. 2022;198: 114953.
58. Wesseldijk F, Huygen FJ, Heijmans-Antonissen C, Niehof SP, Zijlstra EJ. Six years follow-up of the levels of TNF-alpha and IL-6 in patients with complex regional pain syndrome type 1. *Mediators Inflamm*. 2008;2008: 469439.
59. Wong GY, Gavva NR. Therapeutic potential of vanilloid receptor TRPV1 agonists and antagonists as analgesics: Recent advances and setbacks. *Brain Res Rev*. 2009;60:267–77.
60. Woolf CJ, Salter MW. Neuronal plasticity: increasing the gain in pain. *Science*. 2000. <https://doi.org/10.1126/science.288.5472.1765>.
61. Yu HM, Wang Q, Sun WB. Silencing of FKBP51 alleviates the mechanical pain threshold, inhibits DRG inflammatory factors and pain mediators through the NF- $\kappa$ B signaling pathway. *Gene*. 2017;627:169–75.
62. Yu XB, Liu HJ, Hamel KA, Morvan MG, Yu S, Ieff J, Guan ZH, Braz JM, Basbaum AI. Dorsal root ganglion macrophages contribute to both the initiation and persistence of neuropathic pain. *Nat Commun*. 2020. <https://doi.org/10.1038/s41467-019-13839-2>.

## Publisher's Note

Springer Nature remains neutral with regard to jurisdictional claims in published maps and institutional affiliations.

Ready to submit your research? Choose BMC and benefit from:

- fast, convenient online submission
- thorough peer review by experienced researchers in your field
- rapid publication on acceptance
- support for research data, including large and complex data types
- gold Open Access which fosters wider collaboration and increased citations
- maximum visibility for your research: over 100M website views per year

At BMC, research is always in progress.

Learn more [biomedcentral.com/submissions](https://biomedcentral.com/submissions)





---

## 2.3 Supplemental file

### Additional file 1

#### **SAFit2 reduces neuroinflammation and ameliorates nerve injury-induced neuropathic pain**

Saskia Wedel<sup>1</sup>, Praveen Mathdoor<sup>2</sup>, Oliver Rauh<sup>3</sup>, Tim Heymann<sup>4</sup>, Cosmin I. Ciotu<sup>5</sup>, Dominik C. Fuhrmann<sup>2</sup>, Michael J. M. Fischer<sup>5</sup>, Andreas Weigert<sup>2</sup>, Natasja de Bruin<sup>5</sup>, Felix Hausch<sup>4</sup>, Gerd Geisslinger<sup>1,6</sup> and Marco Sisignano<sup>1,6\*</sup>

<sup>1</sup> Institute of Clinical Pharmacology, *pharmazentrum frankfurt/ZAFES*, University Hospital, Goethe-University, 60590 Frankfurt am Main, Germany

<sup>2</sup> Institute of Biochemistry I, Faculty of Medicine, Goethe-University Frankfurt, 60590 Frankfurt am Main, Germany

<sup>3</sup> Membrane Biophysics, Department of Biology, Technical University of Darmstadt, 64287 Darmstadt, Germany

<sup>4</sup> Department of Chemistry, Technical University of Darmstadt, 64287 Darmstadt, Germany

<sup>5</sup> Center of Physiology and Pharmacology, Medical University of Vienna, 1090 Vienna, Austria

<sup>6</sup> Fraunhofer Institute for Translational Medicine and Pharmacology ITMP and Fraunhofer Cluster of Excellence for Immune Mediated Diseases CIMD, 60596 Frankfurt am Main, Germany

Figures: 8

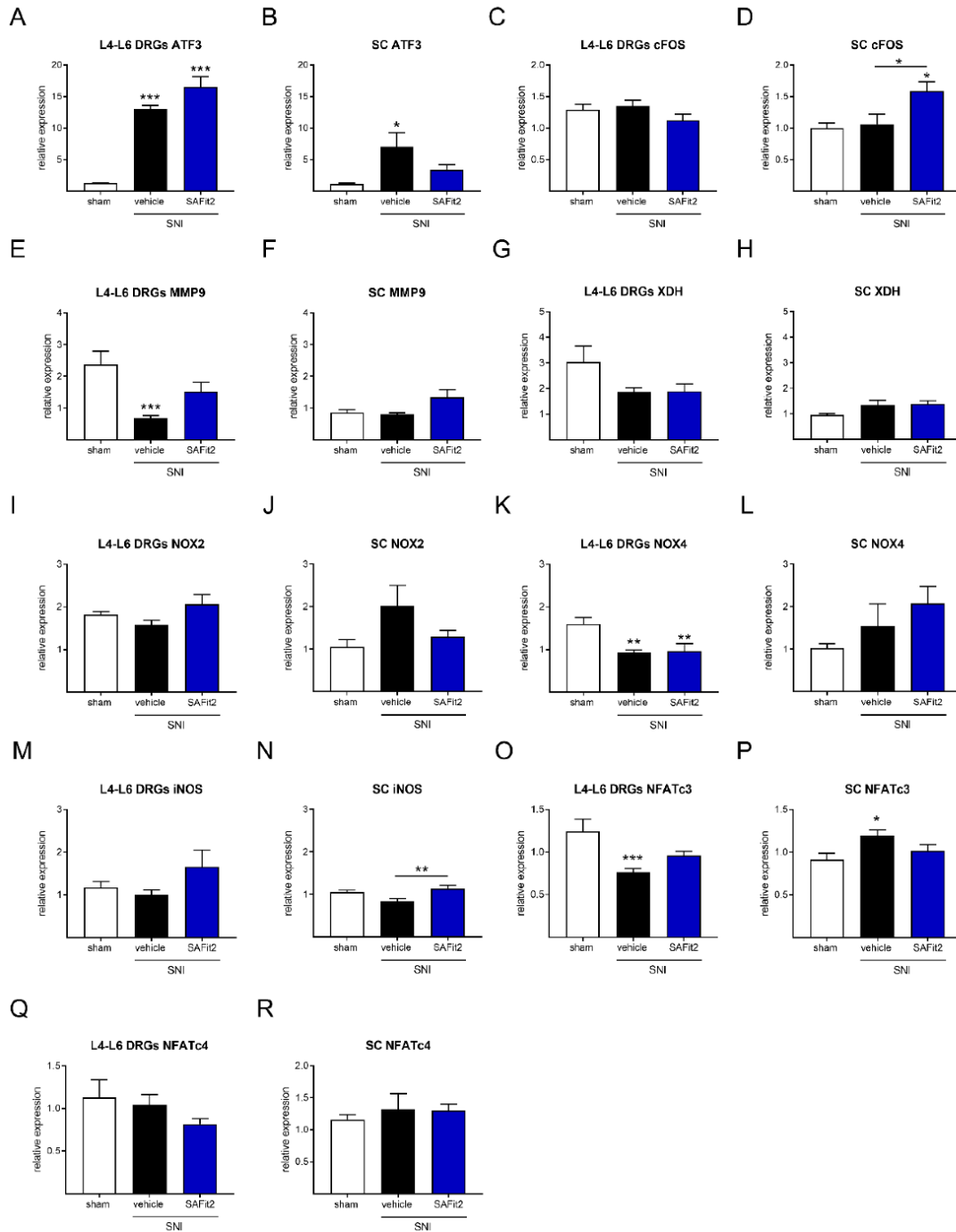


**Figure S1: Gene expression of neuronal stress and oxidative stress markers in lumbar DRGs and spinal cord of SAFit2 treated mice 21 days after SNI.** Mice underwent a SNI surgery and were then treated with either vehicle or 10 mg/kg SAFit2 from day five to ten after the surgery. After 21 days, the expression of neuronal stress

---

markers: ATF3 (A,B), cFOS (C,D), MMP9 (E,F), oxidative stress markers: XDH (G,H), NOX2 (I,J), NOX4 (K,L), iNOS (M,N) and NFAT subunits: NFATc3 and NFATc4 (O-R) was measured. The data represents the mean  $\pm$  SEM of 3-4 mice per group, measured in technical triplicates respectively. \*  $p < 0.05$ , \*\*  $p < 0.01$ , \*\*\*  $p < 0.001$  one-way ANOVA with Tukey's post hoc test. Abbreviations: SAFit2: selective antagonist of FKBP51 by induced fit 2, SNI: spared nerve injury, ATF3: activating transcription factor 3, MMP9: matrix metalloproteinase 9, XDH: xanthine dehydrogenase, NOX2/4: NADPH oxidase 2/4, iNOS: inducible nitric oxide synthase, NFAT: nuclear factor of activated T cells

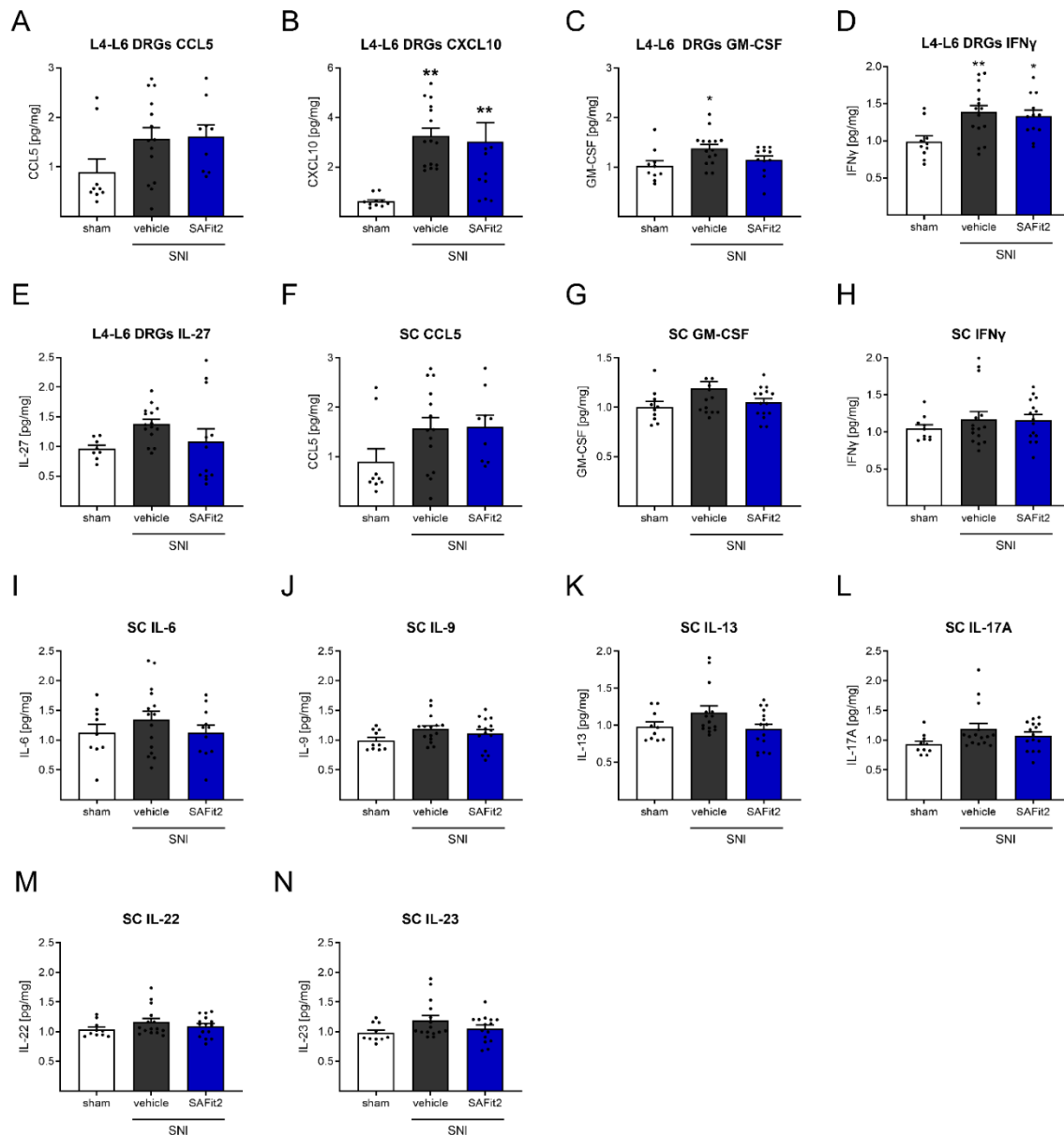
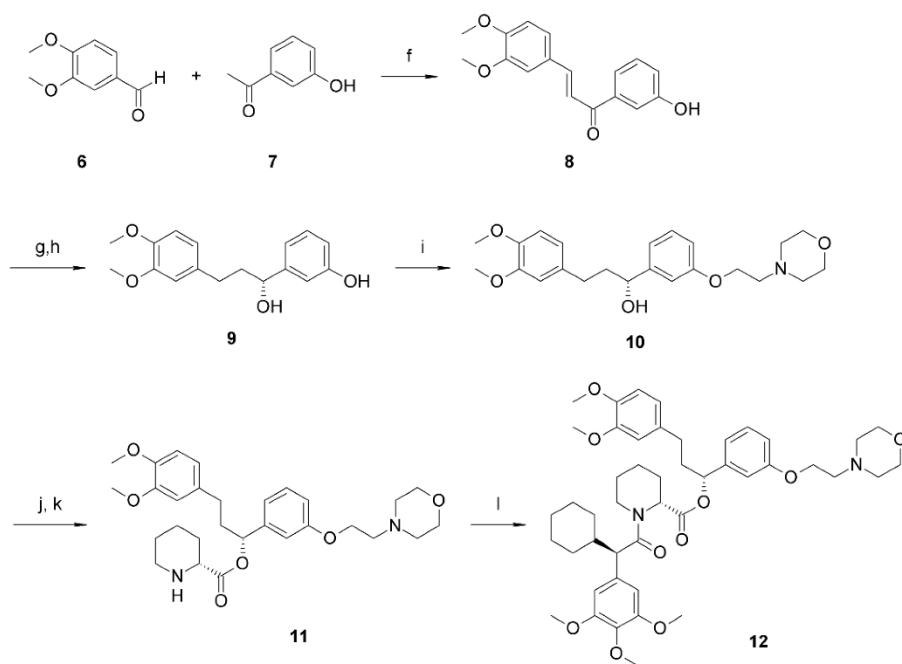
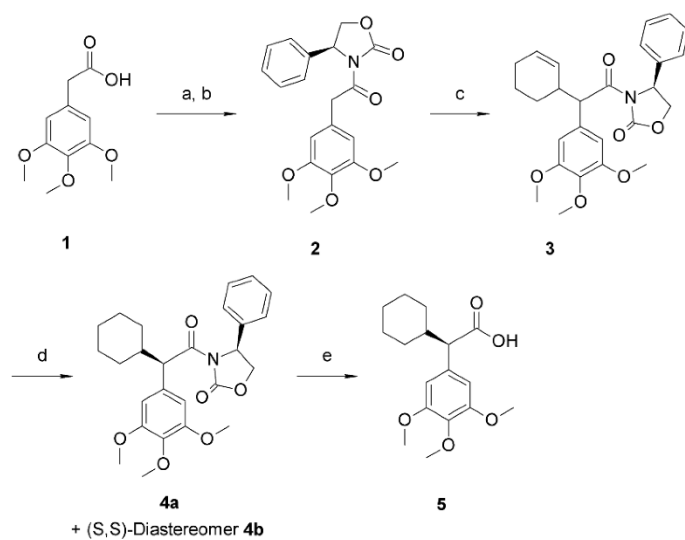


**Figure S2: Cytokine and chemokine levels in lumbar DRGs and spinal cord of SAFit2 treated SNI mice after 21 days.** Mice underwent SNI surgery and were then treated with either vehicle or 10 mg/kg SAFit2 from day five to ten after the surgery. After 21 days, L4-L6 DRGs and spinal cord were isolated from ipsilateral and contralateral sides with which lysates a multiplex immunoassay was performed including a panel of 26 cytokines and chemokines. Shown is a section of mediators measured in L4-L6 DRGs (**A-E**) and spinal cord (**F-N**) after SAFit2 treatment. The data

---

represents the mean  $\pm$  SEM from 5 mice per group, measured in technical triplicates respectively. The raw data was related to the total protein amount of the sample and the ipsilateral (injured) value was normalized to the contralateral (control) value per animal. \*  $p < 0.05$ , \*\*  $p < 0.01$ , \*\*\*  $p < 0.001$  one-way ANOVA with Tukey's post hoc test. Abbreviations: SNI: spared nerve injury, DRGs: dorsal root ganglia, SC: spinal cord, SAFit2: selective antagonist of FKBP51 by induced fit 2

A



B

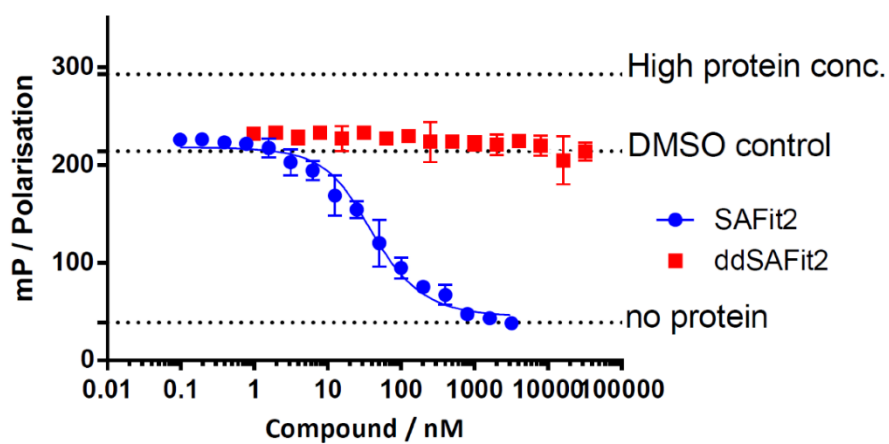


**Figure S3: Synthesis of ddSAFit 12 and competitive fluorescence assay (FPA) of SAFit2 and ddSAFit2. (A)** **a)** Pentafluorophenol, EDC · HCl, DMAP, DCM 0 °C, 74% yield, **b)** (S)-4-phenyloxazolidin-2-one, n-BuLi, THF, -78 °C, 76% yield, **c)** LiHMDS, 3-bromo cyclohexene, THF -78 °C, 74% yield, **d)** 1 bar H<sub>2</sub>, Pd/C, MeOH, 19% of 4a and 70% of the diastereomer 4b, **e)** LiOH/H<sub>2</sub>O<sub>2</sub>, THF/H<sub>2</sub>O 8:5, 0 °C, 69% yield, **f)** KOH, H<sub>2</sub>O/EtOH, 0 °C, 99% yield, **g)** Zn/NH<sub>4</sub>Ac, MeOH, r.t., 84% yield, **h)** atmospheric H<sub>2</sub>, KOtBu, Noyori catalyst, IPA, r.t., 95%, **i)** K<sub>2</sub>CO<sub>3</sub>, 2-chloroethylmorpholine hydrochloride, MeCN, reflux, 78% yield, **j)** EDC · HCl, DMAP, R)-1-(tert-butoxycarbonyl)piperidine-2-carboxylic acid, DCM, 0 °C, 78% yield, **k)** DCM/TFA 2:1, r.t., quant. yield, **l)** HATU, 4a, DiPEA, DCM/DMF, r.t., 78% yield. **(B)** Competitive fluorescence polarization assay (FPA) of SAFit2 (blue dots) and ddSAFit2 (red squares), high protein control, DMSO control, and no protein control are indicated by a tick mark and dashed lines. Fitting the curve results in a K<sub>d</sub> of 8 nM for SAFit2 and > 80000 nM for ddSAFit2. FPA was performed as described previously (Bauder et al., 2021 (<https://doi.org/10.1021/acs.jmedchem.0c02195>)).

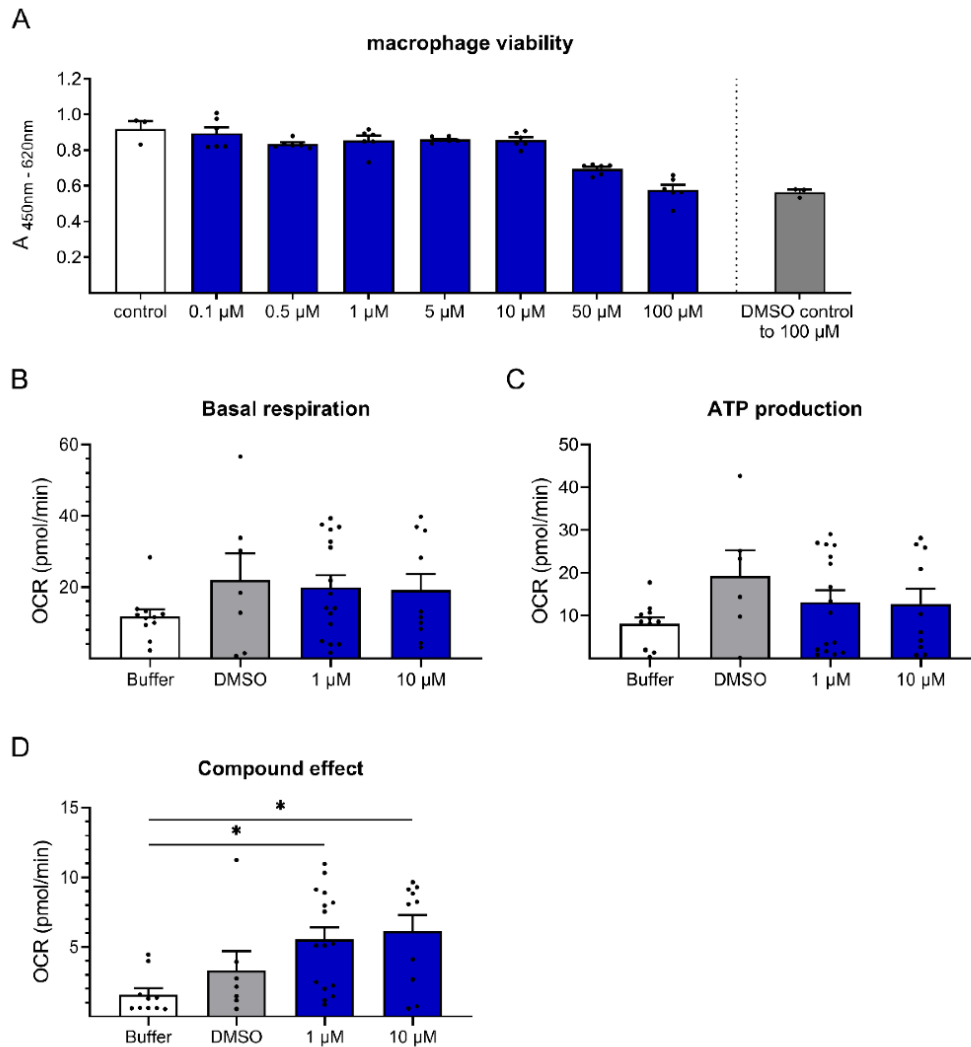


**Figure S4: Cytotoxic and metabolic influence of SAFit2 on primary bone marrow derived macrophages. (A)** The effect of SAFit2 on the macrophage viability was assessed in a WST-1 assay showing that SAFit2 has no influence on the cell viability. The data represents the mean  $\pm$  SEM of 3-6 per group **(B-D)** The influence of SAFit2 the macrophage metabolism was analyzed with a Seahorse bioanalyzer measuring the oxygen consumption rate (OCR). SAFit2 affects neither the basal respiration **(B)** nor the ATP production **(C)** of macrophages. It slightly increases the total respiration of macrophages compared to the buffer control, which is negligible since the DMSO control is also slightly increased. **(D)**. The data represents the mean  $\pm$  SEM of 1-2 runs



---

per group, measured in several technical replicates respectively. \*  $p < 0.05$  one-way ANOVA with Tukey's post hoc test.

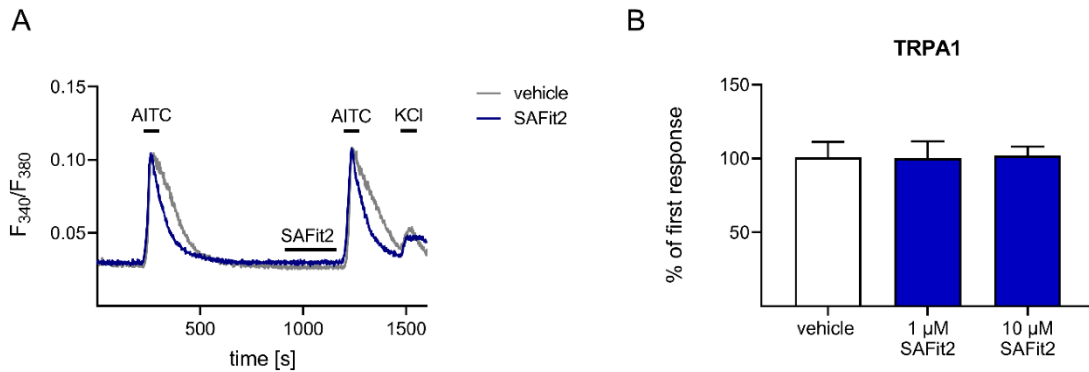


**Figure S5: SAFit2 has no impact on the TRPA1 activity in primary sensory neurons.** Primary sensory neurons were isolated from mice and the effect of SAFit2 on the TRPA1 channel activity was assessed in calcium imaging experiments. **(A)** Representative traces of TRPA1 calcium fluxes from sensory neurons, which were pre-incubated with SAFit2 for 2 minutes and stimulated with the gold standard TRPA1 agonist allyl isothiocyanate (AITC) (100  $\mu$ M, 45 s) afterwards and KCl (50 mM) as a positive control for neuronal response at the end of each experiment. **(B)** Quantification of the treated calcium response (second stimulus) related to the untreated calcium response (first stimulus). The data represents the mean  $\pm$  SEM of 37-51 sensory neurons per group.

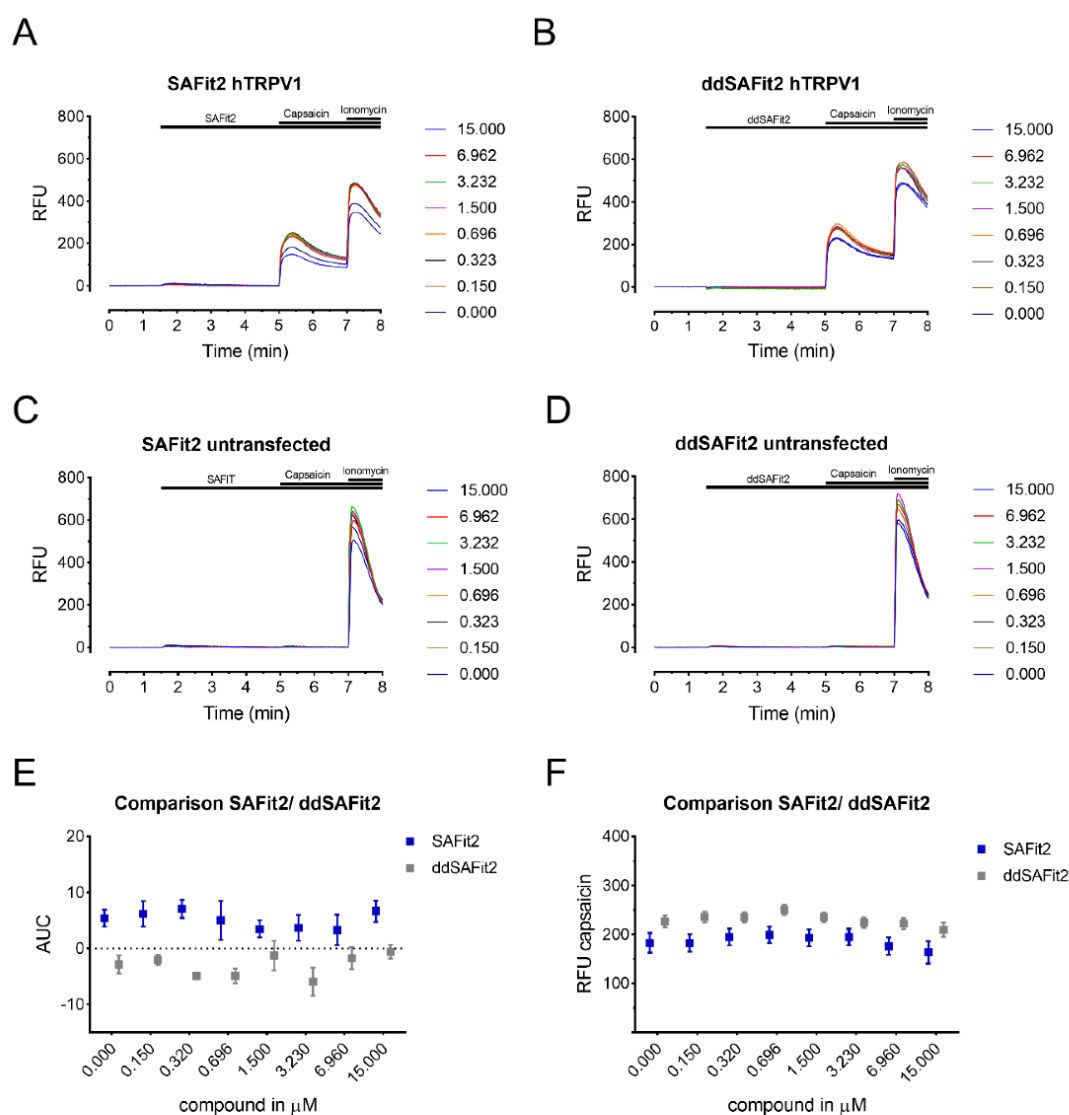


**Figure S6: SAFit2 has no direct impact on the human hTRPV1 channel in HEK-293t cells. (A, B)** Mean relative fluorescence intensity (RFU) traces of hTRPV1 transfected HEK-293t cells after the treatment with up to 15  $\mu$ M SAFit2 (A) and ddSAFit2 (B), followed by a stimulation with 200 nM capsaicin and 2  $\mu$ M ionomycin as a positive control. (C, D) Mean relative fluorescence intensity (RFU) traces of untransfected HEK-293t cells after the treatment with up to 15  $\mu$ M SAFit2 (C) and ddSAFit2 (D), followed by a stimulation with 200 nM capsaicin and a positive control with 2  $\mu$ M ionomycin. (E) Shown is the comparison of the total area under the curve (AUC) values of SAFit2 and ddSAFit2 for respective concentrations. (F) Shown is the

---

calculated RFU with its error for capsaicin stimulations after SAFit2 and ddSAFit2 treatment with respective concentrations. The data represents the mean  $\pm$  SD of 3 measurements.

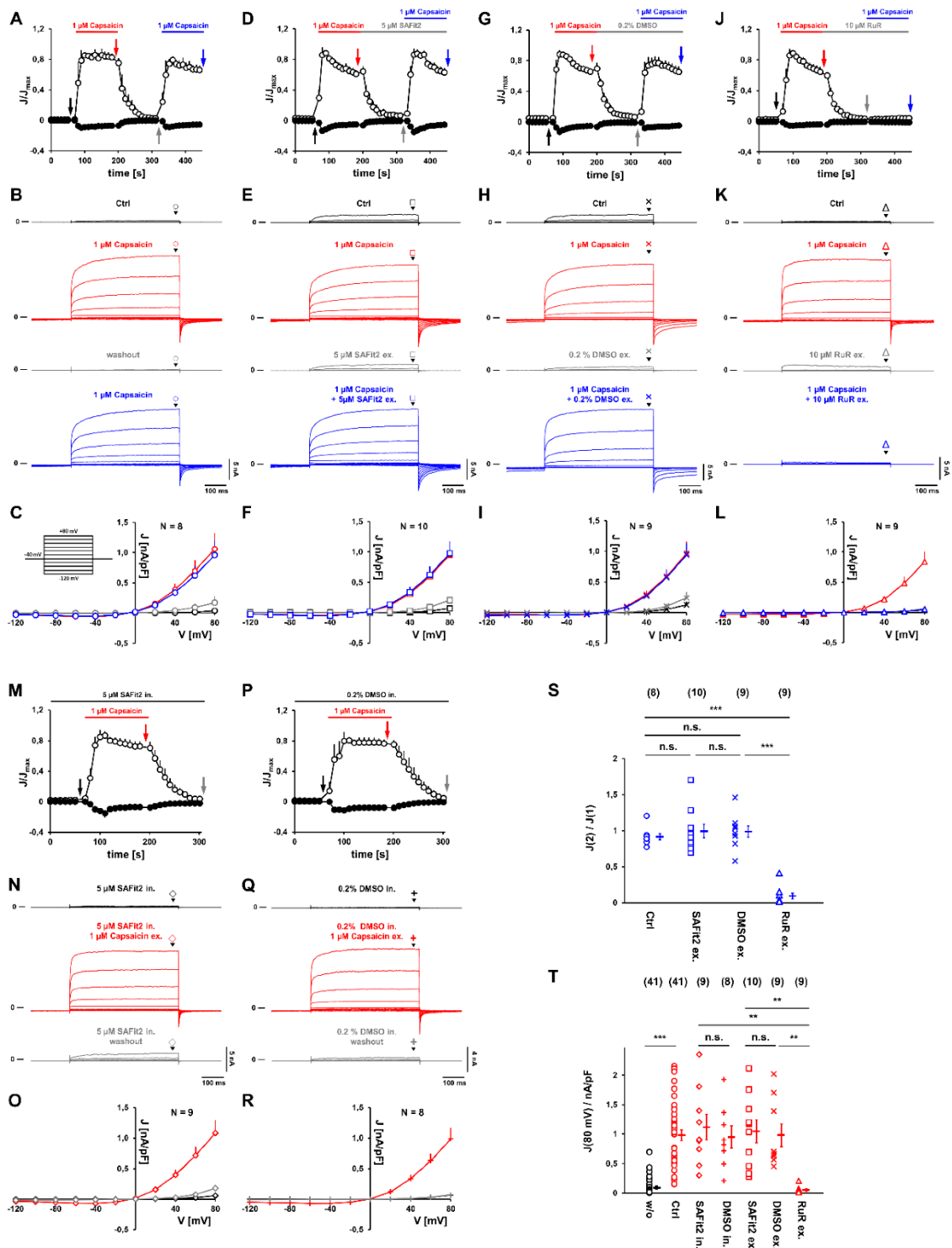


**Figure S7: Extracellularly or intracellularly administered SAFit2 has no effect on the amplitude and kinetics of capsaicin-activated TRPV1 currents in HEK-293 cells.** Whole-cell patch-clamp experiments were performed on HEK-293 cells transiently expressing TRPV1-GFP. TRPV1 currents were activated by addition of

---

1  $\mu\text{M}$  capsaicin to the bath solution. **(A-L)** To determine the effect of extracellularly added compounds on TRPV1 activation, capsaicin was applied twice for two minutes each: the first application was used to determine TRPV1 activity in the absence, the second in the presence of the compound. The compound was administered during washout after the first capsaicin application by perfusion with bath solution. The following compounds were tested: no compound **(A-C)**, SAFit2 **(D-F)**, DMSO (vehicle control) **(G-I)**, and Ruthenium Red (RuR, positive control) **(J-K)**. **(A,D,G,J)** Time courses of normalized current densities at -60 mV (closed circles) and +60 mV (open circles) as obtained by repeatedly applying 500 ms voltage ramps from -60 mV to +60 mV. Current densities were normalized for each cell to the maximal current density measured at +60 mV during the first capsaicin application. Data points represent arithmetic mean  $\pm$  SEM of N = 4-10 cells. **(B,E,H,K)** Representative whole-cell current traces evoked by the voltage-step protocol shown in **(C)**. The time points at which the voltage-step protocol was applied are indicated in the time courses in **A,D,G,J** with arrows of the corresponding color. **(C,F,I,L)** Steady-state current densities obtained from voltage-clamp measurements as shown in **B,E,H,K**. The time points at which the current densities were measured are highlighted in **B,E,H,K** with the corresponding symbols. Data points represent arithmetic mean  $\pm$  SEM. The number of measured cells N is indicated in the graphs. **(M-R)** To determine whether SAFit2 can directly affect TRPV1 activity from the intracellular side of the plasma membrane, patch-clamp experiments were performed with 5  $\mu\text{M}$  SAFit2 **(M-O)** and with 0.2% DMSO (vehicle) added to the pipette solution **(P-R)**. **(M,P)** Time courses of normalized current densities at -60 mV (closed circles) and +60 mV (open circles) as obtained by repeatedly applying 500 ms voltage ramps from -60 mV to +60 mV. Current densities were normalized for each cell to the maximal current density measured at +60 mV. Data points represent arithmetic mean  $\pm$  SEM of N = 5-9 cells. **(N,Q)** Representative whole-

---

cell current traces evoked by the voltage-step protocol shown in **(C)**. The time points at which the voltage-step protocol was applied are indicated in the time courses in **(M,P)** with arrows of the corresponding color. **(O,R)** Steady-state current densities obtained from voltage-clamp measurements as shown in **(N,Q)**. The time points at which the current densities were measured are highlighted in **(N,Q)** with the corresponding symbols. Data points represent arithmetic mean  $\pm$  SEM. The number of measured cells in **N** is indicated in the graphs. **(S)** Ratios  $J(2)/J(1)$  of steady-state current densities measured at +80 mV at the end of the first ( $J(1)$ ) and second ( $J(2)$ ) capsaicin application in the voltage-clamp experiments shown in **(A-L)**. **(T)** Steady-state current densities at +80 mV obtained from the voltage-clamp experiments shown in **(A-R)** without (w/o, black circles) and after 2 minutes of capsaicin application (red symbols) to the bath solution in the absence (Ctrl) or presence of 5  $\mu$ M SAFit2, 0.2% DMSO (vehicle) or 10  $\mu$ M ruthenium red (RuR) in the pipette (in.) or bath solution (ex.). **(S)** and **(T)** show the values of the individual measurements as well as the arithmetic mean  $\pm$  SEM. The number of measured cells is given in brackets above each group. Not significant (n.s.)  $p \geq 0.05$ , \*  $p < 0.05$ , \*\*  $p < 0.01$ , \*\*\*  $p < 0.001$  student t-test with Welch's correction.

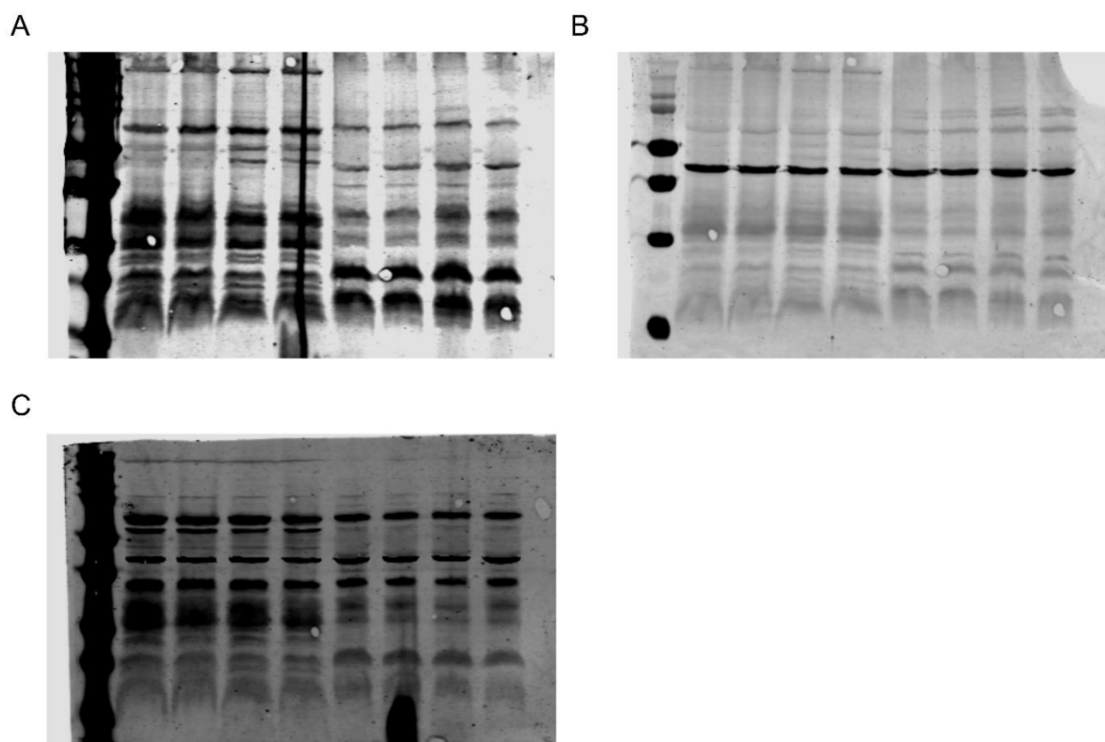


**Figure S8: Uncropped Western Blot images for NF-κB signaling pathway.** Images of (A) phosphorylated p65 and IκBα, (B) β-Actin loading control for phosphorylated proteins and (C) total protein amount of IKKβ, p65, IκBα and the respective loading control β-Actin.

#### **Methods for the synthesis of ddSAFit2**

If not mentioned otherwise, reactions were performed in an oven dried flask under argon atmosphere.  $^1\text{H}$ - and  $^{13}\text{C}$ -NMR spectra were recorded at the NMR department of chemistry of the Technical University of Darmstadt (TUD) on a Bruker DRX500 and at the Thiele lab by Johann Primožic and Matthias Brauser on a Bruker Avance III 600 MHz and Bruker Avance III HD 700 MHz spectrometer. Chemical shifts for  $^1\text{H}$  and  $^{13}\text{C}$  are given in ppm ( $\delta$ ) relative to the tetramethylsilane (TMS) internal standard. Deuterated chloroform ( $\text{CDCl}_3$ ) was used as solvent and the spectra calibrated according to their corresponding peak. The multiplicities are abbreviated as follows:



---

singlet (s), doublet (d), triplet (t), quartet (q), doublet of doublets (dd), multiplet (m). HRMS spectra were acquired on an LTQ Orbitrap XL that was calibrated using the calmix solution of the manufacturer at least a week before the measurements were conducted. Chiral HPLC was performed using a Beckman System Gold 125S Solvent Module with a Beckman System Gold Diode Array Detector Module 168 recording UV spectra at 220 nm using a Daicel chemical industries Ltd, Chiralcel OD-H, normal phase analytical column, 250 × 4.6 mm, 5 μm with an isocratic gradient given for each compound using n heptane as solvent A and isopropyl alcohol (IPA) as solvent B. UHPLC-MS measurements were performed on an Agilent 1260 infinity II system consisting out of a flexible pump, a Vialsampler, a multicolumn compartment with a column oven, a DAD detector, and a 6125B MSD. Data was acquired with a 50 × 2.1 mm, 1.9 μm EC-C18 Poroshell 120 column using a gradient starting with an isocratic hold of 0.2 min at 5% solvent B up to 100% solvent B over 1.8 min followed by a hold for 1 min with solvent A being water with 0.1% formic acid and solvent B acetonitrile with 0.1% formic acid. Purity is determined by UV detection at 220 nm and given in percent. LC-MS measurements were performed using a Beckman System Gold 125 Solvent Module and Beckman System Gold 199 Detector Module with a YMC Pack Pro C8, 100 × 4.6 mm, 3 μm column using a 0 - 100% B gradient in 19 min with a 1 mL/min flow using solvent A: 95% H<sub>2</sub>O, 5% MeCN, 0.1% formic acid and solvent B: 95% MeCN, 5% H<sub>2</sub>O, 0.1% formic acid with a LCQ Deca XP Plus operated in ESI mode. Flash chromatography is performed using an Isolera system from Biotage using the flash columns of the manufacturer with DAD-UV detection. If not mentioned otherwise, separations are performed with a linear 10 column volume gradient. Manual column chromatography was performed using Kieselgel 60 from Roth, 0.04 – 0.063 mm with the solvent mixture mentioned for each compound. Preparative HPLC is performed on an Interchim Puriflash 5.250 system with UV detection.

Purifications are performed using a Luna 250 x 21.2 mm, 5  $\mu$ m C18 column with a 100 Å pore size using a gradient from 5% B to 100% B in ten column volumes at a flow rate of 30 mL/min unless mentioned otherwise. Solvent A is water with 0.1 TFA and solvent B acetonitrile with 0.1% TFA.

**(E)-3-(3,4-Dimethoxyphenyl)-1-(3-hydroxyphenyl)prop-2-en-1-one (8):** 9.0 g (54.2 mmol, 1.0 eq) 3,4-Dimethoxybenzaldehyde and 7.37 g (54.2 mmol, 1.0 eq) 3-Hydroxyacetophenone are dissolved in 90 mL EtOH and the mixture is cooled to 0 °C. 24.5 g (217 mmol, 4.0 eq) potassium hydroxide are dissolved in 60 mL water and to the aforementioned mixture. The mixture is stirred for 2 h and then quenched by adding ice and then 3 M HCl until a pH of 2 is reached. The mixture is crystallized from the quenched reaction mixture to yield 15.3 g (99%) as a yellow solid. <sup>1</sup>H-NMR (500 MHz, CDCl<sub>3</sub>):  $\delta$  7.77 (dd, J = 15.6, 1.4 Hz, 1H), 7.67 – 7.59 (m, 1H), 7.56 (d, J = 7.7 Hz, 1H), 7.40 – 7.33 (m, 2H), 7.22 (dt, J = 8.4, 1.8 Hz, 1H), 7.15 (t, J = 1.8 Hz, 1H), 7.13 – 7.07 (m, 1H), 6.89 (dd, J = 8.3, 1.5 Hz, 1H), 6.64 (s, 1H), 3.94 (s, 3H), 3.93 (s, 3H). <sup>13</sup>C-NMR (126 MHz, CDCl<sub>3</sub>):  $\delta$  190.9, 156.6, 151.7, 149.4, 145.7, 139.9, 130.0, 127.9, 123.5, 120.9, 120.3, 120.0, 115.3, 111.3, 110.3, 56.2, 56.1. UHPLC-MS:  $t_R$  = 1.753 min (99%), m/z: calculated = 285.11 [M+H]<sup>+</sup>, found = 285.2 [M+H]<sup>+</sup>.

**3-(3,4-Dimethoxyphenyl)-1-(3-hydroxyphenyl)propan-1-one:** 14.0 g (215 mmol, 10 eq) zinc and 16.5 g (215 mmol, 10 eq) ammonium acetate are suspended in 100 mL MeOH. 6.1 g (21.5 mmol, 1.0 eq) **8** are dissolved in 100 mL MeOH and added dropwise to the aforementioned mixture. The solids are filtered, washed with MeOH and the crude product is precipitated from the filtrate by addition of water. The crude product is purified by recrystallization from water/methanol to yield 5.17 g (84%) as a white solid. <sup>1</sup>H-NMR (500 MHz, CDCl<sub>3</sub>):  $\delta$  7.54 (dd, J = 2.7, 1.6 Hz, 1H), 7.49 (dq, J = 7.9, 1.2 Hz, 1H), 7.31 (td, J = 8.0, 1.1 Hz, 1H), 7.08 (ddd, J = 8.0, 2.6, 0.9 Hz, 1H), 6.83 – 6.73 (m, 3H), 6.63 (d, J = 42.6 Hz, 1H), 3.84 (s, 3H), 3.84 (s, 3H), 3.26 (dd, J =

8.3, 6.9 Hz, 2H), 3.05 – 2.97 (m, 2H). <sup>13</sup>C-NMR (126 MHz, CDCl<sub>3</sub>): δ 200.4, 156.6, 149.0, 147.5, 138.3, 133.9, 130.0, 120.8, 120.6, 120.3, 114.7, 112.1, 111.6, 56.1, 56.0, 40.9, 30.0. UHPLC-MS: t<sub>R</sub> = 1.778 min (98 %), m/z: calculated = 287.13 [M+H]<sup>+</sup>, found = 287.2 [M+H]<sup>+</sup>.

**(R)-3-(3-(3,4-Dimethoxyphenyl)-1-hydroxypropyl)phenol (9):** 9.70 g (33.9 mmol, 1 eq) **3-(3,4-Dimethoxyphenyl)-1-(3-hydroxyphenyl)propan-1-one** and 50.8 mL (50.8 mmol, 1.5 eq) 1 M potassium butoxide were dissolved in 100 mL IPA. The mixture was degassed with Ar and 270 mg (0.27 mmol, 0.01 eq) RuCl<sub>2</sub>[(S)-dm-segphos] [(S)-daipen] were added. The mixture was saturated with hydrogen for 15 min before the flask was sealed with a rubber septum and equipped with a hydrogen balloon. The mixture is stirred for 72 h before the reaction is stopped by degassing with Ar and removing volatiles under reduced pressure. The crude product is purified by recrystallization from DCM to yield 9.28 g (95%) as a white solid. <sup>1</sup>H-NMR (500 MHz, CDCl<sub>3</sub>): δ 7.14 (t, J = 7.8 Hz, 1H), 6.86 (t, J = 2.0 Hz, 1H), 6.79 (d, J = 7.7 Hz, 1H), 6.76 – 6.70 (m, 2H), 6.69 – 6.61 (m, 2H), 4.58 (dd, J = 7.6, 5.4 Hz, 1H), 3.80 (s, 3H), 3.78 (s, 3H), 2.71 – 2.47 (m, 2H), 2.13 – 1.85 (m, 2H). <sup>13</sup>C-NMR (126 MHz, CDCl<sub>3</sub>): δ 156.3, 148.9, 147.2, 146.1, 134.4, 129.8, 120.4, 118.2, 114.9, 112.9, 112.1, 111.5, 74.0, 56.0, 55.9, 40.3, 31.6. LC-MS: t<sub>R</sub> = 9.87 min (99%), m/z: calculated = 271.13 [M+H-H<sub>2</sub>O]<sup>+</sup>, found = 271.26 [M+H-H<sub>2</sub>O]<sup>+</sup>. Chiral HPLC (30% B): t<sub>R</sub> = 8.78 min (> 99%)

**(R)-3-(3,4-Dimethoxyphenyl)-1-(3-(2-morpholinoethoxy)phenyl)propan-1-ol (10):** 3.33 g (11.5 mmol, 1 eq) **9**, 2.15 g (11.5 mmol, 1 eq) 2-Chloroethylmorpholine hydrochloride, and 6.38 g (66.1 mmol, 4 eq) potassium carbonate are suspended in 50 mL MeCN. The suspension is refluxed for 24 h before the reaction is stopped by filtering off the solids and removing volatiles under reduced pressure. The crude product is purified by manual silica column (EA/TEA/MeOH 100:3:1) to yield 3.60 g (78%) as a yellow oil. <sup>1</sup>H-NMR (500 MHz, CDCl<sub>3</sub>): δ 7.28 – 7.21 (m, 1H), 6.92 (dt, J =

6.6, 1.4 Hz, 2H), 6.83 – 6.79 (m, 1H), 6.79 – 6.77 (m, 1H), 6.75 – 6.69 (m, 2H), 4.65 (dd,  $J = 7.9, 5.2$  Hz, 1H), 4.15 – 4.06 (m, 2H), 3.85 (s, 3H), 3.84 (s, 3H), 3.74 – 3.68 (m, 4H), 2.78 (td,  $J = 5.7, 1.2$  Hz, 2H), 2.75 – 2.56 (m, 2H), 2.58 – 2.53 (m, 4H), 2.14 – 1.93 (m, 2H).  $^{13}\text{C}$ -NMR (126 MHz,  $\text{CDCl}_3$ ):  $\delta$  159.1, 149.0, 147.3, 146.6, 134.5, 129.6, 120.3, 118.6, 113.7, 112.3, 111.9, 111.4, 73.8, 67.0, 65.9, 57.8, 56.1, 56.0, 54.2, 40.7, 31.8. UHPLC-MS:  $t_R = 1.358$  min (98%),  $m/z$ : calculated = 402.23  $[\text{M}+\text{H}]^+$ , found = 402.2  $[\text{M}+\text{H}]^+$ .

**Perfluorophenyl 2-(3,4,5-trimethoxyphenyl)acetate:** 50 g (221 mmol, 1.0 eq) 3,4,5,-Trimethoxyphenylacetic acid, 40.7 g (221 mmol, 1.0 eq) pentafluorophenol, and 4.96 g (44.2 mmol, 0.2 eq) DMAP are dissolved in 500 mL DCM and cooled to 0 °C, 46.6 g (243 mmol, 1.1 eq) EDC · HCl are added and the mixture is stirred overnight at room temperature. After quenching the reaction by adding brine, the mixture is extracted three times using DCM, the combined organic phases are washed twice with 1 M HCl, dried over  $\text{MgSO}_4$ , and volatiles are removed under reduced pressure. The crude product is recrystallized from MeOH to yield 64.2 g (74%) as a white solid.  $^1\text{H}$ -NMR (500 MHz,  $\text{CDCl}_3$ ):  $\delta$  6.57 (s, 2H), 3.90 (s, 2H), 3.88 (s, 6H), 3.85 (s, 3H).  $^{13}\text{C}$ -NMR (126 MHz,  $\text{CDCl}_3$ ):  $\delta$  153.2, 136.4, 127.9, 106.4, 60.8, 56.1. LC-MS:  $t_R = 13.43$  min (99%),  $m/z$ : calculated = 393.08  $[\text{M}+\text{H}]^+$ , found = 393.07  $[\text{M}+\text{H}]^+$ .

**(S)-4-Phenyl-3-(2-(3,4,5-trimethoxyphenyl)acetyl)oxazolidin-2-one (2):** 28.19 g (173 mmol, 1.1 eq) (S)-4-Phenyloxazolidin-2-one are dissolved in 620 mL THF and cooled to -78 °C. 68.0 mL (173 mmol, 1.1 eq) *n*-butyl lithium are slowly added and the mixture is stirred for 15 min. 61.6 g (157 mmol, 1.0 eq of **Perfluorophenyl 2-(3,4,5-trimethoxyphenyl)acetate** are added and the mixture is stirred for 2 h at -78 °C before the reaction is quenched by addition of isopropyl alcohol (IPA). The mixture was extracted with EA, dried over  $\text{MgSO}_4$ , and volatiles are removed under reduced pressure. The crude product is purified by flash column chromatography (Cy/EA

gradient) to yield 40.0 g (76%) as a white solid. <sup>1</sup>H-NMR (500 MHz, CDCl<sub>3</sub>): δ 7.37 – 7.28 (m, 3H), 7.23 – 7.15 (m, 2H), 6.45 (s, 2H), 5.43 (dd, J = 8.8, 4.0 Hz, 1H), 4.69 (t, J = 8.9 Hz, 1H), 4.30 – 4.23 (m, 2H), 4.16 (d, J = 14.8 Hz, 1H), 3.82 (s, 3H), 3.77 (s, 6H). <sup>13</sup>C-NMR (126 MHz, CDCl<sub>3</sub>): δ 170.6, 153.7, 153.3, 138.8, 137.3, 134.1, 129.2, 128.9, 126.1, 106.8, 70.0, 61.0, 57.9, 56.2, 41.8. UHPLC-MS: t<sub>R</sub> = 1.98 min (96%), m/z: calculated = 372.15 [M+H]<sup>+</sup>, found = 372.2 [M+H]<sup>+</sup>.

**(4S)-3-(2-(cyclohex-2-en-1-yl)-2-(3,4,5-trimethoxyphenyl)acetyl)-4-**

**phenyloxazolidin-2-one:** 40.0 g (108 mmol, 1.0 eq) **2** are dissolved in 240 mL THF and cooled to 78 °C. 118 mL (118 mmol, 1.1 eq) of 1 M LiHMDS are added and the mixture is stirred for 2 h at -78 °C. 18.9 mL (162 mmol, 1.5 eq) 3-bromocyclohexene are added and the mixture is stirred for another 2 h before the reaction is quenched by addition of NH<sub>4</sub>Cl solution. The mixture was extracted with EA, dried over MgSO<sub>4</sub>, and volatiles are removed under reduced pressure. The crude product is purified by flash column chromatography (Cy/EA gradient) to yield 35.9 g (74%) as a white solid as a mixture of diastereomers. <sup>1</sup>H-NMR (500 MHz, CDCl<sub>3</sub>): δ 7.43 – 7.37 (m, 2H), 7.36 – 7.30 (m, 3H), 6.67 (d, J = 8.7 Hz, 2H), 5.61 (dq, J = 9.7, 4.6, 1.8 Hz, 1H), 5.36 (ddd, J = 9.2, 5.6, 3.7 Hz, 1H), 5.04 (dq, J = 10.2, 2.3 Hz, 1H), 4.83 (d, J = 11.3 Hz, 1H), 4.57 (td, J = 8.9, 3.2 Hz, 1H), 4.20 (ddd, J = 8.9, 3.8, 2.1 Hz, 1H), 3.83 (d, J = 2.8 Hz, 6H), 3.81 (d, J = 0.7 Hz, 3H), 2.80 (ddp, J = 16.1, 7.7, 2.6 Hz, 1H), 1.93 (ddq, J = 12.4, 5.9, 3.3 Hz, 2H), 1.70 – 1.58 (m, 1H), 1.49 – 1.28 (m, 2H), 1.11 (tdd, J = 12.7, 6.2, 2.6 Hz, 1H). <sup>13</sup>C-NMR (126 MHz, CDCl<sub>3</sub>): δ 173.5, 153.5, 153.4, 153.2, 139.4, 139.4, 137.4, 132.7, 132.6, 129.4, 129.2, 129.1, 128.9, 128.8, 128.5, 128.0, 126.1, 126.0, 106.4, 106.2, 69.5, 69.5, 60.8, 58.2, 58.2, 56.2, 56.2, 53.6, 53.4, 39.7, 39.6, 27.6, 26.1, 25.3, 25.2, 21.1, 20.4. UHPLC-MS: t<sub>R</sub> = 1.150 min (99%), m/z: calculated = 452.21 [M+H]<sup>+</sup>, found = 452.2 [M+H]<sup>+</sup>.

**(S)-3-((R)-2-cyclohexyl-2-(3,4,5-trimethoxyphenyl)acetyl)-4-phenyloxazolidin-2-one (4a)** and **(S)-3-((S)-2-Cyclohexyl-2-(3,4,5-trimethoxyphenyl)acetyl)-4-phenyloxazolidin-2-one (4b)**: 23.2 g (51.4 mmol, 1.0 eq) **(4S)-3-(2-(cyclohex-2-en-1-yl)-2-(3,4,5-trimethoxyphen-yl)acetyl)-4-phenyloxazolidin-2-one** are dissolved in 220 mL MeOH and the mixture is degassed with Ar for 15 min before 2.73 g (2.57 mmol, 0.05 eq) Pd/C are added. The mixture is then saturated with hydrogen gas for 15 min before the flask is sealed with a rubber septum and equipped with a hydrogen balloon. The reaction is stirred overnight at room temperature and then stopped by degassing the solution for 15 min with Ar before filtering over silica. Volatiles are removed under reduced pressure. The crude product is purified by flash column chromatography (Cy/EA gradient) to yield **11a** 16.38 g (70%) as a white solid and **11b** 4.38 g (19%) as a white solid.

**4a**: <sup>1</sup>H-NMR (500 MHz, CDCl<sub>3</sub>): δ 7.22 – 7.12 (m, 3H), 6.85 – 6.79 (m, 2H), 6.27 (s, 2H), 5.44 (dd, J = 9.0, 5.0 Hz, 1H), 4.72 (d, J = 10.7 Hz, 1H), 4.68 – 4.58 (m, 1H), 3.83 (s, 3H), 3.63 (s, 6H), 2.05 – 1.92 (m, 1H), 1.85 (dt, J = 12.4, 3.1 Hz, 1H), 1.70 (dt, J = 14.7, 3.9 Hz, 1H), 1.65 – 1.57 (m, 3H), 1.35 – 1.20 (m, 2H), 1.20 – 1.07 (m, 2H), 1.02 (tdd, J = 12.4, 10.8, 3.6 Hz, 1H), 0.82 (qd, J = 11.8, 3.0 Hz, 1H). <sup>13</sup>C-NMR (126 MHz, CDCl<sub>3</sub>): δ 172.7, 153.3, 153.0, 138.4, 137.1, 132.1, 128.8, 128.5, 125.9, 106.0, 69.5, 60.9, 57.9, 56.0, 55.9, 39.8, 32.4, 30.3, 26.5, 26.1, 26.1. UHPLC-MS: t<sub>R</sub> = 1.186 min (99%), m/z: calculated = 454.23 [M+H]<sup>+</sup>, found = 454.2 [M+H]<sup>+</sup>.

**4b**: <sup>1</sup>H-NMR (500 MHz, CDCl<sub>3</sub>): δ 7.46 – 7.26 (m, 5H), 5.36 (dd, J = 8.8, 3.6 Hz, 1H), 4.79 (d, J = 10.8 Hz, 1H), 4.58 (t, J = 8.8 Hz, 1H), 4.21 (dd, J = 8.9, 3.6 Hz, 1H), 3.84 (s, 6H), 3.82 (s, 3H), 2.08 – 1.89 (m, 1H), 1.58 (d, J = 16.1 Hz, 4H), 1.36 – 1.20 (m, 3H), 1.09 (d, J = 8.3 Hz, 2H), 1.01 – 0.62 (m, 1H). <sup>13</sup>C-NMR (126 MHz, CDCl<sub>3</sub>): δ 174.0, 153.7, 153.1, 139.5, 137.2, 133.2, 129.3, 128.9, 126.0, 106.2, 69.5, 61.0, 58.3, 56.2,

54.7, 42.2, 31.5, 30.3, 26.4, 26.0, 25.9. UHPLC-MS:  $t_R = 1.238$  min (99%),  $m/z$ : calculated = 454.23  $[M+H]^+$ , found = 454.2  $[M+H]^+$ .

**(S)-2-Cyclohexyl-2-(3,4,5-trimethoxyphenyl)acetic acid:** 16.38 g (36.1 mmol, 1.0 eq) **4b** are dissolved in 160 mL THF and added to a mixture of 2.59 g (108 mmol, 3.0 eq) LiOH and 18.4 mL (181 mmol, 5.0 eq)  $H_2O_2$  dissolved in 80 mL water. The mixture is stirred overnight at room temperature before the reaction is quenched by addition of 1 M HCl. The mixture is extracted with ether, dried over  $MgSO_4$ , and the solvent is removed under reduced pressure. The crude product is purified by flash column chromatography (Cy/EA+1% of formic acid gradient) to yield 9.7 g (87%) as a pale yellow solid.  $^1H$ -NMR (500 MHz,  $CDCl_3$ ):  $\delta$  6.54 (s, 2H), 3.84 (s, 6H), 3.82 (s, 3H), 3.12 (d,  $J = 10.7$  Hz, 1H), 1.95 (tt,  $J = 11.0, 3.3$  Hz, 1H), 1.92 – 1.86 (m, 1H), 1.79 – 1.71 (m, 1H), 1.64 (dq,  $J = 8.0, 3.9$  Hz, 2H), 1.43 – 1.34 (m, 1H), 1.34 – 1.24 (m, 1H), 1.22 – 1.13 (m, 2H), 1.07 (tdd,  $J = 12.6, 10.8, 3.5$  Hz, 1H), 0.81 – 0.69 (m, 1H).  $^{13}C$ -NMR (126 MHz,  $CDCl_3$ ):  $\delta$  180.0, 153.3, 137.5, 133.0, 105.8, 60.9, 59.1, 56.3, 41.0, 32.0, 30.4, 26.4, 26.0. UHPLC-MS:  $t_R = 1.863$  min (99%),  $m/z$ : calculated = 309.2  $[M+H]^+$ , found = 309.2  $[M+H]^+$ .

**(R)-2-Cyclohexyl-2-(3,4,5-trimethoxyphenyl)acetic acid (5):** 4.34 g (9.57 mmol, 1.0 eq) **4a** are dissolved in 80 mL THF. The mixture is cooled to 0 °C and 0.69 g (28.7 mmol, 3.0 eq) LiOH and 4.89 mL (47.9 mmol, 5.0 eq)  $H_2O_2$  dissolved in 50 mL are added. The mixture is stirred overnight at room temperature before the reaction is quenched by addition of diluted HCl. The mixture is extracted with EA, dried with  $MgSO_4$ , and volatiles are removed under reduced pressure. The crude product is purified by flash column chromatography (DCM/MeOH + 1% FA) to yield 2.03 g (69%) as a white solid.  $^1H$ -NMR (500 MHz,  $CDCl_3$ ):  $\delta$  6.54 (s, 2H), 3.84 (s, 6H), 3.82 (s, 3H), 3.12 (d,  $J = 10.7$  Hz, 1H), 2.02 – 1.85 (m, 2H), 1.79 – 1.71 (m, 1H), 1.68 – 1.58 (m, 2H), 1.41 – 1.23 (m, 2H), 1.22 – 1.01 (m, 3H), 0.81 – 0.69 (m, 1H).  $^{13}C$ -NMR (126 MHz,

CDCl<sub>3</sub>): δ 179.9, 153.3, 137.5, 133.0, 129.3, 126.1, 105.8, 61.0, 59.1, 56.3, 41.0, 32.1, 30.4, 26.4, 26.1. UHPLC-MS: t<sub>R</sub> = 0.492 min (97%), m/z: calculated = 309.18 [M+H]<sup>+</sup>, found = 309.2 [M+H]<sup>+</sup>.

**(S)-1-Tert-butyl 2-((R)-3-(3,4-dimethoxyphenyl)-1-(3-(2-**

**morpholinoethoxy)phenyl)pro-pyl) piperidine-1,2-dicarboxylate:** 31.3 g (77.8 mmol, 1.0 eq) **10**, 18.74 g (81.7 mmol, 1.05 eq) (S)-N-Boc-pipecolate, and 1.90 g (15.6 mmol, 0.2 eq) DMAP are dissolved in 350 mL DCM. The mixture is cooled to 0 °C and 15.7 g (81.7 mmol, 1.05 eq) EDC · HCl are added. The mixture is stirred overnight at room temperature before the reaction is quenched by addition of brine. The mixture is extracted with DCM, dried with MgSO<sub>4</sub>, and volatiles are removed under reduced pressure. The crude product is purified by flash column chromatography (Cy/EA + 3% TEA) to yield 42.2 g (97%) as a pale yellow oil. <sup>1</sup>H-NMR (500 MHz, CDCl<sub>3</sub>): δ 7.24 (t, J = 8.2 Hz, 2H), 6.91 (d, J = 7.8 Hz, 2H), 6.87 (s, 2H), 6.82 (d, J = 8.2 Hz, 1H), 6.77 (d, J = 8.1 Hz, 1H), 6.67 (q, J = 6.6 Hz, 3H), 5.76 (s, 1H), 5.04 – 4.89 (m, 1H), 4.75 (d, J = 6.0 Hz, 1H), 4.10 (p, J = 6.3 Hz, 5H), 4.06 – 3.90 (m, 1H), 3.84 (d, J = 2.5 Hz, 9H), 3.80 – 3.68 (m, 7H), 2.79 (t, J = 5.7 Hz, 3H), 2.67 – 2.42 (m, 4H), 2.25 (dd, J = 26.2, 13.2 Hz, 4H), 2.04 (d, J = 8.3 Hz, 4H), 1.77 – 1.55 (m, 5H), 1.47 (s, 6H), 1.36 (d, J = 7.2 Hz, 7H), 1.22 – 1.02 (m, 1H). <sup>13</sup>C-NMR (126 MHz, CDCl<sub>3</sub>): δ 171.5, 171.2, 158.9, 155.5, 149.0, 147.5, 141.9, 133.8, 133.6, 129.7, 120.3, 119.2, 114.2, 114.0, 113.1, 111.8, 111.4, 80.0, 76.2, 67.0, 65.9, 60.5, 57.8, 56.0, 55.9, 55.9, 55.1, 54.2, 54.0, 49.2, 42.3, 41.2, 38.4, 38.2, 34.1, 31.5, 31.2, 28.5, 28.4, 26.9, 25.7, 25.1, 25.0, 24.7, 21.1, 21.0, 20.8, 14.3. UHPLC-MS: t<sub>R</sub> = 2.072 min (99%), m/z: calculated = 613.35 [M+H]<sup>+</sup>, found = 613.4 [M+H]<sup>+</sup>.

**(S)-(R)-3-(3,4-Dimethoxyphenyl)-1-(3-(2-morpholinoethoxy)phenyl)propyl**

**piperidine-2-carboxylate:** 42.2 g (68.9 mmol, 1.0 eq) **(S)-1-Tert-butyl 2-((R)-3-(3,4-dimethoxyphenyl)-1-(3-(2-morpholinoethoxy)phenyl)pro-pyl) piperidine-1,2-**



**dicarboxylate** are dissolved in 40 mL of DCM and 20 mL TFA. The mixture is stirred for 2 h at room temperature before the reaction is quenched by addition of NaHCO<sub>3</sub>. The mixture is extracted with DCM, dried with MgSO<sub>4</sub>, and volatiles are removed under reduced pressure. The crude product (35.3 g quant.) is used without further purification. <sup>1</sup>H-NMR (500 MHz, CDCl<sub>3</sub>): δ 7.22 – 7.15 (m, 1H), 6.86 (d, J = 7.6 Hz, 1H), 6.82 (d, J = 2.5 Hz, 1H), 6.77 (dd, J = 8.2, 2.5 Hz, 1H), 6.73 (d, J = 8.1 Hz, 1H), 6.65 – 6.56 (m, 2H), 5.70 (dd, J = 8.1, 5.5 Hz, 1H), 4.04 (t, J = 5.6 Hz, 2H), 3.80 (s, 3H), 3.79 (s, 3H), 3.68 (t, J = 4.5 Hz, 4H), 3.32 (dd, J = 10.1, 3.3 Hz, 1H), 3.02 (dt, J = 12.2, 3.8 Hz, 1H), 2.74 (t, J = 5.8 Hz, 2H), 2.65 – 2.54 (m, 1H), 2.54 – 2.44 (m, 6H), 2.18 (ddt, J = 14.7, 9.0, 4.2 Hz, 1H), 2.05 – 1.94 (m, 2H), 1.75 (dt, J = 8.5, 4.8 Hz, 1H), 1.59 – 1.48 (m, 2H), 1.47 – 1.36 (m, 2H), 1.16 – 0.96 (m, 1H). <sup>13</sup>C-NMR (126 MHz, CDCl<sub>3</sub>): δ 172.8, 158.8, 148.8, 147.3, 141.8, 133.6, 129.5, 120.1, 120.1, 119.0, 119.0, 113.8, 113.0, 111.7, 111.7, 111.3, 75.5, 67.0, 66.9, 65.7, 58.7, 57.6, 55.9, 55.8, 55.8, 54.1, 52.9, 45.9, 45.6, 38.0, 33.9, 31.3, 31.3, 29.3, 25.8, 25.7, 25.0, 24.1, 9.3, 8.1. UHPLC-MS: t<sub>R</sub> = 1.302 min (98%), m/z: calculated = 513.30 [M+H]<sup>+</sup>, found = 513.2 [M+H]<sup>+</sup>.

**(S)-(R)-3-(3,4-Dimethoxyphenyl)-1-(3-(2-morpholinoethoxy)phenyl)propyl**

**1-((S)-2-cyclohexyl-2-(3,4,5-trimethoxyphenyl)acetyl)piperidine-2-carboxylate**

**(SAFit2):** 13.4 g (43.3 mmol, 1.0 eq) **(S)-2-Cyclohexyl-2-(3,4,5-trimethoxyphenyl)acetic acid**, 18.1 g (47.6 mmol, 1.1 eq) HATU, and 30.2 mL (173 mmol, 4.0 eq) DiPEA are dissolved in 20 mL of DMF. The mixture is stirred for 30 min at room temperature before 33.3 g (64.9 mmol, 1.5 eq) **(S)-(R)-3-(3,4-Dimethoxyphenyl)-1-(3-(2-morpholinoethoxy)phenyl)propyl piperidine-2-carboxylate** dissolved in 250 mL DCM are added. The mixture is stirred overnight at room temperature before the reaction is quenched by addition of brine. The mixture is extracted with DCM, dried with MgSO<sub>4</sub>, and volatiles are removed under reduced

pressure. The crude product is purified by preparative HPLC and flash column chromatography (Cy/EA+3% TEA) to yield 19.5 g (56%) as a white solid. <sup>1</sup>H-NMR (700 MHz, CDCl<sub>3</sub>): δ 7.28 (t, J = 7.9 Hz, 0H), 7.09 (t, J = 7.9 Hz, 1H), 6.95 (d, J = 7.6 Hz, 0H), 6.90 (t, J = 2.1 Hz, 0H), 6.88 – 6.84 (m, 0H), 6.78 (d, J = 8.2 Hz, 0H), 6.76 – 6.73 (m, 2H), 6.69 (t, J = 2.0 Hz, 1H), 6.68 (dd, J = 8.2, 2.0 Hz, 0H), 6.65 (d, J = 2.0 Hz, 0H), 6.63 – 6.60 (m, 2H), 6.47 (s, 2H), 6.41 (s, 1H), 6.39 (d, J = 7.6 Hz, 1H), 5.79 (t, J = 7.0 Hz, 0H), 5.55 (dd, J = 8.2, 5.5 Hz, 1H), 5.46 (d, J = 5.6 Hz, 1H), 4.71 (d, J = 5.8 Hz, 0H), 4.55 (d, J = 13.6 Hz, 0H), 4.14 – 4.08 (m, 1H), 4.06 (t, J = 5.7 Hz, 2H), 3.93 (d, J = 13.6 Hz, 1H), 3.85 (s, 1H), 3.84 (s, 1H), 3.84 (s, 3H), 3.83 (s, 5H), 3.82 (s, 1H), 3.76 (s, 3H), 3.71 (t, J = 4.7 Hz, 6H), 3.70 (s, 5H), 3.36 (d, J = 9.8 Hz, 1H), 2.96 (d, J = 9.7 Hz, 0H), 2.81 – 2.78 (m, 1H), 2.77 (t, J = 5.7 Hz, 2H), 2.65 – 2.52 (m, 6H), 2.46 (ddd, J = 14.4, 9.4, 5.3 Hz, 1H), 2.37 (ddd, J = 13.9, 9.1, 7.0 Hz, 1H), 2.28 (d, J = 13.7 Hz, 1H), 2.13 – 2.04 (m, 2H), 2.03 (s, 0H), 1.95 (dtd, J = 14.0, 8.7, 5.3 Hz, 1H), 1.87 (d, J = 11.9 Hz, 1H), 1.85 – 1.75 (m, 1H), 1.72 – 1.64 (m, 2H), 1.64 – 1.61 (m, 2H), 1.61 – 1.52 (m, 2H), 1.45 – 1.37 (m, 1H), 1.36 – 1.27 (m, 2H), 1.27 – 1.21 (m, 1H), 1.19 – 1.07 (m, 3H), 0.99 (t, J = 12.6 Hz, 0H), 0.89 (qd, J = 12.5, 3.5 Hz, 1H), 0.78 – 0.71 (m, 1H), 0.64 – 0.50 (m, 1H). <sup>13</sup>C-NMR (176 MHz, CDCl<sub>3</sub>): δ 172.4, 172.3, 171.2, 170.7, 170.6, 159.1, 158.7, 153.4, 153.1, 149.1, 148.9, 147.6, 147.4, 141.9, 141.6, 137.1, 136.9, 134.4, 133.7, 133.6, 133.4, 129.9, 129.6, 120.3, 120.2, 119.2, 118.5, 114.2, 113.8, 113.4, 113.2, 111.9, 111.8, 111.5, 111.4, 105.9, 105.4, 76.9, 75.7, 67.0, 67.0, 65.9, 65.8, 61.0, 60.9, 60.5, 57.8, 56.4, 56.1, 56.0, 56.0, 56.0, 56.0, 55.9, 55.9, 55.8, 55.1, 54.2, 52.1, 43.7, 41.5, 41.2, 39.5, 38.1, 37.9, 33.1, 32.9, 31.6, 31.1, 30.8, 30.6, 26.9, 26.7, 26.5, 26.3, 26.3, 26.2, 25.6, 24.4, 21.1, 21.1, 20.8, 14.3. UHPLC-MS: t<sub>R</sub> = 1.614 min (> 99%), m/z: calculated = 803.45 [M+H]<sup>+</sup>, found = 803.4 [M+H]<sup>+</sup>.

**(R)-1-tert-Butyl 2-((R)-3-(3,4-dimethoxyphenyl)-1-(3-(2-morpholinoethoxy)phenyl)prop-yl) piperidine-1,2-dicarboxylate: 4.00 g**

(10.0 mmol, 1.0 eq) **10**, 2.40 g (10.5 mmol, 1.05 eq) *R*-N-Boc-pipecolate, and 0.24 g (2.0 mmol, 0.2 eq) DMAP are dissolved in 50 mL DCM. The mixture is cooled to 0 °C and 2.01 g (10.5 mmol, 1.05 eq) DCC are added. The mixture is stirred overnight at room temperature before the reaction is quenched by addition of brine. The mixture is extracted with DCM, dried with MgSO<sub>4</sub>, and volatiles are removed under reduced pressure. The crude product is purified by manual column chromatography (EA/TEA/MeOH 100:3:1) to yield 4.78 g (78%) as a white solid. <sup>1</sup>H-NMR (500 MHz, CDCl<sub>3</sub>): δ 7.23 (td, J = 7.9, 5.2 Hz, 1H), 6.90 (q, J = 6.9 Hz, 1H), 6.85 (d, J = 1.8 Hz, 1H), 6.84 – 6.79 (m, 2H), 6.77 (d, J = 8.1 Hz, 1H), 6.68 (dd, J = 8.0, 2.0 Hz, 1H), 6.66 (d, J = 2.0 Hz, 1H), 5.74 (dt, J = 32.3, 6.9 Hz, 1H), 4.98 – 4.88 (m, 1H), 4.77 (s, 0H), 4.09 (t, J = 5.8 Hz, 2H), 3.88 – 3.82 (m, 6H), 3.75 – 3.69 (m, 4H), 2.93 (dt, J = 34.6, 13.1 Hz, 1H), 2.78 (t, J = 5.7 Hz, 2H), 2.66 – 2.47 (m, 6H), 2.22 (qd, J = 15.3, 10.0 Hz, 3H), 2.04 (ddd, J = 16.2, 12.9, 6.4 Hz, 1H), 1.72 – 1.52 (m, 3H), 1.43 (d, J = 32.0 Hz, 11H), 1.22 – 1.02 (m, 1H). <sup>13</sup>C-NMR (126 MHz, CDCl<sub>3</sub>): δ 171.5, 171.3, 159.0, 156.1, 155.4, 149.0, 147.5, 142.3, 141.9, 133.8, 133.7, 129.6, 120.3, 118.8, 114.1, 113.9, 113.2, 112.6, 111.9, 111.5, 80.1, 80.0, 76.2, 76.1, 67.0, 65.9, 57.8, 56.0, 56.0, 55.0, 54.2, 53.9, 42.3, 41.2, 38.5, 38.4, 31.6, 31.4, 28.5, 26.9, 26.8, 24.9, 24.7, 20.8, 20.7. UHPLC-MS: t<sub>R</sub> = 1.786 min (97%), m/z: calculated = 613.35 [M+H]<sup>+</sup>, found = 613.2 [M+H]<sup>+</sup>.

**(R)-(R)-3-(3,4-Dimethoxyphenyl)-1-(3-(2-morpholinoethoxy)phenyl)propyl-piperidine-2-carboxylate (11)**: 4.78 g (7.8 mmol, 1.0 eq) **(R)-1-tert-Butyl 2-((R)-3-(3,4-dimethoxyphenyl)-1-(3-(2-morpholinoethoxy)phenyl)prop-yl) piperidine-1,2-dicarboxylate** is dissolved in 24 mL DCM and 12 mL TFA. The mixture is stirred for 1.5 h at room temperature before the mixture was concentrated under reduced pressure and the reaction was neutralized with sodium carbonate. The mixture is extracted with DCM, dried with MgSO<sub>4</sub>, and volatiles are removed under reduced

pressure. The crude product (4.0 g quant.) is used without further purification. <sup>1</sup>H-NMR (500 MHz, CDCl<sub>3</sub>): δ 7.22 (td, J = 7.9, 1.4 Hz, 1H), 6.89 (dt, J = 7.7, 1.3 Hz, 1H), 6.85 (dd, J = 2.6, 1.6 Hz, 1H), 6.80 (ddd, J = 8.2, 2.6, 1.0 Hz, 1H), 6.76 (dd, J = 7.9, 1.4 Hz, 1H), 6.69 – 6.62 (m, 2H), 5.74 (dd, J = 7.9, 5.8 Hz, 1H), 4.08 (td, J = 5.8, 2.3 Hz, 2H), 3.84 (d, J = 1.3 Hz, 3H), 3.83 (d, J = 1.3 Hz, 3H), 3.74 – 3.69 (m, 4H), 3.42 – 3.32 (m, 1H), 3.06 (dt, J = 12.2, 3.7 Hz, 1H), 2.77 (td, J = 5.8, 1.4 Hz, 2H), 2.69 – 2.60 (m, 1H), 2.59 – 2.47 (m, 6H), 2.28 – 2.17 (m, 1H), 2.10 – 1.99 (m, 2H), 1.98 – 1.91 (m, 1H), 1.74 (dq, J = 7.7, 3.4 Hz, 1H), 1.60 – 1.53 (m, 1H), 1.51 – 1.33 (m, 3H). <sup>13</sup>C-NMR (126 MHz, CDCl<sub>3</sub>): δ 172.8, 158.9, 148.9, 147.4, 142.0, 133.7, 129.6, 120.2, 119.0, 113.9, 113.2, 113.1, 111.8, 111.4, 75.7, 67.0, 65.9, 58.7, 57.7, 56.0, 55.9, 54.2, 45.8, 37.9, 31.4, 29.3, 26.0, 24.1. UHPLC-MS: t<sub>R</sub> = 1.256 min (97%), m/z: calculated = 513.30 [M+H]<sup>+</sup>, found = 513.2 [M+H]<sup>+</sup>.

**(R)-(R)-3-(3,4-Dimethoxyphenyl)-1-(3-(2-morpholinoethoxy)phenyl)propyl**

**1-((R)-2-cyclohexyl-2-(3,4,5-trimethoxyphenyl)acetyl)piperidine-2-carboxylate**

**(ddSAFit, 12):** 2.03 g (6.6 mmol, 1.0 eq) **4a**, and 2.63 g (6.9 mmol, 1.05 eq) HATU, and 4.6 mL (26.3 mmol, 4.0 eq) DiPEA are dissolved in 10 mL of DMF. The mixture is stirred for 30 min at room temperature before 4.0 g (7.8 mmol, 1.2 eq) **11** dissolved in 50 mL DCM are added. The mixture is stirred overnight at room temperature before the reaction is quenched by addition of brine. The mixture is extracted with EA, dried with MgSO<sub>4</sub>, and volatiles are removed under reduced pressure. The crude product is purified by preparative HPLC and flash column chromatography (Cy/EA+3% TEA) to yield 4.12 g (78%) as a white solid. <sup>1</sup>H-NMR (700 MHz, CDCl<sub>3</sub>): δ 7.29 – 7.25 (m, 0H), 7.18 (t, J = 8.0 Hz, 1H), 6.94 (d, J = 7.6 Hz, 0H), 6.93 – 6.83 (m, 1H), 6.80 – 6.73 (m, 3H), 6.71 – 6.64 (m, 1H), 6.62 – 6.56 (m, 2H), 6.49 (s, 1H), 6.41 (s, 1H), 5.78 (dd, J = 7.9, 6.2 Hz, 0H), 5.55 (dd, J = 8.4, 5.2 Hz, 1H), 5.43 – 5.40 (m, 1H), 4.73 (d, J = 5.6 Hz, 0H), 4.66 (d, J = 13.6 Hz, 0H), 4.12 – 4.02 (m, 2H), 3.96 (d, J = 13.8 Hz, 1H), 3.87

– 3.80 (m, 9H), 3.77 (s, 6H), 3.74 – 3.69 (m, 4H), 3.38 (d, J = 9.8 Hz, 1H), 3.10 (d, J = 9.6 Hz, 0H), 2.97 (td, J = 13.4, 2.9 Hz, 1H), 2.78 (dt, J = 17.0, 5.7 Hz, 2H), 2.65 – 2.51 (m, 5H), 2.47 (ddd, J = 14.3, 9.0, 5.5 Hz, 1H), 2.36 (dt, J = 14.6, 7.8 Hz, 1H), 2.26 (dd, J = 12.0, 4.1 Hz, 1H), 2.15 – 2.02 (m, 2H), 1.98 – 1.85 (m, 3H), 1.74 – 1.50 (m, 5H), 1.43 (q, J = 12.9 Hz, 1H), 1.37 – 1.08 (m, 4H), 1.06 – 0.97 (m, 0H), 0.92 (qd, J = 12.4, 3.5 Hz, 1H), 0.82 – 0.55 (m, 1H). <sup>13</sup>C-NMR (176 MHz, CDCl<sub>3</sub>): δ 172.8, 171.9, 170.6, 170.5, 159.0, 153.4, 153.1, 149.1, 149.0, 147.6, 147.4, 142.3, 141.3, 137.1, 136.9, 134.3, 133.6, 133.6, 133.4, 129.8, 129.7, 120.3, 120.3, 120.2, 119.3, 118.5, 114.1, 113.8, 113.6, 112.7, 111.9, 111.8, 111.5, 111.4, 105.9, 105.4, 77.0, 75.7, 67.0, 67.0, 66.0, 65.9, 61.0, 60.8, 57.8, 57.8, 56.3, 56.2, 56.1, 56.1, 55.9, 55.8, 55.1, 54.2, 54.2, 52.3, 43.7, 41.6, 41.2, 39.7, 38.2, 37.9, 33.2, 32.9, 31.6, 31.3, 30.8, 30.8, 26.9, 26.8, 26.7, 26.7, 26.4, 26.3, 26.3, 26.3, 25.6, 24.6, 21.0, 20.8. UHPLC-MS: t<sub>R</sub> = 1.881 min (> 99%), m/z: calculated = 803.45 [M+H]<sup>+</sup>, found = 803.4 [M+H]<sup>+</sup>. HRMS: m/z: calculated = 803.4477, found = 803.4461 [M+H]<sup>+</sup> (1.99 ppm error)

---

### 3 Publication 2

---

## The FKBP51 Inhibitor SAFit2 Restores the Pain-Relieving C16 Dihydroceramide after Nerve Injury

Saskia Wedel<sup>1</sup>, Lisa Hahnefeld<sup>1,2</sup>, Mohamad Wessam Alnouri<sup>3</sup>, Stefan Offermanns<sup>3,4</sup>, Felix Hausch<sup>5</sup>, Gerd Geisslinger<sup>1,2</sup> and Marco Sisignano<sup>1,2</sup>

<sup>1</sup> Institute of Clinical Pharmacology, Pharmazentrum Frankfurt/ZAFES, University Hospital, Goethe-University, 60590 Frankfurt am Main, Germany

<sup>2</sup> Fraunhofer Institute for Translational Medicine and Pharmacology ITMP, Fraunhofer Cluster of Excellence for Immune Mediated Diseases CIMD, 60596 Frankfurt am Main, Germany

<sup>3</sup> Max Planck Institute for Heart and Lung Research, 61231 Bad Nauheim, Germany

<sup>4</sup> Center for Molecular Medicine, Goethe-University Frankfurt, 60590 Frankfurt am Main, Germany

<sup>5</sup> Department of Biochemistry, Technical University Darmstadt, 64287 Darmstadt, Germany

### 3.1 Author contributions

Conceptualization: FH, MS and GG conceptualized the project.

Funding acquisition: MS and FH acquired the funding.

Experimental design: **SW**, SO, and MS designed the experiments.

Data acquisition: **SW** performed the qPCRs, calcium imaging experiments and *in vivo* experiments. LH conducted the LC-HRMS measurement and MWA performed the GPCR screen.

Data analysis: **SW** analyzed all the data. LH helped with the LC-HRMS analysis.

Data curation: **SW** performed the data curation.

Original draft preparation: **SW** and MS wrote and revised the manuscript.

All authors approved the final manuscript.

## 3.2 Manuscript





International Journal of  
Molecular Sciences



Article

# The FKBP51 Inhibitor SAFit2 Restores the Pain-Relieving C16 Dihydroceramide after Nerve Injury

Saskia Wedel<sup>1</sup>, Lisa Hahnefeld<sup>1,2</sup> , Mohamad Wessam Alnouri<sup>3</sup>, Stefan Offermanns<sup>3,4</sup>, Felix Hausch<sup>5</sup>, Gerd Geisslinger<sup>1,2</sup> and Marco Sisignano<sup>1,2,\*</sup> 

- <sup>1</sup> Institute of Clinical Pharmacology, Pharmazentrum Frankfurt/ZAFES, University Hospital, Goethe-University, 60590 Frankfurt am Main, Germany
  - <sup>2</sup> Fraunhofer Institute for Translational Medicine and Pharmacology ITMP, Fraunhofer Cluster of Excellence for Immune Mediated Diseases CIMD, 60596 Frankfurt am Main, Germany
  - <sup>3</sup> Max Planck Institute for Heart and Lung Research, 61231 Bad Nauheim, Germany
  - <sup>4</sup> Center for Molecular Medicine, Goethe-University Frankfurt, Theodor-Stern-Kai 7, 60590 Frankfurt am Main, Germany
  - <sup>5</sup> Department of Biochemistry, Technical University Darmstadt, 64287 Darmstadt, Germany
- \* Correspondence: marco.sisignano@med.uni-frankfurt.de

**Abstract:** Neuropathic pain is a pathological pain state with a broad symptom scope that affects patients after nerve injuries, but it can also arise after infections or exposure to toxic substances. Current treatment possibilities are still limited because of the low efficacy and severe adverse effects of available therapeutics, highlighting an emerging need for novel analgesics and for a detailed understanding of the pathophysiological alterations in the onset and maintenance of neuropathic pain. Here, we show that the novel and highly specific FKBP51 inhibitor SAFit2 restores lipid signaling and metabolism in nervous tissue after nerve injury. More specifically, we identify that SAFit2 restores the levels of the C16 dihydroceramide, which significantly reduces the sensitization of the pain-mediating TRPV1 channel and subsequently the secretion of the pro-inflammatory neuropeptide CGRP in primary sensory neurons. Furthermore, we show that the C16 dihydroceramide is capable of reducing acute thermal hypersensitivity in a capsaicin mouse model. In conclusion, we report for the first time the C16 dihydroceramide as a novel and crucial lipid mediator in the context of neuropathic pain as it has analgesic properties, contributing to the pain-relieving properties of SAFit2.

**Keywords:** neuropathic pain; lipid mediators; ceramides; sensory neurons; nerve injury; FKBP51



**Citation:** Wedel, S.; Hahnefeld, L.; Alnouri, M.W.; Offermanns, S.; Hausch, F.; Geisslinger, G.; Sisignano, M. The FKBP51 Inhibitor SAFit2 Restores the Pain-Relieving C16 Dihydroceramide after Nerve Injury. *Int. J. Mol. Sci.* **2022**, *23*, 14274. <https://doi.org/10.3390/ijms232214274>

Academic Editor: Hartmut Kthn

Received: 26 October 2022

Accepted: 16 November 2022

Published: 17 November 2022

**Publisher's Note:** MDPI stays neutral with regard to jurisdictional claims in published maps and institutional affiliations.



**Copyright:** © 2022 by the authors. Licensee MDPI, Basel, Switzerland. This article is an open access article distributed under the terms and conditions of the Creative Commons Attribution (CC BY) license (<https://creativecommons.org/licenses/by/4.0/>).

## 1. Introduction

Chronic pain and especially neuropathic pain as persistent pain states affect patients worldwide after nerve injuries, chemotherapies, or diseases such as diabetes and multiple sclerosis. However, the available therapeutics for efficient pain relief are currently inadequate, pointing out neuropathic pain as a pathological entity with a lack of treatment possibilities and a broad symptom scope [1,2]. Former studies revealed FK506 binding protein 51 (FKBP51), which is encoded by the FKBP5 gene, as a novel and promising target for various pathologies, since it is involved in many different pathological processes, such as the establishment of chronic pain [3,4], stress endocrinology difficulties [5], and glucocorticoid signaling-related diseases [6]. Moreover, the highly potent FKBP51 inhibitor SAFit2 has been shown to pass the blood-brain barrier [7,8], indicating that SAFit2 is also able to pass the blood spinal cord barrier and can mediate analgesic effects in the central and peripheral nervous system. Likewise, we recently showed that SAFit2 ameliorates neuropathic pain in vivo as it counteracts the enhanced neuronal activity and reduces neuroinflammation after nerve injury [9]. These previous reports highlight the concept of FKBP51 inhibitors as a potential novel treatment approach for neuropathic pain.

Mechanistically, SAFit2 reduces the NF- $\kappa$ B pathway activation after nerve injury, potentially also modulating crucial target genes in the NF- $\kappa$ B downstream signaling [9]. NF- $\kappa$ B itself is a crucial transcription factor in lipid metabolism as it regulates the expression of various enzymes, such as cyclooxygenases, lipoxygenases, and phospholipases [10,11]. These enzymes metabolize and oxidize eicosanoids, linoleic acid metabolites, and sphingolipids, generating lipid mediators that can act as autocrine and paracrine signaling mediators [12]. In addition, previous studies have already demonstrated that lipid mediators can contribute to pain hypersensitivities after chemotherapeutic treatment or nerve injury [13–15]. Importantly, it was shown that lipid mediators can affect the sensitivity or activation threshold of ion channels in sensory neurons, especially of pain-mediating transient receptor potential cation (TRP) channels, which can result in an enhanced neuronal activity, leading to increased pain perception and neuroinflammation [14,16–20]. Moreover, alterations in the subset of lipid mediators were shown to be associated with nerve dysfunctions and chronic pain.

In the development of neuropathic pain, metabolites from the ceramide/sphingolipid pathway were identified as potential targets for treating neuroinflammation, as they were implicated to be crucial regulators at the neuroimmune interface [21]. Particularly, the sphingolipid sphingosine1-phosphate (S1P) is known to sensitize TRP subfamily V member 1 (TRPV1) in inflammatory processes, leading to hypersensitivity and enhanced neuropathic pain [21–23]. However, the influence of other S1P pathway metabolites, such as ceramides and dihydroceramides, on TRP channels has not yet been investigated in the context of neuropathic pain.

In the present study, we focus on the peripheral nervous system and the interface between the peripheral and the central nervous system. We investigated the expression of lipid-generating enzymes and performed lipidomic analysis in sensory neurons of the dorsal root ganglia, as they are the central location of the cell somata of peripheral sensory neurons, and in the dorsal spinal cord. Here, we detected that the neuropathic pain-ameliorating FKBP51 inhibitor SAFit2 also affects the expression of lipid-oxidizing enzymes, such as lipoxygenases, as well as ceramide synthases in the context of nerve injury-induced neuropathic pain in mice. An unbiased LC-HRMS-based lipidomics screening from lumbar dorsal root ganglia (DRGs) and spinal cords revealed that SAFit2 is capable of counteracting the nerve injury-induced alterations in lipid levels after SNI. While the levels of classical eicosanoids were not significantly altered, SAFit2 especially restores the levels of the C16 dihydroceramide (N-palmitoyl-D-erythro-sphinganine) after nerve injury. Neurobiological characterization of the C16 dihydroceramide showed that it significantly reduces the sensitization of TRPV1 in sensory neurons and subsequently the release of the pro-inflammatory neuropeptide CGRP (calcitonin gene-related peptide). Furthermore, the C16 dihydroceramide was shown to significantly decrease the thermal hypersensitivity of mice in an acute pain model, attributing C16 dihydroceramide potential analgesic or antihyperalgesic properties. In summary, we discovered that interfering with the FKBP51 signaling with the inhibitor SAFit2 can influence lipid signaling and metabolism in nervous tissue after nerve injury. In addition, we identified the C16 dihydroceramide as a novel and previously unrelated crucial lipid mediator in the context of neuropathic pain.

## 2. Results

### 2.1. SAFit2 Reduces the Upregulation of Lipid-Oxidizing and -Metabolizing Enzymes after SNI

To investigate the influence of SAFit2 on lipid metabolism after nerve injuries, we first analyzed the expression of lipid-oxidizing enzymes, which play a crucial role in the generation of signaling lipids and lipid metabolites, and which can influence the onset and maintenance of inflammation [12]. Therefore, we performed a spared nerve injury model on mice and treated them intraperitoneally with either 10 mg/kg SAFit2 or vehicle two times daily on six consecutive days (days five to ten) after SNI (Figure 1A). After 21 days, the mice were sacrificed, and lumbar L4-L6 dorsal root ganglia (DRGs) as well as the corresponding section of the spinal cord (SC) were collected to measure the expression



of ceramide synthases, lipoxygenases, cyclooxygenases, phospholipases, and cytochrome-P<sub>450</sub>-oxygenases (Figure 1B–I).

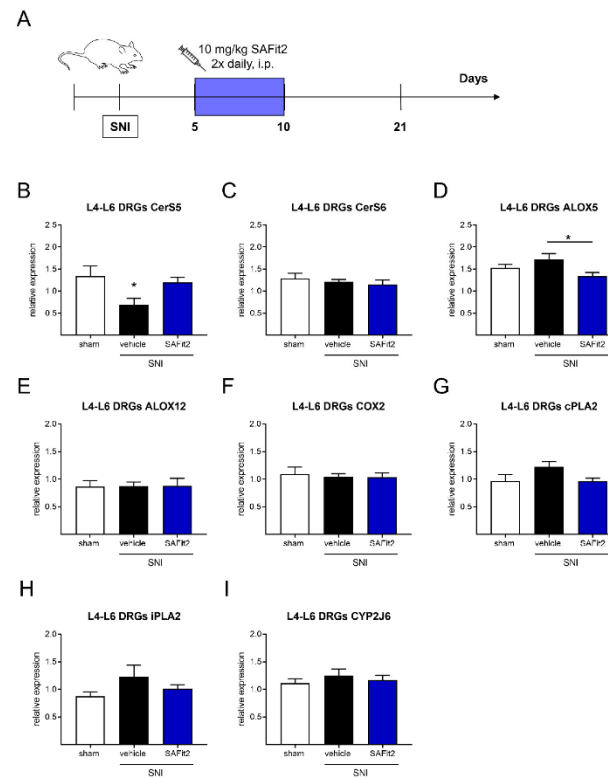


**Figure 1.** Gene expression of ceramide synthases, lipoxygenases, phospholipases, and epoxygenases in lumbar DRGs of nerve-injured mice after additional SAFit2 treatment. (A) Schematic illustration of the experimental procedure: SNI surgery was performed followed by a treatment with either 10 mg/kg SAFit2 or vehicle on six consecutive days (days five to ten) after SNI. The gene expression of ceramide synthases (B,C), lipoxygenases (D–F), phospholipases (G,H), and epoxygenase (I) was measured 21 days after the surgery. The data are displayed as the mean  $\pm$  SEM of technical replicates from three to four mice per treatment. \*  $p < 0.05$ , as per one-way ANOVA with Tukey’s post-hoc test. Abbreviations: DRGs: dorsal root ganglia; SAFit2: selective antagonist of FKBP51 by induced fit 2; SNI: spared nerve injury; CerS: ceramide synthase; ALOX: arachidonate lipoxygenase; COX2: cyclooxygenase 2; cPLA2: cytosolic phospholipase A2; iPLA2: calcium-independent phospholipase A2; CYP2J6: cytochrome P450 family 2 subfamily j polypeptide 6.

Interestingly, we detected a significant reduction in ceramide synthase 5 (CerS5), which is required for the synthesis of long-chain ceramides [24], in the lumbar DRGs after SNI (Figure 1B), after conducting a one-way ANOVA with Tukey’s post-hoc test. In addition, we observed a significant difference in the expression of the arachidonate lipoxygenase 5 (ALOX5) in DRGs between the vehicle and SAFit2-treated animals (Figure 1D). However, the cyclooxygenase 2 (COX2, Figure 1F), which is typically upregulated in inflammatory processes synthesizing prostaglandins [25], shows an unaltered expression after SNI at our investigated time point. Likewise, the expression of other enzymes, such as ceramide synthase 6 (CerS6, Figure 1C), arachidonate lipoxygenase 12 (ALOX12, Figure 1E), phospholipases cPLA2 and iPLA2 (Figure 1G,H), and cytochrome-P<sub>450</sub>-oxygenase CYP2J6 (Figure 1I), were not significantly altered in the lumbar DRGs after SNI, when comparing treatments using one-way ANOVA with a Tukey’s post-hoc test. In addition, the expres-

sion of the arachidonate lipoxygenase 15 (ALOX15) and the cytochrome-P<sub>450</sub>-oxygenase CYP3a11 was below the detection limit in lumbar DRGs.

As we analyzed the expression of the same enzymes in the respective segments of the spinal cord and determined significant alterations with a one-way ANOVA and Tukey's post-hoc test (Figure 2), we again detected an alteration in the expression of ceramide synthases and lipoxygenases. However, this time ceramide synthases 5 and 6 were both significantly upregulated in the vehicle-treated SNI animals (Figure 2B,C). In addition, the expression of the ceramide synthase 6 differs significantly between the vehicle and SAFit2-treated SNI animals, whereas it is quite comparable between SAFit2 and the sham treatment in the spinal cord after SNI (Figure 2C). Furthermore, the expression of arachidonate lipoxygenase 12 (ALOX12) was significantly altered between the vehicle and SAFit2-treated animals in the spinal cord (Figure 2E). The expression of the other lipoxygenases, cyclooxygenases, phospholipases, and cytochrome-P<sub>450</sub>-oxygenases was not changed in the spinal cord after SNI (Figure 2D,F–I). Expression of arachidonate lipoxygenase 15 (ALOX15) and cytochrome-P<sub>450</sub>-oxygenase CYP3a11 was not detectable in the spinal cord.

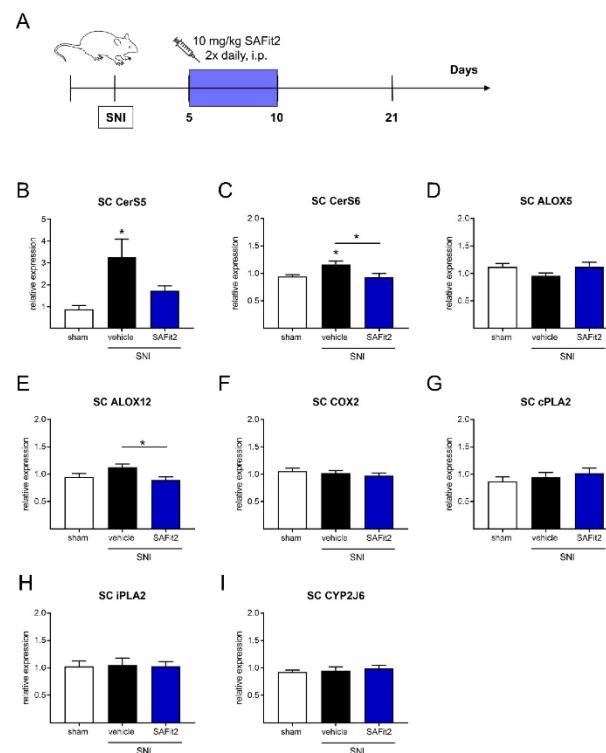


**Figure 2.** Gene expression of ceramide synthases, lipoxygenases, phospholipases, and epoxygenases in the spinal cord of nerve-injured mice after additional SAFit2 treatment. (A) Schematic illustration of the experimental procedure: SNI surgery was performed followed by treatment with either 10 mg/kg SAFit2 or the vehicle on six consecutive days (days five to ten) after SNI, as depicted in Figure 1. The gene expression of ceramide synthases (B,C), lipoxygenases (D–F), phospholipases (G,H), and epoxygenase (I) was measured 21 days after the surgery. The data are displayed as the mean  $\pm$  SEM of technical replicates of three to four mice per treatment. \*  $p < 0.05$ , as per one-way ANOVA with a Tukey's post-hoc test. Abbreviations: SAFit2: selective antagonist of FKBP51 by induced fit 2; SNI: spared nerve injury; CerS: ceramide synthase; ALOX: arachidonate lipoxygenase; COX2: cyclooxygenase 2; cPLA2: cytosolic phospholipase A2; iPLA2: calcium-independent phospholipase A2; CYP2J6: cytochrome P450 family 2 subfamily j polypeptide 6.

## 2.2. The Influence of SAFit2 on Lipid Levels after SNI

Next, we performed an untargeted lipid screening using LC-HRMS to investigate the influence of SAFit2 on lipids after nerve injury. Therefore, we analyzed the lipid distribution in L4-L6 DRGs and the respective parts of the spinal cord 21 days after SNI surgery (Figure 3). In the lipid screening, we detected 249 lipids from 14 classes—fatty acids, ceramides, diglycerides, lysophosphatidylcholines, -ethanolamines, -glycerols, -inositols, phosphatidylcholines, -ethanols, -glycerols, -inositols, -serines, sphingomyelins, and triglycerides—which can be partially further divided into subclasses (Figure 3A). For further analysis, the analytes were sorted into their lipid classes and ipsilateral values and normalized to the contralateral values, performed for every lipid. In addition, the differences between the normalized treatments were compared in heat maps for the spinal cord (Figure 3B) and lumbar DRGs (Figure 3C), separately. For lipids in the spinal cord, only slight changes were observed after nerve injury (Figure 3B). Nevertheless, some lipid classes show minor trends, such as the downregulation of fatty acids or the upregulation of lysophosphatidylethanol and phosphatidylcholines after SNI. However, these effects could be counteracted with a 10 mg/kg SAFit2 treatment after SNI. In contrast, the alterations between the treatments were stronger in the lumbar DRGs comparing the vehicle and SAFit2 treatment after SNI (Figure 3C). The classes of ceramides, diglycerides, fatty acids, lysophosphatidylglycerols, and phosphatidylcholins were clearly downregulated in the vehicle-treated SNI animals compared to the sham-treated animals. Whereas, the SAFit2 treatment counteracted this downregulation after nerve injury, adjusting the concentrations to levels comparable to the sham. In contrast, the lysophosphatidylcholins and lysophosphatidylethanol were upregulated after SNI in the vehicle-treated group while these lipids were less upregulated in the SAFit2-treated group. In summary, SAFit2 seems to compensate the SNI-induced alterations and shifts in lipid synthesis and metabolism in the respective tissues.

For investigating the effect of SAFit2 on individual lipids, we plotted the logarithmic *p*-value, which was calculated with of a two-way ANOVA and Tukey's post-hoc test, of the two treatments against the logarithmic fold change in volcano plots for DRGs, as we have seen major differences in this tissue (Figure 3D). In Figure 3D (top), we compared the vehicle-treated SNI animals with sham animals to elucidate the impact of nerve injury on lipids, discovering four significantly altered lipids. In this comparison, the C16 dihydroceramide (d18:0/16:0), the 36:4 diglyceride, and the polyunsaturated fatty acid docosahexaenoic acid were significantly downregulated, whereas the 16:1 ether-lysophosphatidylcholine was significantly upregulated after nerve injury. Interestingly, the comparison of the vehicle and SAFit2-treated SNI animals revealed only the C16 dihydroceramide (d18:0/16:0) as a significantly altered lipid (Figure 3D (bottom)).

For showing the whole LC-HRMS dataset, the relative amount of each individual lipid is displayed in violin plots in Supplementary Material Figures S1–S3 for DRGs, and for the spinal cord samples, in Supplementary Material Figures S4–S6. The internal standards and the LC-gradient used for the analysis are highlighted in Tables S1 and S2. Summarizing the results from this broad screen, we detected that some lipid mediators, such as the C16 dihydroceramide (d18:0/16:0), 36:4 diglyceride, and docosahexaenoic acid, were significantly downregulated, and the 16:1 ether-lysophosphatidylcholine was significantly upregulated after SNI. However, the C16 dihydroceramide (d18:0/16:0) was the only lipid that was significantly altered comparing the vehicle and SAFit2 treatment after nerve injury. Based on this, we hypothesized that this C16 dihydroceramide might play a crucial role in the analgesic mechanism of SAFit2.

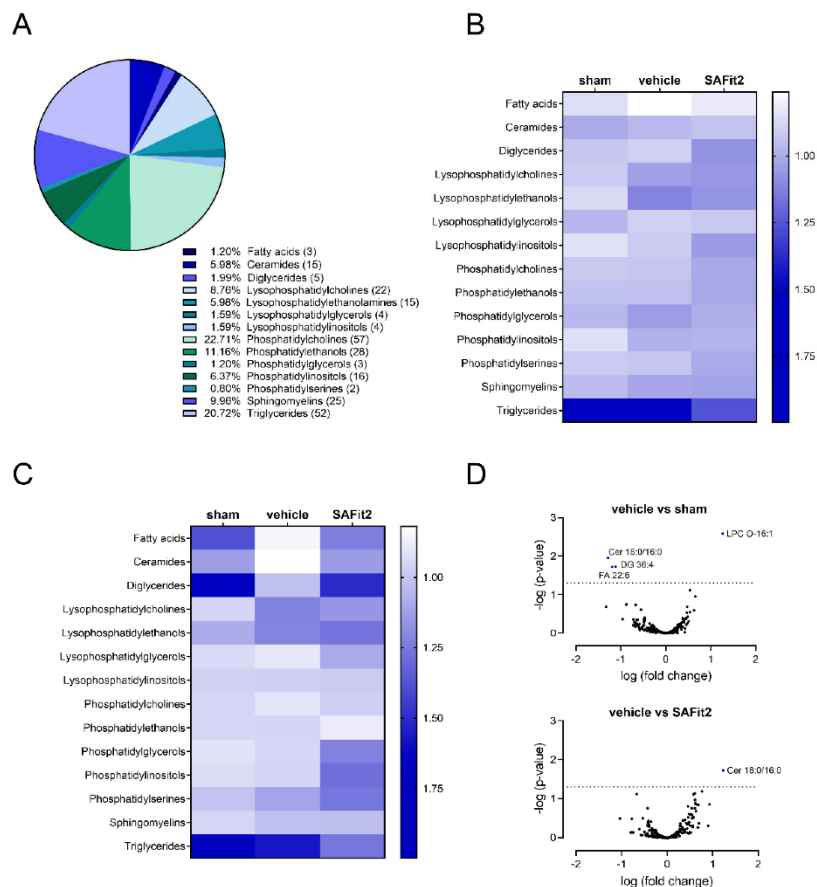


**Figure 3.** LC–HRMS lipid analysis of lumbar DRGs (L4–L6) and the respective segments of spinal cord from nerve-injured mice after additional SAFit2 treatment. **(A)** Distribution of the number of measured analytes per lipid class in LC–HRMS analysis. **(B)** Abundance of lipid classes in the spinal cord of the vehicle and 10 mg/kg SAFit2 treated SNI animals as well as sham animals. **(C)** Lipid levels of the lipid classes in lumbar DRGs of the vehicle and 10 mg/kg SAFit2-treated animals after SNI, and the sham animals. **(D)** Volcano plots comparing the lipid levels of the sham and vehicle-treated SNI animals (top) and vehicle and SAFit2-treated animals after SNI (bottom). A  $p$ -value of 0.05 was determined as a threshold for significance, which was calculated with a two-way ANOVA with a Tukey’s post-hoc test. All significantly altered lipids were labeled and depicted in blue. Abbreviations: DRGs: dorsal root ganglia; LC–HRMS: liquid chromatography–high-resolution mass spectrometry; SAFit2: selective antagonist of FKBP51 by induced fit 2; SNI: spared nerve injury.

### 2.3. C16 Dihydroceramide Desensitizes the TRPV1 Channel in Sensory Neurons

Based on the previous findings that SAFit2 reduces mechanical hypersensitivity after nerve injury [9], we investigated the influence of the C16 dihydroceramide (d18:0/16:0), which is named as C16 or C16 dihydroceramide in the following, on pain-sensing calcium channels. Firstly, we characterized the impact of C16 on the TRPV1 channel, as it is the most important and most abundantly expressed pain-mediating, ligand-gated calcium channel in sensory neurons, and plays a crucial role in the development of various pain conditions, including neuropathic pain [26].

To investigate the impact of C16 on TRPV1, we isolated sensory neurons from DRGs of naïve mice and analyzed the calcium transients of TRPV1 after C16 treatment in live cell

calcium imaging (Figure 4). For comparing the calcium transients with and without C16 treatment, a protocol was established in which the TRPV1 was stimulated twice: first, only with the agonist capsaicin, and second, with the pre-incubation of C16 (2 min), to verify whether C16 has an influence on the channel-mediated calcium influx (Figure 4A). Interestingly, we detected that C16 concentration-dependently reduced the calcium transients of TRPV1 in sensory neurons (Figure 4B), after comparing the different conditions using a one-way ANOVA with a Tukey's multiple-comparison test.

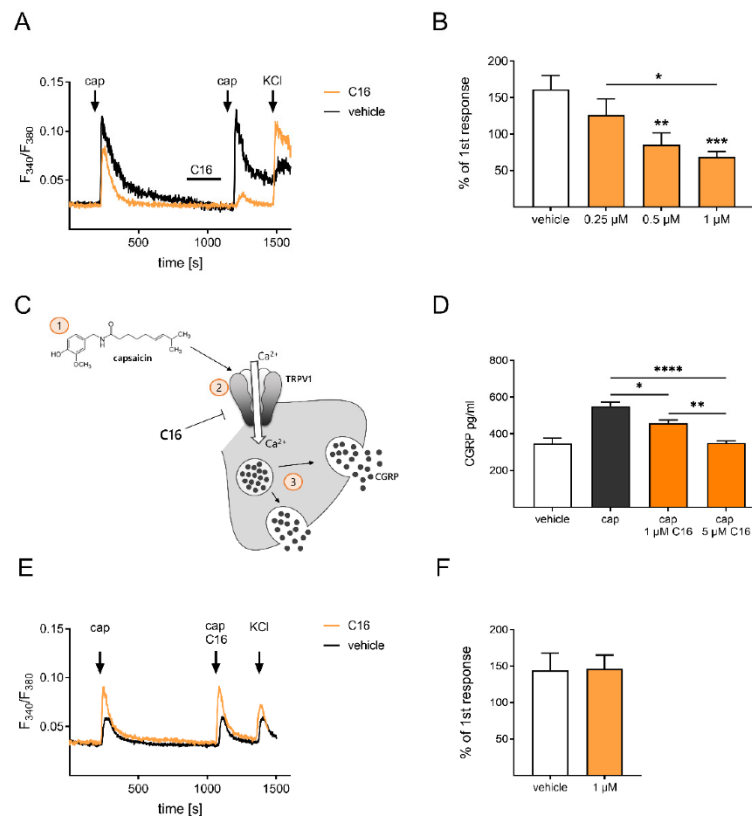


**Figure 4.** C16 dihydroceramide causes a desensitization of the TRPV1 channel and subsequently leads to a reduced CGRP release from primary sensory neurons. (A) Representative calcium responses of sensory neurons, which were pre-treated with C16 for 2 min, followed by an activation of the TRPV1 channel with the agonist capsaicin (100 nM, 30 s). Afterwards, the cells were treated with potassium chloride (50 mM, 45s) to discriminate reacting cells as neurons. (B) Quantification of the two calcium responses in (A) after capsaicin stimulation (untreated and C16 treated). (C) The schematic illustration displays the downstream signaling of TRPV1 after capsaicin activation, which results in the release of CGRP from sensory neurons. A scheme depicting the mechanism was designed using images from motifolio. (D) CGRP amount measured in the supernatant of C16 and capsaicin treated sensory neurons. (E) Representative calcium responses of sensory neurons, which were treated with both capsaicin (100 nM, 45 s) and C16 (1 μM, 45 s) at the same time point. (F) Quantification of the double stimulation from (E), ruling out antagonist properties of C16. (B,D) Each condition displays the mean  $\pm$  SEM of 23–38 measured primary sensory neurons. \*  $p < 0.05$ , \*\*  $p < 0.01$ , and \*\*\*  $p < 0.001$ , and \*\*\*\*  $p < 0.0001$ , as per one-way ANOVA with a Tukey's post-hoc test. Abbreviations: CGRP: calcitonin gene-related peptide; cap: capsaicin; KCl: potassium chloride; TRPV1: transient receptor potential cation channel subfamily V member 1.

Next, we further evaluated whether this reduced calcium flux has an impact on the TRPV1 downstream signaling pathway. Therefore, the release of the peptide calcitonin gene-related peptide (CGRP) was assessed in primary sensory neuron cultures via ELISA. The neuropeptide CGRP was released from sensory neurons due to increasing intracellular calcium concentrations and functions as a mediator in neuropathic pain (Figure 4C) [27,28]. Interestingly, we observed that the C16 concentration dependently also reduced the CGRP amount in the supernatant of the primary sensory neurons, which were treated with capsaicin beforehand (Figure 4D). Furthermore, the concentration dependency was considered as statistically significant after performing a one-way ANOVA with a Tukey's multiple-comparison test. Based on these results, we concluded that C16 reduces TRPV1-mediated calcium transients and subsequently reduces CGRP-mediated neuroinflammation.

Since many direct TRPV1 antagonists lead to severe side effects and failed in clinical trials [29], we next determined whether C16 inhibits or desensitizes the TRPV1 channel. Therefore, we changed the calcium imaging protocol in which we left out the pre-incubation step with C16, this time applying C16 together with capsaicin at the second stimulation time point (Figure 4E). However, we detected no alterations in the TRPV1-mediated calcium flux between the first and second stimulus (Figure 4F), summarizing that C16 does not directly inhibit the TRPV1 channel.

Next, we tried to elucidate how C16 reduces TRPV1-mediated calcium transients. We hypothesized that the reduced TRPV1 open probability is due to the desensitization of TRPV1, which may be indirectly mediated by a G protein coupled receptor (GPCR). To test this hypothesis, we performed a GPCR screen using three reporter assays to investigate the effect of C16 on 314 different GPCRs (Supplementary Material Figure S7, Table S3). However, we did not detect any C16-induced activation of a GPCR, concluding that C16 probably affects the TRPV1 open probability indirectly, possibly via interacting with the cell membrane.

#### 2.4. C16 Dihydroceramide Does Not Affect TRPA1 and P2X3 in Primary Sensory Neurons

For further characterizing C16 in the context of pain, we examined the influence of C16 on other TRP channels. As a first approach, we applied 1  $\mu$ M and 10  $\mu$ M C16 to sensory neurons to investigate whether C16 activates any calcium channels in sensory neurons (Supplementary Material Figure S8). However, we did not detect any calcium transients after the stimulation with C16.

Since we detected an influence of C16 on the TRPV1 channel, and since the TRPA1 channel (transient receptor potential ankyrin 1) is both co-expressed in a subgroup of TRPV1-positive sensory neurons as well as closely associated to the TRPV1, we also assessed the impact of C16 on the TRPA1 channel [30]. To examine this, we again performed a protocol involving two stimuli, however this time using allyl isothiocyanate (AITC) as the gold standard agonist of the TRPA1 channel (Figure 5A). We detected a slight increase in calcium transients after a pre-incubation with C16 compared to the vehicle control (Figure 5B). Nevertheless, the calcium transients were also increased after a pre-incubation with cremophor, using cremophor EL as a second, more lipophilic vehicle control. Based on these results, we suggest that C16 and cremophor EL does not sensitize the TRPA1; however, it increases the solubility of the lipophilic agonist AITC in Ringer's solution, which leads to a more efficient stimulation of sensory neurons.

Moreover, we analyzed the effect of C16 on the purinergic ligand-gated calcium channel P2X3, since it also plays a critical role in the development of neuropathic pain [31]. To stimulate the P2X3 channel, we used  $\alpha,\beta$ -methyleneadenosine 5'-triphosphate trisodium salt (meATP) as agonist (Figure 5C). As we compared calcium transients of P2X3 with and without C16 pre-incubation, we detected no differences (Figure 5D). In summary, we observed that C16 does not directly activate any calcium channel, has a desensitizing effect on TRPV1, and no influence on the activity of TRPA1 and P2X3.

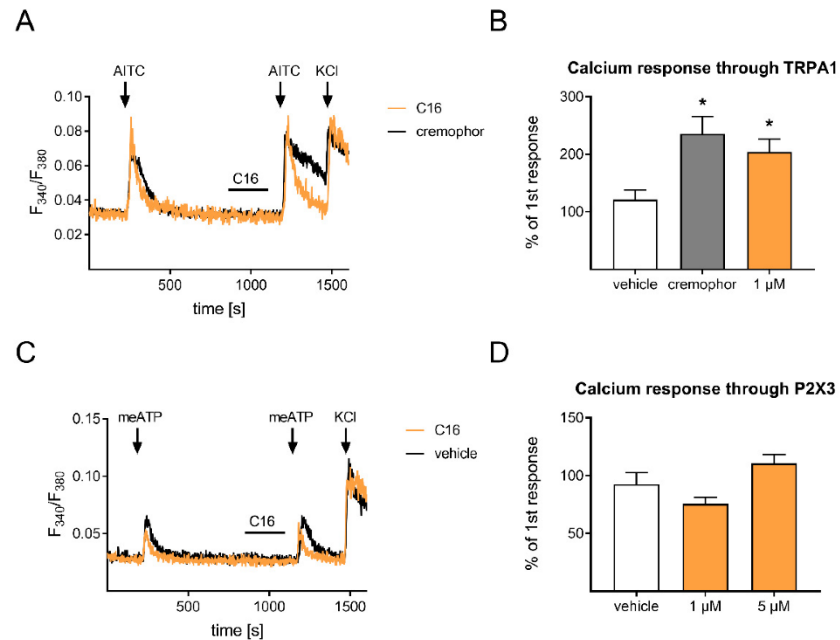


**Figure 5.** C16 dihydroceramide has no influence on the activity of TRPA1 and P2X3 in primary sensory neurons. (A) Representative calcium responses of sensory neurons, which were pre-incubated with C16 (2 min) and stimulated with the TRPA1 agonist AITC (100  $\mu$ M, 45 s) followed by a KCl (50 mM) treatment as a positive control. (B) Quantification of the two calcium responses in (A) after AITC stimulation (untreated and C16 treated). (C) Representative calcium responses of sensory neurons, which were pre-incubated with C16 (2 min) and stimulated with the P2X3 agonist meATP (50  $\mu$ M, 30 s) followed by a KCl (50 mM) treatment as a positive control. (D) Quantification of the two calcium responses in (C) after meATP stimulation (untreated and C16 treated). (B,D) The data represents the mean  $\pm$  SEM of 23–30 sensory neurons per group. \*  $p < 0.05$ , as per one-way ANOVA with a Tukey's post-hoc test. Abbreviations: TRPA1: transient receptor potential cation channel subfamily A member 1; AITC: allyl isothiocyanate; meATP:  $\alpha,\beta$ -methyleneadenosine 5' triphosphate trisodium salt; KCl: potassium chloride.

### 2.5. C16 Dihydroceramide Reduces Thermal Hypersensitivity after Capsaicin Treatment

As final step, we wanted to examine whether C16 can influence the thermal hypersensitivity of capsaicin-treated mice, as we detected a reduced TRPV1 activity after C16 treatment in vitro. Therefore, the thermal pain threshold of every mouse was assessed with the radiant heat test two times before treatment. Then, the mice were treated intraplantar with either 50  $\mu$ M C16 or vehicle and 400  $\mu$ M capsaicin. Afterwards, the thermal sensitivity of the mice paws was assessed over 4 h with a radiant heat test. Interestingly, we detected that the C16 treatment prevented the development of thermal hypersensitivity after capsaicin treatment in mice (Figure 6). In addition, the paw withdrawal latencies were significantly different comparing the vehicle and C16-treated mice for the time points 0.5, 1, 2, 3, and 4 h, as per assessment with a two-way ANOVA with Bonferroni's post-hoc test. These results reveal the analgesic properties of C16, pointing out that the desensitization of TRPV1 reduces the thermal hypersensitivity of mice.

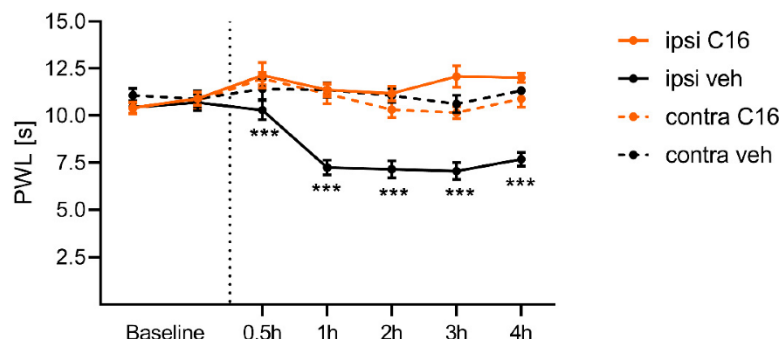


**Figure 6.** C16 dihydroceramide reduces the thermal hypersensitivity after capsaicin treatment in mice. We analyzed the baseline levels the day before and on the day of treatment. The mice were treated intraplantarly with either capsaicin and the C16 dihydroceramide or capsaicin and vehicle to analyze the analgesic properties of C16. The thermal pain threshold was assessed 30 min, 1 h, 2 h, 3 h, and 4 h after treatment. The data represent the mean  $\pm$  SEM from seven mice per group, \*\*\*  $p < 0.001$ , as per two-way ANOVA with Bonferroni's post-hoc test.

### 3. Discussion

Neuropathic pain affects around 10 percent of the general population and is induced by lesions and diseases of the somatosensory system, infections, or toxic substances [2]. However, the available therapies are very scarce because of their low efficacy and severe adverse effects [32]. Based on these circumstances, there is a high medical need for novel, safe, effective treatment approaches for neuropathic pain [32]. Nevertheless, the development of many therapy strategies failed, having faced the challenge that neuropathic pain is a multifunctional event mediated by various mediators with pleiotropic effects. In addition, the underlying mechanisms of this complex pain state are barely understood yet. In line with this, investigation of the endogenous mechanisms and alterations, for example, after nerve injury, is becoming increasingly important. Therefore, we tried to discover the alterations in lipids after SNI and assessed the influence of the potential therapeutic approach SAFit2 on these alterations.

The distribution and abundance of lipids affects various mechanisms and conditions, such as the structure of the myelin sheath, the fluidity of membranes, energy storage, and signaling pathways. In the last decades, a growing number of endogenous lipid mediators has been described to be involved in several signaling pathways and to modulate the activity of the TRP channels in sensory neurons [33]. Likewise, these endogenous lipid mediators play a crucial role in the context of persistent pain states, such as neuropathic pain and chronic pain [12,19,33,34]. Especially alterations and dysregulations in specific lipids were associated with nerve dysfunctions and neuropathic pain. A prominent example for lipid metabolism dysregulation, which results in neuropathic pain, is treatment with the cytostatic bortezomib, which significantly alters the sphingosine/ceramide pathway [20]. In contrast, the FDA-approved, S1P receptor-inhibiting substance fingolimod was shown to reduce neuropathic pain after nerve injury and in multiples sclerosis as it targets the sphingosine/ceramide pathway [35,36]. Nevertheless, alterations in the anandamide metabolism were previously associated with the development of chronic pain [37]. Furthermore, several studies have pointed out the importance of anti-inflammatory and analgesic lipid mediators, such as resolvins, in the resolution of inflammation and pain [38–41].

Here, we reveal that the selective FKBP51 inhibitor SAFit2 is capable to counteract pathophysiological alterations in lipid metabolism after SNI. More specifically, we observed that SAFit2 counteracts alterations in the expression of lipid-oxidizing enzymes as well as dysregulations in lipid classes. Likewise, the lipid classes of free fatty acids and ceramides were markedly downregulated in lumbar dorsal root ganglia and spinal cord after SNI, which were not downregulated in SAFit2-treated SNI animals. Interestingly, we could not



observe any difference in arachidonic acid levels after SAFit2 treatment, indicating that the synthesis of eicosanoids, such as prostanoids, EETs (epoxyeicosatrienoic acids), and HETEs (hydroxyl-eicosatetraenoic acids), is unaffected.

Nevertheless, we detected a significant reduction in the free fatty acid (and precursor of several specialized pro-resolving mediators (SPMs)) docosahexaenoic acid (FA 22:6, DHA) in the vehicle-treated SNI mice. However, a SAFit2 treatment was capable to restore the physiological level of DHA after SNI to a level comparable to sham mice. Since docosahexaenoic acid metabolites were identified as endogenous TRP inhibitors, which can contribute to the relief of inflammation and pain [33], these results indicate that SAFit2 can restore omega-3 polyunsaturated fatty acids as precursors for potentially antihyperalgesic lipids, thereby resolving mechanical hypersensitivity after SNI [9]. Nonetheless, synthesis, signaling, and occurrence of SPM in tissues have been the subject of controversies, because of the inability and inconsistency of their detection with analytical methods in biological samples [42].

Interestingly, we detected one lipid in the untargeted screening that shows both a significant downregulation after SNI and a significantly increased level after SAFit2 treatment. These alterations reveal the C16 dihydroceramide as a novel and crucial lipid mediator in the context of neuropathic pain. However, the knowledge about ceramides is very limited in the research field of pain, although the group of sphingosines from the sphingosine/ceramide pathway are well characterized in the context of neuropathic pain [21–23,43–48]. Based on that, we decided to assess the impact of the C16 dihydroceramide on pain mediating TRP channels and its function in acute pain. We showed that the C16 dihydroceramide reduces the sensitivity of the mechanical and thermal pain-mediating TRPV1 channel. However, it does not inhibit the calcium channel directly, which is quite a crucial property, since many TRPV1 antagonists lead to hyperthermia as they disturbed the complex regulatory role of TRPV1 for normal body temperature maintenance [13,29,49]. Based on that, it might be beneficial to maintain the TRPV1 activity in a physiological state and to reduce its sensitization, which mainly occurs in inflammation-related pain states. In conclusion, the desensitizing effects of the C16 dihydroceramide further contribute to the analgesic effects of SAFit2, which are capable of mediating pain relief after nerve injury [9].

It is still unclear how SAFit2 alters the levels of the C16 dihydroceramide. Possibly, SAFit2 is involved in regulating the expression of ceramide synthase 5 (CerS5) in sensory neurons. This may be caused by the interference of SAFit2 in NF- $\kappa$ B signaling [9]. In addition, it has previously been shown that NF- $\kappa$ B signaling can be influenced by the ceramide synthase 4 [50]. SAFit2 may also enhance or restore activity or expression of phospholipases, leading to enhanced release and availability of free fatty acids after treatment.

Since we detected no direct effect of the C16 dihydroceramide on TRPV1, we analyzed whether the lipid mediator might desensitize the TRPV1 indirectly via a G protein coupled receptor. However, we also did not detect any activation of a G protein coupled receptor, when screening a library consisting of 314 GPCRs. Based on these results, we suggest that the C16 dihydroceramide modulates the TRPV1 indirectly, as it alters the biophysical plasma membrane properties or may act as an allosteric modulator of TRPV1, as was previously described for cholesterol and other lysophospholipids [51–53]. In addition, we observed an influence of the C16 dihydroceramide on the downstream signaling of TRPV1, as it reduces the release of the pro-inflammatory neuropeptide CGRP in sensory neurons. CGRP is secreted upon enhanced neuronal activity and can cause neuroinflammation via GPCRs, leading to the development of persistent pain states [27,28,54]. We further confirmed these analgesic properties in an acute mouse model in which we could show that the C16 dihydroceramide significantly reduced capsaicin-induced thermal hypersensitivity to a physiological normal level. Here, we identify the C16 dihydroceramide as a novel antihyperalgesic lipid mediator and observe the effects of SAFit2 on the expression of ceramide synthase 5 and on the free fatty acid levels in nervous tissue. These findings help explain the mechanism of SAFit2-mediated analgesic effects and they provide additional

evidence for the involvement of lipids as a regulatory interface for antihyperalgesia in nervous tissue in the context of neuropathic pain.

A limitation of the study is the lack of female mice in our *in vivo* experiments. Previous studies revealed evidence for sex differences in inflammatory pain models and the development of neuropathic pain [55]. However, the SAFit2-inhibiting target FKBP51 was previously shown to be sex-independently involved in the development of neuropathic pain [4]. In addition, the sex dimorphism in inflammatory and neuropathic pain models was attributed to the involvement of different immune cells in the development of pain [56]. However, our *in vivo* study focused on acute TRPV1-mediated nociception, which is sex independent and does not involve the influence of any immune cells.

In summary, we report that the highly selective FKBP51 inhibitor SAFit2 is capable of counteracting the alterations in lipid metabolism and signaling after SNI. More specifically, SAFit2 restored the levels of the C16 dihydroceramide, which reduced the TRPV1 activity, as well as the subsequent secretion of CGRP in primary sensory neurons. Both effects indicate the analgesic properties of the C16 dihydroceramide, revealing this lipid as a novel and crucial lipid mediator in the context of neuropathic pain.

Collectively, these findings can mechanistically explain the analgesic effects of SAFit2 *in vivo*. They also raise the question whether C16 dihydroceramide itself can serve as a treatment for neuropathic pain. However, due to the short half-life and limited distribution and bioavailability of this lipid [57,58], we do not consider it as a direct therapeutic option for the treatment of neuropathic pain.

#### 4. Materials and Methods

##### 4.1. Spared Nerve Injury Surgery and SAFit2 Treatment

For all animal experiments, we obtained wild type mice with a C57BL/NRj background from commercial breeding companies, such as Janvier and Charles River. Mice were matched regarding age (8–10 weeks) for the *in vivo* treatments. For analyzing the effect of SAFit2 after nerve injury, we conducted the well-characterized and robust spared nerve injury (SNI) model. Therefore, surgery was performed under anesthesia, in which we firstly ligated the common peroneal and tibial branches of the sciatic nerve and then dissected the sciatic nerve distally from the ligature on the level of the knee joint. The third nerve branch was left intact [59]. After surgery, we treated the mice intraperitoneally with either 10 mg/kg SAFit2 or vehicle (PBS supplemented with 5% Tween, 5% PEG400, and 0.7% ethanol) twice daily from Day 5 to 10.

##### 4.2. Tissue Isolation

On Day 21 after surgery, the mice were sacrificed, and lumbar dorsal root ganglia (DRGs) (L4–L6) and the respective segments of the spinal cord (SC) were dissected. The respective tissue was isolated from injured (ipsilateral) and unimpaired (contralateral) sites and frozen in liquid nitrogen for either RNA isolation or LC-HRMS analysis.

##### 4.3. Quantitative Real-Time PCR

The total RNA was isolated from lumbar DRGs (L4–L6) and the respective segments of spinal cord using the mirVana miRNA Isolation Kit (Applied Biosystems, Waltham, MA, USA). The isolation was performed according to the manufacturer's instructions. As a next step, we measured the RNA concentrations using a NanoDrop ND-1000 spectrophotometer (NanoDrop Technologies, Wilmington, DE, USA). The reverse transcription was conducted with 200 ng RNA for DRG samples and 400 ng RNA for spinal cord samples using the First Strand cDNA Synthesis Kit (Thermo Fisher Scientific, Waltham, MA, USA), compliant with the manufacturer's instructions. Quantification of gene expression was assessed with a quantitative real-time PCR, which was performed using the TaqMan<sup>®</sup> Gene Expression Assay System with respective assay primers (Thermo Fisher Scientific) and the QuantStudio<sup>™</sup> Design & Analysis Software v 1.4.3 (Thermo Fisher Scientific). The experimental settings were adjusted compliant to the manufacturer's instructions and using the assay primers

listed in Table 1. The raw data were evaluated with the  $\Delta\Delta C(T)$  method to calculate the relative expression of the target genes, as described previously [60,61].

**Table 1.** List of used TaqMan<sup>®</sup> Gene Expression Assays.

Target	Gene	Article Number	Company
ALOX12	Arachidonate 12-lipoxygenase	Mm00545833_m1	Thermo Fisher
ALOX15	Arachidonate 15-lipoxygenase	Mm00507789_m1	Thermo Fisher
ALOX5	Arachidonate 5-lipoxygenase	Mm01182747_m1	Thermo Fisher
CerS5	Ceramide synthase 5	Mm00556165_m1	Thermo Fisher
CerS6	Ceramide synthase 6	Mm00510998_m1	Thermo Fisher
COX2	Cytochrome c oxidase subunit II	Mm03294838_g1	Thermo Fisher
CYP2J6	Cytochrome P450, family 2, subfamily j, polypeptide 6	Mm01268197_m1	Thermo Fisher
CYP3a11	Cytochrome P450, family 3, subfamily a, polypeptide 11	Mm00731567_m1	Thermo Fisher
GAPDH	Glycerinaldehyde-3-phosphate dehydrogenase	Mm99999915_g1	Thermo Fisher
PLA2g4a	Phospholipase A2, group 4a	Mm00447040_m1	Thermo Fisher
PLA2g4c	Phospholipase A2, group 4c	Mm01195718_m1	Thermo Fisher

#### 4.4. Liquid Chromatography–High Resolution Mass Spectrometry (LC-HRMS)

For LC-HRMS purposes, DRGs and spinal cord (SC) were homogenized using a pellet pestle mixer (Thermo Fisher scientific). A volume of 79 or 237  $\mu\text{L}$  of ethanol:water (1:9, *v/v*) was added to approximately 1 mg (DRGs) or 3 mg (SC) of tissue and grinded for 30 to 60 s, including short breaks to avoid overheating.

For lipid extraction, 75  $\mu\text{L}$  of internal standards, solved in methanol (see Supplementary Material), were added to 20  $\mu\text{L}$  of tissue homogenate. Next, 250  $\mu\text{L}$  of methyl-tert-butyl-ether (MTBE, HPLC-grade) and 50  $\mu\text{L}$  of 50 mM ammonium formate (for mass spectrometry,  $\geq 99.0$  was purchased from Sigma-Aldrich, Munich, Germany) were added and the samples mixed for 1 min. After 5 min of centrifugation at ambient temperature and  $20,000\times g$ , the upper phase was transferred and the lower phase reextracted using 100  $\mu\text{L}$  of MTBE:methanol:water (10:3:2.5, *v/v/v*, upper phase), again followed by centrifugation. The combined upper phases were dried under a nitrogen stream at 45  $^{\circ}\text{C}$ , stored at  $-80^{\circ}\text{C}$  and redissolved in 100  $\mu\text{L}$  of methanol prior to analysis. For analysis, an Exploris 480 Orbitrap mass spectrometer coupled with a Vanquish horizon LC-system (both Thermo Fisher Scientific) was used.

Chromatographic separation was performed using a Zorbax RRHD Eclipse Plus C8 column (1.8  $\mu\text{m}$  50  $\times$  2.1 mm ID, Agilent) with a precolumn of the same type and a 14-min binary gradient. The samples were analyzed in positive and negative ionization mode with a scan range from 180 to 1500 *m/z* and 120,000 mass resolution. Additionally, data-dependent spectra were acquired at a 15,000 resolution and a total cycle time of 600 ms. Acquisition was performed using XCalibur software v4.4, and for evaluation, TraceFinder software v5.1 was applied (both Thermo Fisher Scientific). Lipids were identified as previously described, with a mass error of 5 ppm [62]. The first ten spinal cord samples were pooled, and multiple replicates were analyzed over the run-time to verify system stability. The results were normalized to the protein concentration, which was determined after tissue homogenization with a Bradford assay.

#### 4.5. Isolation of Dorsal Root Ganglia (DRGs)

For performing assays with primary sensory neurons, naïve mice were sacrificed and DRGs isolated, which were stored in precooled HBSS, supplemented with  $\text{CaCl}_2$  and  $\text{MgCl}_2$  (Gibco), on ice during dissection until further purification. For purification purposes, we substituted HBSS with a collagenase/dispase solution containing 500 U/mL collagenase and 2.5 U/mL dispase diluted in neurobasal medium (Gibco). The isolated DRGs were incubated with the collagenase/dispase solution for 75 min at 37  $^{\circ}\text{C}$ . Next, we removed the

enzyme solution by centrifuging and discarding the supernatant, followed by two washing steps with neurobasal medium, supplemented with 10% FCS (*v/v*). Afterwards, the DRGs were further enzymatically dissociated via an incubation step with 0.05% trypsin (*v/v*) (Gibco) for 10 min at 37 °C. The DRGs were again washed twice with neurobasal medium containing 10% FCS. After the enzymatic dissociation, we dissociated the DRGs mechanically in neurobasal medium (Gibco) supplemented with L-glutamine (2 mM; Gibco), penicillin (100 U/mL; Gibco), streptomycin (100 µg/mL; Gibco), B-27 supplement (Gibco), and gentamicin (50 µg/mL; Gibco). Finally, 30 µL of the primary sensory neuron suspension were plated on poly-L-lysine-coated cover slips or 48-well plates and incubated at 37 °C for two hours to allow adhesion of the sensory neurons. After the attachment phase, we added another 2 mL of neurobasal medium to each dish.

#### 4.6. Calcium Imaging

To analyze the calcium levels in primary sensory neurons, we stained sensory neuron cultures with Fura-2-AM for at least 45 min prior the measurement. Afterwards, the cells were washed twice with freshly prepared Ringer's solution. We also used Ringer's solution during live cell calcium imaging as we measured the baseline levels. In addition, we applied Ringer's solution after and in between stimulations for wash-out purposes. The Ringer's solution consisted of 145 mM NaCl, 1.25 mM CaCl<sub>2</sub> × 2 H<sub>2</sub>O, 1 mM MgCl<sub>2</sub> × 6 H<sub>2</sub>O, 5 mM KCl, 10 mM D-glucose, and 10 mM HEPES, and its pH was adjusted to a physiological level of 7.3 using NaOH. To analyze the influence of the C16 dihydroceramide on different calcium channels, we pre-incubated primary sensory neurons with the C16 dihydroceramide for two minutes (0.25–5 µM) and stimulated the cells with the following agonists, respectively: 100 nM capsaicin for 30 s (TRPV1 agonist), 100 µM allyl isothiocyanate for 45 s (AITC, TRPA1 agonist), and 50 µM α,β-methyleneadenosine 5' triphosphate trisodium salt (meATP, P2X3 agonist). Control experiments were performed with the respective volume of the corresponding vehicle, which was either DMSO or cremophor EL. The agonists as well as the C16 dihydroceramide were diluted from stock solutions in Ringer's solution to their final concentrations. The calcium live cell imaging measurements were conducted using an automated perfusion system (ValveBank II, AutoMate Scientific, San Diego, CA, USA) and recorded with a DMI4000 B Microscope, with a compact light source CTR550 HS (Leica Microsystems, Wetzlar, Germany).

#### 4.7. Calcitonin Gene-Related Peptide Assay

To investigate the influence of the C16 dihydroceramide on calcitonin gene-related peptide (CGRP) secretion, the amount of CGRP was measured in the supernatant of sensory neurons after TRPV1 stimulation. Therefore, sensory neurons were isolated from DRGs as previously described and stimulated with a mixture of capsaicin and C16 dihydroceramide the next day. To prepare the primary sensory neurons for the secretion assay, we washed them with HBSS previously. Afterwards, we treated the cells with either vehicle as negative control, capsaicin as positive control, or a mixture of capsaicin and C16 dihydroceramide for 15 min. All compounds were diluted in HBSS. The amount of CGRP in the supernatant was detected with an ELISA kit from Bertin Bioreagent, in accordance with the manufacturer's instructions, measuring the absorption at 405 nm. The quantification was performed with linear regression, as described in the manufacturer's manual.

#### 4.8. Screen for C16 Dihydroceramide Activated GPCRs

##### 4.8.1. β-Arrestin Assay

In total, 5000 HTLA cells were seeded into a white, transparent, and poly-L-Lysine-coated 384-well plate from PerkinElmer. The cells were co-transfected after 6 h with a plasmid from the PRESTO-Tango GPCR library (Addgene, Watertown, MA, USA, [63]). We used a mixture of 10 ng plasmid and 0.04 µL Lipofectamine 2000 per well when performing the transfection, as described by [63]. We used GFP as a transfection control and 100 µM carbachol and the muscarinic M5 receptor as a positive control. After 24 h, the medium

was replaced by 45  $\mu$ L of serum-free medium. The ligand (5  $\mu$ L) was then added at a final concentration of 30  $\mu$ M for approximately 24 h. Afterwards, the medium was aspirated, and the cells lysed using 50  $\mu$ L of bright-Glo reagent (Promega, Madison, WI, USA) diluted 10 times with PBS. After 15 min of incubation with lysis buffer, the luminescence (endpoint, 1500 ms integration time) was measured using a flexstation 3 plate reader.

#### 4.8.2. cAMP Reporter Assay

In total, 5000 HEK293 cells were seeded in a white, transparent and ploy-L-Lysin-coated 384-well plate from PerkinElmer. The cells were co-transfected after 6 h with the cAMP reporter pGL4.29 plasmid (Promega) and a plasmid from the PRESTO-Tango GPCR library (10 ng from each plasmid and 0.04  $\mu$ L Lipofectamine 2000 per well). As a transfection control, we used GFP and as a positive control we used 10 nM GLP-1 acting on the GLP-1 receptor. After 48 h, the medium was replaced by 45  $\mu$ L of serum-free medium for one hour. The ligand (5  $\mu$ L) was then added at a final concentration of 15  $\mu$ M for 5 h. Afterwards, the medium was aspirated, and the cells were lysed using 50  $\mu$ L of a mixture of bright-Glo reagent (Promega) diluted 10 times with PBS. After 15 min of incubation with lysis buffer, the luminescence (endpoint, 1500 ms integration time) was determined using a flexstation 3 plate reader.

#### 4.8.3. RhoA Reporter Assay

In total, 5000 HEK293 cells were seeded in a white, transparent and ploy-L-Lysin coated 384-well plate from PerkinElmer. The cells were co-transfected after 6 h with the pGL4.34 plasmid (Promega) and a plasmid from the PRESTO-Tango GPCR library (10 ng from each plasmid and 0.04  $\mu$ L Lipofectamine 2000 per well). As a transfection control, we used GFP and as a positive control we used FBS on cells transfected only with the reporter plasmid pGL4.34. The medium was aspirated after 24 h, and serum-free medium was added instead. After 48 h, the medium was replaced by 45  $\mu$ L of serum-free medium, and cells were incubated for one more hour. The ligand (5  $\mu$ L) was then added at a final concentration of 15  $\mu$ M for 5 h. Afterwards, the medium was aspirated, and the cells were lysed using 50  $\mu$ L of a mixture of bright-Glo reagent (Promega) diluted 10 times with PBS. After 15 min of incubation with lysis buffer, the luminescence (endpoint, 1500 ms integration time) was measured using a flexstation 3 plate reader.

#### 4.9. Radiant Heat Assay

During the behavioral experiment, the experimenter was blinded. All animals were transferred into respective test cages for at least one hour before the measurement to allow habituation, as described previously [64]. For assessing the thermal withdrawal latency, a radiant heat test was performed using a Plantar Analgesia Meter with a high-intensity projector lamp (IITC Life Science, Woodland Hill, CA, USA). The cut-off time for this experiment was set to 20 s.

#### 4.10. Data Analysis and Statistics

All animal numbers and in vitro replicates are depicted in the figure legends. In addition, the data are displayed as the mean  $\pm$  SEM. The statistical analysis was performed with GraphPad Prism software version 9. The normal distribution of the raw data was verified and confirmed with the Shapiro–Wilk test. We performed an unpaired and heteroskedastic Student's *t*-test with Welch's correction for comparing two groups for the in vitro experiments. To determine the significance between more than two groups, we conducted a one-way analysis of variance (ANOVA). In line with this, we used a two-way ANOVA when comparing more than three groups. To evaluate the significance levels for behavioral assays, we performed a two-way ANOVA with Bonferroni's multiple-comparisons post-hoc test. We considered a *p*-value lower than 0.05 as statistically significant.

**Supplementary Materials:** The supporting information can be downloaded at: <https://www.mdpi.com/article/10.3390/ijms232214274/s1>.

**Author Contributions:** Conceptualization: S.W., S.O., F.H., G.G. and M.S.; experimental investigations: S.W., L.H. and M.W.A.; data curation: S.W.; writing and original draft preparation: S.W. and M.S. All authors have read and agreed to the published version of the manuscript.

**Funding:** For conducting this research, the authors received grants 51TaValP of the Federal German Ministry of Education and Research (BMBF) and SFB1039 A09, A04, and Z01, as well as 445757098, from the Deutsche Forschungsgemeinschaft (German Research Foundation). We also received grants from the Fraunhofer Foundation Project: Neuropathic Pain, as well as from the Fraunhofer Cluster of Excellence for Immune-Mediated Diseases (CIMD).

**Institutional Review Board Statement:** The animal study protocols were granted by the local Ethics Committee for Animal Research (Darmstadt) with the permit numbers FU/2018, F152/1021 and FK/1113. Furthermore, all animal experiments were performed in accordance with the recommendations of the Preclinical Pain Research Consortium for Investigating Safety and Efficacy (PPRECISE) Working Group [65] and the updated ARRIVE guidelines for reporting animal research [66] and guidelines as defined by European Quality In Preclinical Data (EQIPD) [67]. All efforts were made to minimize animal suffering.

**Informed Consent Statement:** Not applicable.

**Data Availability Statement:** Not applicable.

**Conflicts of Interest:** The authors declare no conflict of interest.

## References

1. Finnerup, N.B.; Attal, N.; Haroutounian, S.; McNicol, E.; Baron, R.; Dworkin, R.H.; Gilron, I.; Haanpää, M.; Hansson, P.; Jensen, T.S.; et al. Pharmacotherapy for neuropathic pain in adults: A systematic review and meta-analysis. *Lancet Neurol.* **2015**, *14*, 162–173. [CrossRef]
2. Colloca, L.; Ludman, T.; Bouhassira, D.; Baron, R.; Dickenson, A.H.; Yarnitsky, D.; Freeman, R.; Truini, A.; Attal, N.; Finnerup, N.B.; et al. Neuropathic pain. *Nat. Rev. Dis. Primers* **2017**, *3*, 17002. [CrossRef]
3. Maiarù, M.; Tochiki, K.K.; Cox, M.B.; Annan, L.V.; Bell, C.G.; Feng, X.; Hausch, F.; Géranton, S.M. The stress regulator FKBP51 drives chronic pain by modulating spinal glucocorticoid signaling. *Sci. Transl. Med.* **2016**, *8*, 325ra19. [CrossRef]
4. Maiaru, M.; Morgan, O.B.; Mao, T.; Breitsamer, M.; Bamber, H.; Pöhlmann, M.; Schmidt, M.V.; Winter, G.; Hausch, F.; Géranton, S.M. The stress regulator FKBP51: A novel and promising druggable target for the treatment of persistent pain states across sexes. *Pain* **2018**, *159*, 1224–1234. [CrossRef]
5. Storer, C.L.; Dickey, C.A.; Galigniana, M.D.; Rein, T.; Cox, M.B. FKBP51 and FKBP52 in signaling and disease. *Trends Endocrinol. Metab.* **2011**, *22*, 481–490. [CrossRef]
6. Hähle, A.; Merz, S.; Meyners, C.; Hausch, F. The Many Faces of FKBP51. *Biomolecules* **2019**, *9*, 35. [CrossRef]
7. Gabani, B.B.; Sulochana, S.P.; Siddesh, A.H.; Kiran, V.; Saini, N.K.; Samanta, S.K.; Hallur, M.S.; Rajagopal, S.; Mullangi, R. Validated LC-MS/MS Method for Simultaneous Quantitation of SAFit-1 and SAFit-2 in Mice Plasma: Application to a Pharmacokinetic Study. *Drug Res.* **2020**, *70*, 325–332. [CrossRef]
8. Gaali, S.; Kirschner, A.; Cuboni, S.; Hartmann, J.; Kozany, C.; Balsevich, G.; Namendorf, C.; Fernandez-Vizarra, P.; Sippel, C.; Zannas, A.S.; et al. Selective inhibitors of the FK506-binding protein 51 by induced fit. *Nat. Chem. Biol.* **2015**, *11*, 33–37. [CrossRef]
9. Wedel, S.; Mathoor, P.; Rauh, O.; Heymann, T.; Ciotu, C.I.; Fuhrmann, D.C.; Fischer, M.J.M.; Weigert, A.; de Bruin, N.; Hausch, F.; et al. SAFit2 reduces neuroinflammation and ameliorates nerve injury-induced neuropathic pain. *J. Neuroinflammation* **2022**, *19*, 1–21. [CrossRef]
10. Morgan, M.J.; Liu, Z.G. Crosstalk of reactive oxygen species and NF-kappaB signaling. *Cell Res.* **2011**, *21*, 103–115. [CrossRef]
11. Liu, T.; Zhang, L.; Joo, D.; Sun, S.C. NF-kappaB signaling in inflammation. *Signal Transduct. Target. Ther.* **2017**, *2*, 17023. [CrossRef]
12. Osthuys, T.; Sisignano, M. Oxidized Lipids in Persistent Pain States. *Front. Pharmacol.* **2019**, *10*, 1147. [CrossRef]
13. Julius, D. TRP channels and pain. *Annu. Rev. Cell Dev. Biol.* **2013**, *29*, 355–384. [CrossRef]
14. Hohmann, S.W.; Angioni, C.; Tunaru, S.; Lee, S.; Woolf, C.J.; Offermanns, S.; Geisslinger, G.; Scholich, K.; Sisignano, M. The G2A receptor (GPR132) contributes to oxaliplatin-induced mechanical pain hypersensitivity. *Sci. Rep.* **2017**, *7*, 446. [CrossRef]
15. Ji, R.-R.; Xu, Z.-Z.; Gao, Y.-J. Emerging targets in neuroinflammation-driven chronic pain. *Nat. Rev. Drug Discov.* **2014**, *13*, 533–548. [CrossRef]
16. Patwardhan, A.M.; Akopian, A.N.; Ruparel, N.B.; Diogenes, A.; Weintraub, S.T.; Uhlson, C.; Murphy, R.C.; Hargreaves, K.M. Heat generates oxidized linoleic acid metabolites that activate TRPV1 and produce pain in rodents. *J. Clin. Investig.* **2010**, *120*, 1617–1626. [CrossRef]

17. Sisignano, M.; Angioni, C.; Park, C.-K.; Dos Santos, S.M.; Jordan, H.; Kuzikov, M.; Liu, D.; Zinn, S.; Hohman, S.W.; Schreiber, Y.; et al. Targeting CYP2J to reduce paclitaxel-induced peripheral neuropathic pain. *Proc. Natl. Acad. Sci. USA* **2016**, *113*, 12544–12549. [[CrossRef](#)]
18. Ramsden, C.E.; Domenichiello, A.F.; Yuan, Z.-X.; Sapio, M.R.; Keyes, G.S.; Mishra, S.K.; Gross, J.R.; Majchrzak-Hong, S.; Zamora, D.; Horowitz, M.S.; et al. A systems approach for discovering linoleic acid derivatives that potentially mediate pain and itch. *Sci. Signal.* **2017**, *10*, eaa15241. [[CrossRef](#)]
19. Zimmer, B.; Angioni, C.; Osthues, T.; Toewe, A.; Thomas, D.; Pierre, S.C.; Geisslinger, G.; Scholich, K.; Sisignano, M. The oxidized linoleic acid metabolite 12,13-DiHOME mediates thermal hyperalgesia during inflammatory pain. *Biochim. Biophys. Acta (BBA) Mol. Cell Biol. Lipids* **2018**, *1863*, 669–678. [[CrossRef](#)]
20. Stockstill, K.; Doyle, T.M.; Yan, X.; Chen, Z.; Janes, K.; Little, J.W.; Braden, K.; Lauro, F.; Giacotti, L.A.; Harada, C.M.; et al. Dysregulation of sphingolipid metabolism contributes to bortezomib-induced neuropathic pain. *J. Exp. Med.* **2018**, *215*, 1301–1313. [[CrossRef](#)]
21. Langeslag, M.; Kress, M. The ceramide-S1P pathway as a druggable target to alleviate peripheral neuropathic pain. *Expert Opin. Ther. Targets* **2020**, *24*, 869–884. [[CrossRef](#)]
22. Mair, N.; Benetti, C.; Andratsch, M.; Leitner, M.; Constantin, C.E.; Camprubí-Robles, M.; Quarta, S.; Biasio, W.; Kuner, R.; Gibbins, I.L.; et al. Genetic Evidence for Involvement of Neuronally Expressed S1P1 Receptor in Nociceptor Sensitization and Inflammatory Pain. *PLoS ONE* **2011**, *6*, e17268. [[CrossRef](#)]
23. Doyle, T.M.; Janes, K.; Chen, Z.; Grace, P.M.; Esposito, E.; Cuzzocrea, S.; Largent-Milnes, T.M.; Neumann, W.L.; Watkins, L.R.; Spiegel, S.; et al. Activation of sphingosine-1-phosphate receptor subtype 1 in the central nervous system contributes to morphine-induced hyperalgesia and antinociceptive tolerance in rodents. *Pain* **2020**, *161*, 2107–2118. [[CrossRef](#)]
24. Grösch, S.; Schiffmann, S.; Geisslinger, G. Chain length-specific properties of ceramides. *Prog. Lipid Res.* **2011**, *51*, 50–62. [[CrossRef](#)]
25. Nørregaard, R.; Kwon, T.-H.; Frøkiær, J. Physiology and pathophysiology of cyclooxygenase-2 and prostaglandin E2 in the kidney. *Kidney Res. Clin. Pract.* **2015**, *34*, 194–200. [[CrossRef](#)]
26. Szallasi, A.; Cortright, D.N.; Blum, C.A.; Eid, S.R. The vanilloid receptor TRPV1: 10 years from channel cloning to antagonist proof-of-concept. *Nat. Rev. Drug Discov.* **2007**, *6*, 357–372. [[CrossRef](#)]
27. Geppetti, P.; Capone, J.G.; Trevisani, M.; Nicoletti, P.; Zagli, G.; Tola, M.R. CGRP and migraine: Neurogenic inflammation revisited. *J. Headache Pain* **2005**, *6*, 61–70. [[CrossRef](#)]
28. Walsh, D.A.; Mapp, P.I.; Kelly, S. Calcitonin gene-related peptide in the joint: Contributions to pain and inflammation. *Br. J. Clin. Pharmacol.* **2015**, *80*, 965–978. [[CrossRef](#)]
29. Wong, G.Y.; Gavva, N.R. Therapeutic potential of vanilloid receptor TRPV1 agonists and antagonists as analgesics: Recent advances and setbacks. *Brain Res. Rev.* **2009**, *60*, 267–277. [[CrossRef](#)]
30. Bautista, D.M.; Pellegrino, M.; Tsunozaki, M. TRPA1: A Gatekeeper for Inflammation. *Annu. Rev. Physiol.* **2013**, *75*, 181–200. [[CrossRef](#)]
31. Nuñez-Badinez, P.; Sepúlveda, H.; Diaz, E.; Greffrath, W.; Treede, R.; Stehberg, J.; Montecino, M.; van Zundert, B. Variable transcriptional responsiveness of the P2X3 receptor gene during CFA-induced inflammatory hyperalgesia. *J. Cell. Biochem.* **2018**, *119*, 3922–3935. [[CrossRef](#)] [[PubMed](#)]
32. Sisignano, M.; Gribbon, P.; Geisslinger, G. Drug Repurposing to Target Neuroinflammation and Sensory Neuron-Dependent Pain. *Drugs* **2022**, *82*, 357–373. [[CrossRef](#)] [[PubMed](#)]
33. Sisignano, M.; Bennett, D.L.; Geisslinger, G.; Scholich, K. TRP-channels as key integrators of lipid pathways in nociceptive neurons. *Prog. Lipid Res.* **2013**, *53*, 93–107. [[CrossRef](#)] [[PubMed](#)]
34. Wedel, S.; Osthues, T.; Zimmer, B.; Angioni, C.; Geisslinger, G.; Sisignano, M. Oxidized linoleic acid metabolites maintain mechanical and thermal hypersensitivity during sub-chronic inflammatory pain. *Biochem. Pharmacol.* **2022**, *198*, 114953. [[CrossRef](#)]
35. Salvemini, D.; Doyle, T.; Kress, M.; Nicol, G. Therapeutic targeting of the ceramide-to-sphingosine 1-phosphate pathway in pain. *Trends Pharmacol. Sci.* **2013**, *34*, 110–118. [[CrossRef](#)]
36. Doolen, S.; Iannitti, T.; Donahue, R.R.; Shaw, B.C.; Grachen, C.M.; Taylor, B.K. Fingolimod reduces neuropathic pain behaviors in a mouse model of multiple sclerosis by a sphingosine-1 phosphate receptor 1-dependent inhibition of central sensitization in the dorsal horn. *Pain* **2017**, *159*, 224–238. [[CrossRef](#)]
37. Malek, N.; Kucharczyk, M.; Starowicz, K. Alterations in the Anandamide Metabolism in the Development of Neuropathic Pain. *BioMed Res. Int.* **2014**, *2014*, 1–12. [[CrossRef](#)]
38. Ji, R.-R.; Xu, Z.-Z.; Strichartz, G.; Serhan, C.N. Emerging roles of resolvins in the resolution of inflammation and pain. *Trends Neurosci.* **2011**, *34*, 599–609. [[CrossRef](#)]
39. Luo, X.; Gu, Y.; Tao, X.; Serhan, C.N.; Ji, R.-R. Resolvin D5 Inhibits Neuropathic and Inflammatory Pain in Male But Not Female Mice: Distinct Actions of D-Series Resolvins in Chemotherapy-Induced Peripheral Neuropathy. *Front. Pharmacol.* **2019**, *10*, 745. [[CrossRef](#)]
40. Xu, Z.-Z.; Berta, T.; Ji, R.-R. Resolvin E1 Inhibits Neuropathic Pain and Spinal Cord Microglial Activation Following Peripheral Nerve Injury. *J. Neuroimmune Pharmacol.* **2012**, *8*, 37–41. [[CrossRef](#)]
41. Meesawatson, P.; Hathway, G.; Bennett, A.; Constantin-Teodosiu, D.; Chapman, V. Spinal neuronal excitability and neuroinflammation in a model of chemotherapeutic neuropathic pain: Targeting the resolution pathways. *J. Neuroinflamm.* **2020**, *17*, 1–17. [[CrossRef](#)] [[PubMed](#)]

42. Schebb, N.H.; Kühn, H.; Kahnt, A.S.; Rund, K.M.; O'Donnell, V.B.; Flamand, N.; Peters-Golden, M.; Jakobsson, P.J.; Weylandt, K.H.; Rohwer, N.; et al. Formation, Signaling and Occurrence of Specialized Pro-Resolving Lipid Mediators-What is the Evidence so far? *Front. Pharmacol.* **2022**, *13*, 838782. [[CrossRef](#)] [[PubMed](#)]
43. Finley, A.; Chen, Z.; Esposito, E.; Cuzzocrea, S.; Sabbadini, R.; Salvemini, D. Sphingosine 1-Phosphate Mediates Hyperalgesia via a Neutrophil-Dependent Mechanism. *PLoS ONE* **2013**, *8*, e55255. [[CrossRef](#)] [[PubMed](#)]
44. Chen, Z.; Doyle, T.M.; Luongo, L.; Largent-Milnes, T.M.; Giacotti, L.A.; Kolar, G.; Squillace, S.; Boccella, S.; Walker, J.K.; Pendleton, A.; et al. Sphingosine-1-phosphate receptor 1 activation in astrocytes contributes to neuropathic pain. *Proc. Natl. Acad. Sci. USA* **2019**, *116*, 10557–10562. [[CrossRef](#)]
45. Singh, S.K.; Spiegel, S. Sphingosine-1-phosphate signaling: A novel target for simultaneous adjuvant treatment of triple negative breast cancer and chemotherapy-induced neuropathic pain. *Adv. Biol. Regul.* **2019**, *75*, 100670. [[CrossRef](#)]
46. Camprubi-Robles, M.; Mair, N.; Andratsch, M.; Benetti, C.; Beroukas, D.; Rukwied, R.; Langeslag, M.; Proia, R.; Schmelz, M.; Montiel, A.V.F.; et al. Sphingosine-1-Phosphate-Induced Nociceptor Excitation and Ongoing Pain Behavior in Mice and Humans Is Largely Mediated by S1P3 Receptor. *J. Neurosci.* **2013**, *33*, 2582–2592. [[CrossRef](#)]
47. Spiegel, S.; Milstien, S. Sphingosine-1-phosphate: An enigmatic signalling lipid. *Nat. Rev. Mol. Cell Biol.* **2003**, *4*, 397–407. [[CrossRef](#)]
48. Spiegel, S. Sphingosine-1-phosphate: From insipid lipid to a key regulator. *J. Biol. Chem.* **2020**, *295*, 3371–3384. [[CrossRef](#)]
49. Koivisto, A.-P.; Belvisi, M.G.; Gaudet, R.; Szallasi, A. Advances in TRP channel drug discovery: From target validation to clinical studies. *Nat. Rev. Drug Discov.* **2021**, *21*, 41–59. [[CrossRef](#)]
50. Chen, J.; Li, X.; Ma, D.; Liu, T.; Tian, P.; Wu, C. Ceramide synthase-4 orchestrates the cell proliferation and tumor growth of liver cancer in vitro and in vivo through the nuclear factor- $\kappa$ B signaling pathway. *Oncol. Lett.* **2017**, *14*, 1477–1483. [[CrossRef](#)]
51. Morales-Lázaro, S.L.; Rosenbaum, T. Cholesterol as a Key Molecule That Regulates TRPV1 Channel Function. *Adv. Exp. Med. Biol.* **2019**, *1135*, 105–117. [[CrossRef](#)] [[PubMed](#)]
52. Ciardo, M.G.; Ferrer-Montiel, A. Lipids as central modulators of sensory TRP channels. *Biochim. Biophys. Acta (BBA) Biomembr.* **2017**, *1859*, 1615–1628. [[CrossRef](#)] [[PubMed](#)]
53. Taberner, F.J.; Fernández-Ballester, G.; Fernández-Carvajal, A.; Ferrer-Montiel, A. TRP channels interaction with lipids and its implications in disease. *Biochim. Biophys. Acta (BBA) Biomembr.* **2015**, *1848*, 1818–1827. [[CrossRef](#)] [[PubMed](#)]
54. Benarroch, E.E. CGRP: Sensory neuropeptide with multiple neurologic implications. *Neurology* **2011**, *77*, 281–287. [[CrossRef](#)] [[PubMed](#)]
55. Mogil, J.S. Qualitative sex differences in pain processing: Emerging evidence of a biased literature. *Nat. Rev. Neurosci.* **2020**, *21*, 353–365. [[CrossRef](#)] [[PubMed](#)]
56. Sorge, R.E.; Mapplebeck, J.C.S.; Rosen, S.; Beggs, S.; Taves, S.; Alexander, J.K.; Martin, L.J.; Austin, J.-S.; Sotocinal, S.G.; Chen, D.; et al. Different immune cells mediate mechanical pain hypersensitivity in male and female mice. *Nat. Neurosci.* **2015**, *18*, 1081–1083. [[CrossRef](#)]
57. Chen, Y.; Berejniaia, O.; Liu, J.; Wang, S.-P.; Daurio, N.A.; Yin, W.; Mayoral, R.; Petrov, A.; Kasumov, T.; Zhang, G.-F.; et al. Quantifying ceramide kinetics in vivo using stable isotope tracers and LC-MS/MS. *Am. J. Physiol. Metab.* **2018**, *315*, E416–E424. [[CrossRef](#)]
58. Zelnik, I.D.; Volpert, G.; Viiri, L.E.; Kauhanen, D.; Arazi, T.; Aalto-Setälä, K.; Laaksonen, R.; Futerman, A.H. Different rates of flux through the biosynthetic pathway for long-chain versus very-long-chain sphingolipids. *J. Lipid Res.* **2020**, *61*, 1341–1346. [[CrossRef](#)]
59. Decosterd, I.; Woolf, C.J. Spared nerve injury: An animal model of persistent peripheral neuropathic pain. *Pain* **2000**, *87*, 149–158. [[CrossRef](#)]
60. Livak, K.J.; Schmittgen, T.D. Analysis of relative gene expression data using real-time quantitative PCR and the 2<sup>(-Delta Delta C(T))</sup> Method. *Methods* **2001**, *25*, 402–408. [[CrossRef](#)]
61. Schmittgen, T.D.; Livak, K.J. Analyzing real-time PCR data by the comparative C(T) method. *Nat. Protoc.* **2008**, *3*, 1101–1108. [[CrossRef](#)]
62. Hahnefeld, L.; Gurke, R.; Thomas, D.; Schreiber, Y.; Schäfer, S.M.; Trautmann, S.; Snodgrass, I.F.; Kratza, D.; Geisslinger, G.; Ferreira, N.; et al. Implementation of lipidomics in clinical routine: Can fluoride/citrate blood sampling tubes improve preanalytical stability? *Talanta* **2020**, *209*, 120593. [[CrossRef](#)] [[PubMed](#)]
63. Kroeze, W.K.; Sassano, M.F.; Huang, X.-P.; Lansu, K.; McCorvy, J.D.; Giguère, P.M.; Sciaky, N.; Roth, B.L. PRESTO-Tango as an open-source resource for interrogation of the druggable human GPCRome. *Nat. Struct. Mol. Biol.* **2015**, *22*, 362–369. [[CrossRef](#)] [[PubMed](#)]
64. Sisignano, M.; Park, C.-K.; Angioni, C.; Zhang, D.D.; Von Hehn, C.; Cobos, E.J.; Ghasemlou, N.; Xu, Z.-Z.; Kumaran, V.; Lu, R.; et al. 5,6-EET Is Released upon Neuronal Activity and Induces Mechanical Pain Hypersensitivity via TRPA1 on Central Afferent Terminals. *J. Neurosci.* **2012**, *32*, 6364–6372. [[CrossRef](#)] [[PubMed](#)]
65. Andrews, N.A.; Latrémolière, A.; Basbaum, A.I.; Mogil, J.S.; Porreca, F.; Rice, A.S.; Woolf, C.J.; Currie, G.L.; Dworkin, R.H.; Eisenach, J.C.; et al. Ensuring transparency and minimization of methodologic bias in preclinical pain research: PPRECISE considerations. *Pain* **2016**, *157*, 901–909. [[CrossRef](#)]



66. Percie du Sert, N.; Hurst, V.; Ahluwalia, A.; Alam, S.; Avey, M.T.; Baker, M.; Browne, W.J.; Clark, A.; Cuthill, I.C.; Dirnagl, U.; et al. The ARRIVE guidelines 2.0: Updated guidelines for reporting animal research. *PLoS Biol.* **2020**, *18*, e3000410.
67. Bespalov, A.; Bernard, R.; Gilis, A.; Gerlach, B.; Guillén, J.; Castagné, V.; Lefevre, I.; Ducrey, F.A.; Monk, L.; Bongiovanni, S.; et al. Introduction to the EQIPD quality system. *eLife* **2021**, *10*, e63294. [[CrossRef](#)]

---

### 3.3 Supplemental file

## Supplemental Information

### The FKBP51 inhibitor SAFit2 restores the pain relieving C16 dihydroceramide after nerve injury

Saskia Wedel<sup>1</sup>, Lisa Hahnefeld<sup>1,5</sup>, Mohamad Wessam Alnouri<sup>2</sup>, Stefan Offermanns<sup>2,3</sup>,  
Felix Hausch<sup>4</sup>, Gerd Geisslinger<sup>1,5</sup> and Marco Sisignano<sup>1,5\*</sup>

<sup>1</sup> Institute of Clinical Pharmacology, *pharmazentrum frankfurt/ZAFES*, University Hospital, Goethe-University, 60590 Frankfurt am Main, Germany

<sup>2</sup> Max Planck Institute for Heart and Lung Research, 61231 Bad Nauheim, Germany

<sup>3</sup> Center for Molecular Medicine, Goethe-University Frankfurt, 60590 Frankfurt am Main, Germany

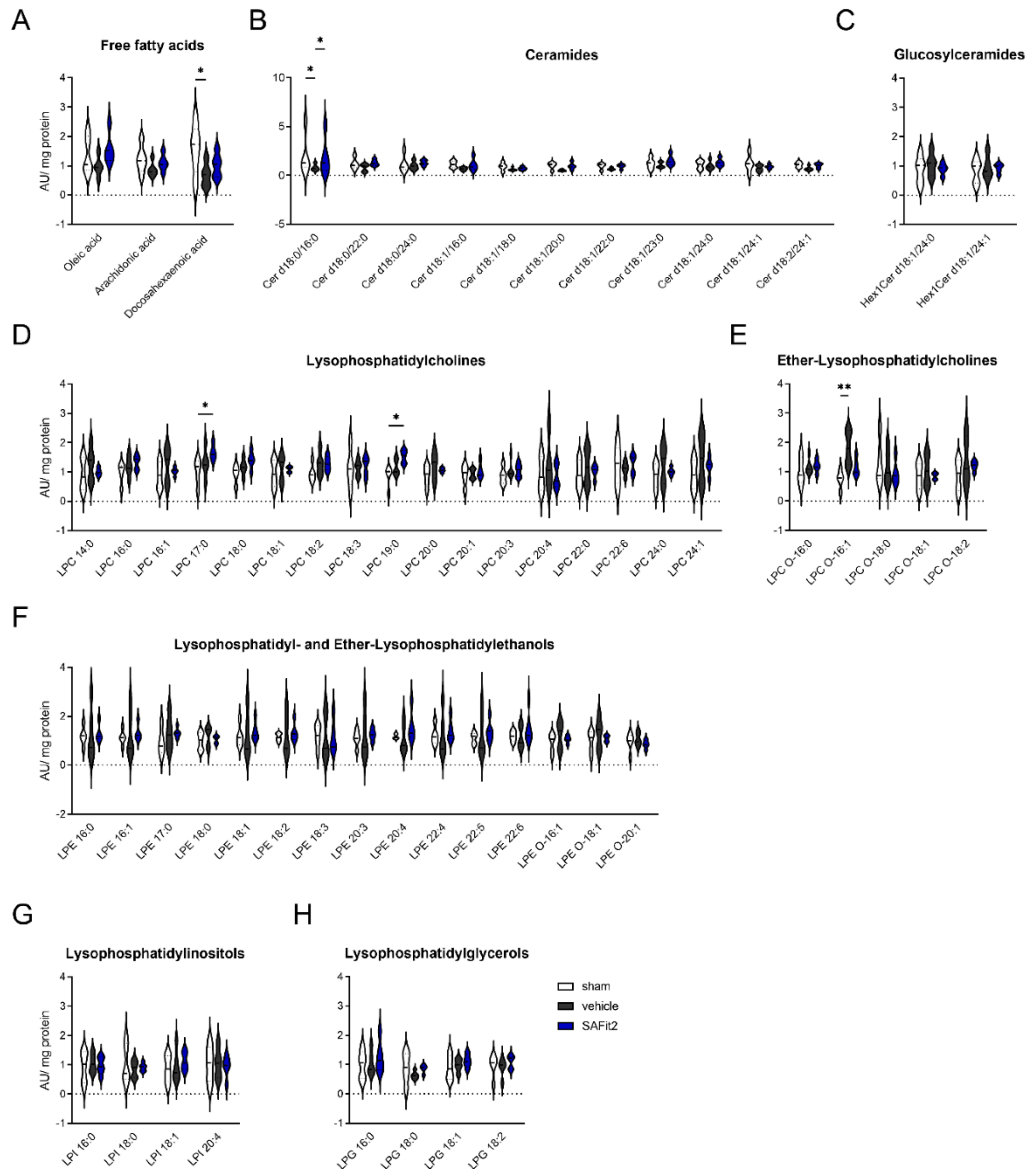
<sup>4</sup> Department of Biochemistry, Technical University Darmstadt, 64287 Darmstadt, Germany

<sup>5</sup> Fraunhofer Institute for Translational Medicine and Pharmacology ITMP, and Fraunhofer Cluster of Excellence for Immune Mediated Diseases CIMD, 60596 Frankfurt am Main, Germany

\*Address correspondence to: Dr. Marco Sisignano, *pharmazentrum frankfurt/ZAFES*, Institute of Clinical Pharmacology, University Hospital, Goethe-University, D-60590 Frankfurt am Main, Germany, Phone: +49 (0)69-6301-7819, E-mail: Marco.Sisignano@med.uni-frankfurt.de

Supplementary Figures: 8

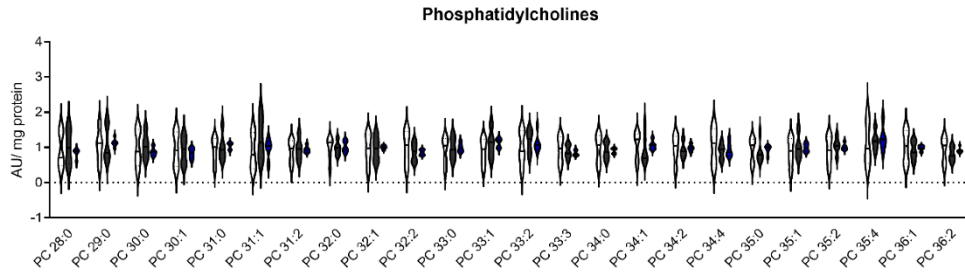
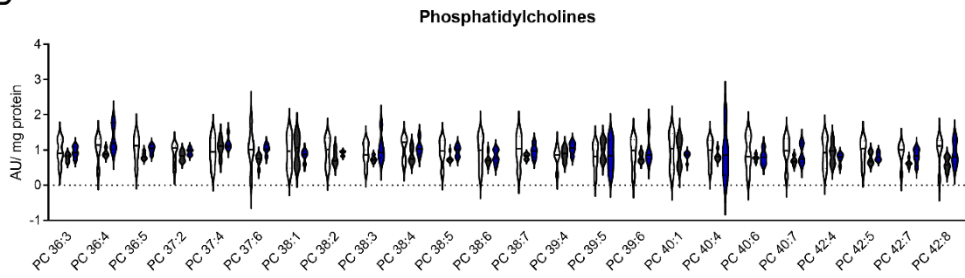
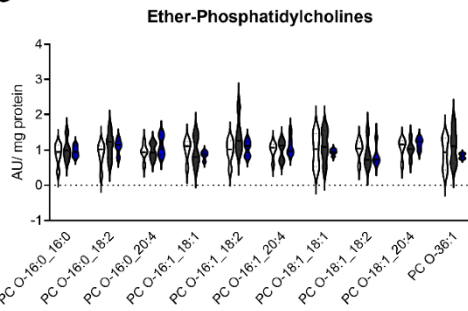
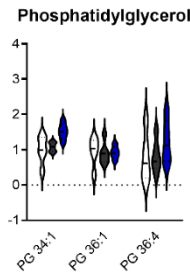
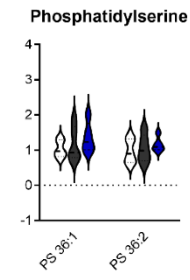
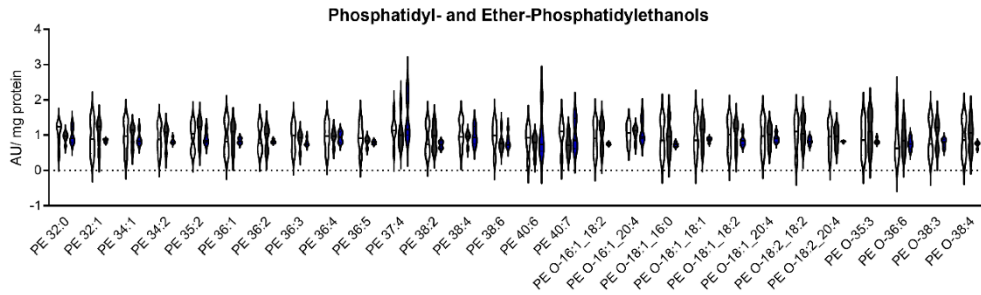
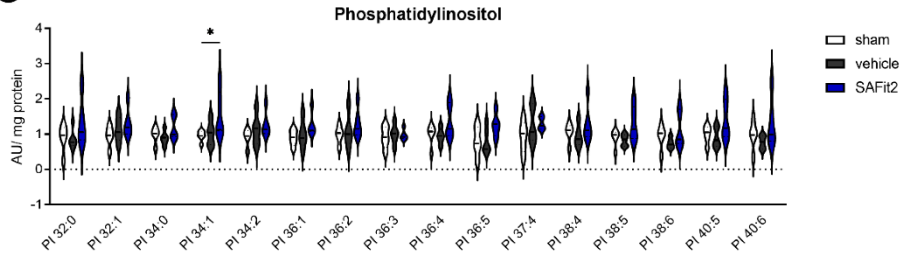
Supplementary Tables: 3



**Figure S1: Normalized lipid concentrations of free fatty acids, ceramides and lysophospholipids in lumbar DRGs 21 days after SNI.** Mice underwent SNI surgery and were treated with either vehicle or 10 mg/kg SAFit2 from day five to ten after the surgery. After 21 days, the lumbar DRGs were isolated from ipsilateral and contralateral sides, lysed and lipids were measured in an untargeted LC-HRMS screening. The distribution of normalized lipids is displayed treatment-wise for each lipid, which are further grouped in classes: **(A)** fatty acids **(B)** ceramides, **(C)** glucosylceramides, **(D)** lysophosphatidylcholines, **(E)** ether-

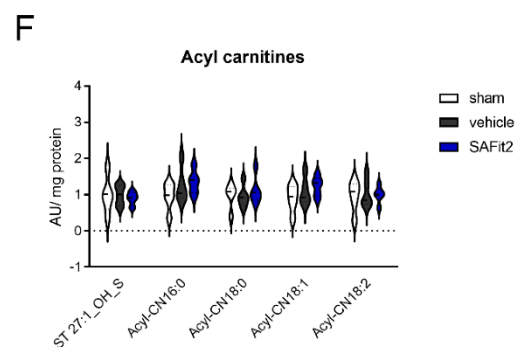
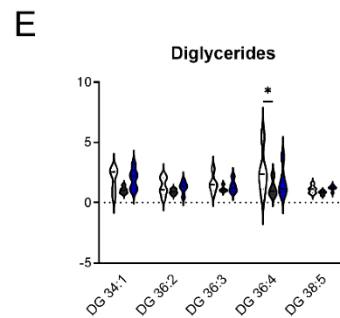
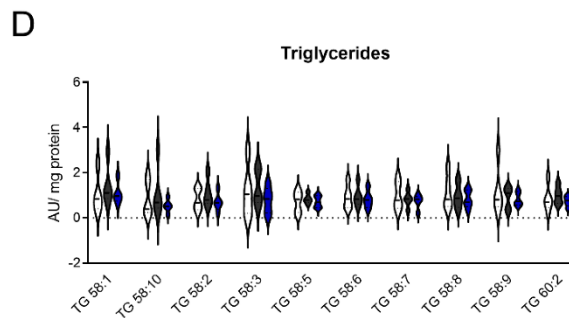
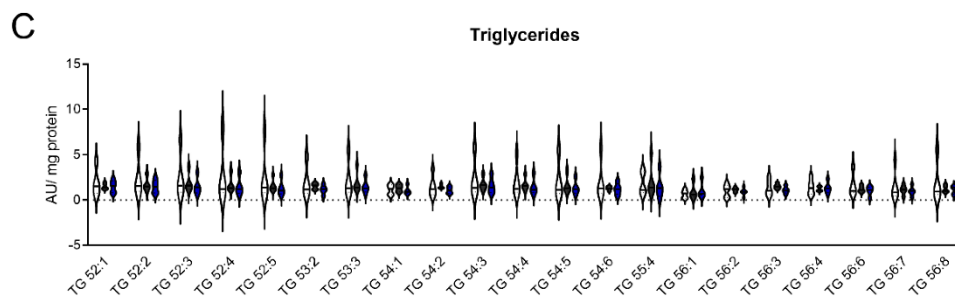
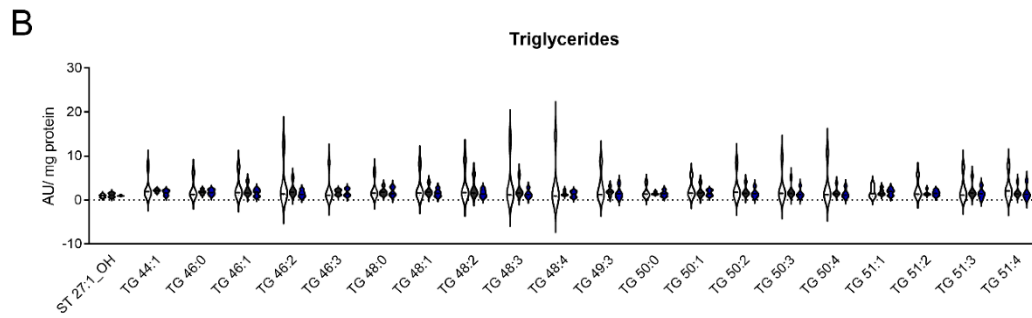
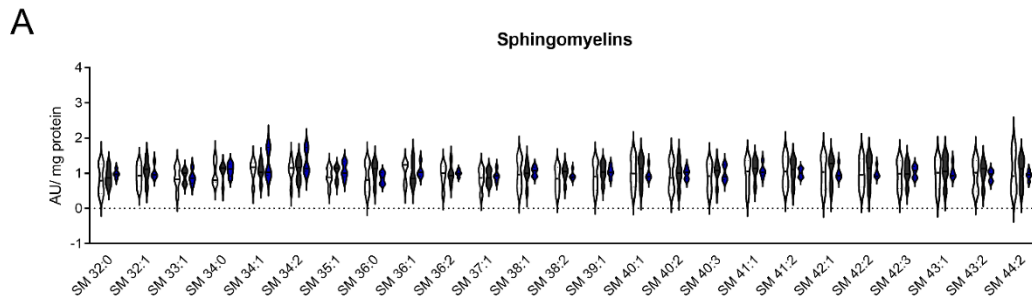
---

lysophosphatidylcholines, **(F)** lysophosphatidyl- and ether-lysophosphatidylethanol, **(G)** lysophosphatidylinositols, **(H)** lysophosphatidylglycerols. \*  $p < 0.05$  two-way ANOVA with Tukey's post hoc test. Abbreviations: DRGs: dorsal root ganglia, SAFit2: selective antagonist of FKBP51 by induced fit 2, SNI: spared nerve injury, LC-HRMS: liquid chromatography-high-resolution mass spectrometry

**A****B****C****D****E****F****G**

---

**Figure S2: Normalized lipid concentrations of phosphatidylcholines, -glycerols, -serines, -ethanols and -inositols in lumbar DRGs 21 days after SNI.** Mice underwent SNI surgery and were treated with either vehicle or 10 mg/kg SAFit2 from day five to ten after the surgery. After 21 days, the lumbar DRGs were isolated from ipsilateral and contralateral sides, lysed and lipids were measured in an untargeted LC-HRMS screen. The distribution of normalized lipids is displayed treatment-wise for each lipid, which are further grouped in classes: **(A, B)** phosphatidylcholines, **(C)** ether-phosphatidylcholines, **(D)** phosphatidylglycerols, **(E)** phosphatidylserines, **(F)** phosphatidyl- and ether-phosphatidylethanols, **(G)** phosphatidylinositols. \*  $p < 0.05$  two-way ANOVA with Tukey's post hoc test. Abbreviations: DRGs: dorsal root ganglia, SAFit2: selective antagonist of FKBP51 by induced fit 2, SNI: spared nerve injury, LC-HRMS: liquid chromatography-high-resolution mass spectrometry



---

**Figure S3: Normalized lipid concentrations of sphingomyelins, triglycerides, diglycerides and acyl carnitines in lumbar DRGs 21 days after SNI.** Mice underwent SNI surgery and were treated with either vehicle or 10 mg/kg SAFit2 from day five to ten after the surgery. After 21 days, the lumbar DRGs were isolated from ipsilateral and contralateral sides, lysed and lipids were measured in an untargeted LC-HRMS screen. The distribution of normalized lipids is displayed treatment-wise for each lipid, which are further grouped in classes: **(A)** sphingomyelins, **(B-D)** triglycerides, **(E)** diglycerides, **(F)** acyl carnitines. \*  $p < 0.05$  two-way ANOVA with Tukey's post hoc test. Abbreviations: DRGs: dorsal root ganglia, SAFit2: selective antagonist of FKBP51 by induced fit 2, SNI: spared nerve injury, LC-HRMS: liquid chromatography-high-resolution mass spectrometry



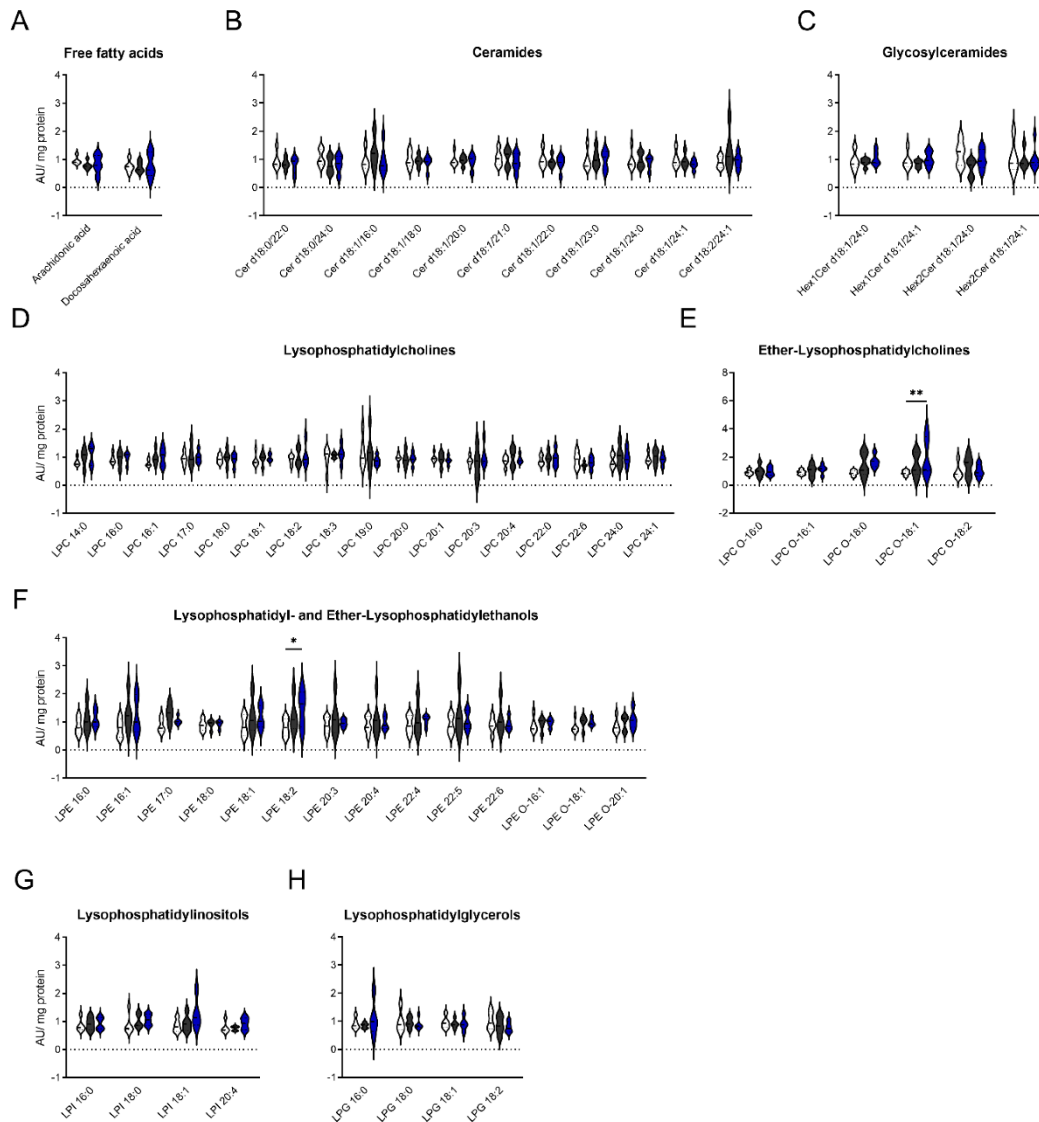
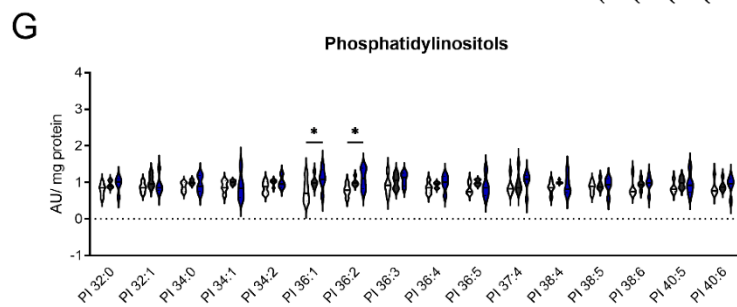
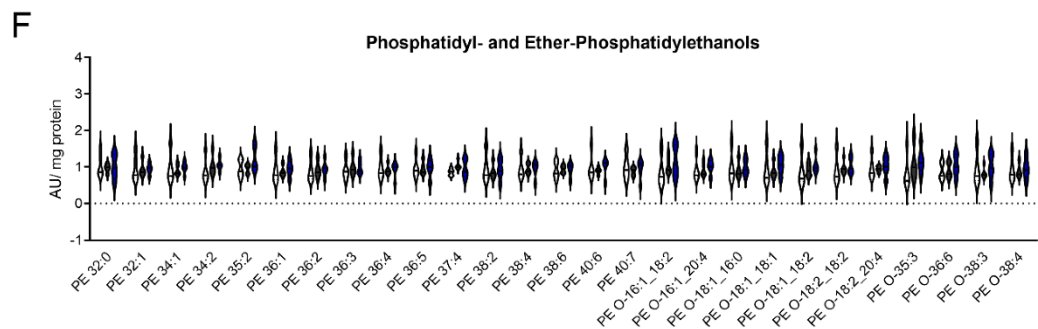
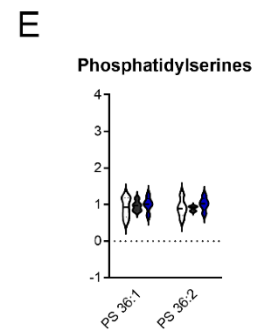
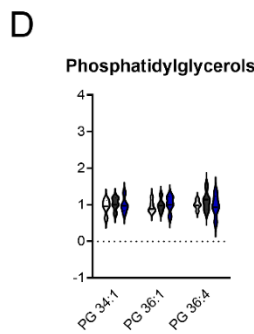
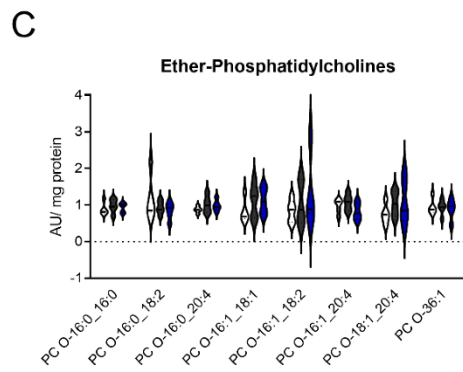
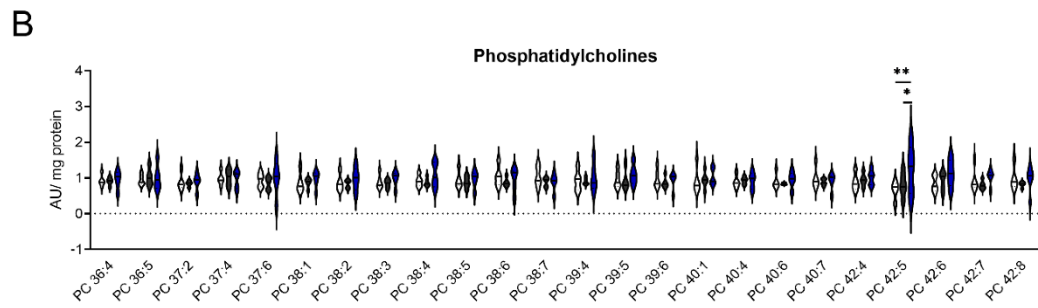
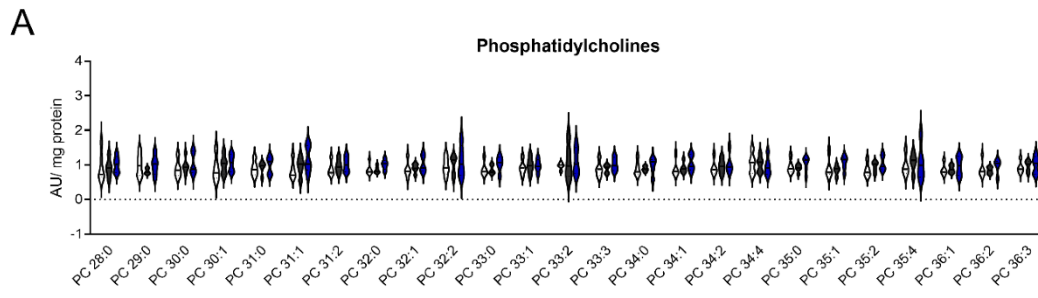


**Figure S4: Normalized lipid concentrations of free fatty acids, ceramides and lysophospholipids in spinal cord 21 days after SNI.** Mice underwent SNI surgery and were treated with either vehicle or 10 mg/kg SAFit2 from day five to ten after the surgery. After 21 days, the spinal cord was isolated from ipsilateral and contralateral sides, lysed and lipids were measured in an untargeted LC-HRMS screen. The distribution of normalized lipids is displayed treatment-wise for each lipid, which are grouped in classes: **(A)** fatty acids **(B)** ceramides, **(C)** glycosylceramides, **(D)** lysophosphatidylcholines, **(E)** ether-lysophosphatidylcholines, **(F)** lysophosphatidyl-

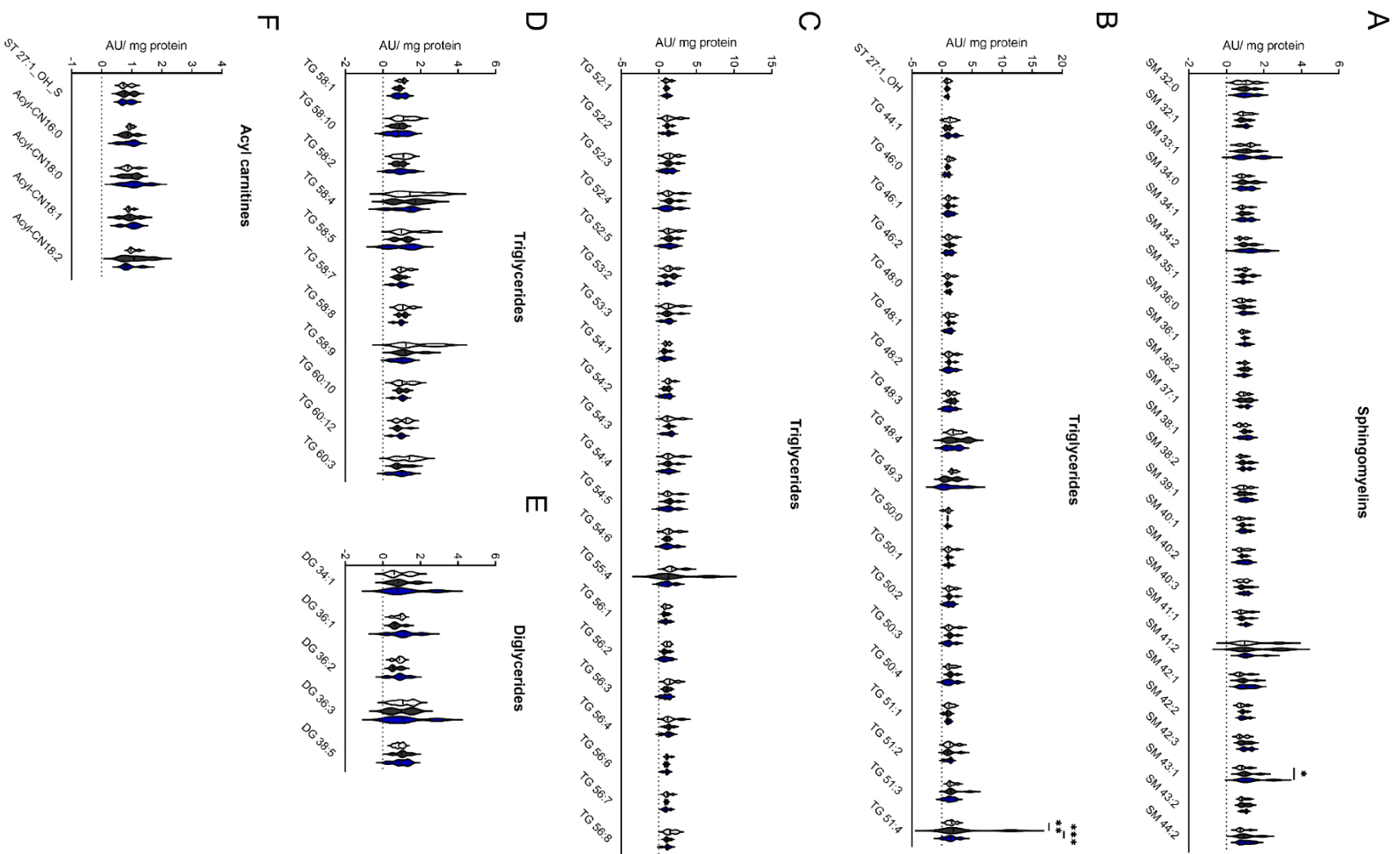
---

and ether-lysophosphatidylethanol, **(G)** lysophosphatidylinositols, **(H)** lysophosphatidylglycerols. \*  $p < 0.05$  two-way ANOVA with Tukey's post hoc test. Abbreviations: SC: spinal cord, SAFit2: selective antagonist of FKBP51 by induced fit 2, SNI: spared nerve injury, LC-HRMS: liquid chromatography-high-resolution mass spectrometry



---

**Figure S5: Normalized lipid concentrations of phosphatidylcholines, -glycerols, -serines, -ethanols and -inositols in spinal cord 21 days after SNI.** Mice underwent SNI surgery and were treated with either vehicle or 10 mg/kg SAFit2 from day five to ten after the surgery. After 21 days, the spinal cord was isolated from ipsilateral and contralateral sides, lysed and lipids were measured in an untargeted LC-HRMS screen. The distribution of normalized lipids is displayed treatment-wise for each lipid, which are grouped in classes: **(A, B)** phosphatidylcholines, **(C)** ether-phosphatidylcholines, **(D)** phosphatidylglycerols, **(E)** phosphatidylserines, **(F)** phosphatidyl- and ether-phosphatidylethanols, **(G)** phosphatidylinositols. \*  $p < 0.05$  two-way ANOVA with Tukey's post hoc test. Abbreviations: SC: spinal cord, SAFit2: selective antagonist of FKBP51 by induced fit 2, SNI: spared nerve injury, LC-HRMS: liquid chromatography-high-resolution mass spectrometry



---

**Figure S6: Normalized lipid concentrations of sphingomyelins, triglycerides, diglycerides and acyl cyanides in spinal cord after 21 days after SNI.** Mice underwent SNI surgery and were treated with either vehicle or 10 mg/kg SAFit2 from day five to ten after the surgery. After 21 days, the spinal cord was isolated from ipsilateral and contralateral sides, lysed and lipids were measured in an untargeted LC-HRMS screen. The distribution of normalized lipids is displayed treatment-wise for each lipid, which are grouped in classes: **(A)** sphingomyelins, **(B-D)** triglycerides, **(E)** diglycerides, **(F)** acyl carnitines. \*  $p < 0.05$  two-way ANOVA with Tukey's post hoc test. Abbreviations: SC: spinal cord, SAFit2: selective antagonist of FKBP51 by induced fit 2, SNI: spared nerve injury, LC-HRMS: liquid chromatography-high-resolution mass spectrometry

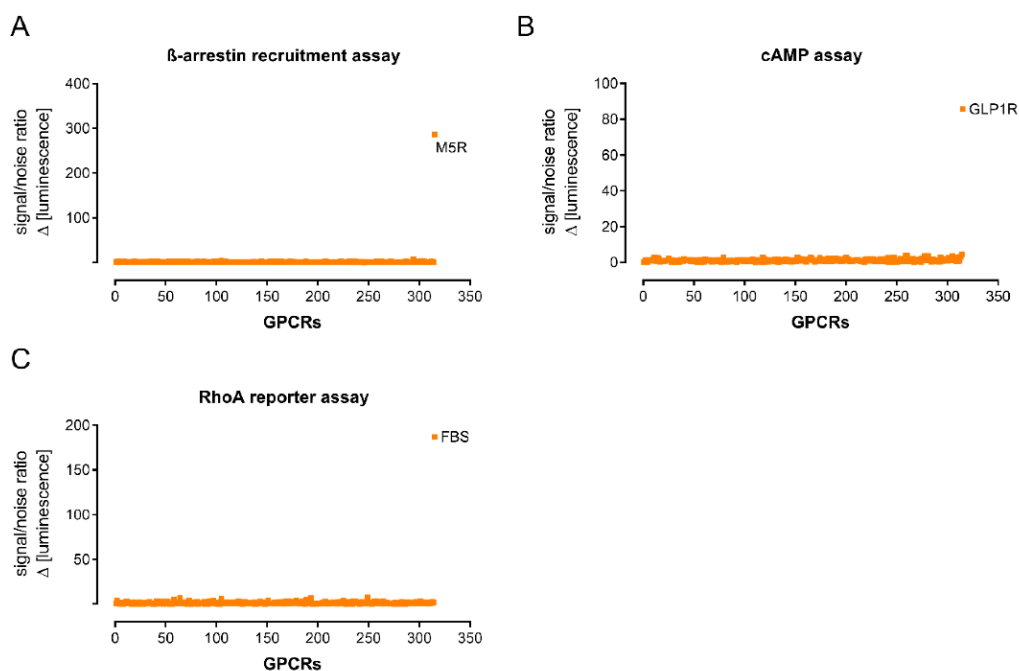


**Figure S7: Results of a GPCR screen using C16 dihydroceramide as a potential interaction partner.** To screen a library of 314 GPCRs in search for a potential receptor activated by the C16 dihydroceramide, a  $\beta$ -arrestin recruitment assay (A), a cAMP assay (B), and a RhoA reporter assay (C) were performed. The C16 was added at a final concentration of 30  $\mu$ M (A) or 15  $\mu$ M (B,C). As positive controls 100  $\mu$ M carbachol and the muscarinic M5 receptor (A), 10 nM GLP-1 and the GLP-1 receptor (B), and FBS (C) were used. For details see method section. The GPCRs analyzed are listed in table S1.

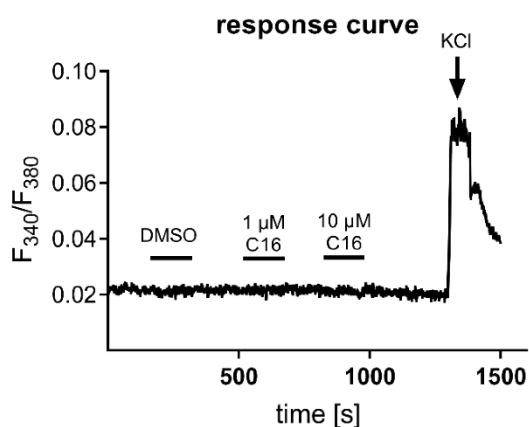


**Figure S8: Representative response curve of calcium fluxes in C16 dihydroceramide treated sensory neurons.** The primary cells were treated with 1 and 10  $\mu\text{M}$  C16 dihydroceramide and the corresponding solvent control (DMSO) followed by a KCl (50 mM) treatment as a positive control.

**Table S1: Internal standards and their concentrations in the working solutions for the lipid screening** (all from Avanti Polar Lipids, Alabaster, AL, USA)

Analyte	Concentration ( $\mu\text{g/mL}$ )
Arachidonic acid-d8	0.1
CE 18:1-d7	5
Cer d18:1/16:0-d7	0.02
Cholesterol-d7	7.5
DG 15:0/18:1-d7	0.3
LacCer d18:1/17:0	0.06
LPC 18:1-d7	0.3
LPC O-16:0-d4	0.02
LPE 18:1-d7	0.02
LPG 17:1	0.02
LPI 17:1	0.02
PC 15:0/18:1-d7	2
PC O-18:0/18:1-d9	0.2
PE 15:0/18:1-d7	0.1
PG 15:0/18:1-d7	0.1
PI 15:0/18:1-d7	0.1
PS 15:0/18:1-d7	0.025
SM d18:1/18:1-d9	0.4
TG 14:0/16:1/14:0-d5	0.6
TG 15:0/18:1-d7/15:0	0.6
TG 20:0/20:1/20:0-d5	0.6



**Table S2: LC-gradient**

Time (min)	Sol. A (%)	Sol. B (%)
0.00	75.0	25.0
0.30	75.0	25.0
1.50	20.0	80.0
11.00	0.0	100.0
12.00	0.0	100.0
12.50	75.0	25.0
14.00	75.0	25.0

### Instrumentation

Mass spectrometer Orbitrap Exploris 480 (Thermo Fisher Scientific, Dreiech, Germany)

HESI-source

HPLC Vanquish Horizon (Thermo Fisher Scientific, Dreiech, Germany)

Vanquish Compartment H

Vanquish Split Sampler HT

Vanquish Pump H

LC-column Zorbax RRHD Eclipse Plus C8 1.8  $\mu\text{m}$  50 x 2.1 mm ID (Agilent, Waldbronn, Germany), heated at 40 °C, flow rate 300  $\mu\text{L}/\text{min}$

Precolumn: ZORBAX Eclipse Plus C8, 2.1 mm, 1.8  $\mu\text{m}$  (Agilent, Waldbronn, Germany)

Solvent A Water + 0.1% formic acid + 10 mM ammonium formate

Solvent B Acetonitrile:isopropanole 2:3 (v/v) + 0.1% formic acid

Injection volume 2  $\mu\text{L}$  (positive ion mode), 5  $\mu\text{L}$  (negative ion mode)

**Table S3: List of GPCRs which were screened for potential activation by the C16 dihydroceramide**

n	description	n	description	n	description	n	description	n	description	n	description
1	ADCYAP1R1	51	CX3C1	101	GPR119	151	GPR4	201	HTR1F	301	TA1
2	ADORA1	52	CXCR1	102	GPR12	152	GPR44	202	HTR2A	302	TAAR2
3	ADORA2A	53	CXCR2	103	GPR120	153	GPR45	203	HTR2B	303	TAAR5
4	ADORA2B	54	CXCR3	104	GPR123	154	GPR50	204	HTR2C	304	TAAR6
5	ADORA3	55	CXCR4	105	GPR124	155	GPR52	205	HTR4	305	TAAR8
6	ADRA1A	56	CXCR5	106	GPR125	156	GPR55	206	HTR5	306	TAAR9
7	ADRA1B	57	CXCR6	107	GPR126	157	GPR56	207	HTR6	307	TACR1
8	ADRA1D	58	CXCR7	108	GPR132	158	GPR6	208	HTR7	308	TACR2
9	ADRA2A	59	CYSLTR1	109	GPR133	159	GPR61	209	KISSPEPTIN	309	TACR3
10	ADRA2B	60	CYSLTR2	110	GPR135	160	GPR62	210	LHCGR	310	TBXA2R
11	ADRA2C	61	DRD1	111	GPR141	161	GPR63	211	LPAR1	311	TSHR
12	ADRB1	62	DRD2	112	GPR142	162	GPR64	212	LPAR2	312	UTS2R
13	ADRB2	63	DRD3	113	GPR143	163	GPR65	213	LPAR4	313	VIPR1
14	ADRB3	64	DRD4	114	GPR144	164	GPR68	214	LPAR5	314	VIPR2
15	AGTR1	65	DRD5	115	GPR146	165	GPR75	215	LPAR6		
16	AGTR2	66	EDNRA	116	GPR148	166	GPR77	216	LTB4R		
17	APJ	67	EDNRB	117	GPR149	167	GPR78	217	LTB4R2B		
18	AVPR1A	68	ELTD1	118	GPR15	168	GPR82	218	MAS1		
19	AVPR1B	69	F2R	119	GPR150	169	GPR83	219	MAS1L		
20	AVPR2	70	F2RL1	120	GPR151	170	GPR84	220	MC1R		
21	BB3	71	F2RL2	121	GPR152	171	GPR85	221	MC2R		
22	BDKRB1	72	F2RL3	122	GPR153	172	GPR87	222	MC3R		
23	BDKRB2	73	FFA1 (GPR40)	123	GPR156	173	GPR88	223	MC4R		
24	C3AR1	74	FFA2 (GPR43)	124	GPR157	174	GPR97	224	MC5R		
25	C5A	75	FFA3 (GPR41)	125	GPR158	175	GPRC5A	225	MCHR1		
26	CALCRb	76	FPR1	126	GPR160	176	GPRC5B	226	MCHR2		
27	CALCRL	77	FPR2	127	GPR161	177	GPRC5C	227	MLNR		
28	CASR	78	FPR3	128	GPR162	178	GPRC5D	228	MRGPRD		
29	CCKAR	79	FSHR	129	GPR17	179	GPRC6A	229	MRGPRE		
30	CCKBR	80	GABBR1	130	GPR171	180	GRM1	230	MRGPRF		
31	CCR10	81	GAL1	131	GPR173	181	GRM2	231	MRGPRG		
32	CCR2	82	GAL2	132	GPR174	182	GRM4	232	MRGPRX1		
33	CCR3	83	GAL3	133	GPR18	183	GRM5	233	MRGPRX2		
34	CCR4	84	GCGR	134	GPR182	184	GRM6	234	MRGPRX3		
35	CCR5	85	GHRHR	135	GPR183	185	GRM7	235	MRGPRX4		
36	CCR6	86	GHSR	136	GPR19	186	GRM8	236	MTNR1A		
37	CCR7	87	GIPR	137	GPR20	187	GRPR	237	MTNR1B		
38	CCR8	88	GLP1R	138	GPR21	188	HCA1	238	NMBR		
39	CCRL2	89	GLP2R	139	GPR22	189	HCA2	239	NMUR1		
40	CD97	90	GNRHR	140	GPR25	190	HCA3	240	NMUR2		
41	CHRM1	91	GPBA	141	GPR26	191	HCTR1	241	NPBW1		
42	CHRM2	92	GPBR	142	GPR27	192	HCTR2	242	NPBW2		
43	CHRM3	93	GPR1	143	GPR3	193	HRH1	243	NPFF1		
44	CHRM4	94	GPR101	144	GPR31	194	HRH2	244	NPFF2		
45	CHRM5	95	GPR110	145	GPR32	195	HRH3	245	NPS		
46	CMKLR1	96	GPR111	146	GPR34	196	HRH4	246	NPY1R		
47	CNR1	97	GPR113	147	GPR35	197	HTR1A	247	NPY2R		
48	CNR2	98	GPR114	148	GPR37	198	HTR1B	248	NPY4R		
49	CRHR1	99	GPR115	149	GPR37L1	199	HTR1D	249	NPY5R		
50	CRHR2	100	GPR116	150	GPR39	200	HTR1E	250	NTSR1		

---

## 4 Publication 3

---

### SAFit2 ameliorates paclitaxel-induced neuropathic pain by reducing spinal gliosis and elevating pro-resolving lipid mediators

Saskia Wedel<sup>1</sup>, Lisa Hahnefeld<sup>1,2</sup>, Yannick Schreiber<sup>2</sup>, Christian Namendorf<sup>3</sup>, Tim Heymann<sup>4</sup>, Manfred Uhr<sup>3</sup>, Mathias V. Schmidt<sup>3</sup>, Natasja de Bruin<sup>2</sup>, Felix Hausch<sup>4</sup>, Dominique Thomas<sup>1,2</sup>, Gerd Geisslinger<sup>1,2</sup> and Marco Sisignano<sup>1,2\*</sup>

<sup>1</sup> Institute of Clinical Pharmacology, Pharmazentrum Frankfurt/ZAFES, University Hospital, Goethe-University, 60590 Frankfurt am Main, Germany

<sup>2</sup> Fraunhofer Institute for Translational Medicine and Pharmacology ITMP, Fraunhofer Cluster of Excellence for Immune Mediated Diseases CIMD, 60596 Frankfurt am Main, Germany

<sup>3</sup> Core Unit Analytics and Mass Spectrometry, Max Planck Institute of Psychiatry, 80804 Munich, Germany

<sup>4</sup> Department of Biochemistry, Technical University Darmstadt, 64287 Darmstadt, Germany

#### 4.1 Author contributions

Conceptualization: FH, MS and GG conceptualized the project.

Funding acquisition: MS, FH, and NdB acquired the funding.

Experimental design: **SW**, NdB, MU and MS designed the experiments.

Data acquisition: **SW** performed the behavioral experiments and isolated the tissue. **SW** further performed multiplex assays, qPCRs, immunohistochemistry stainings, PLA2 assays and prepared tissue samples for measurements. NdB supervised the behavioral study and the pharmacokinetic study together with MVS. CN performed LC-MS/MS measurements for the pharmacokinetic study and LH conducted the LC-HRMS as well as LC-MS/MS for lipid measurements. DT established the LC-MS/MS oxylipin method. TH synthesized the batch of SAFit2.

Data analysis: **SW** analyzed all the data. LH helped with the LC-HRMS as well as CN and LH helped with the LC-MS/MS analysis. NdB helped with the pharmacokinetic study analysis.

Data curation: **SW** performed the data curation.

Original draft preparation: **SW** and MS wrote and revised the manuscript.

All authors approved the final manuscript

## 4.2 Manuscript

Wedel et al. *Journal of Neuroinflammation* (2023) 20:149  
<https://doi.org/10.1186/s12974-023-02835-5>

Journal of Neuroinflammation

### RESEARCH

### Open Access



# SAFit2 ameliorates paclitaxel-induced neuropathic pain by reducing spinal gliosis and elevating pro-resolving lipid mediators

Saskia Wedel<sup>1</sup>, Lisa Hahnefeld<sup>1,2</sup>, Yannick Schreiber<sup>2</sup>, Christian Namendorf<sup>3</sup>, Tim Heymann<sup>4</sup>, Manfred Uhr<sup>3</sup>, Mathias V. Schmidt<sup>3</sup>, Natasja de Bruin<sup>2</sup>, Felix Hausch<sup>4</sup>, Dominique Thomas<sup>1,2</sup>, Gerd Geisslinger<sup>1,2</sup> and Marco Sisignano<sup>1,2\*</sup>

#### Abstract

**Background** Chemotherapy-induced neuropathic pain (CIPN) describes a pathological pain state that occurs dose-dependently as a side effect and can limit or even impede an effective cancer therapy. Unfortunately, current treatment possibilities for CIPN are remarkably confined and mostly inadequate as CIPN therapeutics themselves consist of low effectiveness and may induce severe side effects, pointing out CIPN as pathological entity with an emerging need for novel treatment targets. Here, we investigated whether the novel and highly specific FKBP51 inhibitor SAFit2 reduces paclitaxel-induced neuropathic pain.

**Methods** In this study, we used a well-established multiple low-dose paclitaxel model to investigate analgesic and anti-inflammatory properties of SAFit2. For this purpose, the behavior of the mice was recorded over 14 days and the mouse tissue was then analyzed using biochemical methods.

**Results** Here, we show that SAFit2 is capable to reduce paclitaxel-induced mechanical hypersensitivity in mice. In addition, we detected that SAFit2 shifts lipid levels in nervous tissue toward an anti-inflammatory and pro-resolving lipid profile that counteracts peripheral sensitization after paclitaxel treatment. Furthermore, SAFit2 reduced the activation of astrocytes and microglia in the spinal cord as well as the levels of pain-mediating chemokines. Its treatment also increased anti-inflammatory cytokines levels in neuronal tissues, ultimately leading to a resolution of neuroinflammation.

**Conclusions** In summary, SAFit2 shows antihyperalgesic properties as it ameliorates paclitaxel-induced neuropathic pain by reducing peripheral sensitization and resolving neuroinflammation. Therefore, we consider SAFit2 as a potential novel drug candidate for the treatment of paclitaxel-induced neuropathic pain.

**Keywords** SAFit2, FKBP51, Neuropathic pain, Chemotherapy, Oxylipins

\*Correspondence:

Marco Sisignano

[Marco.Sisignano@med.uni-frankfurt.de](mailto:Marco.Sisignano@med.uni-frankfurt.de)

Full list of author information is available at the end of the article



© The Author(s) 2023. **Open Access** This article is licensed under a Creative Commons Attribution 4.0 International License, which permits use, sharing, adaptation, distribution and reproduction in any medium or format, as long as you give appropriate credit to the original author(s) and the source, provide a link to the Creative Commons licence, and indicate if changes were made. The images or other third party material in this article are included in the article's Creative Commons licence, unless indicated otherwise in a credit line to the material. If material is not included in the article's Creative Commons licence and your intended use is not permitted by statutory regulation or exceeds the permitted use, you will need to obtain permission directly from the copyright holder. To view a copy of this licence, visit <http://creativecommons.org/licenses/by/4.0/>. The Creative Commons Public Domain Dedication waiver (<http://creativecommons.org/publicdomain/zero/1.0/>) applies to the data made available in this article, unless otherwise stated in a credit line to the data.

## Background

Paclitaxel is a chemotherapeutic agent, which is used for the treatment of malignancies as it stabilizes microtubule formation and thereby disrupts cell proliferation and cytoskeleton related cellular functions [1, 2]. Based on this mechanism of action, paclitaxel became a very important cytostatic, which enables the treatment of many different tumor types. However, the microtubule-stabilizing property of paclitaxel also affects the axonal transport of sensory neurons in the peripheral nervous system, which leads to axonal degeneration, neuropathy and neuropathic pain [3].

Neuropathic pain is a pathophysiological pain state, which is generally induced by nerve lesions or damages in the somatosensory system and can become chronic [4, 5]. A specific type of neuropathic pain is the chemotherapy-induced peripheral neuropathy (CIPN), which arises during chemotherapy as a severe side effect [6]. CIPN is a dose-dependent side effect that can even limit or impede an effective cancer therapy as chemotherapy often has to be reduced in dose or frequency or interrupted after the occurrence of CIPN [7, 8]. Unfortunately, CIPN affects up to 80 percent of all cancer patients and the majority of paclitaxel-treated patients [3]. Nonetheless, the available treatment possibilities for CIPN are extremely confined and mostly inadequate as the therapeutics of CIPN itself consist of a low effectiveness and may induce severe side effects, pointing out CIPN as pathological entity with an emerging need for novel treatment targets [9]. In addition, CIPN comprises a large symptom scope, which needs to be further investigated and underlying mechanisms to be revealed in order to develop appropriate therapeutic drugs.

Interestingly, previous studies revealed the FK506 binding protein 51 (FKBP51, encoded by the FKBP5 gene) as a novel and potential target for several pathological disorders such as chronic pain [10, 11], stress endocrinology [12] and glucocorticoid signaling related diseases [13]. In the context of chronic pain, FKBP51 was shown to be significantly upregulated in sensory neurons of the dorsal horn in an ankle joint knee inflammation model, indicating its involvement in the development of persistent pain states [10]. Based on these previous findings, we synthesized a highly potent and FKBP51 specific inhibitor named SAFit2 to address the scarcity of therapeutic approaches for chronic and especially paclitaxel-mediated neuropathic pain [14, 15].

To investigate whether or not the novel and specific FKBP51 inhibitor SAFit2 may reduce paclitaxel-induced neuropathic pain and improve paclitaxel-induced dysregulations of endogenous mechanisms, we performed a multiple low-dose paclitaxel mouse model. Previous findings already discovered that paclitaxel mediates

axonal degeneration and its cumulative toxicity induces neuroinflammation and spinal cord gliosis [3]. Here, we confirm that a paclitaxel treatment induces a release of proalgesic mediators in nervous tissue and mediates spinal cord gliosis. In addition, we show that SAFit2 counteracts spinal cord gliosis after paclitaxel treatment and ameliorates paclitaxel-induced mechanical hypersensitivity in vivo. Previous studies have already shown alterations in the distribution of lipids and the levels of lipid mediators in nerve disorders or chronic pain states [4, 16, 17]. However, the role and precise mechanisms of endogenous lipid mediators in the context of paclitaxel-mediated neuropathic pain are still unclear. Based on this lack of understanding, we performed an unbiased lipidomics screen (LC-HRMS) and a targeted LC-MS/MS oxylipin screen from dorsal root ganglia (DRGs) and spinal cord (SC) samples to elucidate changes in the distribution of lipids after paclitaxel treatment. Furthermore, we assessed the influence of SAFit2 on paclitaxel-mediated alterations in lipid levels. Investigating these lipid levels in paclitaxel-treated mice, we observed that a SAFit2 treatment leads to an increase of anti-inflammatory and pro-resolving lipid mediators, which play a crucial role in the resolution of pain states.

## Materials and methods

### Animals

For all experimental approaches, wild-type animals with a C57BL/NRj background were purchased from the breeding companies Janvier and Charles River. All animal experiments, which included treated animals, were started with nine weeks old mice and naïve mice were matched in age and sex, respectively.

### Paclitaxel and SAFit2 treatment

To induce paclitaxel-mediated neuropathic pain in mice, a multiple low-dose model was performed including four injections of 2 mg/kg paclitaxel, which was administered every second day, adding up to a cumulative dose of 8 mg/kg. [18]. The cytostatic paclitaxel was dissolved in a 50:50 (v/v) ethanol-cremophor EL (238470, Millipore) solution and stored at  $-20^{\circ}\text{C}$  until further usage. Before the intraperitoneal injection, the paclitaxel stock-solution was thawed and freshly diluted 1:2 (v/v) with saline solution (NaCl 0.9% (w/v)) to a final concentration of 0.4 mg/ml. For assessing the influence of SAFit2 on paclitaxel-induced neuropathic pain and endogenous mechanisms, the mice were treated intraperitoneally with either 10 mg/kg SAFit2 or vehicle (PBS supplemented with 5% PEG400, 5% Tween and 0.7% ethanol) two times daily on six consecutive days, starting on day five after the first paclitaxel injection. The experimental treatment schedule is displayed in Fig. 1A.

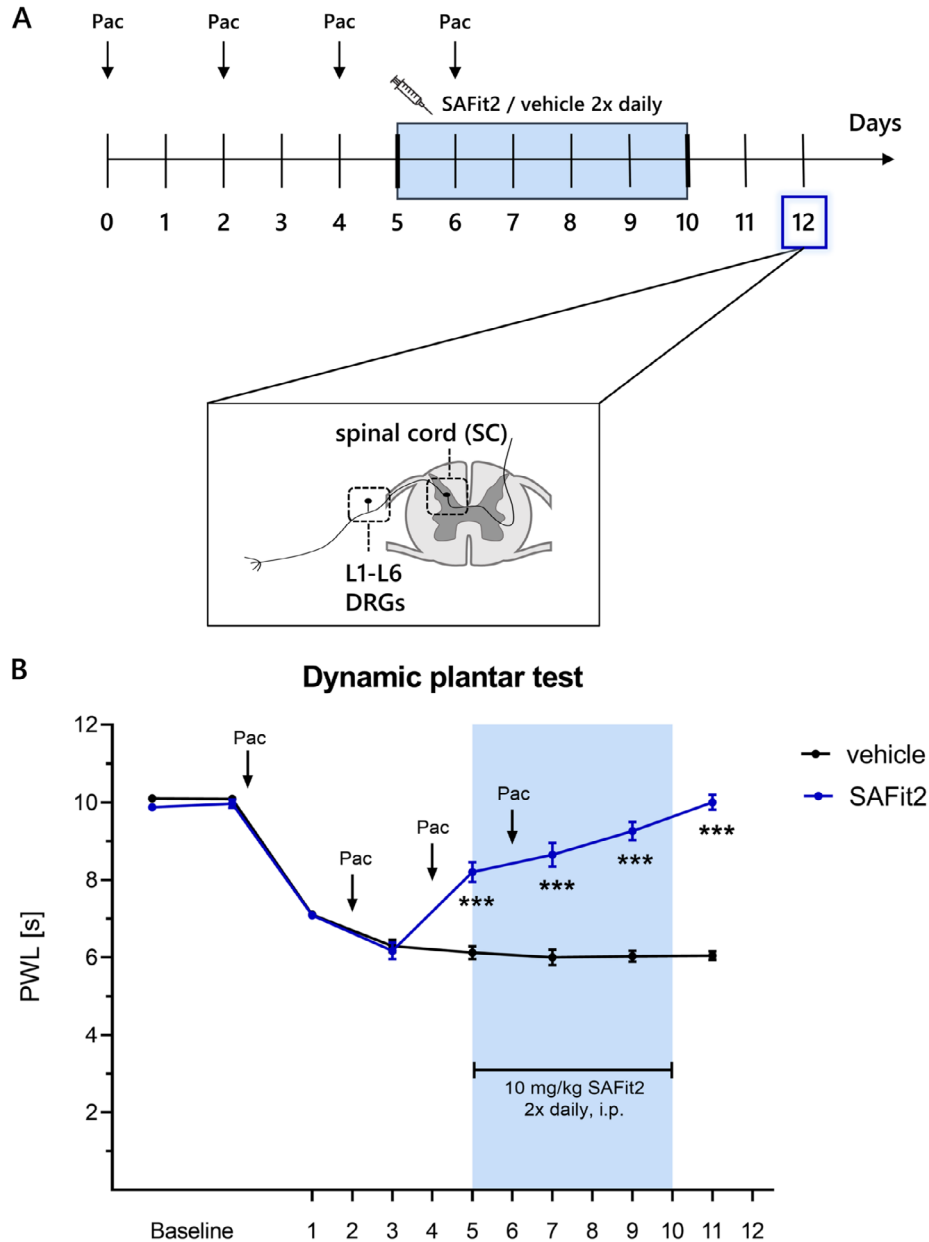


**Fig. 1** SAFit2 reduces paclitaxel-induced mechanical hypersensitivity. **A** Schematic illustration of the animal treatment: neuropathic pain was induced with a multiple low-dose paclitaxel model, including four intraperitoneal injections with 2 mg/kg paclitaxel on day zero, two, four and six. Afterwards, the animals were treated with 10 mg/kg SAFit2 intraperitoneally from day five to ten two times daily. At day twelve, the mice were killed and DRGs and spinal cord samples collected. **B** Baseline measurements were performed on two different days before paclitaxel treatment. The mechanical pain threshold was assessed over 12 days every second day and the behavioral readout within the SAFit2 treatment was recorded between the SAFit2 treatments, approximately three hours after the first dose of SAFit2. The data represent the mean  $\pm$  SEM from 13–14 mice per group. \*\*\* $p < 0.001$  two-way ANOVA with Bonferroni's post hoc test. *Pac* paclitaxel, *DRGs* dorsal root ganglia, *PWL* paw withdrawal latency, *SAFit2* selective antagonist of FKBP51 by induced fit 2

### Behavioral experiments

Before starting the behavioral experiments and treatment phases, the locomotor function of all animals was verified using a rotarod assay [19]. During all behavioral experiments, the experimenter was blinded. For assessing the mechanical pain threshold, the animals were placed at least one hour before the measurement in the respective test cages to allow habituation. After this habituation phase, the mechanical paw withdrawal threshold was assessed using a Dynamic Plantar Aesthesiometer (Ugo Basile) as described previously [20]. The baseline measurements were performed on two consecutive days before the treatment phase and the mechanical pain thresholds were assessed every second day.

### Tissue isolation

For tissue isolation, mice were euthanized by isoflurane anesthesia (2–2.5% isoflurane in carbogen), cardiac puncture, and cervical dislocation 12 days after the first paclitaxel injection. The lumbar (L1–L6) dorsal root ganglia (DRGs) and the respective innervated segments of the spinal cord were dissected followed by freezing tissue samples in liquid nitrogen for either RNA isolation, a multiplex assay or LC–HRMS and LC–MS/MS analysis. For immunohistochemistry staining, the spinal cord was dissected and fixed with 2% paraformaldehyde (PFA) solution until further usage.

### Pharmacokinetic study

In the pharmacokinetic study, a single dose of 40 mg/kg SAFit2, formulated as described above, was applied intraperitoneally. Likewise, a single dose of 100 mg/kg SAFit2, formulated as a slow-release formulation with vesicular phospholipid gel (VPG) [21], was applied subcutaneously. For the first formulation, plasma and brain samples were collected after 15 min, 30 min, 1 h, 3 h, 6 h and 24 h from three animals. For the second formulation, plasma and brain samples were collected after 2 h, 8 h, 24 h, 48 h, 72 h and 96 h from three animals. Mice were euthanized by isoflurane anesthesia (2–2.5% isoflurane in carbogen), cardiac puncture, and cervical dislocation. Brains were weighed and then homogenized in tenfold PBS volume containing Complete Protease Inhibitor Cocktail Tablets (Roche), using a Dispomix Drive (Medic Tools AG). Plasma samples were analyzed using the combined high-performance liquid chromatography/mass spectrometry (HPLC/MS–MS) technique. Analysis was performed using a Shimadzu Nexera X2 (Shimadzu) liquid chromatograph, which was interfaced to the ESI source of a Sciex QTrap 5500 (Sciex) triple quadrupole mass spectrometer. All samples were prepared using Ostro protein precipitation and phospholipid removal plates (Waters).

Chromatography was accomplished using a gradient elution in an Accucore RP-MS column (100×2.1 mm, 2.6 μm Thermo Scientific) at a flow rate of 0.5 ml/min and 30 °C. The composition of eluent B was methanol with 10 mM ammonium formate with 0.1% formic acid and water with 10 mM ammonium formate with 0.1% formic acid was eluent A. The gradient was 0–3 min 60% B, 3–4.5 min 60–90% B, 0.5 min held at 90% B, 5–5.2 min 90–60% B and 5.2–6 min 60% B. The total run time was 6 min and the injection volume was 2 μl. The ion source was operated in the positive mode at 500 °C, and multiple reaction monitoring (MRM) collision-induced dissociation (CID) were performed using nitrogen gas as the collision gas. Deuterated SAFit2 (SAFit2-D3) was used as internal standard.

### Quantitative real-time PCR

To isolate the RNA from lumbar DRGs and the respective segments of the spinal cord, the mirVana miRNA Isolation Kit (Applied Biosystems) was used according to the manufacturer's instructions. Afterwards, RNA concentrations were quantified with a NanoDrop ND-1000 spectrophotometer (NanoDrop Technologies) and a cDNA synthesis was conducted with 200 ng RNA from DRGs and 400 ng RNA from spinal cord. The reverse transcription was performed with the First Strand cDNA Synthesis Kit (Thermo Fisher Scientific) according to the manufacturer's recommendations. The quantitative real-time PCR was performed with the QuantStudio™ Design & Analysis Software v 1.4.3 (Thermo Fisher Scientific) in a TaqMan® Gene Expression Assay System (Table 1, Thermo Fisher Scientific) according to the manufacturer's instructions. The raw data were evaluated using the  $\Delta\Delta C(T)$  method, as described previously [22, 23].

### Multiplex assay

For performing the ProcartaPlex multiplex immunoassay (Thermo Fisher), proteins were isolated with a manufacturer recommended cell lysis buffer, which was further supplemented with a phosphatase inhibitor cocktail (PhosSTOP, Roche) and a protease inhibitor cocktail (cOmplete, Roche). Each lumbar DRG (L1–L6 per animal) sample was suspended in 100 μl and each spinal cord sample, which comprises the respective innervated segments of the spinal cord, in 200 μl cell lysis buffer. The spinal cord samples were further processed by a cell grinder. Afterwards, the tissue was homogenized two times per sample using a Sonopuls Sonicator (Bandelin) with the setting 6×10%. During sonication, the samples were cooled in an ice bath, preventing proteins from degradation. Finally, the samples were centrifuged with 16,000×g at 4 °C for 10 min, followed by collecting the

**Table 1** List of used TaqMan<sup>®</sup> gene expression assays

Target	Gene	Article number	Company
ALOX12	Arachidonate 12-lipoxygenase	Mm00545833_m1	Thermo Fisher
ALOX15	Arachidonate 15-lipoxygenase	Mm00507789_m1	Thermo Fisher
ALOX5	Arachidonate 5-lipoxygenase	Mm01182747_m1	Thermo Fisher
ATF3	Activating transcription factor 3	Mm00476033_m1	Thermo Fisher
CerS5	Ceramide synthase 5	Mm00556165_m1	Thermo Fisher
CerS6	Ceramide synthase 6	Mm00510998_m1	Thermo Fisher
cFOS	FBJ osteosarcoma oncogene	Mm00487425_m1	Thermo Fisher
COX2	Cytochrome c oxidase subunit II	Mm03294838_g1	Thermo Fisher
CYP2J6	Cytochrome P450, family 2, subfamily j, polypeptide 6	Mm01268197_m1	Thermo Fisher
CYP3a11	Cytochrome P450, family 3, subfamily a, polypeptide 11	Mm00731567_m1	Thermo Fisher
GAPDH	Glyceraldehyde-3-phosphate dehydrogenase	Mm99999915_g1	Thermo Fisher
iNOS	Inducible nitric oxide synthase 2	Mm00440502_m1	Thermo Fisher
MMP9	Matrix metalloproteinase 9	Mm00442991_m1	Thermo Fisher
NOX2	NADPH oxidase 2	Mm01287743_m1	Thermo Fisher
NOX4	NADPH oxidase 4	Mm00479246_m1	Thermo Fisher
PLA2g4a	Phospholipase A2, group 4a	Mm00447040_m1	Thermo Fisher
PLA2g4c	Phospholipase A2, group 4c	Mm01195718_m1	Thermo Fisher
XDH	Xanthine dehydrogenase	Mm00442110_m1	Thermo Fisher

supernatant for a protein concentration determination via Bradford.

The ProcartaPlex multiplex immunoassay was performed according to the manufacturer's recommendations. Briefly, a dark wall 96-well plate was prepared by several washing steps and coating steps with respective magnetic beads. Afterwards, standards were prepared in a serial dilution (1:4, (v/v)) and added to the plate, followed by further washing steps. Lastly, the samples were diluted (1:2, (v/v)) and added to the plate, which was sealed and incubated for 40 min with 500 rpm on an orbital shaker at room temperature, overnight at 4 °C and further 50 min with 500 rpm at room temperature. On the next day, the detection antibody mixture was added after a washing step and the plate was further incubated on an orbital shaker for 30 min at room temperature. Again, the plate was washed and streptavidin phycoerythrin (SAPE) was added to the plate and incubated for 30 min as described above. After the last washing step, the plate was prepared with reading buffer, incubated for 5 min with 500 rpm on an orbital shaker, and measured with the Luminex 200 system (Bio-Rad).

#### Immunohistochemistry

Before the immunohistochemical staining, the spinal cord samples were fixed with 2% PFA for 5 h at room temperature, as previously described in the tissue isolation section. As a next step, the tissue was dehydrated

with a concentration series of 20% (w/v) and 30% (w/v) sucrose solutions. Therefore, spinal cord samples were firstly incubated in a 20% sucrose solution at 4 °C overnight and then further dehydrated in a 30% sucrose solution for five hours at 4 °C. Next, the spinal cord samples were embedded in Tissue-Tek and frozen at – 80 °C. The frozen tissue samples were serially sliced into 14-µm tissue slices with a cryostat (Leica Biosystems).

For staining the slices, the samples were fixed with 2% PFA for ten minutes. Afterwards, the fixative was removed and the slices rinsed with PBS. Next, slices were permeabilized with PBS (pH 7.4) containing 0.1% Triton X (v/v) for 15 min. After removing the PBST, the slices were blocked with a 3% BSA (w/v) solution for two hours at room temperature. The primary antibodies anti-GFAP (ab7260, Abcam), anti-IBA1 (019-19741, FUJIFILM Wako Pure Chemical Corporation), anti-ATF3 (sc-188, Santa Cruz) and anti-cFOS (9F3, Cell Signaling) were diluted 1:1000, 1:500, 1:100 and 1:200, respectively, in 1% BSA solution and applied for an overnight incubation at 4 °C. The primary antibody anti-FKBP51 (sc-271547, Santa Cruz) was diluted 1:50 as recommended in 3% BSA solution to minimize cross-reactivity as the host species is mouse.

On the next day, the excess of non-specific binding primary antibodies was removed via three washing steps with PBS, this time incubating the slices with PBS for 5 min. Afterwards, the secondary antibodies, goat



anti-rabbit Alexa Fluor 488 (ab150077, Abcam) and donkey anti-rabbit Alexa Fluor 647 (A-31573, Thermo Fisher) were diluted 1:1000 in 1% BSA solution and applied for one hour at room temperature. The secondary antibodies goat anti-mouse Alexa Fluor 488 (CF488A, Biotium) and sheep anti-mouse Cy3 (C2181, Sigma Aldrich) were diluted in 3% BSA solution. Next, the excess of non-specific binding secondary antibodies was removed, the slices rinsed with PBS and further incubated with DAPI 1:1000 (6335.1, Carl Roth) for ten minutes at room temperature. The slices were mounted with Fluoromount-G mounting medium from Southern Biotech. Images were taken with the fluorescence microscope Observer.Z1 (Carl Zeiss) and processed as well as quantified with ImageJ software. Three to five representative images were taken per stained spinal cord slice, resulting in a total number of 10–20 images per animal. In total, we quantified the number of cells for the markers GFAP and IBA1 by counting cells in 70–80 pictures per condition. For the marker cFOS, we counted the cells in 40 images per condition and for FKBP51, we quantified the mean intensity per image for 40 images per condition.

#### Liquid chromatography–high-resolution mass spectrometry (LC–HRMS)

For LC–HRMS purposes, an approximately 3 mg lumbar DRG sample and 30 mg of the respective parts of the spinal cord (SC) were homogenized using a pellet pestle mixer (Thermo Fisher scientific). The tissue samples were grinded for 30 to 60 s, with short breaks included to avoid overheating, in an ethanol:water (1:9, v/v) solution, using 119  $\mu$ l ethanol for DRG samples and 1190  $\mu$ l ethanol for spinal cord samples. Afterwards, lipid extraction and chromatographic separation was performed as well as the measurement settings and internal standards chosen as previously described [24]. Instrumental setup consisted of a Vanquish Horizon coupled to an Exploris 480 (both Thermo Fisher Scientific) with Zorbax RRHD Eclipse Plus C8 column (2.1  $\times$  50 mm, 1.8  $\mu$ m, Agilent) and a pre-column of the same type. The measured lipid levels were normalized to the respective protein amount of the sample. For all lipidomic measurements, including extraction and analysis, the experimenter was blinded.

#### PLA<sub>2</sub> activity assay

To measure PLA<sub>2</sub> activity in primary sensory neuron lysates, DRGs were collected from two naïve mice and washed with ice-cold PBS. Next, the cells were lysed in 1 ml of ice-cold PBS and homogenized using a Sonopuls Sonicator (Bandelin) three times with the setting 6  $\times$  10%. Afterwards, the homogenate was centrifuged with 10,000 rpm for 15 min at 4 °C and the supernatant collect for the PLA<sub>2</sub> activity assay (Abcam).

The assay was performed according the manufacturer's recommendations.

#### Oxylin screen

For oxylin analysis, dorsal root ganglia (DRG) were homogenized in 10% ethanol with addition of 10 M indomethacin (0.04 mg tissue/ $\mu$ l) with a pellet pestle mixer (fisher scientific). Similarly, spinal cord samples were homogenized in 10% ethanol with addition of 10 M indomethacin (0.075 mg tissue/ $\mu$ l) and 7 zirconium oxide beads using a Precellys 24-Dual tissue homogenizer coupled with a Cryolys cooling module (both Bertin Technologies) that was kept at < 10 °C. The Precellys program encompassed three rounds at 6500  $\times$ g for 20 s with 60 s pauses in between to avoid overheating. Tissue homogenates were stored on ice during extraction. For both tissue types, to 200  $\mu$ l of tissue homogenate, 10  $\mu$ l of 4.4% formic acid, 20  $\mu$ l internal standard solution and 20  $\mu$ l of 0.1% BHT in methanol were added and vortexed for 30 s. Proteins were precipitated by addition of 200  $\mu$ l cold acetonitrile:methanol (8:2, v/v). After vortexing for 120 s and 600 s of centrifugation at approximately 15,000  $\times$ g, the supernatant was used for solid phase extraction using EVOLUTE EXPRESS ABN 30 mg/1 ml cartridges (Biotage) as previously described [25]. Calibration standards and quality control samples were prepared accordingly with 20  $\mu$ l of standard solution in methanol with 0.1% BHT and 200  $\mu$ l of PBS. Additionally, DRG homogenates were diluted by adding 180  $\mu$ l of 10% ethanol with 10 M indomethacin to 20  $\mu$ l of homogenate and processed as described above. LC–MS/MS analysis was then conducted on a QTrap 6500+ (Sciex) coupled to a 1290 Infinity II LC-System (Agilent) using an Acquity UPLC BEH C18 column (1.7  $\mu$ m 100  $\times$  2.1 mm ID) with a pre-column of the same type. For all measurements, including extraction and analysis, the experimenter was blinded. Further details including method parameters can be found in a previous publication [25].

#### Data analysis and statistics

All data are presented as mean  $\pm$  SEM. Normal distribution was confirmed using the Shapiro–Wilk test. The statistical analysis for behavioral experiments was conducted using a two-way analysis of variance (ANOVA) with Bonferroni's post hoc correction. For all ex vivo experiments, an unpaired and heteroskedastic Student's *t* test with Welch correction was performed, when comparing only two groups with each other. For the comparison of more than two groups, a one-way ANOVA was used and for examining the effect of two independent variables on a continuous dependent variable a two-way ANOVA was conducted. For all statistical analysis

the software GraphPad Prism 9.5 was used. A  $p$  value of  $<0.05$  was considered as statistically significant.

## Results

Previous studies already suggested a crucial role of FKBP51 in the context of chronic pain states [10, 11]. However, its upregulation in chemotherapy-induced neuropathic pain is not confirmed yet. Therefore, we performed an immunohistochemistry staining to investigate its expression after paclitaxel treatment in L4–L5 dorsal root ganglia as well as in spinal cord slices (Additional file 1: Fig. S1). For both neuronal tissues, we observed a significant increase of FKBP51 after paclitaxel, when comparing the expression to naïve animals. These data confirm the relevance of FKBP51 in the context of chronic pain states and especially chemotherapy-induced neuropathic pain.

### SAFit2 ameliorates paclitaxel-induced mechanical hypersensitivity

To investigate the influence of SAFit2 on paclitaxel-induced neuropathic pain and underlying mechanisms, we chose a well-established multiple low-dose paclitaxel model as a multiple low-dose model corresponds more to a human chemotherapy, than a single high-dose model. The respective model consists of four intraperitoneal injections of paclitaxel (2 mg/kg) every other day, resulting in a cumulative dose of 8 mg/kg to induce paclitaxel-mediated neuropathic pain (Fig. 1A) [26].

As a first approach, the bioavailability and brain permeability of SAFit2 was monitored in a pharmacokinetic study. Here, we tested two SAFit2 doses and two formulations, measuring SAFit2 concentrations in plasma and brain after treatment (Additional file 1: Fig. S2). SAFit2 was either formulated in PBS supplemented with 5% PEG400, 5% Tween and 0.7% ethanol or as slow-release formulation in vesicular phospholipid gel (VPG, Additional file 1: Fig. S2). We observed that the slow-release VPG formulation led to a strong but transient brain permeability of SAFit2 that did not differ between the two doses or vehicles at later time points.

To analyze the effect of SAFit2 on paclitaxel-induced peripheral neuropathy, we aimed to achieve moderate to high SAFit2 plasma concentrations. However, a single injection of the slow-release formulation was not sufficient to achieve sustained moderate to high plasma concentrations and a single dose of 40 mg/kg SAFit2 led to exceedingly high plasma concentrations of SAFit2 at early time points (Additional file 1: Fig. S2). Based on these results and previous studies in which SAFit2 had been administered *in vivo*, we decided to treat the animals intraperitoneally with either 10 mg/kg SAFit2 or vehicle two times daily from day five to ten to investigate

the therapeutic effect of SAFit2 on paclitaxel-treated mice [14, 24, 27]. After 12 days, the animals were killed and the lumbar DRGs (L1–L6) as well as the respective innervated segments of the spinal cord were isolated and collected separately from each individual animal for further biochemical analysis (Fig. 1A).

To investigate whether SAFit2 has an effect on paclitaxel-mediated neuropathic pain, the pain behavior of mice was assessed before the initiation of the model and during the treatment phase until day twelve by recording the mechanical paw withdrawal threshold (Fig. 1B). Both groups (vehicle and SAFit2) developed a mechanical hypersensitivity over time due to the paclitaxel treatment. However, the SAFit2-treated animals recovered from the mechanical hypersensitivity as their paw withdrawal thresholds significantly increased after the first dose of SAFit2 (Fig. 1B). In addition, the amelioration of pain sensation was sustained after the last treatment of SAFit2 until day twelve (Fig. 1B). In summary, SAFit2 significantly reduced the paclitaxel-induced mechanical hypersensitivity *in vivo*.

### SAFit2 reduces neuronal stress marker expression

As we detected a significant and sustained pain relief through the treatment with SAFit2, we analyzed the expression of neuronal stress markers (Fig. 2A–C) and reactive oxygen species (ROS) (Fig. 2D–G) markers in DRG and spinal cord samples in order to understand how SAFit2 affected underlying mechanisms. In addition, we compared the gene expression of both paclitaxel-treated groups with the basal expression of naïve mice, termed control group in the following.

For the neuronal stress marker activating transcription factor 3 (ATF3), we detected a significantly reduced expression in the DRGs of SAFit2-treated animals compared to vehicle-treated animals (Fig. 2A). In addition, the downregulation of ATF3 was confirmed via an immunohistochemistry staining in L4 and L5 DRGs of SAFit2-treated animals (Additional file 1: Fig. S3). Furthermore, we detected no significant changes in the expression of matrix metalloproteinase 9 (MMP9) (Fig. 2B). In contrast, we detected significantly diverging changes in the expression of the neuronal activity marker cFOS for both tissues (Fig. 2C). However, we observed on a protein level a significant downregulation of cFOS for both tissues after SAFit2 treatment, which we suggest to occur due to posttranscriptional modifications (Additional file 1: Fig. S4). In general, cFOS is known to be biphasically expressed and to contribute to the resolution of neuronal damage as its expression is enhanced in the formation of neuronal and synaptic plasticity [28], however its early upregulation was associated with nociceptive activity. In summary, we detected an enhanced expression of cFOS

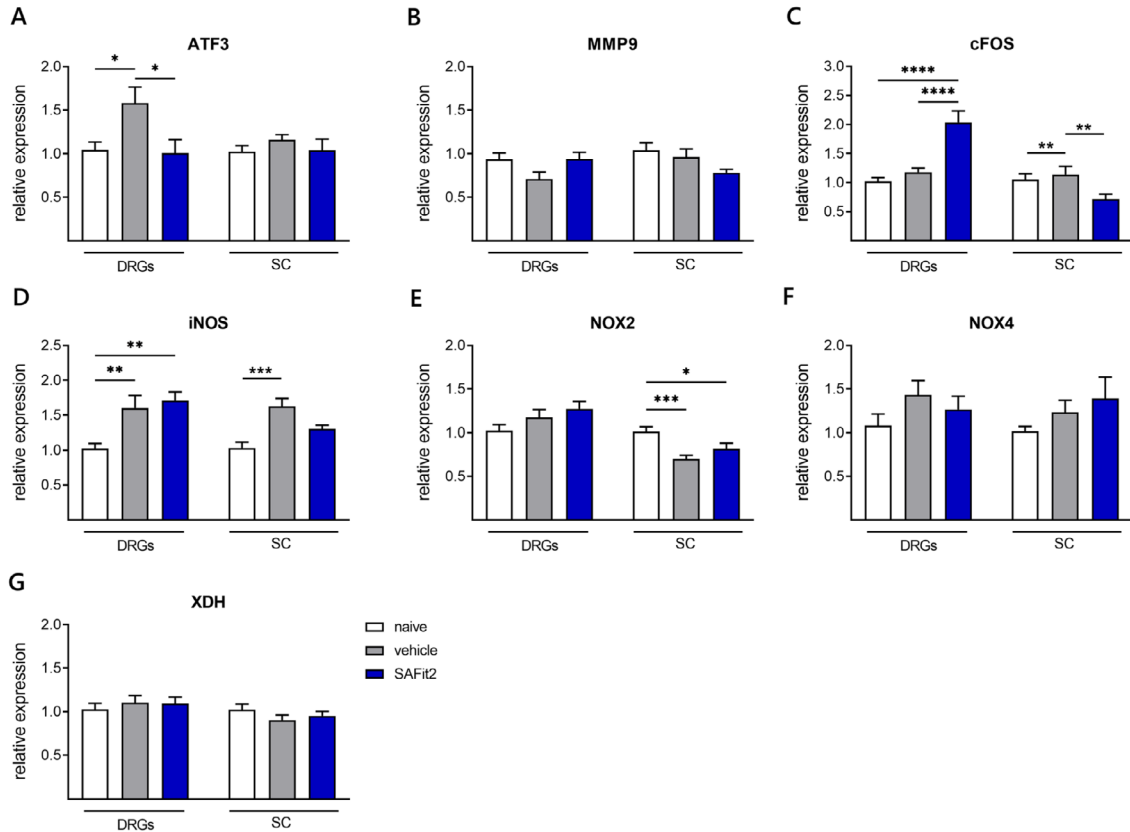


**Fig. 2** Neuronal stress and ROS marker expression in DRGs and spinal cord. After 12 days, the expression of neuronal stress markers (A–C) and ROS markers (D–G) was assessed via qPCR. The expression of vehicle and SAFit2-treated animals were normalized to the expression of naïve animals. The data represent the mean  $\pm$  SEM from 3–4 mice per group, measured in technical triplicates, respectively. \*  $p < 0.05$ , \*\*  $p < 0.01$ , \*\*\*  $p < 0.001$  one-way ANOVA with Tukey’s multiple comparison test per tissue. DRGs dorsal root ganglia, SC spinal cord, SAFit2 selective antagonist of FKBP51 by induced fit 2, ROS reactive oxygen species, ATF3 activating transcription factor 3, MMP9 matrix metalloproteinase 9, XDH xanthine dehydrogenase, NOX2/4 NADPH oxidase 2/4, iNOS inducible nitric oxide synthase

on RNA level in the DRGs and a reduced expression of cFOS on protein level in both tissues after SAFit2 treatment. Furthermore, we observed a reduced expression of ATF3 as neuronal stress marker on RNA and protein level in the DRGs after SAFit2 treatment, which indicates a reduction of neuronal stress after paclitaxel treatment.

Furthermore, we analyzed the expression of ROS markers in lumbar DRGs and spinal cord as the cytostatic paclitaxel is known to induce oxidative stress in sensory neurons [29]. However, we only detected a significant increase in the inducible nitric oxide synthase (Fig. 2D). In line with that, we observed no significant differences in the expression of NADPH oxidase two in the DRGs (Fig. 2E) as well as NADPH oxidase four (Fig. 2F) and the xanthine dehydrogenase (Fig. 2G) in both tissues. From this data, we suggested that the time point of investigation, which was day 12 and already 6 days after the last

paclitaxel treatment, may be too late to measure alterations in ROS responding genes and that their expression changes may be more transient after paclitaxel treatment.

#### SAFit2 reduces pain-mediating chemokine levels and increases anti-inflammatory cytokine levels in DRGs and spinal cord after paclitaxel treatment

Since we did not observe strong differences in the gene expression of neuronal stress and ROS markers except for ATF3 and cFOS after SAFit2 treatment, we next measured the concentrations of inflammatory and proalgesic mediators in the DRGs and the respective segments of the spinal cord. Therefore, we performed a multiplex immunoassay assay, comprising a panel of 26 mediators, to determine differences in the neuroinflammation between vehicle and SAFit2-treated animals in a multiple

low-dose paclitaxel model (Fig. 3, Additional file 1: Figs. S5, S6, S7).

Analyzing these mediators, we observed a significant upregulation of the anti-inflammatory interleukin 22 in the DRGs (Fig. 3A) as well as a significant downregulation of several pain-mediating chemokines such as CCL 2, CCL3, CCL4, CCL5, CCL7 and CXCL10 after SAFit2 treatment (Fig. 3B–G). Moreover, we detected the same tendencies in the spinal cord, since we observed a significant upregulation of the anti-inflammatory cytokine

interleukin 10 (Fig. 3H) and the significant down-regulation of CCL7 (Fig. 3I). Overall, SAFit2 seems to decrease the levels of pain-mediating chemokines and to increase anti-inflammatory mediators in both neural tissues after paclitaxel treatment.

**SAFit2 treatment decreases activation of astrocytes and microglia in the spinal cord of paclitaxel-treated mice**  
Based on the strong effect of SAFit2 on pain-mediating chemokines in the lumbar DRGs and spinal cord, we

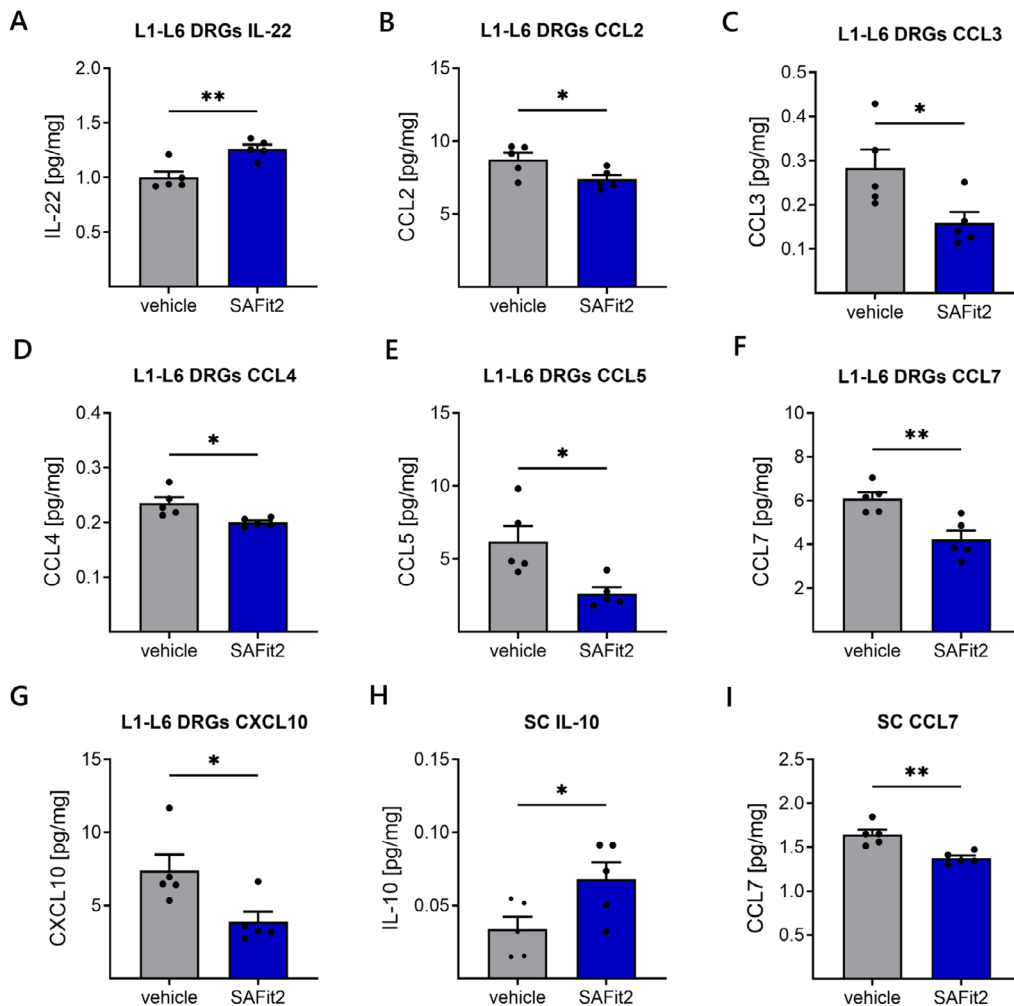


**Fig. 3** Increase of anti-inflammatory cytokines and decrease of pain-mediating chemokines in neuronal tissue of SAFit2-treated animals. After 12 days, DRGs and spinal cord samples were homogenized and analyzed using a multiplex immunoassay including a panel of 26 cytokines and chemokines. This figure displays a section of significantly altered cytokines and chemokines in the DRGs (A–G) and spinal cord (H, I) after vehicle and SAFit2 treatment. The data represent the mean  $\pm$  SEM from 5 mice per group. The raw data were related to the total protein amount of the sample. \*  $p < 0.05$ , \*\*  $p < 0.01$ , \*\*\*  $p < 0.001$  Student's *t*-test with Welch's correction. SAFit2 selective antagonist of FKBP51 by induced fit 2, DRGs dorsal root ganglia, SC spinal cord, IL interleukin, CCL C–C motif ligand, CXCL 10 C–X–C ligand 10

investigated the effect of SAFit2 regarding spinal gliosis, since activated astrocytes and microglia are the predominant source of cytokines and chemokines in the spinal cord [30, 31]. To assess this, we performed immunohistochemical stainings of dorsal horn samples to assess the activation of astrocytes and the number of microglia (Fig. 4).

First, we analyzed the activation of astrocytes with the astrocyte activation marker glial fibrillary acidic protein (GFAP) in dorsal horn cryo-slices (Fig. 4A, C). In these stainings, we could observe a high number of GFAP-positive cells in the vehicle-treated paclitaxel group, indicating a strong activation of astrocytes after paclitaxel treatment (Fig. 4A). In contrast, the number of GFAP-positive cells was lower in the SAFit2-treated paclitaxel group. The control group, which consists of naïve animals, showed no or only a little GFAP-positive cells in comparison. In summary, the staining quantification confirmed these observations and revealed a significant reduction about 50% of astrocyte activation after SAFit2 treatment (Fig. 4D).

Next, we assessed the expression of the microglia marker ionized calcium-binding adaptor molecule 1 (IBA1) in the dorsal horn of the respective groups (Fig. 4B, D). The staining of the vehicle-treated paclitaxel group showed a strong IBA1 expression (Fig. 4B). However, the staining of the SAFit2-treated paclitaxel group showed less IBA1-positive cells. Stainings of the control group showed only weak signals, as expected. Interestingly, the quantification of IBA1-positive cells also revealed a significant reduction of approximately 50% after SAFit2 treatment. In conclusion, we observed that a SAFit2 treatment significantly reduced the number of activated astrocytes and microglia in the spinal cord, indicating that SAFit2 counteracts the paclitaxel-mediated gliosis.

#### SAFit2 treatment leads to increased free fatty acid levels in neuronal tissue

Lipid mediators are important signaling mediators in the context of neuropathic pain as they can be released as paracrine signaling molecules to interact with neurons and glial cells as well as to modulate and resolve neuroinflammation [32]. Based on that, we hypothesized that SAFit2 might have an influence on lipid synthesis or release. For assessing this hypothesis, we first performed

a high-resolution mass spectrometry lipidomic screen (LC-HRMS) to investigate lipid levels in nervous tissue (lumbar DRG and spinal cord samples) on a broad scale comparing vehicle and SAFit2-treated paclitaxel animals.

In this lipid screen, we detected 377 individual lipids that can be further subdivided into the following seventeen lipid classes: fatty acids, ceramides, glycosylceramides, diglycerides, carnitines, lysophosphatidylcholines, -ethanols, -glycerols, -inositols, -serines, phosphatidylcholines, -ethanols, -glycerols, -inositols, -serines, sphingomyelins and triglycerides (Fig. 5A). For further analysis, the values of SAFit2-treated animals were normalized to the values of vehicle-treated animals. Afterwards, the normalized values were compared class wise for DRG and spinal cord samples. Focusing on lipid classes that include potential lipid mediators, we observed a slight increase of lysophosphatidylinositols in the DRGs and ceramides as well as glycosylceramides in the spinal cord after SAFit2 treatment (Fig. 5B). However, we detected a strong increase of fatty acids in the spinal cord through the treatment of SAFit2 (Fig. 5B).

Since the class of fatty acids was strongly elevated after SAFit2 treatment and has a particular relevance in the context of neuropathic pain, we further determined differences between the groups for individual fatty acids. Thereby, we detected increased levels of all measurable fatty acids in the spinal cord. The most drastically changed fatty acids were arachidonic acid (20:4) and docosahexaenoic acid (22:6). We also observed a slight upregulation of myristic acid (14:0) and oleic acid (18:1) (Fig. 5C). In summary, we detected indeed an elevation of free fatty acids and especially of polyunsaturated fatty acids (PUFAs) after SAFit2 treatment, which can be rapidly metabolized into pain-relevant signaling mediators.

PUFAs can be absorbed from nutrition, but they can also be released from the lipid bilayer of cell membranes by the hydrolysis of an ester bond (Fig. 6A). In particular, the phospholipase 2 can hydrolyse the ester bond from the second carbon of a phospholipid, whereby a fatty acid is released. This free fatty acid can consist of different chain length, however, arachidonic acid, linoleic acid, eicosapentaenoic acid and docosahexaenoic acid are the most abundant ones. Nevertheless, these PUFAs are usually rapidly metabolized into both pro- and anti-inflammatory mediators that can regulate and influence the transmission of neuropathic pain [16]. To analyze

(See figure on next page.)

**Fig. 4** Reduced activation of astrocytes and microglia in the spinal cord of SAFit2-treated animals. Immunohistochemistry staining of astrocyte activation marker GFAP (A) and microglia marker IBA1 (B) at 20X magnification (scale bar: 50  $\mu$ m) of spinal cord (dorsal horn) slices. Samples of naïve animals were labeled as control. C Quantification of GFAP-positive cells. D Quantification of IBA1-positive cells. C, D Positive cells were counted in 15–20 images per animal and averaged. Data represent the mean  $\pm$  SEM from 15–20 images of four mice per group. \*\*  $p < 0.01$ , \*\*\*  $p < 0.001$ , \*\*\*\*  $p < 0.0001$  one-way ANOVA with Tukey's multiple comparison test. SAFit2 selective antagonist of FKBP51 by induced fit 2, GFAP glial fibrillary acidic protein, IBA1 ionized calcium-binding adaptor molecule 1

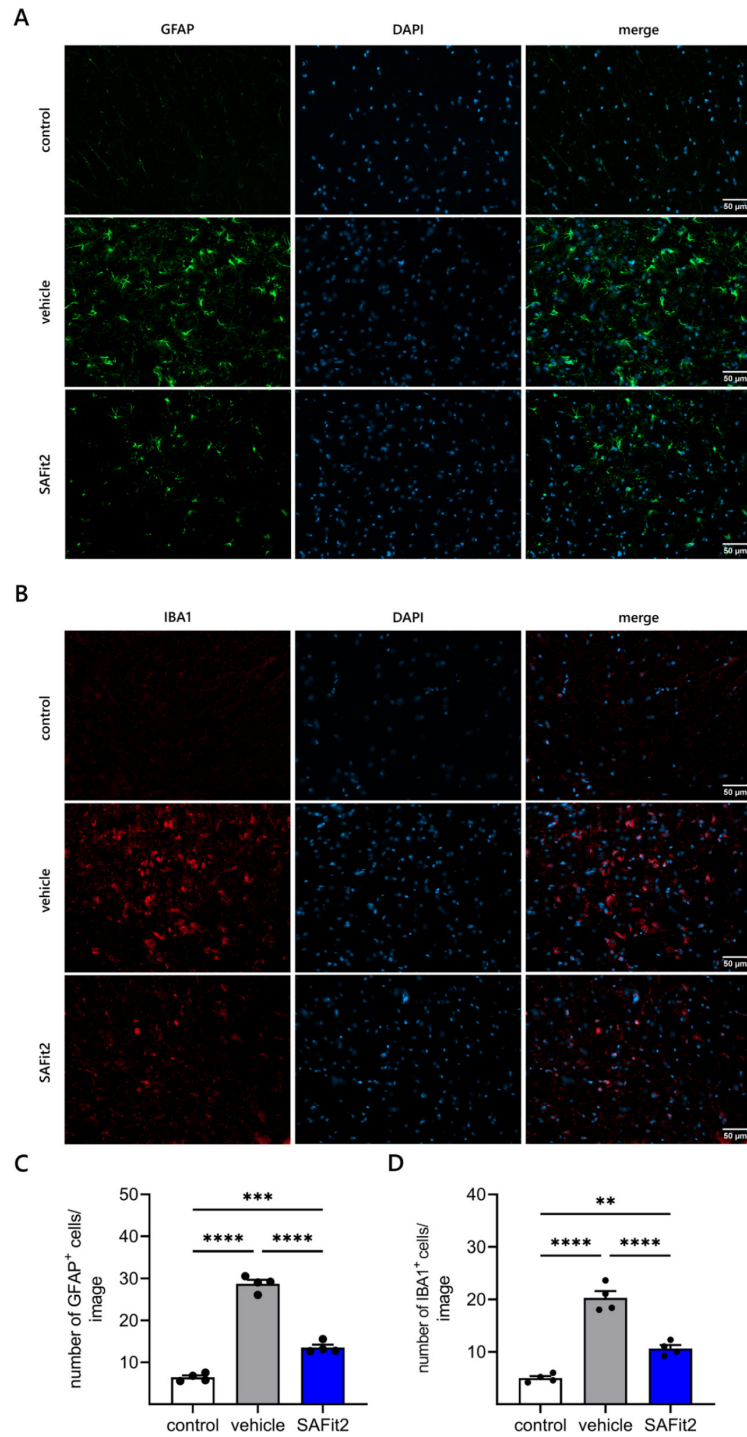


**Fig. 4** (See legend on previous page.)

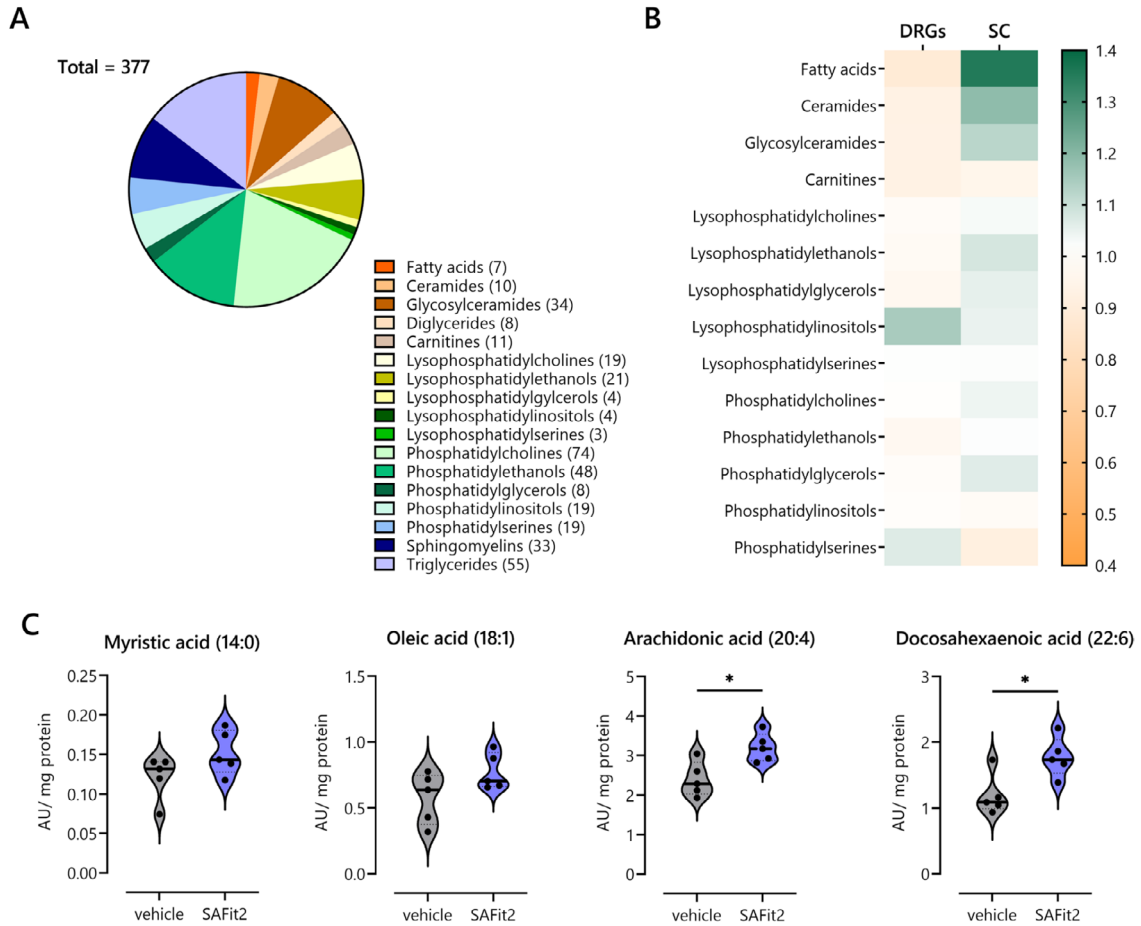


**Fig. 5** LC-HRMS lipid analysis of DRGs and spinal cord from vehicle and SAFit2-treated paclitaxel mice. **A** Distribution of measured lipid classes of both tissues in LC-HRMS analysis. **B** Relative frequencies of lipid classes in lumbar DRGs and spinal cord from SAFit2-treated animals, which were normalized to those of vehicle-treated animals. **C** Violin plots comparing fatty acid levels of spinal cord samples from vehicle and SAFit2-treated animals. The data represent the mean  $\pm$  SEM from five mice per group. \*  $p < 0.05$  Student's *t*-test with Welch's correction. DRGs dorsal root ganglia, SAFit2 selective antagonist of FKBP51 by induced fit 2, LC-HRMS liquid chromatography-high-resolution mass spectrometry

whether SAFit2 can enhance the release of PUFAs, we investigated the effect of SAFit2 on the phospholipase 2 activity in vitro. Interestingly, SAFit2 contributes to an enhanced activity of the phospholipase 2 isoforms cPLA<sub>2</sub>, iPLA<sub>2</sub> and sPLA<sub>2</sub> in primary sensory neuron lysates as we observed a concentration dependent increase of hydrolyzed substrate due to increasing SAFit2 concentrations (Fig. 6B). In summary, we observed that SAFit2 increases PUFA levels in vivo and contributes to the phospholipase 2 mediated release of PUFAs from neuronal membranes.

#### SAFit2 enhances pro-resolving mediators after paclitaxel treatment

As a next step, we investigated the expression of phospholipases and fatty acid metabolizing enzymes as we have observed an increase of free fatty acids after SAFit2 treatment (Fig. 7A–G). Furthermore, we compared the expression of both vehicle and SAFit2-treated paclitaxel groups with the expression of naïve animals.

Consistent with our previous results, we observed an increased expression of the phospholipases cPLA<sub>2</sub> and iPLA<sub>2</sub> in SAFit2-treated paclitaxel animals compared to the expression of control animals (Fig. 7A, B). In addition, we measured a significant upregulation of the lipoxygenase 5 (ALOX5) in the DRGs of SAFit2-treated

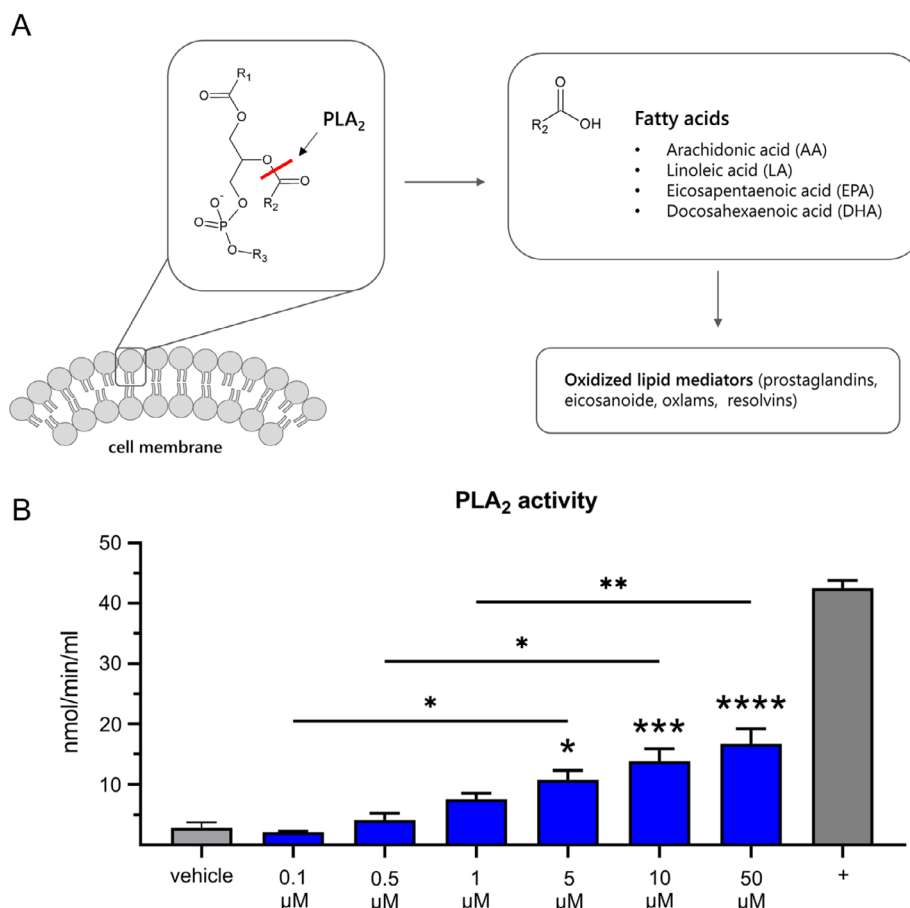


**Fig. 6** Influence of SAFit2 on phospholipase 2 activity in primary sensory neuron lysates. **A** Schematic illustration of the phospholipase 2 function and its products. Phospholipase 2 hydrolyzes the second ester bond of phospholipids that constitute the lipid bilayer of cell membranes. Thereby, polyunsaturated fatty acids were released, which were rapidly metabolized into oxylipins. **B** The influence of SAFit2 (0.1–50 μM) on the phospholipase 2 activity was assessed in lysed primary sensory neurons. Further, the basal phospholipase activity of the lysates was determined, the influence of the solvent DMSO (vehicle) verified and bee venom used as a positive control. Data represent the mean ± SEM. \*  $p < 0.05$ , \*\*  $p < 0.01$ , \*\*\*  $p < 0.001$ , \*\*\*\*  $p < 0.0001$  one-way ANOVA with Tukey's post-multiple comparison test. PLA<sub>2</sub> phospholipase 2, SAFit2 selective antagonist of FKBP51 by induced fit 2

paclitaxel animals (Fig. 7C). In contrast, the expression of this enzyme was significantly lower in the spinal cord of SAFit2-treated animals than in the vehicle-treated paclitaxel animals, yet the expression of both paclitaxel groups was not significantly altered from the control group. Nevertheless, the lipoxygenase 12 (ALOX12) was significantly increased in the DRGs of the SAFit2-treated group compared with both vehicle and control group (Fig. 7D). The expression of the lipoxygenase 15 (ALOX15) was not significantly altered in both tissues (Fig. 7E) and the expression of the cyclooxygenase 2 (COX2) was significantly reduced in the spinal cord for both paclitaxel groups compared to the vehicle group (Fig. 7F). However,

we observed a significant increase of the cytochrome-P<sub>450</sub>-epoxygenase CYP2J6 in the DRGs after SAFit2 treatment (Fig. 7G). The expression of the cytochrome-P<sub>450</sub>-epoxygenase CYP3A11 was lower than the detection limit in both tissues. In summary, we could observe significant differences in the expression of lipoxygenases and CYP2J6 comparing vehicle and SAFit2-treated paclitaxel animals.

Furthermore, we analyzed the expression of sphingosine kinases and ceramide synthases to detect any SAFit2-mediated alterations (Fig. 7F–K). However, we detected no significant changes in expression of vehicle and SAFit2-treated paclitaxel animals for the sphingosine



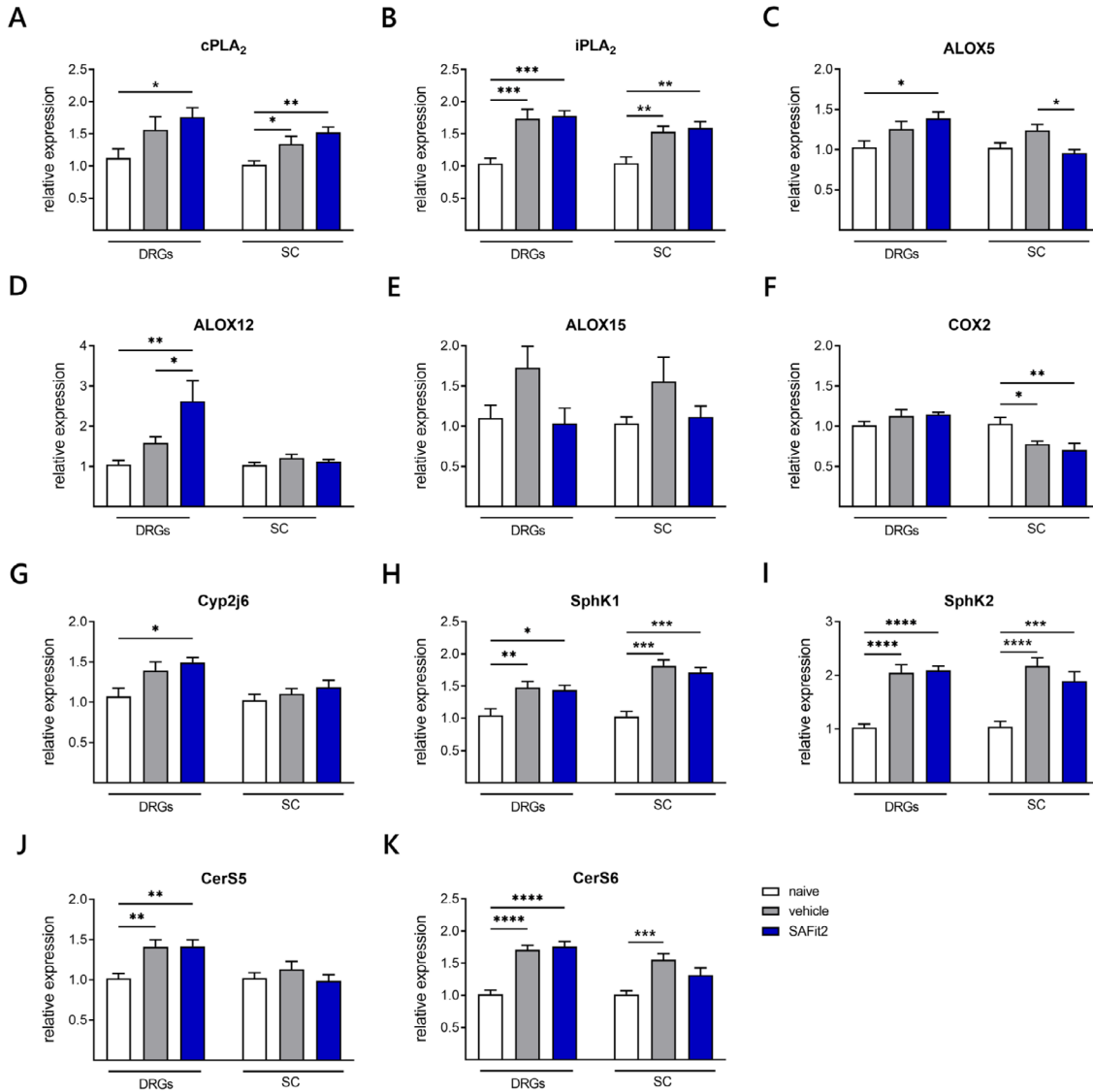


**Fig. 7** Gene expression of lipid synthesizing and metabolizing enzymes in neuronal tissue of SAFit2-treated paclitaxel mice. After twelve days, the expression of phospholipases (A, B), lipoygenases (C–F), epoxygenase (G), sphingosine kinases (H, I) and ceramide synthases (J, K) was assessed via qPCR. The expression levels of vehicle and SAFit2-treated animals were normalized to the expression levels of naïve animals. The data represent the mean  $\pm$  SEM from 3–4 mice per group, measured in technical triplicates, respectively. \*  $p < 0.05$ , \*\*  $p < 0.01$ , \*\*\*  $p < 0.001$  one-way ANOVA with Tukey’s post hoc test was conducted per tissue. DRGs dorsal root ganglia, SC spinal cord, SAFit2 selective antagonist of FKBP51 by induced fit 2, *cPLA<sub>2</sub>* cytosolic phospholipase A2, *iPLA<sub>2</sub>* calcium-independent phospholipase A2, *ALOX* arachidonate lipoxygenase, *CYP2J6* cytochrome P450 family 2 subfamily j polypeptide 6c, *COX2* cyclooxygenase 2, *SphK1/2* sphingosine kinase 1/2, *CerS* ceramide synthase

kinases one and two, though both groups were significantly increased compared to the control group (Fig. 7H, I). In addition, we observed no significant differences in the expression of ceramide synthase five and six for vehicle and SAFit2-treated paclitaxel mice (Fig. 7J, K). In summary, we detected a significant increase in the

expression of fatty acid oxidizing and metabolizing enzymes in the DRGs and spinal cord of SAFit2-treated animals.

Since we observed an increased PLA<sub>2</sub> activity, elevated free fatty acid levels and an increased expression of fatty acid metabolizing enzymes after SAFit2

treatment, we further investigated the influence of SAFit2 on oxylipin levels. Oxylipins are mediators that are generated by the oxidation of free fatty acids and have been shown to play a crucial role as signaling molecules in the pathophysiological context of neuropathic pain [16, 33, 34]. To assess oxylipin levels of vehicle and SAFit2-treated paclitaxel mice as well as naïve mice, we performed a targeted LC–MS/MS analysis with DRG and spinal cord samples of the respective groups in which we were able to detect 27 oxylipins. Afterwards, the oxylipin levels of paclitaxel-treated animals were normalized to those of the control group and clustered in their precursor fatty acids (Fig. 8).

For the arachidonic acid metabolites, we detected a slight decrease of pro-inflammatory prostaglandins in the DRGs after SAFit2 treatment (Fig. 8A), which is shown representatively for prostaglandin D2 (Fig. 8B). Furthermore, we detected an increase of the anti-inflammatory and pro-resolving mediator 8,9-EpETrE in the DRGs. For the linoleic acid and alpha linoleic acid metabolites, we detected a significant decrease of the pro-inflammatory 12,13-DiHOME (Fig. 8C) and a significant increase of the anti-inflammatory 13-HOTrE after SAFit2 treatment (Fig. 8D). Consistently, we detected a significant increase of three docosahexaenoic acid metabolites 14-HDHA, 17-HDHA, 19.20-DiHDPa (Fig. 8E–G), which have also anti-inflammatory and pro-resolving properties. For the spinal cord samples, we could observe an increase of 12-HETE after SAFit2 treatment (Fig. 8A). However, 12-HETE was not significantly increased after SAFit2 treatment (Fig. 8H). Moreover, we measured a slight increase of 14-HDHA after SAFit2 treatment (Fig. 8I). In summary, we observed a decrease of pro-inflammatory and an increase of anti-inflammatory and pro-resolving oxylipins in the DRGs and spinal cord after the treatment with SAFit2.

In conclusion, we observed that SAFit2 enhances the PLA<sub>2</sub> mediated fatty acid release from neuronal membranes in paclitaxel-mediated pain states (Fig. 8)).

Thereby, predominantly the PUFAs arachidonic acid and docosahexaenoic acid were released and oxidized into oxylipins, which have previously been shown to influence and regulate neuropathic pain persistence and transmission. Interestingly, we mainly observed an increase of anti-inflammatory and pro-resolving fatty acid metabolites after SAFit2 treatment. Based on these results, we suggest that SAFit2 treatment leads to an increase of pro-resolving lipid mediators, which counteract neuroinflammation and spinal gliosis, resulting in an amelioration of paclitaxel-mediated neuropathic pain.

## Discussion

The need for CIPN therapeutics is increasing nowadays as available treatment strategies have either a low efficacy or severe side effects [35]. Interestingly, our data show that the novel and specific FKBP51 inhibitor SAFit2 can efficiently reduce mechanical hypersensitivity in paclitaxel-treated mice as it counteracts the paclitaxel-induced peripheral sensitization and neuroinflammation.

### SAFit2 reduces paclitaxel-induced peripheral sensitization

Firstly, we observed that SAFit2 has an influence on endogenous lipid levels as it decreases the levels of pro-inflammatory and transient receptor potential (TRP) channel sensitizing lipids mediators. More specifically, we detected that SAFit2 significantly reduces the levels of 12,13-DiHOME, which is a pro-inflammatory diol lipid that is metabolized from linoleic acid-derived epoxy lipids. Furthermore, 12,13-DiHOME is known to mediate thermal hyperalgesia in mice as it sensitizes the pain-mediating TRPV1 channel and thereby increases the excitability of sensory neurons under inflammatory conditions [36]. In line with that, eicosanoids like the prostaglandin E<sub>2</sub> are also known to sensitize TRP channels and thereby enhance the excitability of sensory neurons [37, 38]. However, we detected a slight decrease of the prostaglandins E<sub>2</sub> and D<sub>2</sub> after SAFit2 treatment. A possible explanation for the decreased prostaglandin levels might

(See figure on next page.)

**Fig. 8** Alteration of oxylipins in DRGs and spinal cord of vehicle and SAFit2-treated paclitaxel mice. **A** Relative amount of oxylipins was measured in the DRGs and spinal cord of both groups and clustered in their precursor fatty acids. The raw data were normalized to the protein amount of the respective sample. **B–I** Violin plots display the relative lipid levels of those lipids, which were altered after SAFit2 treatment. The measured lipid levels of paclitaxel-treated animals were normalized to lipid levels of naïve animals. The analysis was conducted with six animals per group. \*  $p < 0.05$ , \*\*  $p < 0.01$ , \*\*\*  $p < 0.001$  student's *t*-test with Welch's correction. **J** Schematic summary of the effect of SAFit2 on lipid levels. SAFit2 seems to enhance the PLA<sub>2</sub> mediated fatty acid release from phospholipids. In particular, we detected an elevation of arachidonic acid and docosahexaenoic acid after SAFit2 treatment as well as an increase of their pro-resolving metabolites. Pro-inflammatory oxylipins were marked in red, anti-inflammatory/pro-resolving in green, the alteration after SAFit2 treatment is indicated by either a blue arrow for an increase or a blue tilde for no changes. Oxylipins indicated with dashed lines were below the detection limit. DRG dorsal root ganglia, SC spinal cord, SAFit2: selective antagonist of FKBP51 by induced fit 2, AA arachidonic acid, LA linoleic acid, *α*-LA alpha-linolenic acid, DGLA dihomoy-linolenic acid, EPA eicosapentaenoic acid, DHA docosahexaenoic acid, PGE<sub>2</sub> prostaglandin E<sub>2</sub>, PGD<sub>2</sub> prostaglandin D<sub>2</sub>, TXB<sub>2</sub> thromboxane 2, PGF<sub>2α</sub> prostaglandin F<sub>2</sub> alpha, 6-keto PGF<sub>1α</sub> 6-keto prostaglandin F<sub>1</sub> alpha, HETE hydroxyeicosatetraenoic acid, DiHETE dihydroxyeicosatrienoic acid, HHTrE hydroxyheptadecatrienoic acid, EpETrE hydroxyepoxyeicosatrienoic acid, HODE hydroxyoctadecadienoic acid, DiIHOME dihydroxyoctadecenoic acid, HIOTrE hydroxyoctadecatrienoic acid, HETrE hydroxyeicosatrienoic acid. HEPE hydroxyeicosapentaenoic acid, HDHA hydroxydocosahexaenoic acid, DiHDPa: dihydroxydocosapentaenoic acid

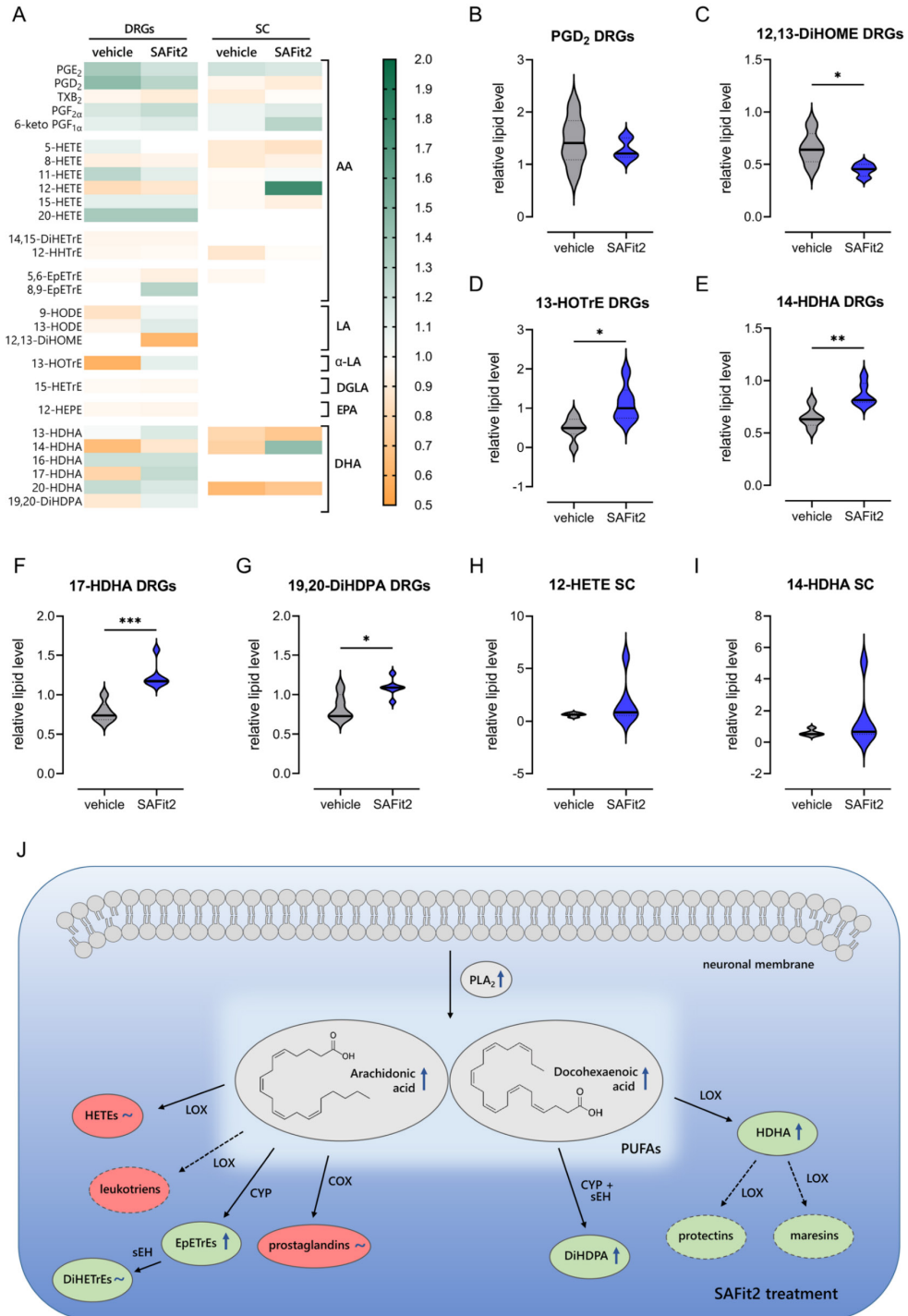


**Fig. 8** (See legend on previous page.)

be a reduced expression of COX2 after SAFit2 treatment, since prostaglandins are predominantly synthesized by the COX2 enzyme [39, 40]. Based on this observation, we assume that a SAFit2 treatment mediates a more anti-inflammatory lipid profile, by shifting oxylipin synthesis towards the LOX and CYP enzymes and not towards COX2, which might reveal one mechanism how SAFit2 is capable to counteract the enhanced excitability of sensory neurons after paclitaxel treatment.

#### **SAFit2 induces the resolution of paclitaxel-induced neuroinflammation**

Peripheral sensitization can also be initiated and regulated by pain-mediating chemokines and pro-inflammatory mediators, that are released from activated glial cells [41]. In addition, it has been shown that paclitaxel-activated glial cells such as microglia and astrocytes can become neurotoxic [3]. Nevertheless, we observed that SAFit2 is capable to reduce gliosis after paclitaxel treatment, which leads to a reduction of pro-inflammatory and pain-mediating cytokines and chemokines in the spinal cord. In line with that, we detected a strong decrease of chemokines such as CCL2 and CCL7, which both are agonists of the C-C chemokine receptor type 2 that is expressed by both sensory neurons and glial cells [42]. The decrease of these chemokines has an essential influence on the pain perception of mice as CCL2 was shown to increase the frequency of excitatory post synaptic currents as well as to enhance the currents of AMPA and NMDA receptors, leading to an enhanced excitability of neurons and a sensitized pain state [43, 44]. In addition, both CCL7 and CCL2 have been shown to be direct activators of microglia [45, 46]. Another crucial pain-mediating chemokine, which is strongly downregulated after SAFit2 treatment, is CCL5, which was previously shown to induce hyperalgesia dose-dependently in mice [47–49]. Although some of the detected inflammatory mediators can be secreted from neurons (CCL2 and CXCL10) [32, 50], most of these mediators are released by immune cells, such as astrocytes (CCL2, CCL5, CCL7, CXCL10, IL-10), microglia (CCL5, CXCL10, IL-10) macrophages (CCL3, CCL4, IL-10) and T-cells (CCL4, IL-22) [51–57].

We did not investigate the levels of immune cells in neuronal tissue after SAFit2 treatment. However, the combined cytokine and chemokine data indicate a reduction of pro-inflammatory macrophages and an increase of anti-inflammatory macrophages and T-cells in DRGs after SAFit2 treatment. These data are also in line with our observations showing reduced numbers of activated astrocytes and microglia in the dorsal spinal cord after SAFit2 treatment. Mechanistically, we assume that SAFit2 on the one hand reduces the levels of these mediators as it counterbalances the enhanced NF- $\kappa$ B

activation [27] and on the other hand causes a more anti-inflammatory lipid profile. Thereby, SAFit2 is capable to decrease neuroinflammation and prevents gliosis and subsequently neurodegeneration in the spinal cord.

Furthermore, emerging evidence indicates that the resolution of neuroinflammation, which is mediated by pro-resolving mediators, becomes an essential issue in the relief of neuropathic pain [58–60]. In line with that, we detected an increase of anti-inflammatory cytokines like interleukin 10 and 22 after the treatment with SAFit2, indicating that SAFit2 even induces a resolution of neuroinflammation, which contributes to a relief of paclitaxel-mediated neuropathic pain.

#### **SAFit2 causes a shift towards an anti-inflammatory lipid profile in nervous tissue**

Besides anti-inflammatory cytokines, PUFAs, such as DHA, have been shown to comprise anti-inflammatory and pro-resolving properties [61]. Interestingly, we observed an enhanced expression and activity of phospholipase 2 after SAFit2 treatment, which resulted in an increase of free polyunsaturated fatty acids and especially of the omega-3 PUFA DHA. These results further confirm our previously suggested SAFit2-mediated anti-inflammatory lipid profile, as DHA was shown to reduce neuropathic pain in a diabetic rat model as well as in a nerve injury rat and mouse model [62]. Moreover, studies reported that DHA has a protective effect on microglia and astrocytes as it counteracts oxidative stress induced calcium dysregulations and ER stress [63, 64].

Nevertheless, PUFAs such as DHA are known to be rapidly metabolized into oxylipins that play a crucial role in the regulation of neuropathic pain [16, 35]. In particular, the free fatty acid DHA gets metabolized by LOX and CYP enzymes into anti-inflammatory specialized pro-resolving mediators (SPMs) such as resolvins, protectins and maresins [65]. In line with that, we observed beside increased DHA levels also an enhanced expression of the respective LOX and CYP enzymes after SAFit2 treatment. Interestingly, these pro-resolving mediators and especially the class of resolvins was shown to dampen inflammatory pain as they interfere in the mechanism of peripheral sensitization and reduce the excitability of sensory neurons [66]. Furthermore, the SPM neuroprotection D1 was able to reduce spinal gliosis and mechanical hypersensitivity in a neuropathic nerve injury model *in vivo* [67]. Unfortunately, we were not capable to detect SPMs in the DRG and spinal cord samples. However, we observed an increase of their anti-inflammatory precursors after SAFit2 treatment. More specifically, we detected an increase of hydroxydocosahexaenoic acids (HDHAs) such as 14-HDHA and 17-HDHA after SAFit2 treatment. Based on the elevation of DHA and

its metabolites after SAFit2 treatment, we conclude that SAFit2 enhances the levels of pro-resolving DHA-originated lipid mediators, which contribute to an anti-inflammatory lipid profile.

Apart from the DHA-originated mediators, we also detected an increase of the alpha linoleic acid metabolite 13-HOTrE. Although less is known about alpha linoleic acid-derived oxylipins in the literature, 13-HOTrE was associated with anti-inflammatory properties as it was shown to suppress the expression of the inflammatory cytokine IL-1 $\beta$  in human chondrocytes and to reduce glomerulomegaly in obese rats [68]. Moreover, we observed an increase in EpETrEs (e.g., 8,9-EpETrEs) after SAFit2 treatment, which are epoxyeicosatrienoic acids that are generated by the oxidation of arachidonic acid [69]. EpETrEs have also been shown to have anti-inflammatory properties as they inhibit the NF- $\kappa$ B translocation into the nucleus and thereby reduce the expression of, e.g., pro-inflammatory mediators or enzymes, that generate pro-inflammatory mediators, such as COX2 [70]. Based on these results, we assume that SAFit2 induces an anti-inflammatory lipid profile after paclitaxel treatment that reduces peripheral sensitization and consequently reduces paclitaxel-mediated mechanical hypersensitivity.

#### Limitations and conclusion

A possible limitation of the study could be the lack of female mice. However, it has been previously shown that the involvement of FKBP51 in neuropathic pain is sex independent and its deficiency leads to an equal pain relief in both sexes [11]. A further limitation could also be the investigation of SAFit2-mediated effects on exclusively the peripheral nervous system and spinal cord regions as these compartments mediate and regulate the development and maintenance of neuropathic pain. Nevertheless, SAFit2 is also capable of affecting FKBP51 levels in the central nervous system as it passes the blood–brain barrier. However, the inhibition of FKBP51 in the brain displays not a disadvantage but rather seems to be beneficial as previous studies have shown that the inhibition of FKBP51 in the brain helps to prevent psychological disorders as well as stress-related and endocrinologic-mediated diseases such as depression, type two diabetes and obesity [71].

Indeed, SAFit2 has already been tested in several neuropathic models and showed promising effects in reducing mechanical and thermal hypersensitivity *in vivo*. The models themselves differ profoundly concerning the degree of neuroinflammation to pain hypersensitivity. While the nerve injury models SNI and CCI (spared nerve injury, chronic constriction injury) are usually connected with a strong spinal gliosis and related neuroinflammation, the chemotherapy-induced neuropathy

models usually show a more neurotoxic and less inflammatory effect, although this depends on the cytostatic drug that is used [32, 72–74].

In line with these reports, we observed elevated levels of cytokines (especially in the dorsal spinal cord) and chemokines (especially in DRGs) in the SNI model, many of which were significantly reduced after SAFit2 treatment [27]. Similar results were observed in animals deficient of FKBP51 [10]. In the current manuscript, we do not see this strong and general increase in (neuro)inflammatory mediators, especially not in pro-inflammatory interleukins, which is in line with previous results [11]. In this model, we observe that SAFit2 rather causes a decrease of pro-inflammatory chemokines in DRGs and an increase of anti-inflammatory mediators (IL-10, IL-22). Moreover, we show, that SAFit2 treatment also causes a shift towards a pro-resolving lipidomic profile within DRGs and the dorsal spinal cord.

In conclusion, we show that the novel and specific FKBP51 inhibitor SAFit2 reduces gliosis in the spinal cord, which leads to a reduction of pain-mediating chemokines. Furthermore, we observed an increase of anti-inflammatory and pro-resolving cytokines and lipid mediators due to a SAFit2 treatment, which contribute to a resolution of neuroinflammation and peripheral sensitization after paclitaxel treatment. In summary, these effects can explain the SAFit2-mediated pain relief after paclitaxel treatment and highlight the role of SAFit2 as potential novel analgesic drug candidate.

#### Abbreviations

AA	Arachidonic acid
CCL	C-C motif ligand
CIPN	Chemotherapy-induced peripheral neuropathy
CXCL	C-X-C motif ligand
DGLA	Dihomo $\gamma$ linolenic acid
DHA	Docosahexaenoic acid
DIHDPA	Dihydroxydocosapentaenoic acid
DIHETE	Dihydroxyeicosatrienoic acid
DIHOME	Dihydroxyoctadecenoic acid
DRGs	Dorsal root ganglia
EPA	Eicosapentaenoic acid
EpETrE	Epoxyeicosatrienoic acid
FKBP51	FK506 binding protein 51
GFAP	Glial fibrillary acidic protein
HDHA	Hydroxydocosahexaenoic acid
HEPE	Hydroxyeicosapentaenoic acid
HETE	Hydroxyeicosatetraenoic acid
HIETE	Hydroxyeicosatrienoic acid
HHTrE	Hydroxyheptadecatrienoic acid
HODE	Hydroxyoctadecadienoic acid
HOTrE	Hydroxyoctadecatrienoic acid
IBA1	Ionized calcium-binding adaptor molecule 1
IL	Interleukin
LA	Linoleic acid
LC-HRMS	Liquid chromatography–high-resolution mass spectrometry
PG	Prostaglandin
PLA <sub>2</sub>	Phospholipase A2
PUFA	Polyunsaturated fatty acids
SAFit2	Selective antagonist of FKBP51 by induced fit

SC	Spinal cord
TRP	Transient receptor potential
TRPV1	Transient receptor potential vanilloid 1 channel
TXB <sub>2</sub>	Thromboxane 2

## Supplementary Information

The online version contains supplementary material available at <https://doi.org/10.1186/s12974-023-02835-5>.

**Additional file 1: Figure S1.** Enhanced FKBP51 expression in spinal cord and L4-L5 DRG slices of paclitaxel-treated animals. **Figure S2.** Pharmacokinetic study of SAFit2 comparing two formulations. **Figure S3.** Reduced AIF3 expression in L4 and L5 DRGs of SAFit2-treated animals. **Figure S4.** Reduced cFOS expression in spinal cord and L4-L5 DRG slices of SAFit2-treated animals. **Figure S5.** Cytokines and chemokines measured in the DRGs of paclitaxel-treated mice. **Figure S6.** Cytokines measured in the spinal cord of paclitaxel-treated mice. **Figure S7.** Chemokines measured in the spinal cord of paclitaxel-treated mice.

### Author contributions

FH, GG and MS conceptualized the project. SW performed the behavioral assays and collected the tissue. SW, LH, YS, DT, CN and MU performed measurements. IH synthesized the batch of SAFit2. NdB supervised the behavioral study and the pharmacokinetic study together with MVS. SW performed the data analysis and curation. SW and MS wrote the original draft. All authors read and approved the final manuscript.

### Funding

Open Access funding enabled and organized by Projekt DEAL. The work of the authors was supported by the Federal German Ministry of Education and Research (BMBF) under the grant number 511aValP, by the German Research Foundation (DFG) grants SFB1039 A09, Z01, 445757098 and from the Fraunhofer Foundation Project Neuropathic Pain, the Fraunhofer Cluster of Excellence for Immune-Mediated Diseases (CIMD) and the Cardiopulmonary Institute EXC 2026 (Project ID 390649896).

### Availability of data and materials

All data generated or analyzed during this study are included in this published article and its additional information file.

### Declarations

#### Ethics approval and consent to participate

All experiments involving animals were approved by the local Ethics Committee for Animal Research (Darmstadt) under the permit numbers F152/1021, F152/1015 and FK1113. Furthermore, all animal experiments were performed according to the recommendations of the Preclinical Pain Research Consortium for Investigating Safety and Efficacy (PPRECISE) Working Group [75], and according to the updated ARRIVE guidelines for reporting animal research [76]. All efforts were made to minimize suffering.

#### Consent for publication

Not applicable.

#### Competing interests

The authors declare that they have no competing interests.

#### Author details

<sup>1</sup>Institute of Clinical Pharmacology, Pharmazentrum Frankfurt/ZAFES, University Hospital, Goethe-University, 60590 Frankfurt am Main, Germany. <sup>2</sup>Fraunhofer Institute for Translational Medicine and Pharmacology ITMP, and Fraunhofer Cluster of Excellence for Immune Mediated Diseases CIMD, 60596 Frankfurt am Main, Germany. <sup>3</sup>Core Unit Analytics and Mass Spectrometry, Max Planck Institute of Psychiatry, 80804 Munich, Germany. <sup>4</sup>Department of Biochemistry, Technical University of Darmstadt, 64287 Darmstadt, Germany.

Received: 25 April 2023 Accepted: 16 June 2023

Published online: 24 June 2023

### References

- Hammad A, Mohamed MSA, Khalifa M, El-Daly M. Mechanisms of Paclitaxel-induced peripheral neuropathy. *J Adv Biomed Pharm Sci.* 2023;6(1):25–35.
- Scripture CD, Figg WD, Sparreboom A. Peripheral neuropathy induced by paclitaxel: recent insights and future perspectives. *Curr Neuropharmacol.* 2006. <https://doi.org/10.2174/157015906776359568>.
- Klein I, Lehmann HC. Pathomechanisms of paclitaxel-induced peripheral neuropathy. *Toxics.* 2021. <https://doi.org/10.3390/toxics9100229>.
- Sisignano M, Lotsch J, Parnham MJ, Geisslinger G. Potential biomarkers for persistent and neuropathic pain therapy. *Pharmacol Ther.* 2019;199:16–29.
- Colloca L, Ludman T, Bouhassira D, Baron R, Dickenson AH, Yarnitsky D, et al. Neuropathic pain. *Nat Rev Dis Primers.* 2017;3:17002.
- Han Y, Smith MT. Pathobiology of cancer chemotherapy-induced peripheral neuropathy (CIPN). *Front Pharmacol.* 2013;4:156.
- Flatters SJJ, Dougherty PM, Colvin LA. Clinical and preclinical perspectives on chemotherapy-induced peripheral neuropathy (CIPN): a narrative review. *Br J Anaesth.* 2017;119(4):737–49.
- Argyriou AA, Bruna J, Marmiroli P, Cavaletti G. Chemotherapy-induced peripheral neurotoxicity (CIPN): an update. *Crit Rev Oncol Hematol.* 2012;82(1):51–77.
- Finnerup NB, Attal N, Haroutounian S, McNicol E, Baron R, Dworkin RH, et al. Pharmacotherapy for neuropathic pain in adults: a systematic review and meta-analysis. *Lancet Neurol.* 2015;14(2):162–73.
- Maiaru M, Tochiki KK, Cox MB, Annan LV, Bell CG, Feng X, et al. The stress regulator FKBP51 drives chronic pain by modulating spinal glucocorticoid signaling. *Sci Transl Med.* 2016;8(325):32519.
- Maiaru M, Morgan OB, Mao T, Breitsamer M, Bamber H, Pohlmann M, et al. The stress regulator FKBP51: a novel and promising druggable target for the treatment of persistent pain states across sexes. *Pain.* 2018;159(7):1224–34.
- Storer CL, Dickey CA, Galigniana MD, Rein T, Cox MB. FKBP51 and FKBP52 in signaling and disease. *Trends Endocrinol Metab.* 2011;22(12):481–90.
- Hähle A, Merz S, Meyners C, Hausch F. The many faces of FKBP51. *Biomolecules.* 2019. <https://doi.org/10.3390/biom9010035>.
- Gaali S, Kirschner A, Cuboni S, Hartmann J, Kozany C, Balsevich G, et al. Selective inhibitors of the FK506-binding protein 51 by induced fit. *Nat Chem Biol.* 2015;11(1):33–7.
- Buffa V, Knaup FH, Heymann T, Springer M, Schmidt MV, Hausch F. Analysis of the selective antagonist SAFit2 as a chemical probe for the FK506 binding protein 51. *ACS Pharmacol Transl Sci.* 2023;6(3):361–71.
- Osthues T, Sisignano M. Oxidized lipids in persistent pain states. *Front Pharmacol.* 2019;10:1147.
- Sisignano M, Bennett DL, Geisslinger G, Scholich K. TRP-channels as key integrators of lipid pathways in nociceptive neurons. *Prog Lipid Res.* 2014;53:93–107.
- Höke A, Ray M. Rodent models of chemotherapy-induced peripheral neuropathy. *ILAR J.* 2014;54(3):273–81.
- Pritchett K, Mulder GB. The Rotarod. *J Am Assoc Lab Anim Sci.* 2003;42(6):49.
- Sisignano M, Angioni C, Ferreiros N, Schuh CD, Suo J, Schreiber Y, et al. Synthesis of lipid mediators during UVB-induced inflammatory hyperalgesia in rats and mice. *PLoS ONE.* 2013;8(12): e81228.
- Pohlmann ML, Hausl AS, Harbich D, Balsevich G, Engelhardt C, Feng X, et al. Pharmacological modulation of the psychiatric risk factor FKBP51 alters efficiency of common antidepressant drugs. *Front Behav Neurosci.* 2018;12:262.
- Livak KJ, Schmittgen TD. Analysis of relative gene expression data using real-time quantitative PCR and the 2(-Delta Delta C(T)) method. *Methods.* 2001;25(4):402–8.
- Schmittgen TD, Livak KJ. Analyzing real-time PCR data by the comparative C(T) method. *Nat Protoc.* 2008;3(6):1101–8.
- Wedel S, Hahnefeld L, Alnouri MW, Offermanns S, Hausch F, Geisslinger G, et al. The FKBP51 inhibitor SAFit2 restores the pain-relieving C16

- dihydroceramide after nerve injury. *Int J Mol Sci.* 2022. <https://doi.org/10.3390/ijms232214274>.
25. Sens A, Rischke S, Hahnefeld L, Dorochow E, Schafer SMG, Thomas D, et al. Pre-analytical sample handling standardization for reliable measurement of metabolites and lipids in LC-MS-based clinical research. *J Mass Spectrom Adv Clin Lab.* 2023;28:35–46.
  26. Nieto FR, Entrena JM, Cendan CM, Del Pozo E, Vela JM, Baeyens JM. Tetradotoxin inhibits the development and expression of neuropathic pain induced by paclitaxel in mice. *Pain.* 2008;137(3):520–31.
  27. Wedel S, Mathoor P, Rauh O, Heymann T, Ciotu CI, Fuhrmann DC, et al. SFAIT2 reduces neuroinflammation and ameliorates nerve injury-induced neuropathic pain. *J Neuroinflamm.* 2022. <https://doi.org/10.1186/s12974-022-02615-7>.
  28. Houle JD, Cote MP. Axon regeneration and exercise-dependent plasticity after spinal cord injury. *Ann NY Acad Sci.* 2013;1279(1):154–63.
  29. Shim HS, Bae C, Wang J, Lee KH, Hanked KM, Kim HK, et al. Peripheral and central oxidative stress in chemotherapy-induced neuropathic pain. *Mol Pain.* 2019;15:1744806919840098.
  30. Calvo M, Bennett DL. The mechanisms of microgliosis and pain following peripheral nerve injury. *Exp Neurol.* 2012;234(2):271–82.
  31. Zhang T, Zhang M, Cui S, Liang W, Jia Z, Guo F, et al. The core of maintaining neuropathic pain: crosstalk between glial cells and neurons (neural cell crosstalk at spinal cord). *Brain Behav.* 2023;13(2):e2868.
  32. Ji RR, Xu ZZ, Gao YJ. Emerging targets in neuroinflammation-driven chronic pain. *Nat Rev Drug Discov.* 2014;13(7):533–48.
  33. Wedel S, Osthues T, Zimmer B, Angioni C, Geisslinger G, Sisignano M. Oxidized linoleic acid metabolites maintain mechanical and thermal hypersensitivity during sub-chronic inflammatory pain. *Biochem Pharmacol.* 2022;198:114953.
  34. Hargreaves KM, Ruparel S. Role of oxidized lipids and TRP channels in orofacial pain and inflammation. *J Dent Res.* 2016;95(10):1117–23.
  35. Sisignano M, Gribbon P, Geisslinger G. Drug repurposing to target neuroinflammation and sensory neuron-dependent pain. *Drugs.* 2022;82(4):357–73.
  36. Zimmer B, Angioni C, Osthues T, Toewe A, Thomas D, Pierre SC, et al. The oxidized linoleic acid metabolite 12,13-DiHOME mediates thermal hyperalgesia during inflammatory pain. *Biochim Biophys Acta Mol Cell Biol Lipids.* 2018;1863(7):669–78.
  37. Benemei S, Patacchini R, Trevisani M, Geppetti P. TRP channels. *Curr Opin Pharmacol.* 2015;22:18–23.
  38. Kawahara K, Hohjoh H, Inazumi T, Tsuchiya S, Sugimoto Y. Prostaglandin E<sub>2</sub>-induced inflammation: relevance of prostaglandin E receptors. *Biochim Biophys Acta.* 2015;1851(4):414–21.
  39. Flower RJ. The development of COX2 inhibitors. *Nat Rev Drug Discov.* 2003;2(3):179–91.
  40. Koehne CH, Dubois RN. COX-2 inhibition and colorectal cancer. *Semin Oncol.* 2004;31(2 Suppl 7):12–21.
  41. Kiguchi N, Kobayashi Y, Kishioka S. Chemokines and cytokines in neuroinflammation leading to neuropathic pain. *Curr Opin Pharmacol.* 2012;12(1):55–61.
  42. Komiya H, Takeuchi H, Ogawa Y, Hatooka Y, Takahashi K, Katsumoto A, et al. CCR2 is localized in microglia and neurons, as well as infiltrating monocytes, in the lumbar spinal cord of ALS mice. *Mol Brain.* 2020;13(1):64.
  43. Zhou Y, Tang H, Liu J, Dong J, Xiong H. Chemokine CCL2 modulation of neuronal excitability and synaptic transmission in rat hippocampal slices. *J Neurochem.* 2011;116(3):406–14.
  44. Spicarova D, Adamek P, Kalynovska N, Mrozkova P, Palecek J. TRPV1 receptor inhibition decreases CCL2-induced hyperalgesia. *Neuropharmacology.* 2014;81:75–84.
  45. Popiolek-Barczyk K, Ciechanowska A, Ciapala K, Pawlik K, Oggioni M, Mercurio D, et al. The CCL2/CCL7/CCL12/CCR2 pathway is substantially and persistently upregulated in mice after traumatic brain injury, and CCL2 modulates the complement system in microglia. *Mol Cell Probes.* 2020;54:101671.
  46. Kwiatkowski K, Popiolek-Barczyk K, Piotrowska A, Rojewska E, Ciapala K, Makuch W, et al. Chemokines CCL2 and CCL7, but not CCL12, play a significant role in the development of pain-related behavior and opioid-induced analgesia. *Cytokine.* 2019;119:202–13.
  47. Liou J-T, Yuan H-B, Mao C-C, Lai Y-S, Day Y-J. Absence of C-C motif chemokine ligand 5 in mice leads to decreased local macrophage recruitment and behavioral hypersensitivity in a murine neuropathic pain model. *Pain.* 2012. <https://doi.org/10.1016/j.pain.2012.03.008>.
  48. Pevida M, Lastra A, Meana A, Hidalgo A, Baamonde A, Menendez L. The chemokine CCL5 induces CCR1-mediated hyperalgesia in mice inoculated with NCTC 2472 tumoral cells. *Neuroscience.* 2014;259:113–25.
  49. Yin Q, Fan Q, Zhao Y, Cheng MY, Liu H, Li J, et al. Spinal NF- $\kappa$ B and chemokine ligand 5 expression during spinal glial cell activation in a neuropathic pain model. *PLoS ONE.* 2015;10(1):e0115120.
  50. McKimmie C, Michlmayr D. Role of CXCL10 in central nervous system inflammation. *Int J Interferon Cytokine Mediat Res.* 2014. <https://doi.org/10.2147/IJICMR.S35953>
  51. Thacker MA, Clark AK, Bishop T, Grist J, Yip PK, Moon LD, et al. CCL2 is a key mediator of microglia activation in neuropathic pain states. *Eur J Pain.* 2009;13(3):263–72.
  52. Kiguchi N, Maeda T, Kobayashi Y, Fukazawa Y, Kishioka S. Macrophage inflammatory protein-1 $\alpha$  mediates the development of neuropathic pain following peripheral nerve injury through interleukin-1 $\beta$  up-regulation. *Pain.* 2010;149(2):305–15.
  53. Sindhu S, Kochumon S, Shenouda S, Wilson A, Al-Mulla F, Ahmad R. The cooperative induction of CCL4 in human monocytic cells by TNF- $\alpha$  and palmitate requires MyD88 and involves MAPK/NF- $\kappa$ B signaling pathways. *Int J Mol Sci.* 2019. <https://doi.org/10.3390/ijms20184658>.
  54. Pittaluga A. CCL5-glutamate cross-talk in astrocyte-neuron communication in multiple sclerosis. *Front Immunol.* 2017;8:1079.
  55. Imai S, Ikegami D, Yamashita A, Shimizu T, Narita M, Niihara K, et al. Epigenetic transcriptional activation of monocyte chemoattractant protein 3 contributes to long-lasting neuropathic pain. *Brain.* 2013;136(Pt 3):828–43.
  56. Burmeister AR, Marriott I. The interleukin-10 family of cytokines and their role in the CNS. *Front Cell Neurosci.* 2018;12:458.
  57. Chen W, Wang J, Yang H, Sun Y, Chen B, Liu Y, et al. Interleukin 22 and its association with neurodegenerative disease activity. *Front Pharmacol.* 2022;13:958022.
  58. Malcangio M. Role of the immune system in neuropathic pain. *Scand J Pain.* 2020;20(1):33–7.
  59. Krukowski K, Eijkelkamp N, Laumet G, Hack CE, Li Y, Dougherty PM, et al. CD8<sup>+</sup> T cells and endogenous IL-10 are required for resolution of chemotherapy-induced neuropathic pain. *J Neurosci.* 2016;36(43):11074–83.
  60. Fiore NT, Debs SR, Hayes JP, Duffy SS, Moalem-Taylor G. Pain-resolving immune mechanisms in neuropathic pain. *Nat Rev Neurol.* 2023. <https://doi.org/10.1038/s41582-023-00777-3>.
  61. Galan-Arriero I, Serrano-Munoz D, Gomez-Soriano J, Goicoechea C, Taylor J, Velasco A, et al. The role of Omega-3 and Omega-9 fatty acids for the treatment of neuropathic pain after neurotrauma. *Biochim Biophys Acta Biomembr.* 2017;1859(9 Pt B):1629–35.
  62. Landa-Juárez AY, Pérez-Severiano F, Castañeda-Hernández G, Ortiz MI, Chávez-Piña AE. The antihyperalgesic effect of docosahexaenoic acid in streptozotocin-induced neuropathic pain in the rat involves the opioidergic system. *Eur J Pharmacol.* 2019;845:32–9.
  63. Begum G, Kintner D, Liu Y, Cramer SW, Sun D. DHA inhibits ER Ca<sup>2+</sup> release and ER stress in astrocytes following in vitro ischemia. *J Neurochem.* 2012;120(4):622–30.
  64. Geng X, Galano J-M, Oger C, Sun GY, Durand T, Lee JC. Neuroprotective effects of DHA-derived peroxidation product 4(RS)-4-F4t-neuroprostane on microglia. *Free Radical Biol Med.* 2022;185:1–5.
  65. Kuda O. Bioactive metabolites of docosahexaenoic acid. *Biochimie.* 2017;136:12–20.
  66. Ji RR, Xu ZZ, Strichartz G, Serhan CN. Emerging roles of resolvins in the resolution of inflammation and pain. *Trends Neurosci.* 2011;34(11):599–609.
  67. Xu ZZ, Liu XJ, Berta T, Park CK, Lu N, Serhan CN, et al. Neuroprotectin/protectin D1 protects against neuropathic pain in mice after nerve trauma. *Ann Neurol.* 2013;74(3):490–5.
  68. Devassy JG, Leng S, Gabbs M, Monirujjaman M, Aukema HM. Omega-3 polyunsaturated fatty acids and oxylipins in neuroinflammation and management of Alzheimer disease. *Adv Nutr.* 2016;7(5):905–16.
  69. Collino S, Montoliu I, Martin FP, Scherer M, Mari D, Salvioli S, et al. Metabolic signatures of extreme longevity in northern Italian centenarians reveal a complex remodeling of lipids, amino acids, and gut microbiota metabolism. *PLoS ONE.* 2013;8(3):e56564.

70. Schmelzer KR, Inceoglu B, Kubala L, Kim I-H, Jinkd SL, Eiserich JP, et al. Enhancement of antinociception by coadministration of nonsteroidal anti-inflammatory drugs and soluble epoxide hydrolase inhibitors. *PNAS*. 2006. <https://doi.org/10.1073/pnas.0605908103>.
71. Schmidt MV, Paez-Pereda M, Holsboer F, Hausch E. The prospect of FKBP51 as a drug target. *ChemMedChem*. 2012;7(8):1351–9.
72. Ellis A, Bennett DL. Neuroinflammation and the generation of neuropathic pain. *Br J Anaesth*. 2013;111(1):26–37.
73. Fumagalli G, Monza I, Cavaletti G, Rigolio R, Meregalli C. Neuroinflammatory process involved in different preclinical models of chemotherapy-induced peripheral neuropathy. *Front Immunol*. 2020;11: 626687.
74. Makker PG, Duffy SS, Lees JG, Perera CJ, Tonkin RS, Butovsky O, et al. Characterisation of immune and neuroinflammatory changes associated with chemotherapy-induced peripheral neuropathy. *PLoS ONE*. 2017;12(1): e0170814.
75. Andrews NA, Latremoliere A, Basbaum AI, Mogil JS, Porreca F, Rice ASC, et al. Ensuring transparency and minimization of methodologic bias in preclinical pain research: PPRECISE considerations. *Pain*. 2016;157(4):901–9.
76. Perciedu Sert N, Hurst V, Ahluwalia A, Alam S, Avey MT, Baker M, et al. The ARRIVE guidelines 2.0: Updated guidelines for reporting animal research. *PLoS Biol*. 2020;18(7): e3000410.

### Publisher's Note

Springer Nature remains neutral with regard to jurisdictional claims in published maps and institutional affiliations.

Ready to submit your research? Choose BMC and benefit from:

- fast, convenient online submission
- thorough peer review by experienced researchers in your field
- rapid publication on acceptance
- support for research data, including large and complex data types
- gold Open Access which fosters wider collaboration and increased citations
- maximum visibility for your research: over 100M website views per year

At BMC, research is always in progress.

Learn more [biomedcentral.com/submissions](https://biomedcentral.com/submissions)





---

## 4.3 Supplemental file

### Additional information

#### **SAFit2 ameliorates paclitaxel-induced neuropathic pain by reducing spinal gliosis and elevating pro-resolving lipid mediators**

Saskia Wedel<sup>1</sup>, Lisa Hahnefeld<sup>1,2</sup>, Yannick Schreiber<sup>2</sup>, Christian Namendorf<sup>3</sup>, Tim Heymann<sup>4</sup>, Manfred Uhr<sup>3</sup>, Mathias V. Schmidt<sup>3</sup>, Natasja de Bruin<sup>2</sup>, Felix Hausch<sup>4</sup>, Dominique Thomas<sup>1,2</sup>, Gerd Geisslinger<sup>1,2</sup> and Marco Sisignano<sup>1,2\*</sup>

<sup>1</sup> Institute of Clinical Pharmacology, *pharmazentrum frankfurt/ZAFES*, University Hospital, Goethe-University, 60590 Frankfurt am Main, Germany

<sup>2</sup> Fraunhofer Institute for Translational Medicine and Pharmacology ITMP and Fraunhofer Cluster of Excellence for Immune Mediated Diseases CIMD, 60596 Frankfurt am Main, Germany

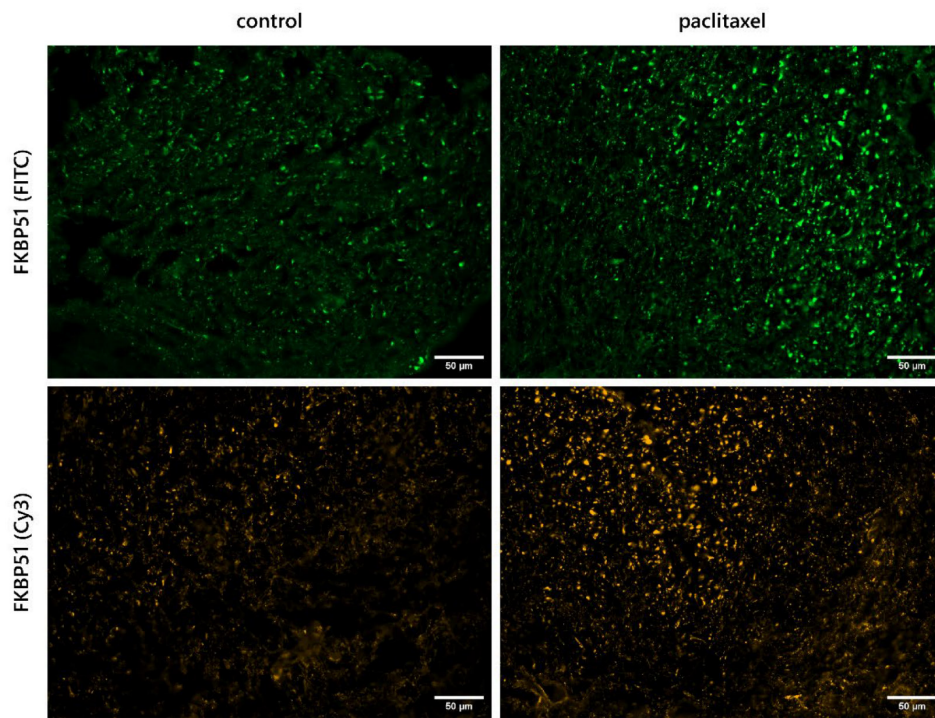
<sup>3</sup> Core Unit Analytics and Mass Spectrometry, Max Planck Institute of Psychiatry, 80804 Munich, Germany

<sup>4</sup> Department of Biochemistry, Technical University of Darmstadt, 64287 Darmstadt, Germany

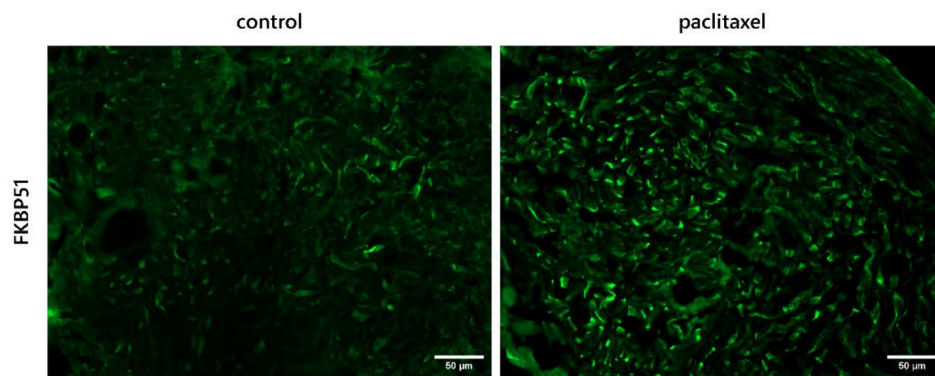
\*Address correspondence to: Dr. Marco Sisignano, *pharmazentrum frankfurt/ZAFES*, Institute of Clinical Pharmacology, University Hospital, Goethe-University, D-60590 Frankfurt am Main, Germany, Phone: +49 (0)69-6301-7819, E-mail: Marco.Sisignano@med.uni-frankfurt.de

Additional Figures: 7

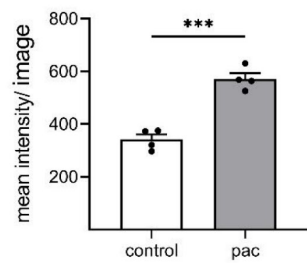
**A**



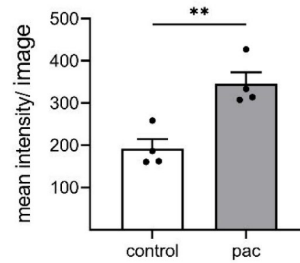
**B**



**C**

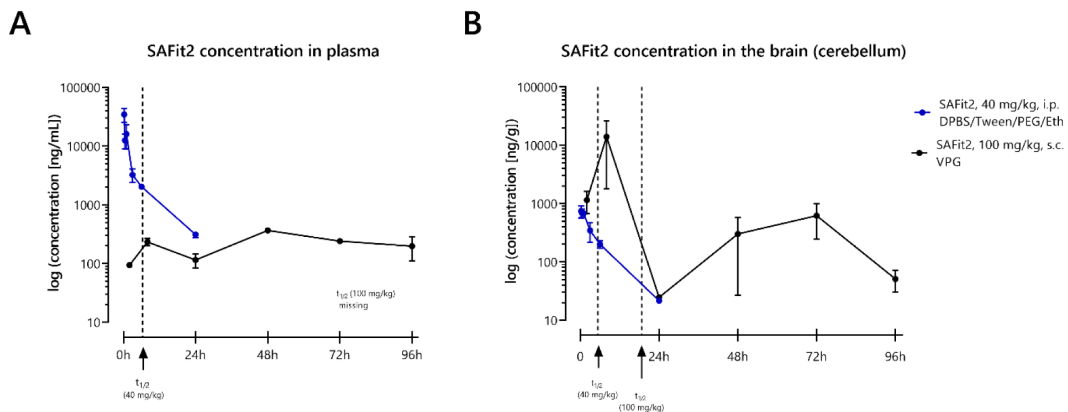


**D**



---

**Figure S1: Enhanced FKBP51 expression in spinal cord and L4-L5 DRG slices of paclitaxel-treated animals.** Immunohistochemistry staining of the protein FKBP51. Representative images of FKBP51 stained spinal cord (dorsal horn) **(A)** and L4-L5 dorsal root ganglia (DRG) **(B)** slices at 20X magnification (scale bar: 50  $\mu$ m). Samples of naïve animals were labeled as control. Quantification of the mean intensity per image for spinal cord samples **(C)** and DRG samples **(D)**. Data represent the mean  $\pm$  SEM from 10 quantified images per mouse. Each condition comprises data from four mice. \*\*  $p < 0.01$ , \*\*\*  $p < 0.001$ , student's t-test with Welch's correction.



C

	plasma		brain	
	SAFit2, 40 mg/kg i.p.	SAFit2, 100 mg/kg VPG s.c.	SAFit2, 40 mg/kg i.p.	SAFit2, 100 mg/kg VPG s.c.
$T_{1/2}$ [h]	6.4	-	5.4	-
$T_{max}$ [h]	0.25	48	0.25	8
$C_{max}$ [ng/ml],[ng/g]	34484	367	741	1801

**Figure S2: Pharmacokinetic study of SAFit2 comparing two formulations.** The animals received one dose of SAFit2 formulated either in PBS supplemented with 5% PEG400, 5% Tween and 0.7% ethanol or as slow-release formulation in vesicular phospholipid gel (VPG). To assess the concentrations of SAFit2 in plasma (A) and brain (B), samples were collected from three mice for each indicated time point. (C) The table shows the calculated half-time as well as the maximum time and the maximum measured concentration of SAFit2.

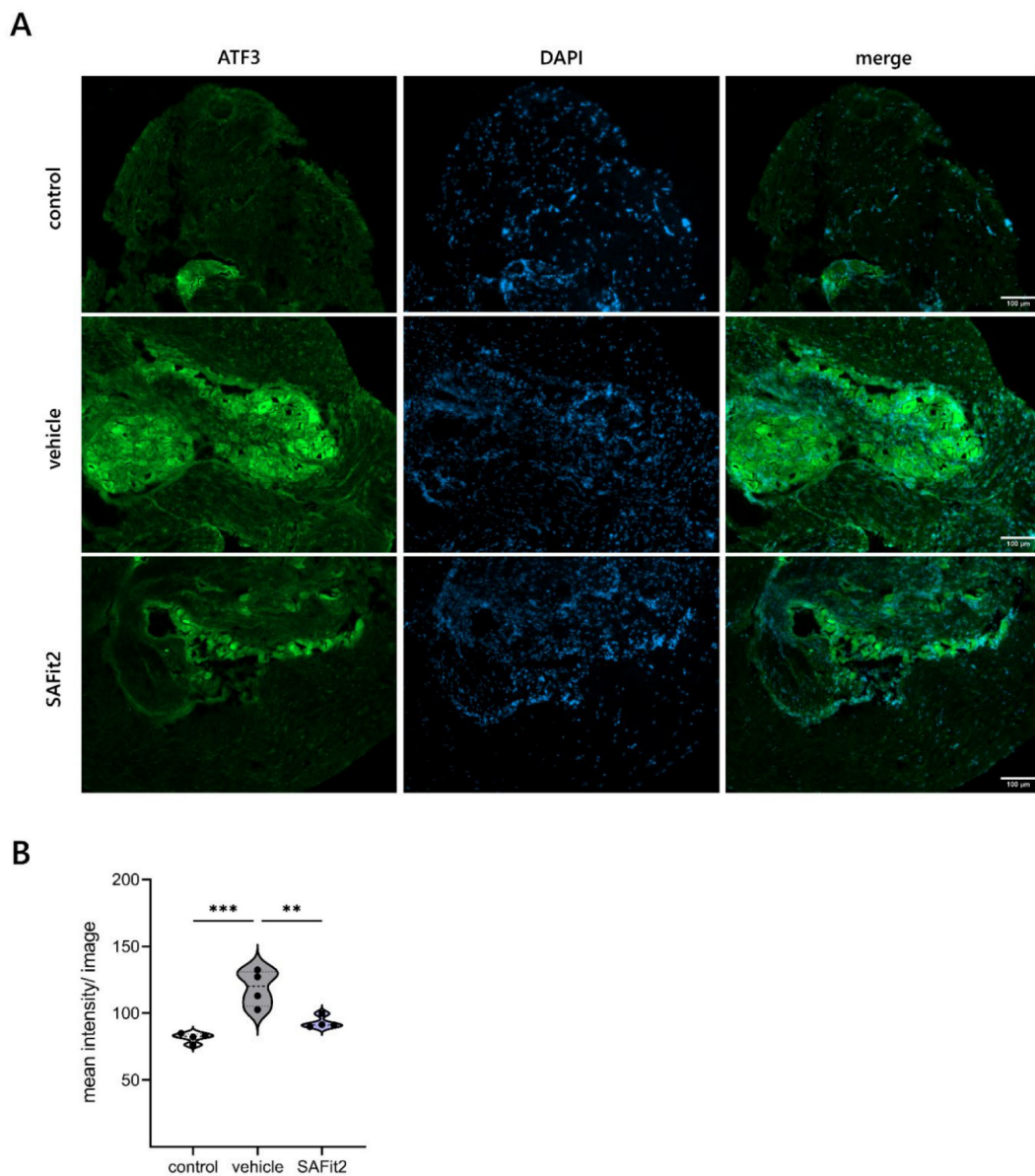
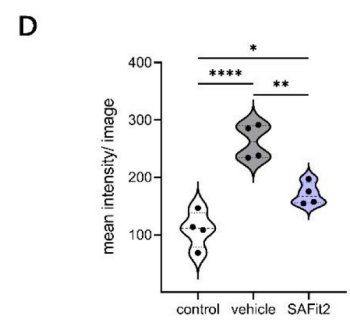
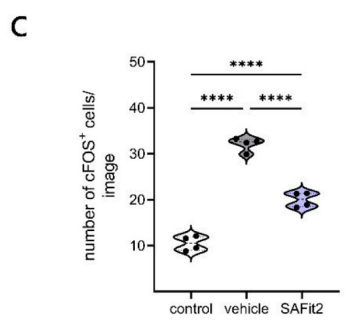
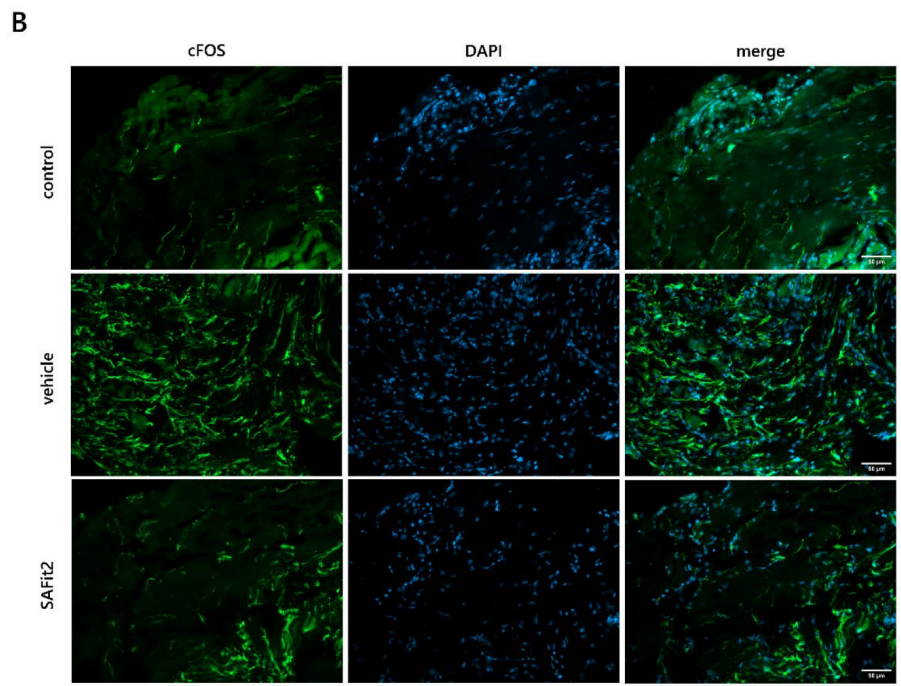
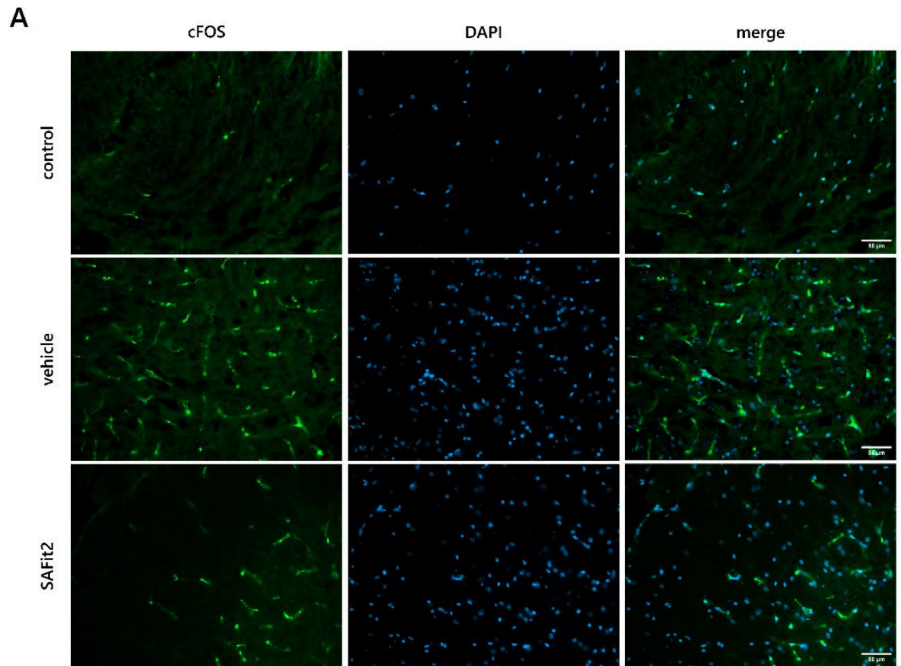


**Figure S3: Reduced ATF3 expression in L4 and L5 DRGs of SAFit2-treated animals.** Immunohistochemistry staining of the neuronal stress marker ATF3. **(A)** Representative images of ATF3 stained L4 and L5 dorsal root ganglia (DRGs) at 10X magnification (scale bar: 100  $\mu$ m). Samples of naïve animals were labeled as control. **(B)** Quantification of the mean intensity per image. Data represent the mean  $\pm$  SEM from 10 quantified images per mouse. Each condition comprises data from four mice. \*\*  $p < 0.01$ , \*\*\*  $p < 0.001$  one-way ANOVA with Tukey's multiple comparison test.



---

**Figure S4: Reduced cFOS expression in spinal cord and L4-L5 DRG slices of SAFit2-treated animals.** Immunohistochemistry staining of the neuronal activity marker cFOS. Representative images of cFOS stained spinal cord (dorsal horn **(A)** and L4-L5 dorsal root ganglia (DRGs) **(B)** slices at 20X magnification (scale bar: 50  $\mu$ m). Samples of naïve animals were labeled as control. **(C)** Quantification of cFOS positive signals per image. **(D)** Quantification of the mean intensity per image. Data represent the mean  $\pm$  SEM from 10 quantified images per mouse. Each condition comprises data from four mice. \*\*  $p < 0.01$ , \*\*\*  $p < 0.001$ , \*\*\*\*  $p < 0.0001$  one-way ANOVA with Tukey's multiple comparison test.

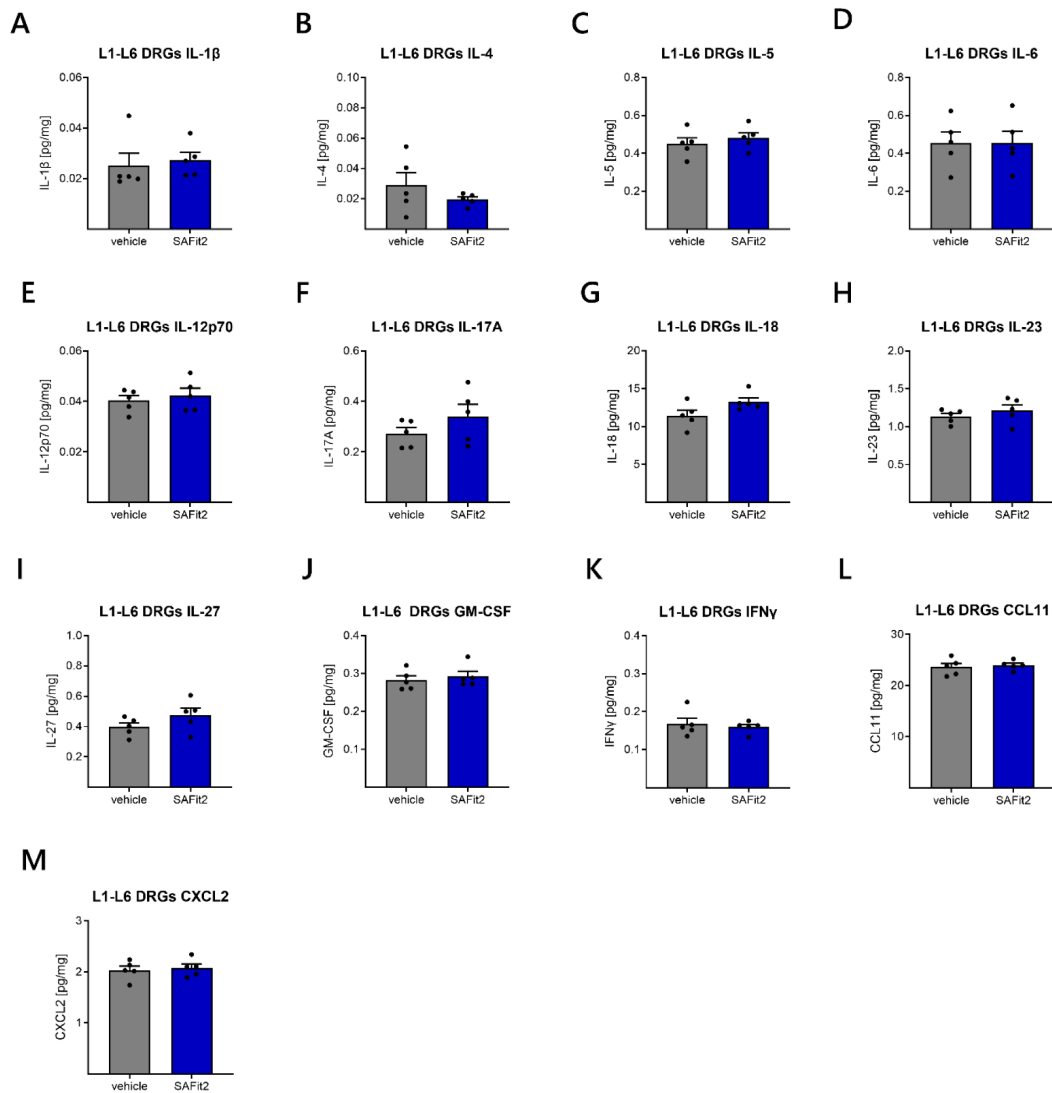


**Figure S5: Cytokines and chemokines measured in the DRGs of paclitaxel treated mice.** After 12 days, DRGs samples were homogenized and analyzed using a multiplex immunoassay including a panel of 26 cytokines and chemokines. The data represents the mean  $\pm$  SEM from 5 mice per group. The raw data was related to the total protein amount of the sample.



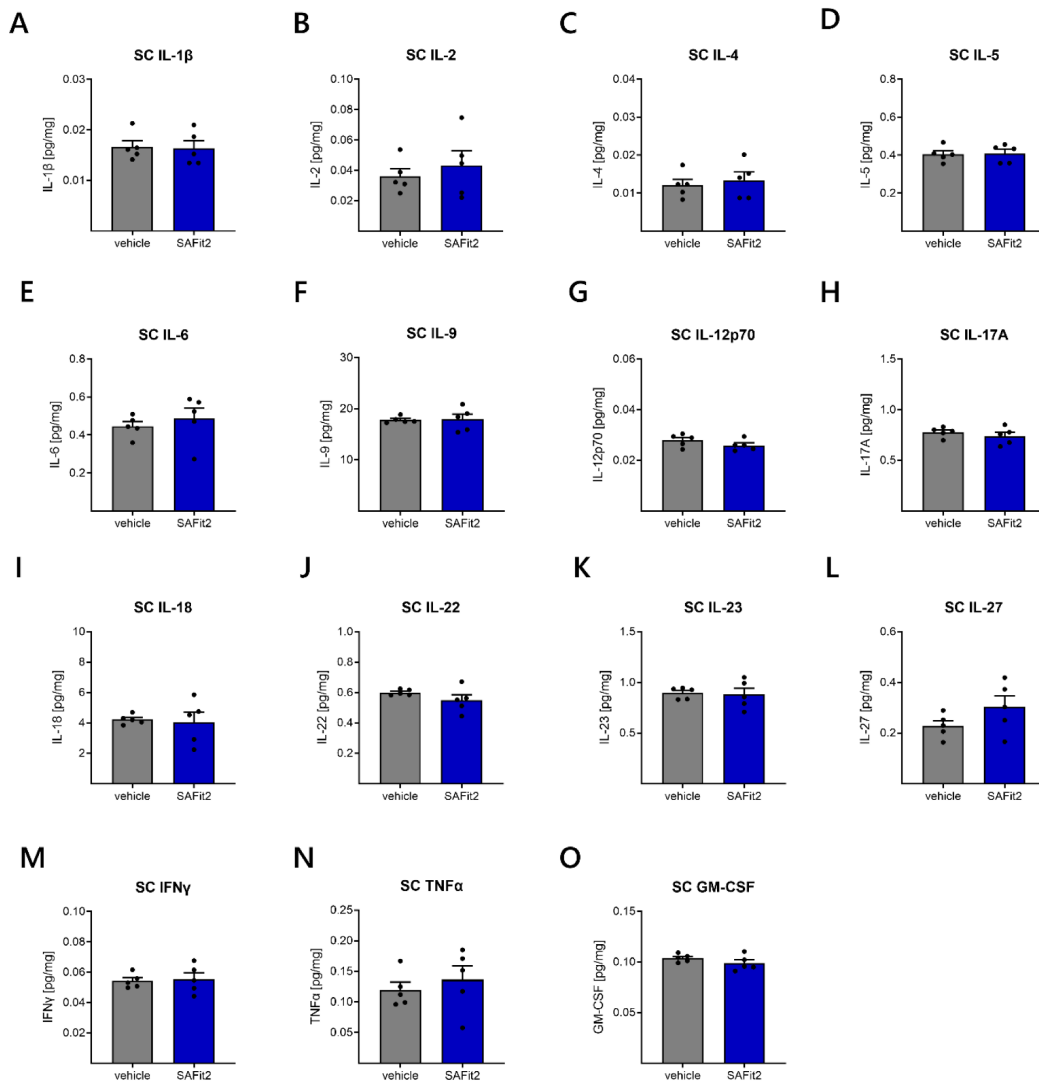


**Figure S6: Cytokines measured in the spinal cord of paclitaxel treated mice.** After 12 days, spinal cord samples were homogenized and analyzed using a multiplex immunoassay including a panel of 26 cytokines and chemokines. The data represents the mean  $\pm$  SEM from 5 mice per group. The raw data was related to the total protein amount of the sample.

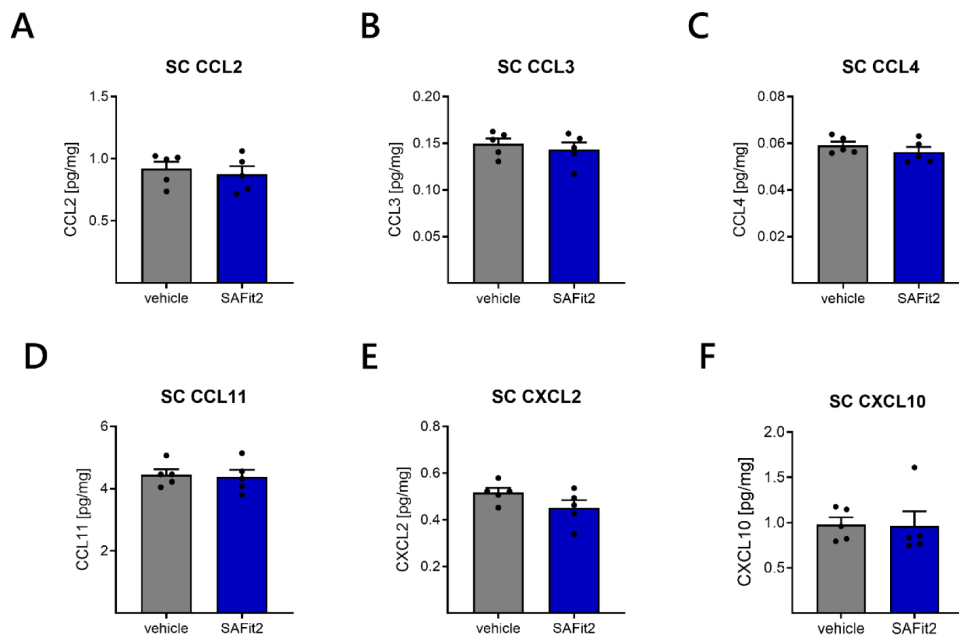


**Figure S7: Chemokines measured in the spinal cord of paclitaxel treated mice.** After 12 days, spinal cord samples were homogenized and analyzed using a multiplex immunoassay including a panel of 26 cytokines and chemokines. The data represents the mean  $\pm$  SEM from 5 mice per group. The raw data was related to the total protein amount of the sample.

---

### **Supplementary Methods section: DRG immunohistochemistry**

The L4 and L5 DRG samples were obtained as described in the “tissue isolation” method section in the main manuscript. Afterwards, the tissue samples were embedded in Tissue-Tek and frozen at -80 °C. For immunohistochemistry stainings, the frozen tissue samples were serially sliced into 12 µm tissue slices with a cryostat (Leica Biosystems). Next, the slices were stained according to the protocol, which is described in the “immunohistochemistry” method section in the main manuscript. The primary antibodies anti-ATF3 (sc-188, Santa Cruz) and anti-cFOS (9F3, Cell Signaling) were diluted 1:50 and 1:200, as recommended, respectively in 1% BSA solution and applied for an overnight incubation at 4 °C. The primary antibody anti-FKBP51 (sc-271547, Santa Cruz) was diluted 1:50 as recommended in 3% BSA solution to minimize cross-reactivity as the host species is mouse. The secondary antibody goat anti-rabbit Alexa Fluor 488 (ab150077, Abcam) was diluted 1:1000 in 1% BSA solution and applied for one hour at room temperature. The secondary antibodies goat anti-mouse Alexa Fluor 488 (CF488A, Biotium) and sheep anti-mouse Cy3 (C2181, Sigma Aldrich) were diluted in 3% BSA solution. For quantification purposes, 10 images were taken per animal per staining. One treatment group comprises samples from four animals as for the spinal cord samples.

---

## 5 General discussion

---

Within this thesis, the central aim was to elucidate whether SAFit2, a selective FKBP51 inhibitor, might serve as potential novel drug candidate for the treatment of nerve injury- and chemotherapy-induced, especially paclitaxel-induced, neuropathic pain. This guiding aim was based on previous data which showed that FKBP51 deficient mice experienced significantly less inflammatory and chronic pain (343, 344). Moreover, the lack of efficient neuropathic pain therapeutics highlights a relevance for novel targets, drug candidates, and treatment strategies. Based on this, we analyzed the impact of SAFit2 on different neuropathic pain states *in vivo* and on pain-associated mechanisms in primary cell cultures and with primary tissue samples *in vitro* (153, 370, 371). In line with this, we discovered that SAFit2 might constitute as novel treatment option for nerve injury- and chemotherapy-induced neuropathic pain as it efficiently relieved pain in both mouse models.

### 5.1 SAFit2-mediated effects in nerve injury- and chemotherapy-induced neuropathic pain in relation to the glucocorticoid receptor signaling

At first, the influence of SAFit2 on pain sensation was assessed in mouse models of nerve injury- and chemotherapy-induced neuropathic pain. Therefore, mice underwent either a surgery to cause a spared nerve injury or were repetitively injected with paclitaxel as cytostatic to induce the respective types of neuropathic pain. Afterwards, the mice were treated either with SAFit2 or the respective vehicle for a distinct period of time. Based on this, we observed an alleviation of mechanical hypersensitivity, which is defined as indication for persistent pain in rodents (373), after SAFit2 treatment in both neuropathic pain models (370, 371). Since SAFit2 gained a pain relief in two models that diverge in their initiation and vary in their underlying mechanisms, a SAFit2-mediated pain relief was suggested to be primarily mediated by an interference of SAFit2 into the disrupted FKBP51-GR interplay.

In line with this assumption, FKBP51-mediated dysregulations in the GR signaling were previously suggested to contribute to the development of neuropathic pain (343, 344). Associated to this, the expression of glucocorticoid receptors was increased in the spinal cord of nerve-injured mice and in the hippocampus of focal brain-injured mice (374, 375). Furthermore, previous studies associated the GR signaling with an upregulation of NMDA receptors, which play an important role in central sensitization mechanisms, in the spinal

---

cord of nerve-injured mice. Likewise, antagonizing GRs reduced the upregulation of NMDA receptors after nerve injury and antagonizing NMDA receptors reduced nerve injury-induced hypersensitivity in rodents (376, 377). Moreover, antagonizing GRs in an ankle joint inflammation model significantly reduced mechanical hypersensitivity in mice (343). However, targeting GRs in naïve mice led to the development of mechanical hypersensitivity. This indicates an anti-nociceptive function of the GR signaling at basal conditions and a pro-nociceptive role of the GR signaling in the development of inflammatory and neuropathic pain states (343). Based on this, the dysregulation of the GR signaling was suggested to mediate pro-nociceptive functions. Accordingly, previous studies indicated that an ablation of FKBP51, which functions as co-chaperone and downstream target of GR, established a constant anti-nociceptive property of the GR signaling (343, 344). According to these insights, counteracting the sustained upregulation of FKBP51 in neuropathic pain states would be beneficial for restoring GR properties and therefore ameliorating neuropathic pain. In line with this, SAFit2 mediated a pain relief in nerve injury- and paclitaxel-induced neuropathic pain states in mice (370, 371), indicating that SAFit2 efficiently interferes in the pathological and FKBP51-mediated dysregulation of the GR signaling (Figure 10).

A dysregulation of the GR signaling and the associated glucocorticoid resistance may also play an essential role in neuropathic pain underlying mechanisms which regulate the development and maintenance of neuropathic pain. More specifically, the GR signaling has been indicated to regulate the activation of the NF- $\kappa$ B signaling pathway and thereby to modulate the transcription of cytokines under physiological conditions (378). Based on this, high levels of glucocorticoids can facilitate a strong anti-inflammatory response. However, studies postulated that in chronic and excessive inflammatory states such as those in neuropathic pain, FKBP51-GR homeostasis is disrupted and GR insensitivity arises (379, 380). In addition, pro-inflammatory cytokines are suggested to mediate such dysregulations as they have been shown to decrease the expression of GRs and to block the GR translocation into the nucleus (381). In consequence, endogenous glucocorticoids fail to resolve neuroinflammation or inflammation in neuropathic and chronic inflammatory pain states.

However, this pathological glucocorticoid resistance might be resolved through an SAFit2 application in neuropathic pain states, since counteracting and preventing the pathologically increased FKBP51 levels, restored FKBP51-GR homeostasis and GR sensitivity *in vivo* (343). In addition, the anti-nociceptive and anti-inflammatory properties of the GR signaling could

---

be restored with SAFit2. In line with this hypothesis, we observed decreased pro-inflammatory cytokine levels in neuronal tissue of nerve-injured mice after SAFit2 treatment (Figure 10). Moreover, we observed a reduction in the NF- $\kappa$ B pathway activation in DRGs and spinal cord of nerve-injured mice after SAFit2 treatment (370). In accordance to this, a reconstituted GR signaling was shown to counteract an inflammation-driven and pathologically increased NF- $\kappa$ B activation (378). Beside the reduction of pro-inflammatory cytokines, paclitaxel-treated animals showed additionally an increase in anti-inflammatory cytokines like IL-10 and IL-22 after SAFit2 treatment. Likewise, the GR signaling is known to repress pro-inflammatory cytokines and to induce the expression of anti-inflammatory cytokines (382, 383), highlighting the complexity of the GR signaling. Nevertheless, these insights lead to the assumption that SAFit2 has the potential of restoring a physiological FKBP51-GR homeostasis in neuropathic pain states.

Interestingly, the comparison of cytokine levels reveals differences between the nerve injury- and the paclitaxel-induced neuropathic pain model after SAFit2 treatment (370, 371). Notably, SAFit2 reduced pro-inflammatory cytokine levels only in nerve-injured mice and not in paclitaxel-treated mice (Figure 10). In addition, SAFit2 increased anti-inflammatory cytokine levels only in paclitaxel-treated mice. These differences might be mediated by the different characteristics of the models. Paclitaxel-induced neuropathic pain encompasses a minor inflammatory component, whereas nerve injury-induced neuropathic pain is characterized by an inflamed injury site. This inflamed nerve injury in turn leads to a strong neuroinflammation, including an enhanced release of pro-inflammatory mediators such as cytokines (237, 261, 265, 274, 384-386).

In contrast to the model-dependent differences, the reduction of chemokine levels was of similar magnitude in DRGs and spinal cord of both models (370, 371). Chemokines are known to play a major role in the transmission of pain as they can directly act on sensory neurons and glial cells (275, 387). Furthermore, chemokines are known to activate glial cells and resident immune cells as well as to facilitate the migration and invasion of immune cells (388, 389). In particular, they serve as chemoattractants and enhance the expression of adhesion molecules in endothelial cells to enable a successful invasion of immune cells into tissue (390). Accordingly, we detected a reduced immune cell infiltration into DRGs and spinal cord of nerve-injured mice and a reduced glial cell activation in the spinal cord of paclitaxel-treated mice (Figure 10). However, we observed no alterations in the number of

immune cells at the site of injury, the sciatic nerve, in nerve-injured mice (370). This is of particular interest, as the application of glucocorticoids and the corresponding GR signaling are associated with systemic anti-inflammatory and immunosuppressive actions (390-392). In comparison, SAFit2- and glucocorticoid-mediated effects show major differences. Whereas glucocorticoids seem to overshoot the system and to switch a GR insensitivity towards a GR hyperactivation, SAFit2 seems to restore a physiological homeostasis of the GR signaling. This restored homeostasis was assumed after SAFit2 treatment since SAFit2 reduced the infiltration of immune cells into DRGs and spinal cord but did not impair the number of immune cells at the site of injury. Thereby, systemic neuroinflammation and sensitization processes were reduced without effecting the resolution of inflammation at the site of injury.

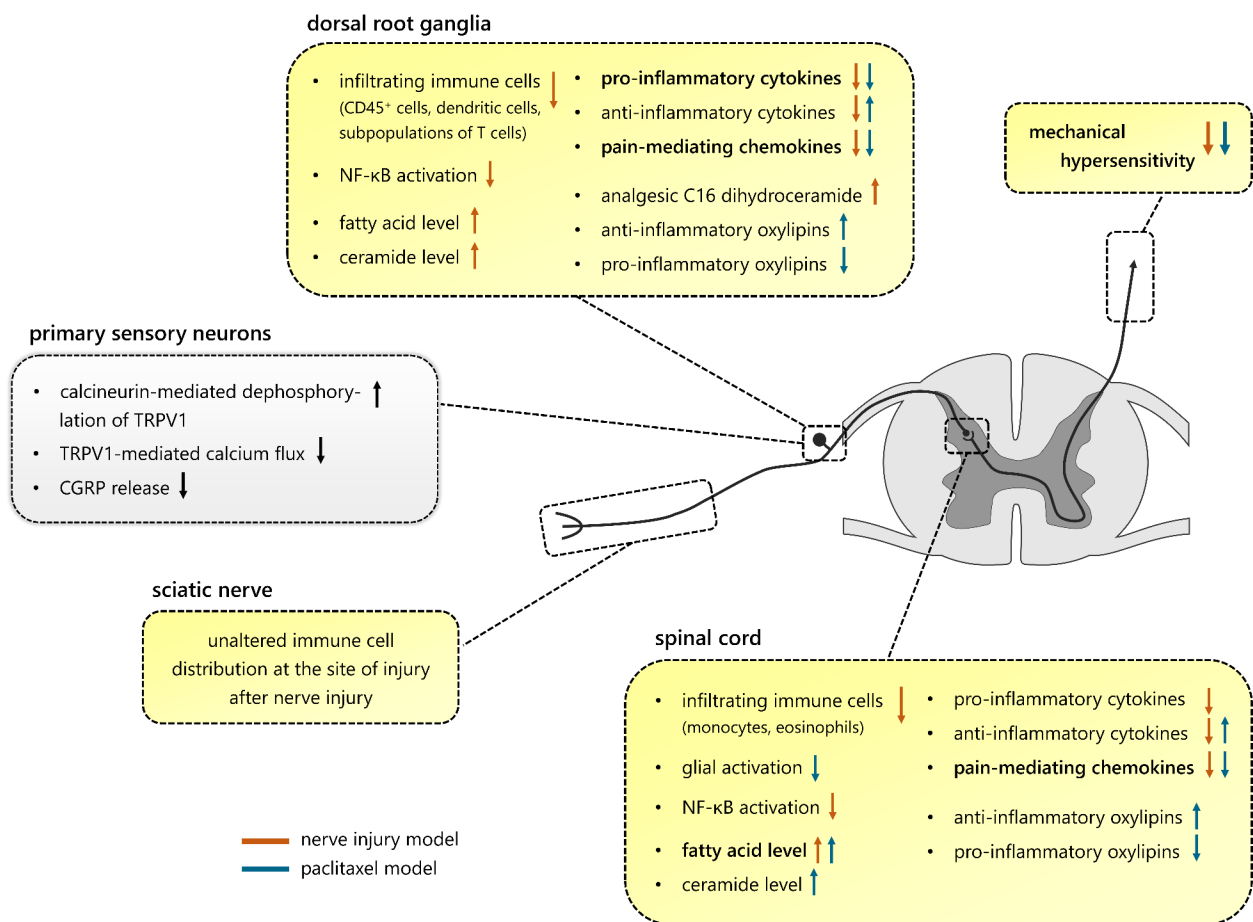


**Figure 10: Summary of SAFit2-mediated effects in nerve injury- and paclitaxel-induced neuropathic pain models.** SAFit2 significantly reduced mechanical hypersensitivity, a symptom of persistent pain, in both models. Furthermore, it significantly reduced levels of pro-inflammatory cytokines and pain-mediating chemokines in DRGs and spinal cord of nerve-injured mice. In contrast, paclitaxel-treated mice showed an increase of anti-inflammatory cytokines and a decrease of pain-mediating chemokines in DRGs and spinal cord

---

after SAFit2 treatment. Nevertheless, SAFit2 leads to changes in the number of activated immune cells in both models. Whereas SAFit2 decreases the invasion of immune cells into DRGs and spinal cord in the nerve injury model, SAFit2 reduces the activation of glial cells in the paclitaxel model. Notably, SAFit2 did not alter the number of immune cells at the site of injury, the sciatic nerve, in the nerve injury model. Moreover, SAFit2 counteracted an enhanced NF- $\kappa$ B pathway activation in DRGs and spinal cord of nerve-injured mice. Besides this, SAFit2 seems to increase the levels of free fatty acids as well as ceramides in both models. Furthermore, it restored the levels of an analgesic ceramide, dihydroceramide C16, after nerve injury and of anti-inflammatory oxylipins after paclitaxel treatment. In primary sensory neurons, SAFit2 leads to the desensitization of the ion channel TRPV1 and a reduced release of the neuropeptide CGRP. Orange arrows represent changes in the nerve injury model, whereas blue arrows display changes in the paclitaxel model. In addition, light orange boxes display either *in vivo* or *ex vivo* data, whereas the grey box illustrates results from primary sensory neuron cultures. SAFit2-mediated effects that are similar in the nerve injury- and the chemotherapy-induced neuropathic pain are printed in bold. The illustration was created with images from motifolio.

The equilibrating property of SAFit2 displays a key benefit in the context of pain treatment, as the GR signaling displays a beneficial pathway for the regulation of anti-inflammatory and anti-nociceptive actions at basal levels (343). However, its homeostasis and regulation seem to be quickly impaired especially in the context of enhanced and chronic inflammation (343, 380, 393, 394). Furthermore, counteracting this disbalance either with GR antagonists or glucocorticoids, GR agonists, resulted in either an analgesic but not anti-inflammatory or strong anti-inflammatory but also immunosuppressive outcome (343, 377, 395-398). In line with this, many studies postulated diverging effects of pain sensation, when targeting the GR signaling with conventional therapeutics in complex mechanisms such as neuroinflammation (399). These contradicting outcomes especially involve mechanisms that include and affect neuronal and immunological components like the activation of astrocytes (400). Based on this, reconstituting the FKBP51-GR homeostasis with SAFit2 seems to be a promising approach to target complex neuroinflammatory mechanisms in pain.

Beside the GR signaling in chronic inflammatory states, glucocorticoids also induce contradictory effects in lipid metabolism. On the one hand, the acute increase of glucocorticoids lead to the release of stored energy like lipids, on the other hand, long term elevated glucocorticoid levels are associated with adipose tissue accumulation (401). However, the investigation of the GR signaling in the context of obesity and type II diabetes increases (402). In line with this, previous studies showed that FKBP51 deficient mice had lower lipid plasma levels, gained less body weight, and comprised less glucose intolerance



---

than wild type animals (339, 403). Nevertheless, the influence of the GR signaling on endogenous lipid mediators such as oxylipins is not well understood yet.

In this work, we firstly assessed lipid levels in nervous tissue after pharmacologically targeting FKBP51 (Figure 10). Thereby, we observed increased poly unsaturated fatty acid and ceramide levels in both models after SAFit2 treatment (369, 371). Although, the role of ceramides is poorly understood in the mediation of neuropathic pain, we identified one dihydroceramide which was significantly altered after SAFit2 treatment in the nerve injury model. Interestingly, we observed that the C16 dihydroceramide comprises analgesic properties as it desensitized the pain-mediating TRPV1 channel *in vitro* as well as reduced thermal hypersensitivity in a capsaicin mouse model (369). Based on this, we firstly revealed a lipid mediator that is restored by SAFit2 after nerve injury. Beside the C16 dihydroceramide, we also observed an increase in PUFAs in DRGs and spinal cord in both neuropathic pain models, highlighting especially the increase of docosahexaenoic acid (DHA) (369, 371). DHA is known as an anti-inflammatory PUFA which is significantly reduced after nerve injury and restored to a sham comparable level after SAFit2 treatment (369). In the paclitaxel model, DHA levels are even increased after SAFit2 treatment compared to the respective vehicle control. Moreover, we observed elevated DHA oxylipin levels, which are precursors for SPMs such as resolvins, after SAFit2 treatment in paclitaxel-treated mice (371). Based on these results among others, we assume that SAFit2 might cause a shift in lipid distribution towards an anti-inflammatory lipid profile and thereby contributes to the resolution of neuropathic pain.

In summary, SAFit2 led to an amelioration of mechanical hypersensitivity in both nerve injury- and paclitaxel-induced neuropathic pain mouse models. Furthermore, it reduced signs of neuroinflammation like the reduction of pro-inflammatory mediators or the activation of glial cells. Lastly, SAFit2 increased anti-inflammatory lipid mediators in nerve injury- and paclitaxel-induced neuropathic pain mouse models, highlighting its comprehensive and multimodal regulation in the context of neuropathic pain.

---

## 5.2 The influence of SAFit2 on TRPV1 sensitization and the phosphatase calcineurin

Besides the promising *in vivo* effects of SAFit2, we observed *in vitro* that SAFit2 desensitizes the pain-mediating TRPV1 channel probably by decreasing its phosphorylation state (370). The dephosphorylation of TRPV1 is mainly mediated by the phosphatase calcineurin in sensory neurons (404, 405). In line with this, we observed that the calcineurin inhibitor cyclosporine reversed the SAFit2-mediated desensitization of TRPV1 in primary sensory neurons (370). Based on this, we investigated the influence of SAFit2 on calcineurin *in vitro*, detecting that SAFit2 enhanced the calcineurin-mediated phosphate release (370). Based on this insight, we suggest that SAFit2 desensitizes the pain-mediating TRPV1 channel in a calcineurin dependent manner. Although these findings would be beneficial in the context of pain and would contribute to a pain relieve *in vivo*, this data also raised the question whether an increased calcineurin-mediated dephosphorylation of TRPV1 might be an off-target effect of SAFit2.

To address this question, the molecular structure of SAFit compounds, which was developed on the molecular basis of FK506, has to be considered (367, 406). FK506 is predominantly known for its immunosuppressive function, mediating the inhibition of calcineurin (407, 408). However, the immunosuppressive capacity of SAFit compounds was neglected in different stimulation assays (367, 409). In those assays, SAFit compounds neither impaired T cell activation nor T cell cytokine secretion, highlighting that SAFit compounds have no immunosuppressive capacity (367). Nevertheless, elucidating whether the calcineurin-mediated TRPV1 desensitization is an on- or off-target effect of SAFit2, becomes a challenging issue, since the regulation of calcineurin is multifarious (Figure 11). Furthermore, the influence of uncomplexed FKBP51 on calcineurin is not fully discovered as only one group proposed the direct inhibition of calcineurin by FKBP51 (410). However, the inhibition of calcineurin by the complex of FKBP1-FK506 was confirmed in various studies (411-414). In line with that, the concept of scavenging either FKBP51 or minimizing the complex of FKBP51-FK506 with SAFit2 would support the assumption of a FKBP51 dependent effect, since SAFit2 directly competes with FK506 in the binding of FKBP51. This assumption was supported by the results which showed that a SAFit2-mediated desensitization of TRPV1 could be reversed by the inhibition of calcineurin in primary sensory neurons (370).

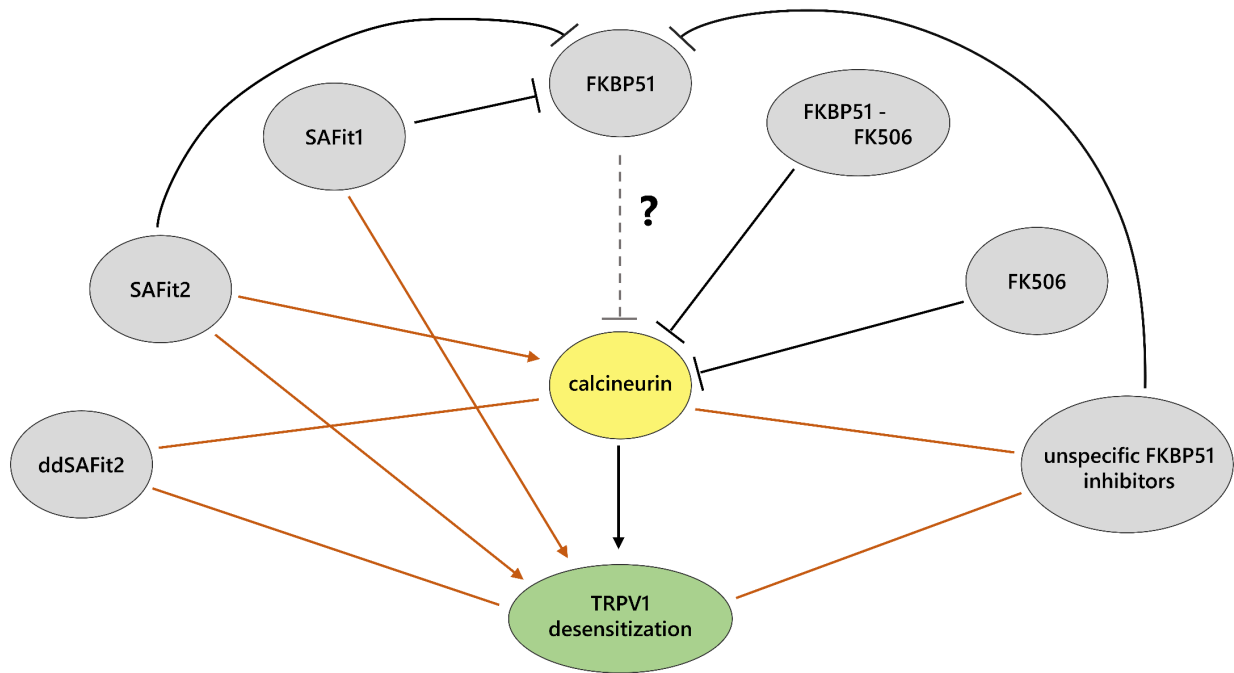


**Figure 11: The SAFit2-FKBP51 network depicted as influencing factors of calcineurin and TRPV1 desensitization.** The influence of FKBP51 on the activity of the phosphatase calcineurin is controversially discussed in literature. However, both the complex of FKBP51 and FK506 as well as FK506 alone have been shown to inhibit the activity of calcineurin, whereas SAFit2 or analogues either have no effect on the activity of calcineurin or increased the calcineurin-mediated phosphate release. Furthermore, calcineurin was shown to mediate the dephosphorylation and subsequent desensitization of TRPV1 in primary sensory neurons. In line with this, SAFit2 and analogues also showed a desensitization of TRPV1 in sensory neurons. However, unspecific FKBP51 inhibitors as well as ddSAFit2, a chiral and biological inactive analogue, did not. Blocking lines indicate an inhibitory effect, arrows an inducing effect and straight lines illustrate neither an induction nor inhibition. Black lines indicate results from literature, whereas orange lines indicate insights from this work.

To verify the effect of SAFit2 on TRPV1, the impact of unspecific FKBP51 inhibitors on TRPV1 was assessed. Interestingly, we observed that unspecific FKBP51 inhibitors, which additionally inhibit other FKBP5s like FKBP12, neither desensitize nor sensitize the TRPV1 channel in primary sensory neurons (370). However, unspecific FKBP51 inhibitors should mediate the same effects as SAFit2, given that they were applied in sufficient high concentrations to efficiently inhibit FKBP51 beside other FKBP5s. Accordingly, other FKBP5s have been shown to inhibit calcineurin in an increased fold in their complexed forms compared to complexed FKBP51 (411). Likewise, independent of the concentration of unspecific FKBP51 inhibitors, they should gain the same effects on calcineurin as SAFit2. Based on this, a SAFit2-mediated desensitization of TRPV1 was suggested to be either an

---

FKBP51 independent effect or can be reasoned by an FKBP51 dependent structural effect of SAFit2, which cannot be achieved by other inhibitors.

Associated with this suggestion, we showed that SAFit2 analogues such as SAFit1, 19a and 19b, which specifically target FKBP51, induced a desensitization of TRPV1 in primary sensory neurons, but with varying potency (415). Based on these insights, a SAFit2-mediated desensitization of TRPV1 can be reasoned by a structural effect of SAFit2 and its analogues. In line with this, a chiral SAFit2 analogue, which is biologically inactive instead, neither desensitized the TRPV1 channel nor increased the calcineurin-mediated phosphate release *in vitro* (370). Furthermore, macrocyclic FKBP51 inhibitors did not show a desensitization at all (unpublished data). Taken together, future research has to be conducted to point out the particular molecular influence of SAFit2 on calcineurin and thereby on TRPV1 sensitization. In summary, the calcineurin-mediated desensitization of TRPV1 is suggested to be caused by a structural effect of SAFit2 and its analogues, derived from their initial lead structure, that has not been identified yet.

### **5.3 Risks and advantages of targeting FKBP51**

The FKBP51-GR signaling is described as a fragile signaling pathway that is involved in the regulation of multifunctional processes (382, 416-418). Moreover, maladaptive dysregulations of the GR signaling were implicated in the context of pain (343, 344, 374, 377). However, targeting this pathway either with glucocorticoids or GR antagonists revealed controversial results (343, 393). Glucocorticoids have been shown to acutely prevent post-operative pain as they strongly counteract inflammation (419). Furthermore, they have been shown to be beneficial in some nerve injury animal models, but at the risk of developing GR insensitivity and possible side effects (396, 399, 402, 420, 421). However, glucocorticoid application in chronic pain states even exacerbated pain sensations in animals and patients (377, 395, 399). In line with this, the application of GR antagonists like mifepristone, which is also used to counteract adverse effects of glucocorticoids, was shown to be beneficial in the context of some chronic pain states (343, 422). These paradoxical effects of GR signaling regulators indicate that targeting FKBP51, as a dysregulated endogenous modulator in neuropathic pain states, can restore the beneficial functions of an FKBP51-GR homeostasis.

---

However, targeting FKBP51 can either additionally affect other processes or might be beneficial in other pathological disorders than in chronic neuroinflammation and neuropathic pain. To evaluate further outcomes of targeting FKBP51, the impact of FKBP51 deficiency has to be analyzed at first in healthy animals. FKBP51 deficient mice displayed no pathophysiological alterations or disorders, no impaired immunity or fertility (423). Furthermore, a long-term treatment with an FKBP51 inhibitor for 30 days, which reflects a model for chronic treatment in rodents, did not induce any pathological phenotype in mice and rats (406). However, both, chronic treatment and complete FKBP51 deficiency, resulted in a leaner phenotype and improved glucose tolerance, although the body temperature, food intake and activity of those animals was not altered (424). These changes can be associated with the tissue specific expression pattern of FKBP51. A comprehensive study in humans revealed that, although FKBP51 is expressed throughout the body, it is expressed the highest in adipocytes, skeletal muscle cells and immune cells beside the brain (340). Based on the high expression especially in adipocytes and muscles, it is conceivable that targeting FKBP51 might affect the energy metabolism of mice (323).

According to the strong expression of FKBP51 in adipocytes, FKBP51 was shown to be involved in both phases of adipogenesis, adipocyte differentiation and maturation (339, 425). Likewise, the deficiency of FKBP51 prevented the development of adipocytes and the accumulation of lipid droplets (426), whereas FKBP51 itself repressed the lipolysis of stored lipids in white adipose tissue (339). Lipolysis is initially mediated by the AKT pathway in muscles and adipocytes, in which the AKT expression is mainly restricted to the isoform AKT2 (340). Upon the activation of AKT through its phosphorylation, it further activates the kinase p38 which subsequently phosphorylates GR $\alpha$  and the peroxisome-activated receptor  $\gamma$  (PPAR $\gamma$ ) (427). Upon the phosphorylation of these two factors, lipolysis is stimulated and adipogenesis repressed (340). However, FKBP51 was shown to scaffold the phosphatase PH domain leucine-rich repeat phosphatase (PHLPP) which dephosphorylates AKT and thereby represses the downstream events, resulting in a repression of lipolysis and an induction of adipogenesis (426, 427). In line with this, FKBP51 deficient mice are protected from gaining weight, obesity and hepatic steatosis in high fat diets (423). Furthermore, they showed less white adipose tissue, revealing FKBP51 as a potential target for obesity (423).

Besides obesity, diabetes displays also an issue in the context of both metabolism and pain. Furthermore, human studies identified a correlation between SNPs of *FKBP5* and type two

---

diabetes, pointing out FKBP51 as marker for insulin resistance (340, 428, 429). In fact, FKBP51 was shown to reduce glucose tolerance by interfering in the AKT signaling pathway. Upon the binding of insulin to muscle cells, the phosphoinositide 3-kinase (PI3K) signaling is activated. This leads to the phosphorylation of AKT by the pyruvate dehydrogenase kinase 1 (PDK1) and mammalian target of rapamycin (mTOR) complex 2 (430-433). Activated AKT in turn activates its downstream effector apoptosis signal-regulating kinase 1 (Ask1) and AS160 (AKT substrate of 160 kDa) through phosphorylation (339, 424). AS160 then promotes the translocation of the glucose transporter 4 (GLUT4) to the cell membrane (424). Based on this mechanism, more glucose can be taken up from skeletal muscle cells and glucose tolerance is increased. However, FKBP51 represses the activation of AKT and its downstream events, leading to the induction of glucose intolerance (429). In line with these insights, FKBP51 deficient mice as well as SAFit2-treated mice showed an improved glucose tolerance under both control and high fat diet conditions, pointing out the involvement of FKBP51 in body glucose homeostasis (424). Considering these insights along with the upregulation of FKBP51 in diabetes type II patients, FKBP51 might also serve as beneficial target in the context of diabetes and insulin intolerance (340, 406, 434).

Nevertheless, studies postulated that FKBP51 is involved in myoblast differentiation and myotube formation (339, 435). This is of particular interest, since deleting FKBP51 could lead to muscle atrophy. In line with this, a study postulated a delayed muscle regeneration in FKBP51 deficient mice (435). This data was supported by another study which showed an enhanced protein expression after FKBP51 overexpression in C2C12 cells (436). Moreover, long term treatment with glucocorticoids or the Cushing's syndrome itself are associated with the occurrence of muscle atrophy (420). Based on this, FKBP51 is suggested to repress the activity of GR $\alpha$  through inhibiting the AKT pathway in those patients and thereby to counteract muscle atrophy (339, 426, 427). According to these recent findings, short-term targeting of FKBP51 could be beneficial to address chronic pain states. In contrast, long-term treatments should be applied with caution, since antagonizing FKBP51 could impair muscle growth and regeneration. However, it has to be taken into account that a complete deficiency of FKBP51 induces more severe effects than inhibiting FKBP51 to a certain amount. In conclusion, further studies need to be performed to further elucidate to which extent FKBP51 comprises a role in the context of muscle regeneration and growth and which impact a SAFit2 treatment would have.

---

Beside the strong expression of FKBP51 in adipocytes and muscles, it has also been shown to be highly expressed in the brain (340). Within the brain, FKBP51 is predominantly linked to many neurological disorders which are caused by a disruption of the GR signaling and will be discussed in a following chapter (321, 437). Beside neurological disorders, FKBP51 was associated to autophagy-mediated processes which play an important role in Huntington disease (438-440). Huntington disease is a rare condition that is predominantly described by the loss of neurons in the CNS and is mediated by a modification of the huntingtin (HTT) gene (441, 442). In addition, lowering the levels of the mutant HTT (mHTT) protein was shown to ameliorate Huntington disease (437). However, FKBP51 was suggested to mediate a conformational change in mHTT that prevents an autophagy-driven clearance of this protein (437). In line with this, lowering FKBP51 levels by pharmacologically targeting FKBP51, lowered the levels of the mutant HTT (mHTT) protein *in vitro* and *in vivo* (437). Associated to this, FKBP51 was shown to be involved in the complex regulation of autophagy in the hippocampus. Neither the complete deficiency nor an overexpression of FKBP51 led to a functional autophagy signaling (439). Exclusively moderate levels of FKBP51 were able to facilitate a functional autophagy signaling (439). In summary, an autophagy signaling can only be facilitated at basal levels of FKBP51 which seems to be restored via targeting FKBP51 with SAFit2. Based on this, targeting FKBP51 to restore autophagy reveals a novel and interesting treatment field since disrupted autophagy is linked to many disorders and diseases (443-445).

In addition to the suggested involvement of FKBP51 in autophagy, FKBP51 has been shown to comprise an essential role in the context of cancer. Furthermore, FKBP51 was postulated as biomarker for cancer by several studies (446-450), although the expression of FKBP51 is controversially discussed in several cancer types. Likewise, a hyperexpression of FKBP51 was recorded in many cancer types such as lymphomas, gliomas, melanoma, idiopathic myelofibrosis, skin melanoma, colon cancer, ovary cancer and prostate cancer (449-452). However, a downregulation of FKBP51 was identified in pancreatic cancer and breast cancer (453-455). The diverging expression levels of FKBP51 in different cancer types has been mainly suggested to depend on the originating cell type and the associated underlying mechanism (352, 449). Based on this, elucidating the underlying mechanisms of FKBP51 in the respective cancer types is crucial for targeting FKBP51 in the context of chemotherapy-

---

induced neuropathic pain. Therefore, suggested mechanisms are described in the following, starting with cancer types that are linked to an FKBP51 overexpression.

In the case of prostate cancer, the signaling of the androgen receptor becomes particularly important. Although FKBP51 represses the activity of GR and PR, it enhances the transcriptional activity of AR (325, 446). In fact, FKBP51 promotes the recruitment of the co-chaperone p23 to the HSP90 complex and thereby facilitates the expression of AR target genes, resulting in cell growth (456). Furthermore, FKBP51 itself displays a target gene of the androgen receptor, forming a short positive feedback loop (457). Based on this, FKBP51 stimulates tumor progression in prostate cancer which reveals FKBP51 as additional target beside common treatment strategies such as irradiation and chemotherapy (446, 456, 458). In line with FKBP51 as cancer target, studies reported a FKBP51-mediated resistance towards chemotherapeutics such as taxanes in ovarian cancer cells (352, 450, 453). Furthermore, silencing FKBP51 in those cells increased the sensitivity and efficiency of paclitaxel as cytostatic (459). These insights highlight a promising treatment strategy of targeting FKBP51 in paclitaxel-treated ovarian and prostate cancer patients with CIPN, enabling both an efficient cancer treatment and a reduction of CIPN.

Beside prostate and ovarian cancer, studies identified FKBP51 as a beneficial target in melanoma and lymphoblastic leukemia cancers based on other underlying mechanisms. Those studies identified that irradiating or chemically treating these cancer types, increased the activation of the NF- $\kappa$ B signaling pathway, while FKBP51 is overexpressed (446). However, counteracting the FKBP51 overexpression in turn reduced the activation of the NF- $\kappa$ B signaling and thereby increased their sensitivity towards irradiation and chemical treatment (355, 357, 364, 451, 460). Furthermore, a study revealed that silencing FKBP51 in melanomas reduced their growth, metastasis, and angiogenesis in a xenograft model (356). Another cancer type, in which the NF- $\kappa$ B signaling plays an essential role, is the ulcerative colitis-associated colorectal cancer as it is developed from a chronic inflammatory state (461). Based on this and in line with data from other NF- $\kappa$ B-related cancers, FKBP51 was postulated as biomarker for the development of colorectal cancer to predict the survival rate of patients (462). Thereby, an increased FKBP51 expression worsens the prognosis of patients (462). In summary, targeting FKBP51 seems to contribute to an efficient cancer treatment in NF- $\kappa$ B signaling related cancer types.



---

In contrast, FKBP51 was shown to play an essential role in breast cancer patients. Breast cancer patients show decreased FKBP51 levels in tumor tissue and 70% of breast cancer patients have an enhanced estrogen receptor alpha (ER $\alpha$ ) expression and activity (463). Unfortunately, ER $\alpha$  interacts with the HSP90 complex and promotes cell proliferation upon transcriptional activity (464). FKBP52 was shown to enhance the ER $\alpha$ -HSP90 complex stability, whereas FKBP51 does not (454). Moreover, FKBP52 was shown to interact with the breast cancer susceptibility gene 1 (BRCA1) which monoubiquitinates ER $\alpha$  and thereby prevents its proteasomal degradation (454, 465). In addition, the deletion of FKBP51 was shown to increase the stability of ER $\alpha$  (454). Based on these insights, targeting FKBP51 in breast cancer patients with CIPN should be avoided until it is discovered whether targeting FKBP51 with SAFit2 or analogues affects the stability of ER $\alpha$ .

Another cancer type which displays low FKBP51 expression is pancreatic cancer (453). In this cancer type, FKBP51 expression was related to a decreased tumor progression, since FKBP51 represses the proliferation-related AKT pathway (466). However, AKT has different isoforms, whereas only AKT1 is related to the regulation of cell cycle and proliferation (340). Furthermore, it has been proven that SAFit2 and its analogues do not interfere in the FKBP51-mediated repression of AKT1 as SAFit2 binds to the binding pocket of FK1 in FKBP51 without sterically impairing its interaction with AKT1 (467). In line with this, targeting FKBP51 pharmacologically with SAFit2 for treating CIPN in AKT1-related cancer types should not enhance AKT-mediated tumor progression.

In summary, all these insights reveal a tissue specificity of FKBP51-mediated effects as its expression varies between tissues as well as the expression of its antagonistic homolog FKBP52 (340, 468). Furthermore, the interaction of FKBP51 with tissue specifically expressed AKT isoforms was controversially discussed in literature (308, 323, 339, 453, 467). Until now, FKBP51 has been proposed to interact with AKT1 and AKT2, but not with AKT3. AKT3 is predominantly expressed in the brain, whereas AKT2 is expressed mainly in muscles and fat, where it regulates glucose homeostasis, and AKT1 has postulated to be widely expressed and to regulate cell proliferation (340). Furthermore, SAFit2 and its analogues have been shown to not interfere in the FKBP51-mediated repression of AKT1, whereas they seem to prevent the FKBP51-mediated repression of AKT2, based on the recent data (340, 424, 467). However, the interaction of FKBP51 with AKT2 in the presence of FKBP51 inhibitors is controversially discussed and has to be investigated in further studies. In conclusion, FKBP51

---

seems to be a promising target in many pathologies such as pain, obesity, diabetes and cancer with FKBP51 overexpression, while targeting FKBP51 could be problematic in disease states like muscle atrophy and breast cancer. Furthermore, unexplored interaction partners of FKBP51 have to be further identified to reduce the risk of side effects.

#### **5.4 SAFit2 as novel treatment option for pathological disorders especially neuropathic pain?**

To date, SAFit2 represents the gold standard for pharmacologically targeting FKBP51 from over 400 other SAFit analogues, as it comprises the best overall profile concerning selectivity, affinity as well as pharmacokinetic and ADME (adsorption-distribution-metabolization-excretion) properties (406). Admittedly, other SAFit analogues showed singly improved parameters, but they did not perform comparably to SAFit2 in multiple parameters (406). SAFit2 comprises a binding affinity around 6 nM towards FKBP51, which is 10,000 times more selective than for its homologue FKBP52, making it a highly specific FKBP51 inhibitor (367). Nevertheless, SAFit2 additionally comprises affinity for FKBP12 and FKBP12.6, which is two times increased and four times lower than for FKBP51, respectively (469). FKBP12 is known to mediate immunosuppression in complex with FK506 through the inhibition of calcineurin (470). However, a study by Gaali et al. identified that SAFit1 does not repress T cell activation and cytokine production at 100 nM *in vitro*, which is a common effect of complexed FKBP12 (367, 471). Nonetheless, SAFit1 shows 10 times less cell permeability than SAFit2 in a Caco2 assay from Eurofins (469). Based on these insights, the influence of SAFit2 on FKBP12-mediated processes should be validated *in vitro*. Furthermore, evaluations of SAFit2-mediated effects should consider an FKBP12 involvement.

Besides the affinity for FKBP12, SAFit2 comprises an appreciable affinity for FKBP12.6. Although less is known about FKBP12.6, it was discussed to interact with the ryanodine receptor type two which is predominantly expressed in cardiac muscles (472). In addition, one study showed that FKBP12.6 dysfunctions can contribute to a disruption in the calcium-induced calcium release (CICR) system *in situ* (473, 474). The CICR system facilitates regular heart contractions, implicating that CICR system disruptions could lead to disruptions in calcium waves and arrhythmias (474). In contrast, an *in vivo* study showed that FKBP12.6 deficient mice did not develop any arrhythmias (475). However, chronic stress was shown to induce angiogenic behavior in mice and to destabilize the binding of FKBP12.6 to ryanodine

---

receptor type two. This behavioral outcome could be prevented by the treatment with a tool compound, which stabilizes the interaction of FKBP12.6 and the ryanodine receptor (476). In summary, previous findings highlight a possible risk of SAFit2 treatment, since its impact on FKBP12.6 and FKBP12.6 interactions is not elucidated yet. Nevertheless, focusing on the cardiovascular impact, a cardiac toxicity test revealed that SAFit2 only marginally affects QT prolongation *in vitro*. In addition, only exceedingly high concentrations of SAFit2 around 10  $\mu$ M, which are not reached *in vivo*, induced a tail current inhibition of 21.4% (406). Based on these insights and numerous *in vivo* studies, which also include chronic SAFit2 treatments, no SAFit2-mediated toxicity was reported (424, 477-484). However, for a further drug development, formal toxicity studies have to be performed.

In addition to SAFit2 specific targets, a broad screen, including 45 CNS-relevant drug targets, was performed to identify potential off-targets of SAFit2. The sigma two receptor was revealed as first off-target with an inhibitory constant of 226 nM (406). Sigma receptors are predominantly expressed in neuronal tissue and comprise remarkably similar binding pockets (485). Although their particular function is not discovered in detail yet, they display promising targets for the treatment of neurodegenerative disorders (486, 487). Furthermore, antagonists for both sigma receptors, one and two, are currently under investigation in clinical or preclinical studies (486). Based on this, inhibiting the sigma two receptor with SAFit2 seems not to raise any safety issues, but rather extend treatment possibilities for SAFit2. Secondly, the histamine receptor four was identified as off-target of SAFit2 with a low inhibition constant ( $K_i$ ) of 3382 nM (406). The histamine receptor four is a GPCR that comprises a high affinity for histamine and was shown to mediate chemotaxis and migration in eosinophils and dendritic cells (488, 489). Moreover, the histamine receptor four is suggested as target for many allergy-driven diseases like asthma and pruritus but also for chronic pulmonary diseases, dermatitis and psoriasis (489). In conclusion, both off-targets of SAFit2 have been revealed as targets for other diseases and do not implicate a risk of developing any severe side effects (487, 490).

Another essential off-target and inhibitory function of SAFit2 is the inhibition of the CYP3A4, inhibiting already 58.1% of CYP3A4 at 1  $\mu$ M (406). The CYP3A4 is the most abundant CYP enzyme with building up one third of the CYP enzymes in the liver. Likewise, CYP3A4 displays the most clinically relevant drug metabolizing enzyme (491). The inhibition of CYP3A4 reduces the metabolism and clearance of numerous drugs which leads either rapidly to

---

toxicity and overdosing or to an impaired efficiency of prodrugs (492). Therefore, the co-administration of SAFit2 with any other drug may lead to pharmacokinetic interactions due to the strong inhibitory effect of SAFit2 on CYP3A4. Regarding the treatment of paclitaxel-induced neuropathic pain, it has to be taken into account that paclitaxel itself comprises cell and neurotoxic properties that could be enhanced by co-treating with SAFit2, since paclitaxel is partially metabolized via the CYP3A4 (493). Based on this, a reduction of CYP3A4 inhibition should be achieved for further optimized clinical lead compounds. Associated to drug metabolism, it is yet unexplored how SAFit2 is metabolized and whether SAFit2 metabolites might have toxic properties (406). However, referring to the previously discussed SAFit2 toxicity, SAFit2 metabolites are suggested to be non-toxic, since chronic treatment with SAFit2 over 30 days and very high doses of 100 mg/kg (unpublished data) did not reveal evidence for any toxicity (406, 424). Nevertheless, the maximal tolerated dosage of SAFit2 is unknown.

Beside metabolism and toxicity, the distribution of SAFit2 was elucidated in pharmacokinetic studies which comprised different formulations and dosages of SAFit2 (367, 371). These revealed a half-life time of SAFit2 of around nine hours in plasma levels and a high volume of distribution with standard formulation (367, 406). A high volume of distribution describes the property of a drug to enter extravascular compartments, meaning that a higher dose is required to achieve high plasma levels (494). In line with this, a moderate brain permeability of SAFit2 was discovered (367). However, SAFit2 concentrations in other tissues such as muscles and fat remain unknown and should be investigated in the future based on the high distribution volume of SAFit2. Nevertheless, a study could show that treating animals with 20 mg/kg two times daily resulted in stable plasma levels between 1500-2000 ng/ml (424). However, to gain stable plasma concentrations repetitive injections of SAFit2 are still necessary, since it is not orally administrable until now (406). Based on this, the bioavailability of future analogues and lead compounds should be improved.

Independent from the improvable pharmacological profile of SAFit2, it has been shown to readjust the balance between FKBP51 and FKBP52 in a neuronal cell line and in primary hippocampal neurons, leading to an enhanced neurite outgrowth (367, 476, 478). Interestingly, FKBP51-deficient neurons did not show an enhanced neurite outgrowth, indicating that especially the balance between FKBP51 and FKBP52 facilitates this mechanism in neurons (476). In line with this, various studies identified FKBP51 and

---

especially FKBP51 dysregulations, which can be either induced by chronic stress or caused by SNPs, as driver of several disorders (329, 335, 336, 363, 466, 495). However, SAFit2 has been shown to successfully address these dysregulations, since SAFit2 readjusted and enhanced the glucocorticoid receptor sensitivity to enable a negative feedback loop towards the HPA axis and thereby reduced corticosterone levels at peak times of secretion (476).

Associated to these counteracting properties of SAFit2, administration of SAFit2 has been shown to prevent stress-induced behavior such as social avoidance and anxiety like behavior in mice and rats (477, 496). These behaviors are highly predominant in psychiatric disorders that are stress induced like depression, post-traumatic stress disorder, and schizophrenia (477, 497, 498). Beside this anxiety like behaviors, SAFit2 was shown to reduce stress-related alcohol consumption and preference in rodents (481, 499). Furthermore, SAFit2 has been shown to limit cocaine re-abuse in male rats, indicating SAFit2 as approach for treating substance abuse disorders (500). This property might also be beneficial in the context of pain, since opioids are less used for pain treatments due to the high risk of abuses, although they are efficiently analgesic (297, 501).

In the context of cancer, SAFit2 was additionally shown to improve cancer treatments as it counteracts the pathological outcomes of FKBP51 overexpression in several cancer types (406, 502). Likewise, overexpression of FKBP51 was shown to enhance proliferation, mediate irradiation and chemotherapy resistance and very recently to protect tumors from their immune environment (354, 446, 503-505). In line with this, SAFit2 was shown to counteract immune evasion of glioblastomas by reducing the expression of programmed cell death ligand-1 (PD-L1) (482). Based on this, SAFit2 reduced tumor growth and activated apoptosis in glioblastomas *in vitro* as well as in a glioblastoma xenograft model *in vivo* (482), revealing SAFit2 as beneficial treatment in the management of cancer. In summary, SAFit2 seems to be a very promising drug precursor for the treatment of many diseases such as stress-related disorders, psychiatric disorders, substance abuse and cancer.

In comparison to first-line treatments for neuropathic pain such as amitriptyline and pregabalin, SAFit2 comprises a broad spectrum of neuroinflammatory effects. Moreover, SAFit2 mediates a quite efficient pain relief in nerve injury-induced and paclitaxel-induced neuropathic pain in mice, whereas human data is not existing yet (370, 371). In contrast, amitriptyline achieved no pain relief in chemotherapy-induced neuropathic pain states in

---

humans (506). Nevertheless, amitriptyline revealed overall a relatively low NNT (number needed to treat) around three to four, indicating that three patients have to be treated with amitriptyline to gain a 50% pain relief (507). However, the distinct mechanism of action of amitriptyline is relatively unknown, since the antidepressant drug is used off-label. Likewise, amitriptyline is not suggested to relieve pain via its unselective serotonin and noradrenalin reuptake inhibiting function, but rather through off-target effects including the inhibition of voltage-dependent sodium channels and the activation of potassium channels. Furthermore, amitriptyline comprises several other interaction partners like muscarinic, histaminergic and dopaminergic receptors, indicating a high unspecificity of amitriptyline (492). In contrast, pregabalin was developed as voltage-dependent calcium channel blocker for the treatment of neuropathic pain, inhibiting the release of neurotransmitters like glutamate, noradrenalin, and substance P (508). However, pregabalin comprises a NNT around seven to eight, besides several side effects like amitriptyline as well and an increasing risk of abuses (507, 509, 510). Based on this, even recommended first-line treatments for neuropathic pain display either a lack of specificity or a low efficacy and comprise a lot of severe side effects. Hence, SAFit2 displays promising properties as drug precursor for neuropathic pain, although it has to be further optimized in pharmacological parameters for a clinical usage.

## 5.5 Future perspectives and conclusion

Beside the beneficial effects of SAFit2 in psychiatric disorders, substance abuse, cancer and neuropathic pain, the influence of SAFit2 or analogues has not been investigated in neurological disorders such as Parkinson disease and Alzheimer disease (352, 363, 437, 511). However, those diseases have been associated with FKBP51 and FKBP5 in general, highlighting further approaches of targeting FKBP51 with either SAFit2 or future improved analogues. Furthermore, SAFit2 efficiently restored glucocorticoid sensitivity *in vivo*, indicating SAFit2 as potential co-treatment for glucocorticoids to prevent the development of a glucocorticoid resistance (353, 476). Glucocorticoids are given in various diverging inflammatory diseases such as multiple sclerosis, rheumatoid arthritis or asthma (512). Notably, the inflammatory component of respective diseases points out another treatment option for SAFit2, since increased FKBP51 levels have been shown to activate the NF- $\kappa$ B signaling pathway, leading to the expression of numerous pro-inflammatory cytokines (308, 353). However, SAFit2 was shown to counteract this enhanced activity and to reduce pro-

---

inflammatory cytokine expression, beside restoring glucocorticoid sensitivity (370). Based on this, SAFit2 might be a potential drug candidate for the treatment of various diseases comprising an inflammatory component independently from their occasion.

Altogether, the involvement of FKBP51 has been identified in numerous diseases. In line with this, the upregulation of FKBP51 was described in different pathological pain forms, especially in neuropathic pain states. Neuropathic pain occurs after nerve lesions and is only barely treatable due to inadequate treatment options, highlighting the need of novel targets and potential drug candidates for neuropathic pain. In this study, it was observed that SAFit2, the recent gold standard for targeting FKBP51, ameliorates nerve injury- and paclitaxel-induced neuropathic pain in mice. Furthermore, it was observed that SAFit2 counteracted neuroinflammation in both mouse models and increased pro-resolving lipid mediator levels in peripheral nervous tissue. In summary, targeting FKBP51 with SAFit2 or future improved analogues seems to be a promising approach for efficiently relieving neuropathic pain after nerve injury and paclitaxel treatment. Furthermore, the influence of SAFit2 on other neuropathic pain types seems to be promising, but has to be investigated separately, since the underlying mechanisms of different neuropathic pain forms are divergent. However, selectivity, pharmacological profile and bioavailability of SAFit2 have to be further optimized in order to develop a clinical lead compound.

---

## References

---

1. Raja SN, Carr DB, Cohen M, Finnerup NB, Flor H, Gibson S, et al. The revised International Association for the Study of Pain definition of pain: concepts, challenges, and compromises. *Pain*. 2020;161(9):1976-82.
2. Basbaum AI, Bautista DM, Scherrer G, Julius D. Cellular and molecular mechanisms of pain. *Cell*. 2009;139(2):267-84.
3. Scholz J, Woolf CJ. Can we conquer pain? *Nat Neurosci*. 2002;5 Suppl:1062-7.
4. Benarroch EE. CGRP: sensory neuropeptide with multiple neurologic implications. *Neurology*. 2011;77(3):281-7.
5. Chudler EH, Dong WK. The role of the basal ganglia in nociception and pain. *Pain*. 1995;60.
6. Costigan M, Woolf CJ. Pain: molecular mechanisms. *J Pain*. 2000;1(3 Suppl):35-44.
7. Hunt SP, Mantyh PW. The molecular dynamics of pain control. *Nature Reviews Neuroscience*. 2001;2(2):83-91.
8. Peirs C, Seal RP. Neural circuits for pain: Recent advances and current views. *Science*. 2016;354(6312):578-84.
9. Eduardo EB. Ion channels in nociceptors. *Neurology*. 2015;84(11):1153.
10. Kidd BL, Urban LA. Mechanisms of inflammatory pain. *Br J Anaesth*. 2001;87(1):3-11.
11. Bautista DM, Pellegrino M, Tsunozaki M. TRPA1: A gatekeeper for inflammation. *Annu Rev Physiol*. 2013;75:181-200.
12. Sandkühler J. Models and Mechanisms of Hyperalgesia and Allodynia. *Physiological Reviews*. 2009;89(2):707-58.
13. Woolf CJ, Ma Q. Nociceptors--noxious stimulus detectors. *Neuron*. 2007;55(3):353-64.
14. Bhave G, Gereau RWt. Posttranslational mechanisms of peripheral sensitization. *J Neurobiol*. 2004;61(1):88-106.
15. Ji RR, Xu ZZ, Strichartz G, Serhan CN. Emerging roles of resolvins in the resolution of inflammation and pain. *Trends Neurosci*. 2011;34(11):599-609.
16. Lawrence T, Gilroy DW. Chronic inflammation: a failure of resolution? *Int J Exp Pathol*. 2007;88(2):85-94.
17. Gold MS, Gebhart GF. Nociceptor sensitization in pain pathogenesis. *Nat Med*. 2010;16(11):1248-57.
18. Kuner R. Central mechanisms of pathological pain. *Nat Med*. 2010;16(11):1258-66.



- 
19. Venkatachalam K, Montell C. TRP channels. *Annu Rev Biochem.* 2007;76:387-417.
  20. Julius D. TRP channels and pain. *Annu Rev Cell Dev Biol.* 2013;29:355-84.
  21. Long-Jun W, Tara-Beth S, David EC. International Union of Basic and Clinical Pharmacology. LXXVI. Current Progress in the Mammalian TRP Ion Channel Family. *Pharmacological Reviews.* 2010;62(3):381.
  22. Chung MK, Jung SJ, Oh SB. Role of TRP channels in pain sensation. *Adv Exp Med Biol.* 2011;704:615-36.
  23. Benemei S, Patacchini R, Trevisani M, Geppetti P. TRP channels. *Curr Opin Pharmacol.* 2015;22:18-23.
  24. Moore C, Gupta R, Jordt SE, Chen Y, Liedtke WB. Regulation of Pain and Itch by TRP Channels. *Neurosci Bull.* 2018;34(1):120-42.
  25. Owsianik G, Talavera K, Voets T, Nilius B. Permeation and selectivity of TRP channels. *Annu Rev Physiol.* 2006;68:685-717.
  26. Gees M, Owsianik G, Nilius B, Voets T. TRP channels. *Compr Physiol.* 2012;2(1):563-608.
  27. Mickle AD, Shepherd AJ, Mohapatra DP. Sensory TRP channels: the key transducers of nociception and pain. *Prog Mol Biol Transl Sci.* 2015;131:73-118.
  28. Moran MM. TRP Channels as Potential Drug Targets. *Annu Rev Pharmacol Toxicol.* 2018;58:309-30.
  29. McKemy DD, Neuhauser WM, Julius D. Identification of a cold receptor reveals a general role for TRP channels in thermosensation. *Nature.* 2002;416(6876):52-8.
  30. Peier AM, Moqrich A, Hergarden AC, Reeve AJ, Andersson DA, Story GM, et al. A TRP channel that senses cold stimuli and menthol. *Cell.* 2002;108(5):705-15.
  31. Mickle AD, Shepherd AJ, Mohapatra DP. Chapter Four - Sensory TRP Channels: The Key Transducers of Nociception and Pain. In: Price TJ, Dussor G, editors. *Progress in Molecular Biology and Translational Science.* 131: Academic Press; 2015. p. 73-118.
  32. Cortright DN, Szallasi A. TRP Channels and Pain. *Current Pharmaceutical Design.* 2009;15.
  33. Tominaga M, Caterina MJ, Malmberg AB, Rosen TA, Gilbert H, Skinner K, et al. The Cloned Capsaicin Receptor Integrates Multiple Pain-Producing Stimuli. *Neuron.* 1998;21(3):531-43.
  34. Ma Q-P. Expression of capsaicin receptor (VR1) by myelinated primary afferent neurons in rats. *Neuroscience Letters.* 2002;319(2):87-90.
  35. Funakoshi K, Nakano M, Atobe Y, Goris RC, Kadota T, Yazama F. Differential development of TRPV1-expressing sensory nerves in peripheral organs. *Cell Tissue Res.* 2006;323(1):27-41.
  36. Spicarova D, Palecek J. The role of spinal cord vanilloid (TRPV1) receptors in pain modulation. *Physiol Res.* 2008;57 Suppl 3:S69-S77.

37. Cavanaugh DJ, Chesler AT, Jackson AC, Sigal YM, Yamanaka H, Grant R, et al. Trpv1 reporter mice reveal highly restricted brain distribution and functional expression in arteriolar smooth muscle cells. *J Neurosci*. 2011;31(13):5067-77.
38. Tominaga M, Tominaga T. Structure and function of TRPV1. *Pflugers Arch*. 2005;451(1):143-50.
39. Vennekens R, Owsianik G, Nilius B. Vanilloid Transient Receptor Potential Cation Channels: An Overview. *Current Pharmaceutical Design*. 2008;14.
40. Brito R, Sheth S, Mukherjea D, Rybak LP, Ramkumar V. TRPV1: A Potential Drug Target for Treating Various Diseases. *Cells*. 2014;3(2):517-45.
41. Benitez-Angeles M, Morales-Lazaro SL, Juarez-Gonzalez E, Rosenbaum T. TRPV1: Structure, Endogenous Agonists, and Mechanisms. *Int J Mol Sci*. 2020;21(10).
42. J. Iadarola M, J. Mannes A. The Vanilloid Agonist Resiniferatoxin for Interventional-Based Pain Control. *Current Topics in Medicinal Chemistry*. 2011;11(17):2171-9.
43. De Petrocellis L, Di Marzo V. Lipids as regulators of the activity of transient receptor potential type V1 (TRPV1) channels. *Life Sciences*. 2005;77(14):1651-66.
44. Suh Y-G, Oh U. Activation and Activators of TRPV1 and Their Pharmaceutical Implication. *Current Pharmaceutical Design*. 2005;11(21):2687-98.
45. Szallasi A, Cortright DN, Blum CA, Eid SR. The vanilloid receptor TRPV1: 10 years from channel cloning to antagonist proof-of-concept. *Nat Rev Drug Discov*. 2007;6(5):357-72.
46. Mantyh PW, Clohisy DR, Koltzenburg M, Hunt SP. Molecular mechanisms of cancer pain. *Nat Rev Cancer*. 2002;2(3):201-9.
47. Touska F, Marsakova L, Teisinger J, Vlachova V. A "Cute" Desensitization of TRPV1. *Current Pharmaceutical Biotechnology*. 2011;12(1):122-9.
48. Yao X, Kwan HY, Huang Y. Regulation of TRP channels by phosphorylation. *Neurosignals*. 2005;14(6):273-80.
49. Jung J, Shin JS, Lee SY, Hwang SW, Koo J, Cho H, et al. Phosphorylation of vanilloid receptor 1 by Ca<sup>2+</sup>/calmodulin-dependent kinase II regulates its vanilloid binding. *J Biol Chem*. 2004;279(8):7048-54.
50. Ji R-R, Samad TA, Jin S-X, Schmoll R, Woolf CJ. p38 MAPK Activation by NGF in Primary Sensory Neurons after Inflammation Increases TRPV1 Levels and Maintains Heat Hyperalgesia. *Neuron*. 2002;36(1):57-68.
51. Zhang X, Huang J, McNaughton PA. NGF rapidly increases membrane expression of TRPV1 heat-gated ion channels. *EMBO J*. 2005;24(24):4211-23.
52. Geppetti P, Capone JG, Trevisani M, Nicoletti P, Zagli G, Tola MR. CGRP and migraine: neurogenic inflammation revisited. *J Headache Pain*. 2005;6(2):61-70.

- 
53. Mohapatra DP, Nau C. Regulation of Ca<sup>2+</sup>-dependent desensitization in the vanilloid receptor TRPV1 by calcineurin and cAMP-dependent protein kinase. *J Biol Chem.* 2005;280(14):13424-32.
  54. Wang H, Woolf CJ. Pain TRPs. *Neuron.* 2005;46(1):9-12.
  55. Por Elaine D, Samelson Bret K, Belugin S, Akopian Armen N, Scott John D, Jeske Nathaniel A. PP2B/calcineurin-mediated desensitization of TRPV1 does not require AKAP150. *Biochemical Journal.* 2010;432(3):549-56.
  56. Szallasi A, Sheta M. Targeting TRPV1 for pain relief: limits, losers and laurels. *Expert Opinion on Investigational Drugs.* 2012;21(9):1351-69.
  57. Jara-Oseguera A, Simon SA, Rosenbaum T. TRPV1: On the Road to Pain Relief. *Current Molecular Pharmacology.* 2008;1(3):255-69.
  58. Khairatkar-Joshi N, Szallasi A. TRPV1 antagonists: the challenges for therapeutic targeting. *Trends Mol Med.* 2009;15(1):14-22.
  59. Gunthorpe MJ, Chizh BA. Clinical development of TRPV1 antagonists: targeting a pivotal point in the pain pathway. *Drug Discov Today.* 2009;14(1-2):56-67.
  60. Iftinca M, Defaye M, Altier C. TRPV1-Targeted Drugs in Development for Human Pain Conditions. *Drugs.* 2021;81(1):7-27.
  61. Immke DC, Gavva NR. The TRPV1 receptor and nociception. *Semin Cell Dev Biol.* 2006;17(5):582-91.
  62. Koivisto AP, Belvisi MG, Gaudet R, Szallasi A. Advances in TRP channel drug discovery: from target validation to clinical studies. *Nat Rev Drug Discov.* 2021.
  63. Meents JE, Ciotu CI, Fischer MJM. TRPA1: a molecular view. *J Neurophysiol.* 2019;121(2):427-43.
  64. Barabas ME, Kossyrev EA, Stucky CL. TRPA1 is functionally expressed primarily by IB4-binding, non-peptidergic mouse and rat sensory neurons. *PLoS One.* 2012;7(10):e47988.
  65. Zygmunt PM, Högestätt ED. TRPA1. In: Nilius B, Flockerzi V, editors. *Mammalian Transient Receptor Potential (TRP) Cation Channels: Volume I.* Berlin, Heidelberg: Springer Berlin Heidelberg; 2014. p. 583-630.
  66. Karashima Y, Talavera K, Everaerts W, Janssens A, Kwan KY, Vennekens R, et al. TRPA1 acts as a cold sensor in vitro and in vivo. *Proceedings of the National Academy of Sciences.* 2009;106(4):1273-8.
  67. Nilius B, Prenen J, Owsianik G. Irritating channels: the case of TRPA1. *J Physiol.* 2011;589(Pt 7):1543-9.
  68. Ramsey IS, Delling M, Clapham DE. An introduction to TRP channels. *Annu Rev Physiol.* 2006;68:619-47.

- 
69. Materazzi S, Nassini R, Andrè E, Campi B, Amadesi S, Trevisani M, et al. Cox-dependent fatty acid metabolites cause pain through activation of the irritant receptor TRPA1. *Proceedings of the National Academy of Sciences*. 2008;105(33):12045-50.
  70. Souza Monteiro de Araujo D, Nassini R, Geppetti P, De Logu F. TRPA1 as a therapeutic target for nociceptive pain. *Expert Opin Ther Targets*. 2020;24(10):997-1008.
  71. Mukaiyama M, Usui T, Nagumo Y. Non-electrophilic TRPA1 agonists, menthol, carvacrol and clotrimazole, open epithelial tight junctions via TRPA1 activation. *J Biochem*. 2020;168(4):407-15.
  72. Kaneko Y, Szallasi A. Transient receptor potential (TRP) channels: a clinical perspective. *Br J Pharmacol*. 2014;171(10):2474-507.
  73. Chen J, Hackos DH. TRPA1 as a drug target--promise and challenges. *Naunyn Schmiedebergs Arch Pharmacol*. 2015;388(4):451-63.
  74. Garrison SR, Stucky CL. The dynamic TRPA1 channel: a suitable pharmacological pain target? *Curr Pharm Biotechnol*. 2011;12(10):1689-97.
  75. Woolf CJ, Salter MW. Neuronal Plasticity: Increasing the Gain in Pain. *Science's Compass*. 2000.
  76. Iyengar S, Ossipov MH, Johnson KW. The role of calcitonin gene-related peptide in peripheral and central pain mechanisms including migraine. *Pain*. 2017;158(4):543-59.
  77. Fabbretti E. ATP P2X3 receptors and neuronal sensitization. *Front Cell Neurosci*. 2013;7:236.
  78. Boddeke EW. Involvement of chemokines in pain. *Eur J Pharmacol*. 2001;429(1-3):115-9.
  79. Ji R-R, Strichartz G. Cell Signaling and the Genesis of Neuropathic Pain. *Science's STKE*. 2004;2004(252):re14-re.
  80. Salzer I, Ray S, Schicker K, Boehm S. Nociceptor Signalling through ion Channel Regulation via GPCRs. *Int J Mol Sci*. 2019;20(10).
  81. Cervero F, Laird JM, Garcia-Nicas E. Secondary hyperalgesia and presynaptic inhibition: an update. *Eur J Pain*. 2003;7(4):345-51.
  82. Ji RR, Kohno T, Moore KA, Woolf CJ. Central sensitization and LTP: do pain and memory share similar mechanisms? *Trends Neurosci*. 2003;26(12):696-705.
  83. Woolf CJ. Pain amplification-A perspective on the how, why, when, and where of central sensitization. *Journal of Applied Biobehavioral Research*. 2018;23(2).
  84. Seybold VS. The Role of Peptides in Central Sensitization. In: Canning BJ, Spina D, editors. *Sensory Nerves*. Berlin, Heidelberg: Springer Berlin Heidelberg; 2009. p. 451-91.
  85. Tao YX. AMPA receptor trafficking in inflammation-induced dorsal horn central sensitization. *Neurosci Bull*. 2012;28(2):111-20.

- 
86. Schaible HG, Ebersberger A, Von Banchet GS. Mechanisms of pain in arthritis. *Ann N Y Acad Sci.* 2002;966:343-54.
  87. Eide PK. Wind-up and the NMDA receptor complex from a clinical perspective. *Eur J Pain.* 2000;4(1):5-15.
  88. Vergne-Salle P, Bertin P. Chronic pain and neuroinflammation. *Joint Bone Spine.* 2021;88(6).
  89. Latremoliere A, Woolf CJ. Central sensitization: a generator of pain hypersensitivity by central neural plasticity. *J Pain.* 2009;10(9):895-926.
  90. Ji RR, Nackley A, Huh Y, Terrando N, Maixner W. Neuroinflammation and Central Sensitization in Chronic and Widespread Pain. *Anesthesiology.* 2018;129(2):343-66.
  91. Chiang CY, Li Z, Dostrovsky JO, Sessle BJ. Central sensitization in medullary dorsal horn involves gap junctions and hemichannels. *Neuroreport.* 2010;21(3):233-7.
  92. Osthues T, Sisignano M. Oxidized Lipids in Persistent Pain States. *Front Pharmacol.* 2019;10:1147.
  93. San Martin VP, Sazo A, Utreras E, Moraga-Cid G, Yevenes GE. Glycine Receptor Subtypes and Their Roles in Nociception and Chronic Pain. *Front Mol Neurosci.* 2022;15:848642.
  94. Fahy E, Cotter D, Sud M, Subramaniam S. Lipid classification, structures and tools. *Biochimica et Biophysica Acta (BBA) - Molecular and Cell Biology of Lipids.* 2011;1811(11):637-47.
  95. Serhan CN, Chiang N, Dalli J, Levy BD. Lipid mediators in the resolution of inflammation. *Cold Spring Harb Perspect Biol.* 2014;7(2):a016311.
  96. van Meer G, Voelker DR, Feigenson GW. Membrane lipids: where they are and how they behave. *Nat Rev Mol Cell Biol.* 2008;9(2):112-24.
  97. Chiurchiu V, Leuti A, Maccarrone M. Bioactive Lipids and Chronic Inflammation: Managing the Fire Within. *Front Immunol.* 2018;9:38.
  98. Piomelli D, Sasso O. Peripheral gating of pain signals by endogenous lipid mediators. *Nat Neurosci.* 2014;17(2):164-74.
  99. Barber CN, Raben DM. Lipid Metabolism Crosstalk in the Brain: Glia and Neurons. *Front Cell Neurosci.* 2019;13:212.
  100. Park KA, Vasko MR. Lipid mediators of sensitivity in sensory neurons. *Trends Pharmacol Sci.* 2005;26(11):571-7.
  101. Malan TP, Jr., Porreca F. Lipid mediators regulating pain sensitivity. *Prostaglandins Other Lipid Mediat.* 2005;77(1-4):123-30.
  102. Ciardo MG, Ferrer-Montiel A. Lipids as central modulators of sensory TRP channels. *Biochim Biophys Acta Biomembr.* 2017;1859(9 Pt B):1615-28.

- 
103. Sisignano M, Lotsch J, Parnham MJ, Geisslinger G. Potential biomarkers for persistent and neuropathic pain therapy. *Pharmacol Ther.* 2019;199:16-29.
  104. Langeslag M, Kress M. The ceramide-S1P pathway as a druggable target to alleviate peripheral neuropathic pain. *Expert Opin Ther Targets.* 2020;24(9):869-84.
  105. Kolesnick R. The therapeutic potential of modulating the ceramide/sphingomyelin pathway. *J Clin Invest.* 2002;110(1):3-8.
  106. Kitatani K, Idkowiak-Baldys J, Hannun YA. The sphingolipid salvage pathway in ceramide metabolism and signaling. *Cell Signal.* 2008;20(6):1010-8.
  107. Salvemini D, Doyle T, Kress M, Nicol G. Therapeutic targeting of the ceramide-to-sphingosine 1-phosphate pathway in pain. *Trends Pharmacol Sci.* 2013;34(2):110-8.
  108. Doolen S, Iannitti T, Donahue RR, Shaw BC, Grachen CM, Taylor BK. Fingolimod reduces neuropathic pain behaviors in a mouse model of multiple sclerosis by a sphingosine-1 phosphate receptor 1-dependent inhibition of central sensitization in the dorsal horn. *Pain.* 2018;159(2):224-38.
  109. Welch SP, Sim-Selley LJ, Selley DE. Sphingosine-1-phosphate receptors as emerging targets for treatment of pain. *Biochem Pharmacol.* 2012;84(12):1551-62.
  110. Stockstill K, Doyle TM, Yan X, Chen Z, Janes K, Little JW, et al. Dysregulation of sphingolipid metabolism contributes to bortezomib-induced neuropathic pain. *J Exp Med.* 2018;215(5):1301-13.
  111. Calder PC. Polyunsaturated fatty acids and inflammation. *Prostaglandins Leukot Essent Fatty Acids.* 2006;75(3):197-202.
  112. Bazinet RP, Laye S. Polyunsaturated fatty acids and their metabolites in brain function and disease. *Nat Rev Neurosci.* 2014;15(12):771-85.
  113. Galan-Arriero I, Serrano-Munoz D, Gomez-Soriano J, Goicoechea C, Taylor J, Velasco A, et al. The role of Omega-3 and Omega-9 fatty acids for the treatment of neuropathic pain after neurotrauma. *Biochim Biophys Acta Biomembr.* 2017;1859(9 Pt B):1629-35.
  114. Yehuda S, Rabinovitz S, L. Carasso R, I. Mostofsky D. The role of polyunsaturated fatty acids in restoring the aging neuronal membrane. *Neurobiology of Aging.* 2002;23(5):843-53.
  115. Vasquez AM, Mouchlis VD, Dennis EA. Review of four major distinct types of human phospholipase A2. *Advances in Biological Regulation.* 2018;67:212-8.
  116. Sun GY, Xu J, Jensen MD, Simonyi A. Phospholipase A2 in the central nervous system: implications for neurodegenerative diseases. *J Lipid Res.* 2004;45(2):205-13.
  117. Peng Z, Chang Y, Fan J, Ji W, Su C. Phospholipase A2 superfamily in cancer. *Cancer Letters.* 2021;497:165-77.
  118. Leslie CC. Cytosolic phospholipase A(2): physiological function and role in disease. *J Lipid Res.* 2015;56(8):1386-402.

119. Niknami M, Patel M, Witting PK, Dong Q. Molecules in focus: cytosolic phospholipase A2-alpha. *Int J Biochem Cell Biol.* 2009;41(5):994-7.
120. Sun GY, Geng X, Teng T, Yang B, Appenteng MK, Greenlief CM, et al. Dynamic Role of Phospholipases A2 in Health and Diseases in the Central Nervous System. *Cells.* 2021;10(11).
121. Hasegawa S, Kohro Y, Tsuda M, Inoue K. Activation of cytosolic phospholipase A2 in dorsal root ganglion neurons by Ca<sup>2+</sup>/calmodulin-dependent protein kinase II after peripheral nerve injury. *Mol Pain.* 2009;5:22.
122. Gijón MA, Leslie CC. Regulation of arachidonic acid release and cytosolic Phospholipase A2 activation. *Journal of Leukocyte Biology.* 1999;65(3):330-6.
123. Burke JE, Dennis EA. Phospholipase A2 structure/function, mechanism, and signaling. *J Lipid Res.* 2009;50 Suppl:S237-42.
124. Richard D, Kefi K, Barbe U, Bausero P, Visioli F. Polyunsaturated fatty acids as antioxidants. *Pharmacol Res.* 2008;57(6):451-5.
125. Spector AA. Arachidonic acid cytochrome P450 epoxygenase pathway. *J Lipid Res.* 2009;50 Suppl(Suppl):S52-6.
126. Motter AL, Ahern GP. TRPA1 is a polyunsaturated fatty acid sensor in mammals. *PLoS One.* 2012;7(6):e38439.
127. Andreou A, Feussner I. Lipoxygenases - Structure and reaction mechanism. *Phytochemistry.* 2009;70(13-14):1504-10.
128. van der Donk WA, Tsai A-L, Kulmacz RJ. The Cyclooxygenase Reaction Mechanism. *Biochemistry.* 2002;41(52):15451-8.
129. Shi Z, He Z, Wang DW. CYP450 Epoxygenase Metabolites, Epoxyeicosatrienoic Acids, as Novel Anti-Inflammatory Mediators. *Molecules.* 2022;27(12).
130. Chandrasekharan NV, Simmons DL. The cyclooxygenases. *Genome Biology.* 2004;5(9):241.
131. Rouzer CA, Marnett LJ. Cyclooxygenases: structural and functional insights. *J Lipid Res.* 2009;50 Suppl(Suppl):S29-34.
132. Prigge ST, Boyington JC, Faig M, Doctor KS, Gaffney BJ, Amzel LM. Structure and mechanism of lipoxygenases. *Biochimie.* 1997;79(11):629-36.
133. Powell WS, Rokach J. Biosynthesis, biological effects, and receptors of hydroxyeicosatetraenoic acids (HETEs) and oxoeicosatetraenoic acids (oxo-ETEs) derived from arachidonic acid. *Biochim Biophys Acta.* 2015;1851(4):340-55.
134. Trostchansky A, Wood I, Rubbo H. Regulation of arachidonic acid oxidation and metabolism by lipid electrophiles. *Prostaglandins & Other Lipid Mediators.* 2021;152:106482.
135. Dennis EA, Norris PC. Eicosanoid storm in infection and inflammation. *Nat Rev Immunol.* 2015;15(8):511-23.

- 
136. Abdulkhaleq LA, Assi MA, Abdullah R, Zamri-Saad M, Taufiq-Yap YH, Hezmee MNM. The crucial roles of inflammatory mediators in inflammation: A review. *Vet World*. 2018;11(5):627-35.
  137. Yagami T, Koma H, Yamamoto Y. Pathophysiological Roles of Cyclooxygenases and Prostaglandins in the Central Nervous System. *Mol Neurobiol*. 2016;53(7):4754-71.
  138. DiNicolantonio JJ, O'Keefe JH. Importance of maintaining a low omega-6/omega-3 ratio for reducing inflammation. *Open Heart*. 2018;5(2):e000946.
  139. Gupta A, Bah M. NSAIDs in the Treatment of Postoperative Pain. *Curr Pain Headache Rep*. 2016;20(11):62.
  140. Jo-Watanabe A, Okuno T, Yokomizo T. The Role of Leukotrienes as Potential Therapeutic Targets in Allergic Disorders. *Int J Mol Sci*. 2019;20(14).
  141. Sisignano M, Angioni C, Park CK, Meyer Dos Santos S, Jordan H, Kuzikov M, et al. Targeting CYP2J to reduce paclitaxel-induced peripheral neuropathic pain. *Proc Natl Acad Sci U S A*. 2016;113(44):12544-9.
  142. Hiesinger K, Wagner KM, Hammock BD, Proschak E, Hwang SH. Development of multitarget agents possessing soluble epoxide hydrolase inhibitory activity. *Prostaglandins Other Lipid Mediat*. 2019;140:31-9.
  143. Sisignano M, Bennett DL, Geisslinger G, Scholich K. TRP-channels as key integrators of lipid pathways in nociceptive neurons. *Prog Lipid Res*. 2014;53:93-107.
  144. Kelly S, Chapman RJ, Woodhams S, Sagar DR, Turner J, Burston JJ, et al. Increased function of pronociceptive TRPV1 at the level of the joint in a rat model of osteoarthritis pain. *Ann Rheum Dis*. 2015;74(1):252-9.
  145. Martinez JA, Wertheim BC, Roe DJ, Taljanovic MS, Chow HS, Chew W, et al. Oxylipins as Biomarkers for Aromatase Inhibitor-Induced Arthralgia (AIA) in Breast Cancer Patients. *Metabolites*. 2023;13(3).
  146. Wen H, Ostman J, Bubb KJ, Panayiotou C, Priestley JV, Baker MD, et al. 20-Hydroxyeicosatetraenoic acid (20-HETE) is a novel activator of transient receptor potential vanilloid 1 (TRPV1) channel. *J Biol Chem*. 2012;287(17):13868-76.
  147. Hwang SH, Wagner K, Xu J, Yang J, Li X, Cao Z, et al. Chemical synthesis and biological evaluation of  $\omega$ -hydroxy polyunsaturated fatty acids. *Bioorganic & Medicinal Chemistry Letters*. 2017;27(3):620-5.
  148. Zhang X, El Demerdash N, Falck JR, Munnuri S, Koehler RC, Yang Z-J. The contribution of TRPV1 channel to 20-HETE—Aggravated ischemic neuronal injury. *Prostaglandins & Other Lipid Mediators*. 2018;137:63-8.
  149. Sisignano M, Park CK, Angioni C, Zhang DD, von Hehn C, Cobos EJ, et al. 5,6-EET is released upon neuronal activity and induces mechanical pain hypersensitivity via TRPA1 on central afferent terminals. *J Neurosci*. 2012;32(18):6364-72.



- 
150. Choque B, Catheline D, Rioux V, Legrand P. Linoleic acid: Between doubts and certainties. *Biochimie*. 2014;96:14-21.
  151. Hildreth K, Kodani SD, Hammock BD, Zhao L. Cytochrome P450-derived linoleic acid metabolites EpOMEs and DiHOMEs: a review of recent studies. *J Nutr Biochem*. 2020;86:108484.
  152. Gaschler MM, Stockwell BR. Lipid peroxidation in cell death. *Biochem Biophys Res Commun*. 2017;482(3):419-25.
  153. Wedel S, Osthues T, Zimmer B, Angioni C, Geisslinger G, Sisignano M. Oxidized linoleic acid metabolites maintain mechanical and thermal hypersensitivity during sub-chronic inflammatory pain. *Biochem Pharmacol*. 2022;198:114953.
  154. Patwardhan AM, Akopian AN, Ruparel NB, Diogenes A, Weintraub ST, Uhlson C, et al. Heat generates oxidized linoleic acid metabolites that activate TRPV1 and produce pain in rodents. *J Clin Invest*. 2010;120(5):1617-26.
  155. Alsalem M, Wong A, Millns P, Arya PH, Chan MS, Bennett A, et al. The contribution of the endogenous TRPV1 ligands 9-HODE and 13-HODE to nociceptive processing and their role in peripheral inflammatory pain mechanisms. *Br J Pharmacol*. 2013;168(8):1961-74.
  156. De Petrocellis L, Schiano Moriello A, Imperatore R, Cristino L, Starowicz K, Di Marzo V. A re-evaluation of 9-HODE activity at TRPV1 channels in comparison with anandamide: enantioselectivity and effects at other TRP channels and in sensory neurons. *Br J Pharmacol*. 2012;167(8):1643-51.
  157. Hohmann SW, Angioni C, Tunaru S, Lee S, Woolf CJ, Offermanns S, et al. The G2A receptor (GPR132) contributes to oxaliplatin-induced mechanical pain hypersensitivity. *Sci Rep*. 2017;7(1):446.
  158. Zhang G, Kodani S, Hammock BD. Stabilized epoxygenated fatty acids regulate inflammation, pain, angiogenesis and cancer. *Prog Lipid Res*. 2014;53:108-23.
  159. Zimmer B, Angioni C, Osthues T, Toewe A, Thomas D, Pierre SC, et al. The oxidized linoleic acid metabolite 12,13-DiHOME mediates thermal hyperalgesia during inflammatory pain. *Biochim Biophys Acta Mol Cell Biol Lipids*. 2018;1863(7):669-78.
  160. Green D, Ruparel S, Gao X, Ruparel N, Patil M, Akopian A, et al. Central activation of TRPV1 and TRPA1 by novel endogenous agonists contributes to mechanical allodynia and thermal hyperalgesia after burn injury. *Mol Pain*. 2016;12.
  161. McReynolds C, Hammock B, Morisseau C. Regulatory lipid vicinal diols counteract the biological activity of epoxy fatty acids and can act as biomarkers and mechanisms for disease progression. *Pharmacology & Therapeutics*. 2023:108454.
  162. Gil Á. Polyunsaturated fatty acids and inflammatory diseases. *Biomedicine & Pharmacotherapy*. 2002;56(8):388-96.

- 
163. Kapoor R, Huang Y-S. Gamma Linolenic Acid: An Antiinflammatory Omega-6 Fatty Acid. *Current Pharmaceutical Biotechnology*. 2006;7(6):531-4.
  164. Cambiaggi L, Chakravarty A, Noureddine N, Hersberger M. The Role of alpha-Linolenic Acid and Its Oxylipins in Human Cardiovascular Diseases. *Int J Mol Sci*. 2023;24(7).
  165. Alagawany M, Elnesr SS, Farag MR, Abd El-Hack ME, Khafaga AF, Taha AE, et al. Omega-3 and Omega-6 Fatty Acids in Poultry Nutrition: Effect on Production Performance and Health. *Animals (Basel)*. 2019;9(8).
  166. Pauls SD, Rodway LA, Winter T, Taylor CG, Zahradka P, Aukema HM. Anti-inflammatory effects of  $\alpha$ -linolenic acid in M1-like macrophages are associated with enhanced production of oxylipins from  $\alpha$ -linolenic and linoleic acid. *The Journal of Nutritional Biochemistry*. 2018;57:121-9.
  167. Kumar N, Gupta G, Anilkumar K, Fatima N, Karnati R, Reddy GV, et al. 15-Lipoxygenase metabolites of alpha-linolenic acid, [13-(S)-HPOTrE and 13-(S)-HOTrE], mediate anti-inflammatory effects by inactivating NLRP3 inflammasome. *Sci Rep*. 2016;6:31649.
  168. Shahidi F, Ambigaipalan P. Omega-3 Polyunsaturated Fatty Acids and Their Health Benefits. *Annu Rev Food Sci Technol*. 2018;9:345-81.
  169. Ji RR. Specialized Pro-Resolving Mediators as Resolution Pharmacology for the Control of Pain and Itch. *Annu Rev Pharmacol Toxicol*. 2023;63:273-93.
  170. Crupi R, Cuzzocrea S. Role of EPA in Inflammation: Mechanisms, Effects, and Clinical Relevance. *Biomolecules*. 2022;12(2).
  171. Weylandt KH, Chiu CY, Gomolka B, Waechter SF, Wiedenmann B. Omega-3 fatty acids and their lipid mediators: towards an understanding of resolvin and protectin formation. *Prostaglandins Other Lipid Mediat*. 2012;97(3-4):73-82.
  172. Ko GD, Nowacki NB, Arseneau L, Eitel M, Hum A. Omega-3 Fatty Acids for Neuropathic Pain: Case Series. *The Clinical Journal of Pain*. 2010;26(2).
  173. Seki H, Tani Y, Arita M. Omega-3 PUFA derived anti-inflammatory lipid mediator resolvin E1. *Prostaglandins Other Lipid Mediat*. 2009;89(3-4):126-30.
  174. Serhan CN, Yacoubian S, Yang R. Anti-inflammatory and proresolving lipid mediators. *Annu Rev Pathol*. 2008;3:279-312.
  175. Serhan CN, Chiang N. Endogenous pro-resolving and anti-inflammatory lipid mediators: a new pharmacologic genus. *Br J Pharmacol*. 2008;153 Suppl 1(Suppl 1):S200-15.
  176. Serhan CN, Chiang N, Van Dyke TE. Resolving inflammation: dual anti-inflammatory and pro-resolution lipid mediators. *Nat Rev Immunol*. 2008;8(5):349-61.
  177. Leuti A, Fava M, Pellegrini N, Maccarrone M. Role of Specialized Pro-Resolving Mediators in Neuropathic Pain. *Front Pharmacol*. 2021;12:717993.

- 
178. Wagner K, Vito S, Inceoglu B, Hammock BD. The role of long chain fatty acids and their epoxide metabolites in nociceptive signaling. *Prostaglandins Other Lipid Mediat.* 2014;113-115:2-12.
  179. Duan J, Song Y, Zhang X, Wang C. Effect of omega-3 Polyunsaturated Fatty Acids-Derived Bioactive Lipids on Metabolic Disorders. *Front Physiol.* 2021;12:646491.
  180. Ostermann AI, Willenberg I, Weylandt KH, Schebb NH. Development of an Online-SPE-LC-MS/MS Method for 26 Hydroxylated Polyunsaturated Fatty Acids as Rapid Targeted Metabolomics Approach for the LOX, CYP, and Autoxidation Pathways of the Arachidonic Acid Cascade. *Chromatographia.* 2014;78(5-6):415-28.
  181. Dasilva G, Munoz S, Lois S, Medina I. Non-Targeted LC-MS/MS Assay for Screening Over 100 Lipid Mediators from ARA, EPA, and DHA in Biological Samples Based on Mass Spectral Fragmentations. *Molecules.* 2019;24(12).
  182. Le Faouder P, Baillif V, Spreadbury I, Motta JP, Rousset P, Chene G, et al. LC-MS/MS method for rapid and concomitant quantification of pro-inflammatory and pro-resolving polyunsaturated fatty acid metabolites. *J Chromatogr B Analyt Technol Biomed Life Sci.* 2013;932:123-33.
  183. Dyll SC. Long-chain omega-3 fatty acids and the brain: a review of the independent and shared effects of EPA, DPA and DHA. *Front Aging Neurosci.* 2015;7:52.
  184. An JU, Kim SE, Oh DK. Molecular insights into lipoxygenases for biocatalytic synthesis of diverse lipid mediators. *Prog Lipid Res.* 2021;83:101110.
  185. Kuda O. Bioactive metabolites of docosahexaenoic acid. *Biochimie.* 2017;136:12-20.
  186. Jensen TS, Baron R, Haanpää M, Kalso E, Loeser JD, Rice ASC, et al. A new definition of neuropathic pain. *PAIN.* 2011;152(10).
  187. Costigan M, Scholz J, Woolf CJ. Neuropathic pain: a maladaptive response of the nervous system to damage. *Annu Rev Neurosci.* 2009;32:1-32.
  188. Bannister K, Sachau J, Baron R, Dickenson AH. Neuropathic Pain: Mechanism-Based Therapeutics. *Annu Rev Pharmacol Toxicol.* 2020;60:257-74.
  189. Becher B, Spath S, Goverman J. Cytokine networks in neuroinflammation. *Nature Reviews Immunology.* 2017;17(1):49-59.
  190. Colloca L, Ludman T, Bouhassira D, Baron R, Dickenson AH, Yarnitsky D, et al. Neuropathic pain. *Nat Rev Dis Primers.* 2017;3:17002.
  191. Dworkin RH. An Overview of Neuropathic Pain: Syndromes, Symptoms, Signs, and Several Mechanisms. *The Clinical Journal of Pain.* 2002;18(6).
  192. Baron R, Binder A, Wasner G. Neuropathic pain: diagnosis, pathophysiological mechanisms, and treatment. *The Lancet Neurology.* 2010;9(8):807-19.
  193. Finnerup NB, Kuner R, Jensen TS. Neuropathic Pain: From Mechanisms to Treatment. *Physiol Rev.* 2021;101(1):259-301.

- 
194. Meacham K, Shepherd A, Mohapatra DP, Haroutounian S. Neuropathic Pain: Central vs. Peripheral Mechanisms. *Curr Pain Headache Rep.* 2017;21(6):28.
  195. Talbot S, Foster SL, Woolf CJ. Neuroimmunity: Physiology and Pathology. *Annu Rev Immunol.* 2016;34:421-47.
  196. Ji RR, Xu ZZ, Gao YJ. Emerging targets in neuroinflammation-driven chronic pain. *Nat Rev Drug Discov.* 2014;13(7):533-48.
  197. Sisignano M, Baron R, Scholich K, Geisslinger G. Mechanism-based treatment for chemotherapy-induced peripheral neuropathic pain. *Nat Rev Neurol.* 2014;10(12):694-707.
  198. Ellis A, Bennett DL. Neuroinflammation and the generation of neuropathic pain. *Br J Anaesth.* 2013;111(1):26-37.
  199. Andersen KG, Aasvang EK, Kroman N, Kehlet H. Intercostobrachial nerve handling and pain after axillary lymph node dissection for breast cancer. *Acta Anaesthesiol Scand.* 2014;58(10):1240-8.
  200. Dowdall T, Robinson I, Meert TF. Comparison of five different rat models of peripheral nerve injury. *Pharmacology Biochemistry and Behavior.* 2005;80(1):93-108.
  201. Høimyr H, Rokkones KA, von Sperling ML, Finnerup K, Jensen TS, Finnerup NB. Persistent pain after lymph node excision in patients with malignant melanoma is neuropathic. *PAIN.* 2011;152(12):2721-8.
  202. Maguire MF, Latter JA, Mahajan R, Beggs FD, Duffy JP. A study exploring the role of intercostal nerve damage in chronic pain after thoracic surgery. *European Journal of Cardio-Thoracic Surgery.* 2006;29(6):873-9.
  203. Haroutiunian S, Nikolajsen L, Finnerup NB, Jensen TS. The neuropathic component in persistent postsurgical pain: a systematic literature review. *Pain.* 2013;154(1):95-102.
  204. Allodi I, Udina E, Navarro X. Specificity of peripheral nerve regeneration: interactions at the axon level. *Prog Neurobiol.* 2012;98(1):16-37.
  205. Perkins NM, Tracey DJ. Hyperalgesia due to nerve injury: role of neutrophils. *Neuroscience.* 2000;101(3):745-57.
  206. Zuo Y, Perkins NM, Tracey DJ, Geczy CL. Inflammation and hyperalgesia induced by nerve injury in the rat: a key role of mast cells. *PAIN.* 2003;105(3).
  207. Zhang T, Zhang M, Cui S, Liang W, Jia Z, Guo F, et al. The core of maintaining neuropathic pain: Crosstalk between glial cells and neurons (neural cell crosstalk at spinal cord). *Brain Behav.* 2023;13(2):e2868.
  208. Breitingner U, Breitingner HG. Excitatory and inhibitory neuronal signaling in inflammatory and diabetic neuropathic pain. *Mol Med.* 2023;29(1):53.
  209. Ji R-R, Chamesian A, Zhang Y-Q. Pain regulation by non-neuronal cells and inflammation. *Science.* 2016;354(6312):572-7.

- 
210. Jha MK, Jeon S, Suk K. Glia as a Link between Neuroinflammation and Neuropathic Pain. in. 2012;12(2):41-7.
  211. Finnerup NB. A review of central neuropathic pain states. *Current Opinion in Anesthesiology*. 2008;21(5).
  212. Lu HJ, Gao YJ. Astrocytes in Chronic Pain: Cellular and Molecular Mechanisms. *Neurosci Bull*. 2023;39(3):425-39.
  213. Calvo M, Bennett DL. The mechanisms of microgliosis and pain following peripheral nerve injury. *Exp Neurol*. 2012;234(2):271-82.
  214. Yu X, Basbaum A, Guan Z. Contribution of colony-stimulating factor 1 to neuropathic pain. *Pain Rep*. 2021;6(1):e883.
  215. Petroianu GA, Aloum L, Adem A. Neuropathic pain: Mechanisms and therapeutic strategies. *Front Cell Dev Biol*. 2023;11:1072629.
  216. Tu H, Chu H, Guan S, Hao F, Xu N, Zhao Z, et al. The role of the M1/M2 microglia in the process from cancer pain to morphine tolerance. *Tissue and Cell*. 2021;68.
  217. Liddelow SA, Guttenplan KA, Clarke LE, Bennett FC, Bohlen CJ, Schirmer L, et al. Neurotoxic reactive astrocytes are induced by activated microglia. *Nature*. 2017;541(7638):481-7.
  218. Korzhevskii DE, Kirik OV. Brain Microglia and Microglial Markers. *Neuroscience and Behavioral Physiology*. 2016;46(3):284-90.
  219. Abbadie C. Chemokines, chemokine receptors and pain. *Trends in Immunology*. 2005;26(10):529-34.
  220. Flynn G, Maru S, Loughlin J, Romero IA, Male D. Regulation of chemokine receptor expression in human microglia and astrocytes. *Journal of Neuroimmunology*. 2003;136(1-2):84-93.
  221. Kierdorf K, Prinz M. Factors regulating microglia activation. *Frontiers in Cellular Neuroscience*. 2013;7.
  222. Shabab T, Khanabdali R, Moghadamtousi SZ, Kadir HA, Mohan G. Neuroinflammation pathways: a general review. *Int J Neurosci*. 2017;127(7):624-33.
  223. Zhang X, Zeng L, Yu T, Xu Y, Pu S, Du D, et al. Positive Feedback Loop of Autocrine BDNF from Microglia Causes Prolonged Microglia Activation. *Cellular Physiology and Biochemistry*. 2014;34(3):715-23.
  224. Salvi V, Sozio F, Sozzani S, Del Prete A. Role of Atypical Chemokine Receptors in Microglial Activation and Polarization. *Frontiers in Aging Neuroscience*. 2017;9.
  225. Pekny M, Nilsson M. Astrocyte activation and reactive gliosis. *Glia*. 2005;50(4):427-34.
  226. Donnelly CR, Andriessen AS, Chen G, Wang K, Jiang C, Maixner W, et al. Central Nervous System Targets: Glial Cell Mechanisms in Chronic Pain. *Neurotherapeutics*. 2020;17(3):846-60.

- 
227. Rozental R, Giaume C, Spray DC. Gap junctions in the nervous system. *Brain Research Reviews*. 2000;32(1):11-5.
228. Van Horn MR, Sild M, Ruthazer ES. D-serine as a gliotransmitter and its roles in brain development and disease. *Front Cell Neurosci*. 2013;7:39.
229. Thompson WL, Van Eldik LJ. Inflammatory cytokines stimulate the chemokines CCL2/MCP-1 and CCL7/MCP-3 through NFkB and MAPK dependent pathways in rat astrocytes [corrected]. *Brain Res*. 2009;1287:47-57.
230. Kim M-O, Suh H-S, Brosnan CF, Lee SC. Regulation of RANTES/CCL5 expression in human astrocytes by interleukin-1 and interferon-beta. *Journal of Neurochemistry*. 2004;90(2):297-308.
231. Ji RR, Donnelly CR, Nedergaard M. Astrocytes in chronic pain and itch. *Nat Rev Neurosci*. 2019;20(11):667-85.
232. Gao Y-J, Ji R-R. Targeting Astrocyte Signaling for Chronic Pain. *Neurotherapeutics*. 2010;7(4):482-93.
233. Inoue K, Tsuda M. Microglia and neuropathic pain. *Glia*. 2009;57(14):1469-79.
234. Inoue K, Tsuda M. Microglia in neuropathic pain: cellular and molecular mechanisms and therapeutic potential. *Nat Rev Neurosci*. 2018;19(3):138-52.
235. Li T, Chen X, Zhang C, Zhang Y, Yao W. An update on reactive astrocytes in chronic pain. *J Neuroinflammation*. 2019;16(1):140.
236. Klein I, Lehmann HC. Pathomechanisms of Paclitaxel-Induced Peripheral Neuropathy. *Toxics*. 2021;9(10).
237. Flatters SJL, Dougherty PM, Colvin LA. Clinical and preclinical perspectives on Chemotherapy-Induced Peripheral Neuropathy (CIPN): a narrative review. *Br J Anaesth*. 2017;119(4):737-49.
238. Carozzi VA, Canta A, Chiorazzi A. Chemotherapy-induced peripheral neuropathy: What do we know about mechanisms? *Neurosci Lett*. 2015;596:90-107.
239. Gutierrez-Gutierrez G, Sereno M, Miralles A, Casado-Saenz E, Gutierrez-Rivas E. Chemotherapy-induced peripheral neuropathy: clinical features, diagnosis, prevention and treatment strategies. *Clin Transl Oncol*. 2010;12(2):81-91.
240. Seretny M, Currie GL, Sena ES, Ramnarine S, Grant R, MacLeod MR, et al. Incidence, prevalence, and predictors of chemotherapy-induced peripheral neuropathy: A systematic review and meta-analysis. *Pain*. 2014;155(12):2461-70.
241. Wolf S, Barton D, Kottschade L, Grothey A, Loprinzi C. Chemotherapy-induced peripheral neuropathy: prevention and treatment strategies. *Eur J Cancer*. 2008;44(11):1507-15.
242. Eldridge S, Guo L, Hamre J, 3rd. A Comparative Review of Chemotherapy-Induced Peripheral Neuropathy in In Vivo and In Vitro Models. *Toxicol Pathol*. 2020;48(1):190-201.

- 
243. Park SB, Goldstein D, Krishnan AV, Lin CS, Friedlander ML, Cassidy J, et al. Chemotherapy-induced peripheral neurotoxicity: a critical analysis. *CA Cancer J Clin.* 2013;63(6):419-37.
  244. Zajackowska R, Kocot-Kepska M, Leppert W, Wrzosek A, Mika J, Wordliczek J. Mechanisms of Chemotherapy-Induced Peripheral Neuropathy. *Int J Mol Sci.* 2019;20(6).
  245. Scripture CD, Figg WD, Sparreboom A. Peripheral Neuropathy Induced by Paclitaxel: Recent Insights and Future Perspectives. *Current Neuropharmacology.* 2006.
  246. Kampan NC, Madondo MT, McNally OM, Quinn M, Plebanski M. Paclitaxel and Its Evolving Role in the Management of Ovarian Cancer. *Biomed Res Int.* 2015;2015:413076.
  247. BfarM. FACHINFORMATION/ ZUSAMMENFASSUNG DER MERKMALE DES ARZNEIMITTELS. 2022.
  248. Perez EA. Paclitaxel in Breast Cancer. *The Oncologist.* 1998;3(6):373-89.
  249. Ramalingam S, Belani CP. Paclitaxel for non-small cell lung cancer. *Expert Opin Pharmacother.* 2004;5(8):1771-80.
  250. Albers P, Park SI, Niegisch G, Fechner G, Steiner U, Lehmann J, et al. Randomized phase III trial of 2nd line gemcitabine and paclitaxel chemotherapy in patients with advanced bladder cancer: short-term versus prolonged treatment [German Association of Urological Oncology (AUO) trial AB 20/99]. *Annals of Oncology.* 2011;22(2):288-94.
  251. Bernabeu E, Cagel M, Lagomarsino E, Moretton M, Chiappetta DA. Paclitaxel: What has been done and the challenges remain ahead. *Int J Pharm.* 2017;526(1-2):474-95.
  252. Banach M, Juranek JK, Zygulska AL. Chemotherapy-induced neuropathies-a growing problem for patients and health care providers. *Brain Behav.* 2017;7(1):e00558.
  253. Yan X, Maixner DW, Yadav R, Gao M, Li P, Bartlett MG, et al. Paclitaxel induces acute pain via directly activating toll like receptor 4. *Mol Pain.* 2015;11:10.
  254. Zhang D, Yang R, Wang S, Dong Z. Paclitaxel: new uses for an old drug. *Drug Des Devel Ther.* 2014;8:279-84.
  255. Xie S, Ogden A, Aneja R, Zhou J. Microtubule-Binding Proteins as Promising Biomarkers of Paclitaxel Sensitivity in Cancer Chemotherapy. *Med Res Rev.* 2016;36(2):300-12.
  256. Ko MH, Hu ME, Hsieh YL, Lan CT, Tseng TJ. Peptidergic intraepidermal nerve fibers in the skin contribute to the neuropathic pain in paclitaxel-induced peripheral neuropathy. *Neuropeptides.* 2014;48(3):109-17.
  257. Boyette-Davis J, Xin W, Zhang H, Dougherty PM. Intraepidermal nerve fiber loss corresponds to the development of Taxol-induced hyperalgesia and can be prevented by treatment with minocycline. *PAIN.* 2011;152(2).
  258. Bobylev I, Joshi AR, Barham M, Ritter C, Neiss WF, Hoke A, et al. Paclitaxel inhibits mRNA transport in axons. *Neurobiol Dis.* 2015;82:321-31.

- 
259. Nicolini G, Monfrini M, Scuteri A. Axonal Transport Impairment in Chemotherapy-Induced Peripheral Neuropathy. *Toxics*. 2015;3(3):322-41.
  260. Alberti P, Semperboni S, Cavaletti G, Scuteri A. Neurons: The Interplay between Cytoskeleton, Ion Channels/Transporters and Mitochondria. *Cells*. 2022;11(16).
  261. Flatters SJL, Bennett GJ. Studies of peripheral sensory nerves in paclitaxel-induced painful peripheral neuropathy: evidence for mitochondrial dysfunction. *Pain*. 2006;122(3):245-57.
  262. Kidd JF, Pilkington MF, Schell MJ, Fogarty KE, Skepper JN, Taylor CW, et al. Paclitaxel affects cytosolic calcium signals by opening the mitochondrial permeability transition pore. *J Biol Chem*. 2002;277(8):6504-10.
  263. Halestrap AP. What is the mitochondrial permeability transition pore? *Journal of Molecular and Cellular Cardiology*. 2009;46(6):821-31.
  264. Zorov DB, Juhaszova M, Sollott SJ. Mitochondrial reactive oxygen species (ROS) and ROS-induced ROS release. *Physiol Rev*. 2014;94(3):909-50.
  265. Vermeer CJC, Hiensch AE, Cleenewerk L, May AM, Eijkelkamp N. Neuro-immune interactions in paclitaxel-induced peripheral neuropathy. *Acta Oncol*. 2021;60(10):1369-82.
  266. Jin HW, Flatters SJ, Xiao WH, Mulhern HL, Bennett GJ. Prevention of paclitaxel-evoked painful peripheral neuropathy by acetyl-L-carnitine: effects on axonal mitochondria, sensory nerve fiber terminal arbors, and cutaneous Langerhans cells. *Exp Neurol*. 2008;210(1):229-37.
  267. Tse KH, Chow KB, Leung WK, Wong YH, Wise H. Primary sensory neurons regulate Toll-like receptor-4-dependent activity of glial cells in dorsal root ganglia. *Neuroscience*. 2014;279:10-22.
  268. Szabo-Pardi TA, Barron LR, Lenert ME, Burton MD. Sensory Neuron TLR4 mediates the development of nerve-injury induced mechanical hypersensitivity in female mice. *Brain, Behavior, and Immunity*. 2021;97:42-60.
  269. Lenert ME, Avona A, Garner KM, Barron LR, Burton MD. Sensory Neurons, Neuroimmunity, and Pain Modulation by Sex Hormones. *Endocrinology*. 2021;162(8).
  270. Piras V, Selvarajoo K. Beyond MyD88 and TRIF Pathways in Toll-Like Receptor Signaling. *Front Immunol*. 2014;5:70.
  271. Kim JJ, Sears DD. TLR4 and Insulin Resistance. *Gastroenterol Res Pract*. 2010;2010.
  272. Lu YC, Yeh WC, Ohashi PS. LPS/TLR4 signal transduction pathway. *Cytokine*. 2008;42(2):145-51.
  273. Brandolini L, d'Angelo M, Antonosante A, Allegretti M, Cimini A. Chemokine Signaling in Chemotherapy-Induced Neuropathic Pain. *Int J Mol Sci*. 2019;20(12).
  274. Velasco-Gonzalez R, Coffeen U. Neurophysiopathological Aspects of Paclitaxel-induced Peripheral Neuropathy. *Neurotox Res*. 2022;40(6):1673-89.



- 
275. Zhang ZJ, Jiang BC, Gao YJ. Chemokines in neuron-glia cell interaction and pathogenesis of neuropathic pain. *Cell Mol Life Sci.* 2017;74(18):3275-91.
276. Vincenzi M, Milella MS, D'Ottavio G, Caprioli D, Reverte I, Maftei D. Targeting Chemokines and Chemokine GPCRs to Enhance Strong Opioid Efficacy in Neuropathic Pain. *Life (Basel).* 2022;12(3).
277. White FA, Jung H, Miller RJ. Chemokines and the pathophysiology of neuropathic pain. *Proceedings of the National Academy of Sciences.* 2007;104(51):20151-8.
278. Zhang H, Boyette-Davis JA, Kosturakis AK, Li Y, Yoon S-Y, Walters ET, et al. Induction of Monocyte Chemoattractant Protein-1 (MCP-1) and Its Receptor CCR2 in Primary Sensory Neurons Contributes to Paclitaxel-Induced Peripheral Neuropathy. *The Journal of Pain.* 2013;14(10):1031-44.
279. Hara T, Chiba T, Abe K, Makabe A, Ikeno S, Kawakami K, et al. Effect of paclitaxel on transient receptor potential vanilloid 1 in rat dorsal root ganglion. *Pain.* 2013;154(6):882-9.
280. Kamata Y, Kambe T, Chiba T, Yamamoto K, Kawakami K, Abe K, et al. Paclitaxel Induces Upregulation of Transient Receptor Potential Vanilloid 1 Expression in the Rat Spinal Cord. *Int J Mol Sci.* 2020;21(12).
281. Li WW, Guo TZ, Shi X, Sun Y, Wei T, Clark DJ, et al. Substance P spinal signaling induces glial activation and nociceptive sensitization after fracture. *Neuroscience.* 2015;310:73-90.
282. Sahbaie P, Shi X, Guo T-Z, Qiao Y, Yeomans DC, Kingery WS, et al. Role of substance P signaling in enhanced nociceptive sensitization and local cytokine production after incision. *PAIN.* 2009;145(3):341-9.
283. Yan X, Li F, Maixner DW, Yadav R, Gao M, Ali MW, et al. Interleukin-1beta released by microglia initiates the enhanced glutamatergic activity in the spinal dorsal horn during paclitaxel-associated acute pain syndrome. *Glia.* 2019;67(3):482-97.
284. Cavalli E, Mammana S, Nicoletti F, Bramanti P, Mazzon E. The neuropathic pain: An overview of the current treatment and future therapeutic approaches. *Int J Immunopathol Pharmacol.* 2019;33:2058738419838383.
285. Verma V, Singh N, Singh Jaggi A. Pregabalin in Neuropathic Pain: Evidences and Possible Mechanisms. *Current Neuropharmacology.* 2014;12(1):44-56.
286. Bennett MI, Simpson KH. Gabapentin in the treatment of neuropathic pain. *Palliative Medicine.* 2004;18(1):5-11.
287. Rao RD, Michalak JC, Sloan JA, Loprinzi CL, Soori GS, Nikcevich DA, et al. Efficacy of gabapentin in the management of chemotherapy-induced peripheral neuropathy: a phase 3 randomized, double-blind, placebo-controlled, crossover trial (N00C3). *Cancer.* 2007;110(9):2110-8.
288. Shinu P, Morsy MA, Nair AB, Mouslem AKA, Venugopala KN, Goyal M, et al. Novel Therapies for the Treatment of Neuropathic Pain: Potential and Pitfalls. *J Clin Med.* 2022;11(11).

- 
289. Ghayur MN. Potential Adverse Consequences of Combination Therapy with Gabapentin and Pregabalin. *Case Rep Med.* 2021;2021:5559981.
  290. Gierthmuhlen J, Baron R. Neuropathic Pain. *Semin Neurol.* 2016;36(5):462-8.
  291. Sindrup SH, Otto M, Finnerup NB, Jensen TS. Antidepressants in the treatment of neuropathic pain. *Basic Clin Pharmacol Toxicol.* 2005;96(6):399-409.
  292. Lee Y-C, Chen P-P. A review of SSRIs and SNRIs in neuropathic pain. *Expert Opinion on Pharmacotherapy.* 2010;11(17):2813-25.
  293. Casale R, Symeonidou Z, Bartolo M. Topical Treatments for Localized Neuropathic Pain. *Curr Pain Headache Rep.* 2017;21(3):15.
  294. Binder A, Baron R. The Pharmacological Therapy of Chronic Neuropathic Pain. *Dtsch Arztebl Int.* 2016;113(37):616-25.
  295. Vadivelu N, Kai A, Maslin B, Kodumudi G, Legler A, Berger JM. Tapentadol extended release in the management of peripheral diabetic neuropathic pain. *Ther Clin Risk Manag.* 2015;11:95-105.
  296. Hartrick CT, Rodríguez Hernández JR. Tapentadol for pain: a treatment evaluation. *Expert Opinion on Pharmacotherapy.* 2012;13(2):283-6.
  297. Quinlan J, Cox F. Acute pain management in patients with drug dependence syndrome. *Pain Rep.* 2017;2(4):e611.
  298. Park J, Park HJ. Botulinum Toxin for the Treatment of Neuropathic Pain. *Toxins (Basel).* 2017;9(9).
  299. Bernetti A, Agostini F, de Sire A, Mangone M, Tognolo L, Di Cesare A, et al. Neuropathic Pain and Rehabilitation: A Systematic Review of International Guidelines. *Diagnostics (Basel).* 2021;11(1).
  300. Klomjai W, Katz R, Lackmy-Vallee A. Basic principles of transcranial magnetic stimulation (TMS) and repetitive TMS (rTMS). *Ann Phys Rehabil Med.* 2015;58(4):208-13.
  301. Caylor J, Reddy R, Yin S, Cui C, Huang M, Huang C, et al. Spinal cord stimulation in chronic pain: evidence and theory for mechanisms of action. *Bioelectron Med.* 2019;5.
  302. Boccard SG, Pereira EA, Aziz TZ. Deep brain stimulation for chronic pain. *J Clin Neurosci.* 2015;22(10):1537-43.
  303. Barik S. Immunophilins: for the love of proteins. *Cell Mol Life Sci.* 2006;63(24):2889-900.
  304. Marks AR. Cellular functions of immunophilins. *Physiological Reviews.* 1996;76(3):631-49.
  305. Wu B, Li P, Liu Y, Lou Z, Ding Y, Shu C, et al. 3D structure of human FK506-binding protein 52: Implications for the assembly of the glucocorticoid receptor/Hsp90/immunophilin heterocomplex. *Proceedings of the National Academy of Sciences.* 2004;101(22):8348-53.

- 
306. Sinars CR, Cheung-Flynn J, Rimerman RA, Scammell JG, Smith DF, Clardy J. Structure of the large FK506-binding protein FKBP51, an Hsp90-binding protein and a component of steroid receptor complexes. *Proceedings of the National Academy of Sciences*. 2003;100(3):868-73.
  307. Bracher A, Kozany C, Thost AK, Hausch F. Structural characterization of the PPlase domain of FKBP51, a cochaperone of human Hsp90. *Acta Crystallogr D Biol Crystallogr*. 2011;67(Pt 6):549-59.
  308. Hähle A, Merz S, Meyners C, Hausch F. The Many Faces of FKBP51. *Biomolecules*. 2019;9(1).
  309. Kumar R, Moche M, Winblad B, Pavlov PF. Combined x-ray crystallography and computational modeling approach to investigate the Hsp90 C-terminal peptide binding to FKBP51. *Sci Rep*. 2017;7(1):14288.
  310. Young JC, Obermann WMJ, Hartl FU. Specific Binding of Tetratricopeptide Repeat Proteins to the C-terminal 12-kDa Domain of hsp90\*. *Journal of Biological Chemistry*. 1998;273(29):18007-10.
  311. Ebong IO, Beilsten-Edmands V, Patel NA, Morgner N, Robinson CV. The interchange of immunophilins leads to parallel pathways and different intermediates in the assembly of Hsp90 glucocorticoid receptor complexes. *Cell Discov*. 2016;2:16002.
  312. Pratt WB, Toft DO. Steroid Receptor Interactions with Heat Shock Protein and Immunophilin Chaperones\*. *Endocrine Reviews*. 1997;18(3):306-60.
  313. Sanchez ER. Chaperoning steroidal physiology: lessons from mouse genetic models of Hsp90 and its cochaperones. *Biochim Biophys Acta*. 2012;1823(3):722-9.
  314. Echeverria PC, Picard D. Molecular chaperones, essential partners of steroid hormone receptors for activity and mobility. *Biochim Biophys Acta*. 2010;1803(6):641-9.
  315. Jääskeläinen T, Makkonen H, Palvimo JJ. Steroid up-regulation of FKBP51 and its role in hormone signaling. *Curr Opin Pharmacol*. 2011;11(4):326-31.
  316. Cioffi DL, Hubler TR, Scammell JG. Organization and function of the FKBP52 and FKBP51 genes. *Curr Opin Pharmacol*. 2011;11(4):308-13.
  317. Smith DF, Toft DO. Minireview: the intersection of steroid receptors with molecular chaperones: observations and questions. *Mol Endocrinol*. 2008;22(10):2229-40.
  318. Beato M, Klug J. Steroid hormone receptors: an update. *Human Reproduction Update*. 2000;6(3):225-36.
  319. Riggs DL, Roberts PJ, Chirillo SC, Cheung-Flynn J, Prapapanich V, Ratajczak T, et al. The Hsp90-binding peptidylprolyl isomerase FKBP52 potentiates glucocorticoid signaling in vivo. *EMBO J*. 2003;22(5):1158-67.
  320. Schülke JP, Wochnik GM, Lang-Rollin I, Gassen NC, Knapp RT, Berning B, et al. Differential impact of tetratricopeptide repeat proteins on the steroid hormone receptors. *PLoS One*. 2010;5(7):e11717.

- 
321. Criado-Marrero M, Rein T, Binder EB, Porter JT, Koren J, 3rd, Blair LJ. Hsp90 and FKBP51: complex regulators of psychiatric diseases. *Philos Trans R Soc Lond B Biol Sci.* 2018;373(1738).
  322. Davies TH, Ning YM, Sanchez ER. A new first step in activation of steroid receptors: hormone-induced switching of FKBP51 and FKBP52 immunophilins. *J Biol Chem.* 2002;277(7):4597-600.
  323. Schmidt MV, Paez-Pereda M, Holsboer F, Hausch F. The prospect of FKBP51 as a drug target. *ChemMedChem.* 2012;7(8):1351-9.
  324. Wochnik GM, Ruegg J, Abel GA, Schmidt U, Holsboer F, Rein T. FK506-binding proteins 51 and 52 differentially regulate dynein interaction and nuclear translocation of the glucocorticoid receptor in mammalian cells. *J Biol Chem.* 2005;280(6):4609-16.
  325. Stechschulte LA, Sanchez ER. FKBP51-a selective modulator of glucocorticoid and androgen sensitivity. *Curr Opin Pharmacol.* 2011;11(4):332-7.
  326. Hartmann J, Wagner KV, Liebl C, Scharf SH, Wang XD, Wolf M, et al. The involvement of FK506-binding protein 51 (FKBP5) in the behavioral and neuroendocrine effects of chronic social defeat stress. *Neuropharmacology.* 2012;62(1):332-9.
  327. Scammell JG. The animal and cell models that uncovered FKBP51 as a regulator of glucocorticoid receptor function. *J Cell Biochem.* 2023.
  328. Binder EB, Bradley RG, Liu W, Epstein MP, Deveau TC, Mercer KB, et al. Association of FKBP5 Polymorphisms and Childhood Abuse With Risk of Posttraumatic Stress Disorder Symptoms in Adults. *JAMA.* 2008;299(11):1291-305.
  329. Binder EB, Salyakina D, Lichtner P, Wochnik GM, Ising M, Putz B, et al. Polymorphisms in FKBP5 are associated with increased recurrence of depressive episodes and rapid response to antidepressant treatment. *Nat Genet.* 2004;36(12):1319-25.
  330. Xie P, Kranzler HR, Poling J, Stein MB, Anton RF, Farrer LA, et al. Interaction of FKBP5 with childhood adversity on risk for post-traumatic stress disorder. *Neuropsychopharmacology.* 2010;35(8):1684-92.
  331. Menke A, Klengel T, Rubel J, Bruckl T, Pfister H, Lucae S, et al. Genetic variation in FKBP5 associated with the extent of stress hormone dysregulation in major depression. *Genes Brain Behav.* 2013;12(3):289-96.
  332. Koenen KC, Uddin M. FKBP5 polymorphisms modify the effects of childhood trauma. *Neuropsychopharmacology.* 2010;35(8):1623-4.
  333. Koenen KC, Saxe G, Purcell S, Smoller JW, Bartholomew D, Miller A, et al. Polymorphisms in FKBP5 are associated with peritraumatic dissociation in medically injured children. *Mol Psychiatry.* 2005;10(12):1058-9.
  334. Roy A, Hodgkinson CA, Deluca V, Goldman D, Enoch MA. Two HPA axis genes, CRHBP and FKBP5, interact with childhood trauma to increase the risk for suicidal behavior. *J Psychiatr Res.* 2012;46(1):72-9.

- 
335. Zannas AS, Wiechmann T, Gassen NC, Binder EB. Gene-Stress-Epigenetic Regulation of FKBP5: Clinical and Translational Implications. *Neuropsychopharmacology*. 2016;41(1):261-74.
  336. Willour VL, Chen H, Toolan J, Belmonte P, Cutler DJ, Goes FS, et al. Family-based association of FKBP5 in bipolar disorder. *Mol Psychiatry*. 2009;14(3):261-8.
  337. Lekman M, Laje G, Charney D, Rush AJ, Wilson AF, Sorant AJ, et al. The FKBP5-gene in depression and treatment response--an association study in the Sequenced Treatment Alternatives to Relieve Depression (STAR\*D) Cohort. *Biol Psychiatry*. 2008;63(12):1103-10.
  338. Kirchheiner J, Lorch R, Lebedeva E, Seeringer A, Roots I, Sasse J, et al. Genetic variants in FKBP5 affecting response to antidepressant drug treatment. *Pharmacogenomics*. 2008;9(7):841-6.
  339. Smedlund KB, Sanchez ER, Hinds TD, Jr. FKBP51 and the molecular chaperoning of metabolism. *Trends Endocrinol Metab*. 2021;32(11):862-74.
  340. Hausl AS, Balsevich G, Gassen NC, Schmidt MV. Focus on FKBP51: A molecular link between stress and metabolic disorders. *Mol Metab*. 2019;29:170-81.
  341. Bortsov AV, Smith JE, Diatchenko L, Soward AC, Ulirsch JC, Rossi C, et al. Polymorphisms in the glucocorticoid receptor co-chaperone FKBP5 predict persistent musculoskeletal pain after traumatic stress exposure. *Pain*. 2013;154(8):1419-26.
  342. Linnstaedt SD, Riker KD, Rueckeis CA, Kutchko KM, Lackey L, McCarthy KR, et al. A Functional riboSNitch in the 3' Untranslated Region of FKBP5 Alters MicroRNA-320a Binding Efficiency and Mediates Vulnerability to Chronic Post-Traumatic Pain. *J Neurosci*. 2018;38(39):8407-20.
  343. Maiaru M, Tochiki KK, Cox MB, Annan LV, Bell CG, Feng X, et al. The stress regulator FKBP51 drives chronic pain by modulating spinal glucocorticoid signaling. *Sci Transl Med*. 2016;8(325):325ra19.
  344. Maiaru M, Morgan OB, Mao T, Breitsamer M, Bamber H, Pohlmann M, et al. The stress regulator FKBP51: a novel and promising druggable target for the treatment of persistent pain states across sexes. *Pain*. 2018;159(7):1224-34.
  345. Bartley EJ, Fillingim RB. Sex differences in pain: a brief review of clinical and experimental findings. *Br J Anaesth*. 2013;111(1):52-8.
  346. Luo X, Chen O, Wang Z, Bang S, Ji J, Lee SH, et al. IL-23/IL-17A/TRPV1 axis produces mechanical pain via macrophage-sensory neuron crosstalk in female mice. *Neuron*. 2021;109(17):2691-706 e5.
  347. Luo X, Gu Y, Tao X, Serhan CN, Ji RR. Resolvin D5 Inhibits Neuropathic and Inflammatory Pain in Male But Not Female Mice: Distinct Actions of D-Series Resolvins in Chemotherapy-Induced Peripheral Neuropathy. *Front Pharmacol*. 2019;10:745.
  348. Sorge RE, Mapplebeck JC, Rosen S, Beggs S, Taves S, Alexander JK, et al. Different immune cells mediate mechanical pain hypersensitivity in male and female mice. *Nat Neurosci*. 2015;18(8):1081-3.

- 
349. Chen G, Luo X, Qadri MY, Berta T, Ji RR. Sex-Dependent Glial Signaling in Pathological Pain: Distinct Roles of Spinal Microglia and Astrocytes. *Neurosci Bull.* 2018;34(1):98-108.
  350. Mukhara D, Oh U, Neigh GN. Chapter 15 - Neuroinflammation. In: Lanzenberger R, Kranz GS, Savic I, editors. *Handbook of Clinical Neurology.* 175: Elsevier; 2020. p. 235-59.
  351. Abraham A, Barnett C, Katzberg HD, Lovblom LE, Perkins BA, Bril V. Sex differences in neuropathic pain intensity in diabetes. *Journal of the Neurological Sciences.* 2018;388:103-6.
  352. Zgajnar NR, De Leo SA, Lotufo CM, Erlejman AG, Piwien-Pilipuk G, Galigniana MD. Biological Actions of the Hsp90-binding Immunophilins FKBP51 and FKBP52. *Biomolecules.* 2019;9(2).
  353. Kaestle M, Kistler B, Lamla T, Bretschneider T, Lamb D, Nicklin P, et al. FKBP51 modulates steroid sensitivity and NFkappaB signalling: A novel anti-inflammatory drug target. *Eur J Immunol.* 2018;48(11):1904-14.
  354. Jiang W, Cazacu S, Xiang C, Zenklusen JC, Fine HA, Berens M, et al. FK506 binding protein mediates glioma cell growth and sensitivity to rapamycin treatment by regulating NF-kappaB signaling pathway. *Neoplasia.* 2008;10(3):235-43.
  355. Romano S, Xiao Y, Nakaya M, D'Angelillo A, Chang M, Jin J, et al. FKBP51 employs both scaffold and isomerase functions to promote NF-kappaB activation in melanoma. *Nucleic Acids Res.* 2015;43(14):6983-93.
  356. Srivastava SK, Bhardwaj A, Arora S, Tyagi N, Singh AP, Carter JE, et al. Interleukin-8 is a key mediator of FKBP51-induced melanoma growth, angiogenesis and metastasis. *Br J Cancer.* 2015;112(11):1772-81.
  357. Romano MF, Avellino R, Petrella A, Bisogni R, Romano S, Venuta S. Rapamycin inhibits doxorubicin-induced NF-kappaB/Rel nuclear activity and enhances the apoptosis of melanoma cells. *Eur J Cancer.* 2004;40(18):2829-36.
  358. Kiguchi N, Kobayashi Y, Kishioka S. Chemokines and cytokines in neuroinflammation leading to neuropathic pain. *Curr Opin Pharmacol.* 2012;12(1):55-61.
  359. Ramesh G, MacLean AG, Philipp MT. Cytokines and chemokines at the crossroads of neuroinflammation, neurodegeneration, and neuropathic pain. *Mediators Inflamm.* 2013;2013:480739.
  360. Soltani Khaboushan A, Yazdanpanah N, Rezaei N. Neuroinflammation and Proinflammatory Cytokines in Epileptogenesis. *Mol Neurobiol.* 2022;59(3):1724-43.
  361. Gao Y, Elamin E, Zhou R, Yan H, Liu S, Hu S, et al. FKBP51 promotes migration and invasion of papillary thyroid carcinoma through NF-kappaB-dependent epithelial-to-mesenchymal transition. *Oncol Lett.* 2018;16(6):7020-8.
  362. Li H, Jiao YL, Zhou RF, Liu S, Cui B, Wang LC, et al. FKBP51 acts as a biomarker of early metastasis and is related to carmustine sensitivity in human glioma cells. *Eur Rev Med Pharmacol Sci.* 2020;24(17):8918-30.

- 
363. Storer CL, Dickey CA, Galigniana MD, Rein T, Cox MB. FKBP51 and FKBP52 in signaling and disease. *Trends Endocrinol Metab.* 2011;22(12):481-90.
  364. Romano S, Mallardo M, Romano MF. FKBP51 and the NF-kappaB regulatory pathway in cancer. *Curr Opin Pharmacol.* 2011;11(4):288-93.
  365. Gaali S, Gopalakrishnan R, Wang Y, Kozany C, Hausch F. The Chemical Biology of Immunophilin Ligands. *Current Medicinal Chemistry.* 2011;18(35):5355-79.
  366. Blackburn EA, Walkinshaw MD. Targeting FKBP isoforms with small-molecule ligands. *Curr Opin Pharmacol.* 2011;11(4):365-71.
  367. Gaali S, Kirschner A, Cuboni S, Hartmann J, Kozany C, Balsevich G, et al. Selective inhibitors of the FK506-binding protein 51 by induced fit. *Nat Chem Biol.* 2015;11(1):33-7.
  368. Feng X, Pomplun S, Hausch F. Recent Progress in FKBP Ligand Development. *Current Molecular Pharmacology.* 2016;9(1):27-36.
  369. Wedel S, Hahnefeld L, Alnouri MW, Offermanns S, Hausch F, Geisslinger G, et al. The FKBP51 Inhibitor SAFit2 Restores the Pain-Relieving C16 Dihydroceramide after Nerve Injury. *Int J Mol Sci.* 2022;23(22).
  370. Wedel S, Mathoor P, Rauh O, Heymann T, Ciotu CI, Fuhrmann DC, et al. SAFit2 reduces neuroinflammation and ameliorates nerve injury-induced neuropathic pain. *Journal of Neuroinflammation.* 2022;19(1).
  371. Wedel S, Hahnefeld L, Schreiber Y, Namendorf C, Heymann T, Uhr M, et al. SAFit2 ameliorates paclitaxel-induced neuropathic pain by reducing spinal gliosis and elevating pro-resolving lipid mediators. *J Neuroinflammation.* 2023;20(1):149.
  372. Draxler SW, Bauer M, Eickmeier C, Nadal S, Nar H, Rangel Rojas D, et al. Hybrid Screening Approach for Very Small Fragments: X-ray and Computational Screening on FKBP51. *J Med Chem.* 2020;63(11):5856-64.
  373. Cruccu G, Sommer C, Anand P, Attal N, Baron R, Garcia-Larrea L, et al. EFNS guidelines on neuropathic pain assessment: revised 2009. *Eur J Neurol.* 2010;17(8):1010-8.
  374. Wang S, Lim G, Zeng Q, Sung B, Ai Y, Guo G, et al. Expression of central glucocorticoid receptors after peripheral nerve injury contributes to neuropathic pain behaviors in rats. *J Neurosci.* 2004;24(39):8595-605.
  375. Takasaki I, Kurihara T, Saegusa H, Zong S, Tanabe T. Effects of glucocorticoid receptor antagonists on allodynia and hyperalgesia in mouse model of neuropathic pain. *European Journal of Pharmacology.* 2005;524(1-3):80-3.
  376. Wang S, Lim G, Zeng Q, Sung B, Yang L, Mao J. Central glucocorticoid receptors modulate the expression and function of spinal NMDA receptors after peripheral nerve injury. *J Neurosci.* 2005;25(2):488-95.

- 
377. Alexander JK, DeVries AC, Kigerl KA, Dahlman JM, Popovich PG. Stress exacerbates neuropathic pain via glucocorticoid and NMDA receptor activation. *Brain Behav Immun.* 2009;23(6):851-60.
378. Neumann M, Naumann M. Beyond I $\kappa$ Bs: alternative regulation of NF- $\kappa$ B activity. *FASEB J.* 2007;21(11):2642-54.
379. Pace TW, Hu F, Miller AH. Cytokine-effects on glucocorticoid receptor function: relevance to glucocorticoid resistance and the pathophysiology and treatment of major depression. *Brain Behav Immun.* 2007;21(1):9-19.
380. Silverman MN, Sternberg EM. Glucocorticoid regulation of inflammation and its functional correlates: from HPA axis to glucocorticoid receptor dysfunction. *Ann N Y Acad Sci.* 2012;1261:55-63.
381. Pace TW, Miller AH. Cytokines and glucocorticoid receptor signaling. Relevance to major depression. *Ann N Y Acad Sci.* 2009;1179:86-105.
382. Baschant U, Tuckermann J. The role of the glucocorticoid receptor in inflammation and immunity. *J Steroid Biochem Mol Biol.* 2010;120(2-3):69-75.
383. Murray PJ. Understanding and exploiting the endogenous interleukin-10/STAT3-mediated anti-inflammatory response. *Curr Opin Pharmacol.* 2006;6(4):379-86.
384. Meunier A, Latrémolière A, Dominguez E, Mauborgne A, Philippe S, Hamon M, et al. Lentiviral-mediated Targeted NF- $\kappa$ B Blockade in Dorsal Spinal Cord Glia Attenuates Sciatic Nerve Injury-induced Neuropathic Pain in the Rat. *Molecular Therapy.* 2007;15(4):687-97.
385. Pottorf TS, Rotterman TM, McCallum WM, Haley-Johnson ZA, Alvarez FJ. The Role of Microglia in Neuroinflammation of the Spinal Cord after Peripheral Nerve Injury. *Cells.* 2022;11(13).
386. Molnar K, Nogradi B, Kristof R, Meszaros A, Pajer K, Siklos L, et al. Motoneuronal inflammasome activation triggers excessive neuroinflammation and impedes regeneration after sciatic nerve injury. *J Neuroinflammation.* 2022;19(1):68.
387. Ambrosini E, Aloisi F. Chemokines and Glial Cells: A Complex Network in the Central Nervous System. *Neurochemical Research.* 2004;29(5):1017-38.
388. Xuan W, Qu Q, Zheng B, Xiong S, Fan G-H. The chemotaxis of M1 and M2 macrophages is regulated by different chemokines. *Journal of Leukocyte Biology.* 2014;97(1):61-9.
389. Babcock AA, Kuziel WA, Rivest S, Owens T. Chemokine Expression by Glial Cells Directs Leukocytes to Sites of Axonal Injury in the CNS. *The Journal of Neuroscience.* 2003;23(21):7922-30.
390. Franchimont D. Overview of the actions of glucocorticoids on the immune response: a good model to characterize new pathways of immunosuppression for new treatment strategies. *Ann N Y Acad Sci.* 2004;1024:124-37.
391. Lowenberg M, Verhaar AP, van den Brink GR, Hommes DW. Glucocorticoid signaling: a nongenomic mechanism for T-cell immunosuppression. *Trends Mol Med.* 2007;13(4):158-63.



- 
392. Coutinho AE, Chapman KE. The anti-inflammatory and immunosuppressive effects of glucocorticoids, recent developments and mechanistic insights. *Mol Cell Endocrinol.* 2011;335(1):2-13.
393. Goecke A, Guerrero J. Glucocorticoid receptor beta in acute and chronic inflammatory conditions: clinical implications. *Immunobiology.* 2006;211(1-2):85-96.
394. Cohen S, Janicki-Deverts D, Doyle WJ, Miller GE, Frank E, Rabin BS, et al. Chronic stress, glucocorticoid receptor resistance, inflammation, and disease risk. *Proc Natl Acad Sci U S A.* 2012;109(16):5995-9.
395. Alexander JK, Cox GM, Tian JB, Zha AM, Wei P, Kigerl KA, et al. Macrophage migration inhibitory factor (MIF) is essential for inflammatory and neuropathic pain and enhances pain in response to stress. *Exp Neurol.* 2012;236(2):351-62.
396. McEwen BS, Kalia M. The role of corticosteroids and stress in chronic pain conditions. *Metabolism.* 2010;59 Suppl 1:S9-15.
397. Cain DW, Cidlowski JA. Immune regulation by glucocorticoids. *Nature Reviews Immunology.* 2017;17(4):233-47.
398. Spies CM, Strehl C, van der Goes MC, Bijlsma JW, Buttgerit F. Glucocorticoids. *Best Pract Res Clin Rheumatol.* 2011;25(6):891-900.
399. Romundstad L, Stubhaug A. Glucocorticoids for Acute and Persistent Postoperative Neuropathic Pain: What Is the Evidence? *Anesthesiology.* 2007;107(3):371-3.
400. Pearson-Leary J, Osborne DM, McNay EC. Role of Glia in Stress-Induced Enhancement and Impairment of Memory. *Front Integr Neurosci.* 2015;9:63.
401. Peckett AJ, Wright DC, Riddell MC. The effects of glucocorticoids on adipose tissue lipid metabolism. *Metabolism.* 2011;60(11):1500-10.
402. Geer EB, Islam J, Buettner C. Mechanisms of glucocorticoid-induced insulin resistance: focus on adipose tissue function and lipid metabolism. *Endocrinol Metab Clin North Am.* 2014;43(1):75-102.
403. Gebru NT, Hill SE, Blair LJ. Genetically engineered mouse models of FK506-binding protein 5. *J Cell Biochem.* 2023.
404. Xu Y, Zhao Y, Gao B. Role of TRPV1 in High Temperature-Induced Mitochondrial Biogenesis in Skeletal Muscle: A Mini Review. *Front Cell Dev Biol.* 2022;10:882578.
405. Bevan S, Quallo T, Andersson DA. TRPV1. In: Nilius B, Flockerzi V, editors. *Mammalian Transient Receptor Potential (TRP) Cation Channels: Volume I.* Berlin, Heidelberg: Springer Berlin Heidelberg; 2014. p. 207-45.
406. Buffa V, Knaup FH, Heymann T, Springer M, Schmidt MV, Hausch F. Analysis of the Selective Antagonist SAFit2 as a Chemical Probe for the FK506-Binding Protein 51. *ACS Pharmacol Transl Sci.* 2023;6(3):361-71.

- 
407. Roy J, Cyert MS. Identifying New Substrates and Functions for an Old Enzyme: Calcineurin. *Cold Spring Harb Perspect Biol.* 2020;12(3).
  408. Li H, Rao A, Hogan PG. Interaction of calcineurin with substrates and targeting proteins. *Trends Cell Biol.* 2011;21(2):91-103.
  409. Babine RE, Villafranca JE, Gold BG. FKBP immunophilin patents for neurological disorders. *Expert Opinion on Therapeutic Patents.* 2005;15(5):555-73.
  410. Li TK, Baksh S, Cristillo AD, Bierer BE. Calcium- and FK506-independent interaction between the immunophilin FKBP51 and calcineurin. *J Cell Biochem.* 2002;84(3):460-71.
  411. Weiwad M, Edlich F, Kilka S, Erdmann F, Jarczowski F, Dorn M, et al. Comparative Analysis of Calcineurin Inhibition by Complexes of Immunosuppressive Drugs with Human FK506 Binding Proteins. *Biochemistry.* 2006;45(51):15776-84.
  412. Baughman G, Wiederrecht GJ, Campbell NF, Martin MM, Bourgeois S. FKBP51, a novel T-cell-specific immunophilin capable of calcineurin inhibition. *Mol Cell Biol.* 1995;15(8):4395-402.
  413. Baughman G, Wiederrecht GJ, Chang F, Martin MM, Bourgeois S. Tissue Distribution and Abundance of Human FKBP51, an FK506-Binding Protein That Can Mediate Calcineurin Inhibition. *Biochemical and Biophysical Research Communications.* 1997;232(2):437-43.
  414. Dumont FJ. FK506, An Immunosuppressant Targeting Calcineurin Function. *Current Medicinal Chemistry.* 2000;7(7):731-48.
  415. Knaup FH, Meyners C, Sugiarto WO, Wedel S, Springer M, Walz C, et al. Structure-Based Discovery of a New Selectivity-Enabling Motif for the FK506-Binding Protein 51. *J Med Chem.* 2023;66(8):5965-80.
  416. Kadmiel M, Cidlowski JA. Glucocorticoid receptor signaling in health and disease. *Trends Pharmacol Sci.* 2013;34(9):518-30.
  417. Oakley RH, Cidlowski JA. The biology of the glucocorticoid receptor: new signaling mechanisms in health and disease. *J Allergy Clin Immunol.* 2013;132(5):1033-44.
  418. Quax RA, Manenschijn L, Koper JW, Hazes JM, Lamberts SWJ, van Rossum EFC, et al. Glucocorticoid sensitivity in health and disease. *Nature Reviews Endocrinology.* 2013;9(11):670-86.
  419. Dahl JB, Nielsen RV, Wetterslev J, Nikolajsen L, Hamunen K, Kontinen VK, et al. Post-operative analgesic effects of paracetamol, NSAIDs, glucocorticoids, gabapentinoids and their combinations: a topical review. *Acta Anaesthesiol Scand.* 2014;58(10):1165-81.
  420. Oray M, Abu Samra K, Ebrahimiadib N, Meese H, Foster CS. Long-term side effects of glucocorticoids. *Expert Opin Drug Saf.* 2016;15(4):457-65.
  421. Cain DW, Cidlowski JA. Specificity and sensitivity of glucocorticoid signaling in health and disease. *Best Pract Res Clin Endocrinol Metab.* 2015;29(4):545-56.

- 
422. Dina OA, Khasar SG, Alessandri-Haber N, Green PG, Messing RO, Levine JD. Alcohol-induced stress in painful alcoholic neuropathy. *Eur J Neurosci*. 2008;27(1):83-92.
  423. Stechschulte LA, Qiu B, Warriar M, Hinds TD, Jr., Zhang M, Gu H, et al. FKBP51 Null Mice Are Resistant to Diet-Induced Obesity and the PPARgamma Agonist Rosiglitazone. *Endocrinology*. 2016;157(10):3888-900.
  424. Balsevich G, Hausl AS, Meyer CW, Karamihalev S, Feng X, Pohlmann ML, et al. Stress-responsive FKBP51 regulates AKT2-AS160 signaling and metabolic function. *Nat Commun*. 2017;8(1):1725.
  425. Toneatto J, Charo NL, Galigniana NM, Piwien-Pilipuk G. Adipogenesis is under surveillance of Hsp90 and the high molecular weight Immunophilin FKBP51. *Adipocyte*. 2015;4(4):239-47.
  426. Stechschulte LA, Hinds TD, Jr., Khuder SS, Shou W, Najjar SM, Sanchez ER. FKBP51 controls cellular adipogenesis through p38 kinase-mediated phosphorylation of GRalpha and PPARgamma. *Mol Endocrinol*. 2014;28(8):1265-75.
  427. Stechschulte LA, Hinds TD, Jr., Ghanem SS, Shou W, Najjar SM, Sanchez ER. FKBP51 reciprocally regulates GRalpha and PPARgamma activation via the Akt-p38 pathway. *Mol Endocrinol*. 2014;28(8):1254-64.
  428. Sidibeh CO, Pereira MJ, Abalo XM, G JB, Skrtic S, Lundkvist P, et al. FKBP5 expression in human adipose tissue: potential role in glucose and lipid metabolism, adipogenesis and type 2 diabetes. *Endocrine*. 2018;62(1):116-28.
  429. Pereira MJ, Palming J, Svensson MK, Rizell M, Dalenback J, Hammar M, et al. FKBP5 expression in human adipose tissue increases following dexamethasone exposure and is associated with insulin resistance. *Metabolism*. 2014;63(9):1198-208.
  430. Sarbassov DD, Guertin DA, Ali SM, Sabatini DM. Phosphorylation and Regulation of Akt/PKB by the Rictor-mTOR Complex. *Science*. 2005;307(5712):1098-101.
  431. Alessi DR, James SR, Downes CP, Holmes AB, Gaffney PRJ, Reese CB, et al. Characterization of a 3-phosphoinositide-dependent protein kinase which phosphorylates and activates protein kinase B $\alpha$ . *Current Biology*. 1997;7(4):261-9.
  432. Alessi DR, Andjelkovic M, Caudwell B, Cron P, Morrice N, Cohen P, et al. Mechanism of activation of protein kinase B by insulin and IGF-1. *The EMBO Journal*. 1996;15(23):6541-51.
  433. Higuchi M, Onishi K, Kikuchi C, Gotoh Y. Scaffolding function of PAK in the PDK1-Akt pathway. *Nat Cell Biol*. 2008;10(11):1356-64.
  434. Ortiz R, Joseph JJ, Lee R, Wand GS, Golden SH. Type 2 diabetes and cardiometabolic risk may be associated with increase in DNA methylation of FKBP5. *Clin Epigenetics*. 2018;10:82.
  435. Ruiz-Estevez M, Staats J, Paatela E, Munson D, Katoku-Kikyo N, Yuan C, et al. Promotion of Myoblast Differentiation by Fkbp5 via Cdk4 Isomerization. *Cell Rep*. 2018;25(9):2537-51 e8.
  436. Shimoide T, Kawao N, Tamura Y, Morita H, Kaji H. Novel roles of FKBP5 in muscle alteration induced by gravity change in mice. *Biochem Biophys Res Commun*. 2016;479(3):602-6.

- 
437. Bailus BJ, Scheeler SM, Simons J, Sanchez MA, Tshilenge KT, Creus-Muncunill J, et al. Modulating FKBP5/FKBP51 and autophagy lowers HTT (huntingtin) levels. *Autophagy*. 2021;17(12):4119-40.
  438. Bajaj T, Häusl AS, Schmidt MV, Gassen NC. FKBP5/FKBP51 on weight watch: central FKBP5 links regulatory WIPI protein networks to autophagy and metabolic control. *Autophagy*. 2022;18(11):2756-8.
  439. Häusl AS, Bajaj T, Brix LM, Pöhlmann ML, Hafner K, De Angelis M, et al. Mediobasal hypothalamic FKBP51 acts as a molecular switch linking autophagy to whole-body metabolism. *Science Advances*.8(10):eabi4797.
  440. Gassen NC, Hartmann J, Schmidt MV, Rein T. FKBP5/FKBP51 enhances autophagy to synergize with antidepressant action. *Autophagy*. 2015;11(3):578-80.
  441. Bates GP, Dorsey R, Gusella JF, Hayden MR, Kay C, Leavitt BR, et al. Huntington disease. *Nat Rev Dis Primers*. 2015;1:15005.
  442. Walker FO. Huntington's disease. *Lancet*. 2007;369(9557):218-28.
  443. Levine B, Kroemer G. Autophagy in the pathogenesis of disease. *Cell*. 2008;132(1):27-42.
  444. Ghavami S, Shojaei S, Yeganeh B, Ande SR, Jangamreddy JR, Mehrpour M, et al. Autophagy and apoptosis dysfunction in neurodegenerative disorders. *Prog Neurobiol*. 2014;112:24-49.
  445. Li L, Zhang X, Le W. Autophagy dysfunction in Alzheimer's disease. *Neurodegener Dis*. 2010;7(4):265-71.
  446. Li L, Lou Z, Wang L. The role of FKBP5 in cancer aetiology and chemoresistance. *Br J Cancer*. 2011;104(1):19-23.
  447. Mazaira GI, Camisay MF, De Leo S, Erlejman AG, Galigniana MD. Biological relevance of Hsp90-binding immunophilins in cancer development and treatment. *Int J Cancer*. 2016;138(4):797-808.
  448. Russo D, Merolla F, Mascolo M, Ilardi G, Romano S, Varricchio S, et al. FKBP51 Immunohistochemical Expression: A New Prognostic Biomarker for OSCC? *Int J Mol Sci*. 2017;18(2).
  449. Staibano S, Mascolo M, Ilardi G, Siano M, De Rosa G. Immunohistochemical analysis of FKBP51 in human cancers. *Curr Opin Pharmacol*. 2011;11(4):338-47.
  450. Solassol J, Mange A, Maudelonde T. FKBP family proteins as promising new biomarkers for cancer. *Curr Opin Pharmacol*. 2011;11(4):320-5.
  451. Romano S, D'Angelillo A, Pacelli R, Staibano S, De Luna E, Bisogni R, et al. Role of FK506-binding protein 51 in the control of apoptosis of irradiated melanoma cells. *Cell Death Differ*. 2010;17(1):145-57.

- 
452. Giraudier S, Chagraoui H, Komura E, Barnache S, Blanchet B, LeCouedic JP, et al. Overexpression of FKBP51 in idiopathic myelofibrosis regulates the growth factor independence of megakaryocyte progenitors. *Blood*. 2002;100(8):2932-40.
  453. Pei H, Li L, Fridley BL, Jenkins GD, Kalari KR, Lingle W, et al. FKBP51 affects cancer cell response to chemotherapy by negatively regulating Akt. *Cancer Cell*. 2009;16(3):259-66.
  454. Habara M, Sato Y, Goshima T, Sakurai M, Imai H, Shimizu H, et al. FKBP52 and FKBP51 differentially regulate the stability of estrogen receptor in breast cancer. *Proc Natl Acad Sci U S A*. 2022;119(15):e2110256119.
  455. Luo K, Li Y, Yin Y, Li L, Wu C, Chen Y, et al. USP49 negatively regulates tumorigenesis and chemoresistance through FKBP51-AKT signaling. *EMBO J*. 2017;36(10):1434-46.
  456. Ni L, Yang CS, Gioeli D, Frierson H, Toft DO, Paschal BM. FKBP51 promotes assembly of the Hsp90 chaperone complex and regulates androgen receptor signaling in prostate cancer cells. *Mol Cell Biol*. 2010;30(5):1243-53.
  457. Febbo Phillip G, Lowenberg M, Thorner Aaron R, Brown M, Loda M, Golub Todd R. Androgen mediated regulation and functional implications of FKBP51 expression in prostate cancer. *Journal of Urology*. 2005;173(5):1772-7.
  458. Maeda K, Habara M, Kawaguchi M, Matsumoto H, Hanaki S, Masaki T, et al. FKBP51 and FKBP52 regulate androgen receptor dimerization and proliferation in prostate cancer cells. *Mol Oncol*. 2022;16(4):940-56.
  459. Sun N-K, Huang S-L, Chang P-Y, Lu H-P, Chao CCK. Transcriptomic profiling of taxol-resistant ovarian cancer cells identifies FKBP5 and the androgen receptor as critical markers of chemotherapeutic response. *Oncotarget*; Vol 5, No 23. 2014.
  460. Avellino R, Romano S, Parasole R, Bisogni R, Lamberti A, Poggi V, et al. Rapamycin stimulates apoptosis of childhood acute lymphoblastic leukemia cells. *Blood*. 2005;106(4):1400-6.
  461. Zhen Y, Luo C, Zhang H. Early detection of ulcerative colitis-associated colorectal cancer. *Gastroenterol Rep (Oxf)*. 2018;6(2):83-92.
  462. Xia Z, Zhang G, Wang C, Feng Y. The role of FKBP51 in the prognosis of ulcerative colitis-associated colorectal cancer. *Adv Med Sci*. 2021;66(1):89-97.
  463. Cook KL, Shajahan AN, Clarke R. Autophagy and endocrine resistance in breast cancer. *Expert Review of Anticancer Therapy*. 2011;11(8):1283-94.
  464. Dhamad AE, Zhou Z, Zhou J, Du Y. Systematic Proteomic Identification of the Heat Shock Proteins (Hsp) that Interact with Estrogen Receptor Alpha (ERalpha) and Biochemical Characterization of the ERalpha-Hsp70 Interaction. *PLoS One*. 2016;11(8):e0160312.
  465. Eakin CM, MacCoss MJ, Finney GL, Klevit RE. Estrogen receptor  $\alpha$  is a putative substrate for the BRCA1 ubiquitin ligase. *Proceedings of the National Academy of Sciences*. 2007;104(14):5794-9.

- 
466. Häusel AS, Brix LM, Hartmann J, Pöhlmann ML, Lopez J-P, Menegaz D, et al. The co-chaperone Fkbp5 shapes the acute stress response in the paraventricular nucleus of the hypothalamus of male mice. *Molecular Psychiatry*. 2021;26(7):3060-76.
467. Fabian AK, Marz A, Neimanis S, Biondi RM, Kozany C, Hausch F. InterAKTions with FKBP5--mutational and pharmacological exploration. *PLoS One*. 2013;8(2):e57508.
468. Uhlen M, Fagerberg L, Hallstrom BM, Lindskog C, Oksvold P, Mardinoglu A, et al. Proteomics. Tissue-based map of the human proteome. *Science*. 2015;347(6220):1260419.
469. Gnatzy MT, Geiger TM, Kuehn A, Gutfreund N, Walz M, Kolos JM, et al. Development of NanoBRET-Binding Assays for FKBP-Ligand Profiling in Living Cells. *Chembiochem*. 2021;22(13):2257-61.
470. Griffith JP, Kim JL, Kim EE, Sintchak MD, Thomson JA, Fitzgibbon MJ, et al. X-ray structure of calcineurin inhibited by the immunophilin-immunosuppressant FKBP12-FK506 complex. *Cell*. 1995;82(3):507-22.
471. Xu X, Su B, Barndt RJ, Chen H, Xin H, Yan G, et al. FKBP12 is the only FK506 binding protein mediating T-cell inhibition by the immunosuppressant FK506. *Transplantation*. 2002;73(11):1835-8.
472. Lanner JT, Georgiou DK, Joshi AD, Hamilton SL. Ryanodine receptors: structure, expression, molecular details, and function in calcium release. *Cold Spring Harb Perspect Biol*. 2010;2(11):a003996.
473. Kolos JM, Voll AM, Bauder M, Hausch F. FKBP Ligands--Where We Are and Where to Go? *Front Pharmacol*. 2018;9:1425.
474. Zhao YT, Guo YB, Gu L, Fan XX, Yang HQ, Chen Z, et al. Sensitized signalling between L-type Ca<sup>2+</sup> channels and ryanodine receptors in the absence or inhibition of FKBP12.6 in cardiomyocytes. *Cardiovasc Res*. 2017;113(3):332-42.
475. Xiao J, Tian X, Jones PP, Bolstad J, Kong H, Wang R, et al. Removal of FKBP12.6 does not alter the conductance and activation of the cardiac ryanodine receptor or the susceptibility to stress-induced ventricular arrhythmias. *J Biol Chem*. 2007;282(48):34828-38.
476. Hausch F. FKBP5 and their role in neuronal signaling. *Biochim Biophys Acta*. 2015;1850(10):2035-40.
477. Hartmann J, Wagner KV, Gaali S, Kirschner A, Kozany C, Ruhter G, et al. Pharmacological Inhibition of the Psychiatric Risk Factor FKBP51 Has Anxiolytic Properties. *J Neurosci*. 2015;35(24):9007-16.
478. Codagnone MG, Kara N, Ratsika A, Levone BR, van de Wouw M, Tan LA, et al. Inhibition of FKBP51 induces stress resilience and alters hippocampal neurogenesis. *Mol Psychiatry*. 2022;27(12):4928-38.
479. McClintick JN, Xuei X, Tischfield JA, Goate A, Foroud T, Wetherill L, et al. Stress-response pathways are altered in the hippocampus of chronic alcoholics. *Alcohol*. 2013;47(7):505-15.

- 
480. Qiu B, Luczak SE, Wall TL, Kirchhoff AM, Xu Y, Eng MY, et al. The FKBP5 Gene Affects Alcohol Drinking in Knockout Mice and Is Implicated in Alcohol Drinking in Humans. *Int J Mol Sci.* 2016;17(8).
481. Konig L, Kalinichenko LS, Huber SE, Voll AM, Bauder M, Kornhuber J, et al. The selective FKBP51 inhibitor SAFit2 reduces alcohol consumption and reinstatement of conditioned alcohol effects in mice. *Addict Biol.* 2020;25(3):e12758.
482. Arrigo P, Russo M, Rea A, Tufano M, Guadagno E, Laura Del Basso De Caro M, et al. A regulatory role for the co-chaperone FKBP51s in PD-L1 expression in glioma. *Oncotarget*; Vol 8, No 40. 2017.
483. D'Arrigo P, Digregorio M, Romano S, Tufano M, Rea A, Hausch F, et al. The splicing FK506-binding protein-51 isoform plays a role in glioblastoma resistance through programmed cell death ligand-1 expression regulation. *Cell Death Discov.* 2019;5:137.
484. Luo X, Du G, Chen B, Yan G, Zhu L, Cui P, et al. Novel immunosuppressive effect of FK506 by upregulation of PD-L1 via FKBP51 in heart transplantation. *Scand J Immunol.* 2022;96(4):e13203.
485. Alon A, Lyu J, Braz JM, Tummino TA, Craik V, O'Meara MJ, et al. Structures of the sigma(2) receptor enable docking for bioactive ligand discovery. *Nature.* 2021;600(7890):759-64.
486. Malar DS, Thitilertdecha P, Ruckvongacheep KS, Brimson S, Tencomnao T, Brimson JM. Targeting Sigma Receptors for the Treatment of Neurodegenerative and Neurodevelopmental Disorders. *CNS Drugs.* 2023;37(5):399-440.
487. Maurice T, Su TP. The pharmacology of sigma-1 receptors. *Pharmacol Ther.* 2009;124(2):195-206.
488. Thurmond RL, Gelfand EW, Dunford PJ. The role of histamine H1 and H4 receptors in allergic inflammation: the search for new antihistamines. *Nat Rev Drug Discov.* 2008;7(1):41-53.
489. Huang J-F, Thurmond RL. The new biology of histamine receptors. *Current Allergy and Asthma Reports.* 2008;8(1):21-7.
490. Thurmond RL, Venable J, Savall B, La D, Snook S, Dunford PJ, et al. Clinical Development of Histamine H4 Receptor Antagonists. In: Hattori Y, Seifert R, editors. *Histamine and Histamine Receptors in Health and Disease.* Cham: Springer International Publishing; 2017. p. 301-20.
491. Rahmioglu N, Heaton J, Clement G, Gill R, Surdulescu G, Zlobecka K, et al. Genetic epidemiology of induced CYP3A4 activity. *Pharmacogenet Genomics.* 2011;21(10):642-51.
492. Geisslinger G, Menzel S, Gudermann T, Hinz B, Ruth P, Mutschler E. Mutschler Arzneimittelwirkungen : Pharmakologie – Klinische Pharmakologie – Toxikologie: BiblioScout; 2019. Available from: <https://biblioscout.net/book/10.52778/9783804740549>.
493. Spratlin J, Sawyer MB. Pharmacogenetics of paclitaxel metabolism. *Crit Rev Oncol Hematol.* 2007;61(3):222-9.

- 
494. Mansoor A, Mahabadi N. Volume of Distribution. StatPearls. Treasure Island (FL)2023.
495. Binder EB. The role of FKBP5, a co-chaperone of the glucocorticoid receptor in the pathogenesis and therapy of affective and anxiety disorders. *Psychoneuroendocrinology*. 2009;34 Suppl 1:S186-95.
496. Pohlmann ML, Hausl AS, Harbich D, Balsevich G, Engelhardt C, Feng X, et al. Pharmacological Modulation of the Psychiatric Risk Factor FKBP51 Alters Efficiency of Common Antidepressant Drugs. *Front Behav Neurosci*. 2018;12:262.
497. Lupien SJ, McEwen BS, Gunnar MR, Heim C. Effects of stress throughout the lifespan on the brain, behaviour and cognition. *Nat Rev Neurosci*. 2009;10(6):434-45.
498. Chrousos GP. Stress and disorders of the stress system. *Nat Rev Endocrinol*. 2009;5(7):374-81.
499. Cruz B, Vozella V, Carper BA, Xu JC, Kirson D, Hirsch S, et al. FKBP5 inhibitors modulate alcohol drinking and trauma-related behaviors in a model of comorbid post-traumatic stress and alcohol use disorder. *Neuropsychopharmacology*. 2022.
500. Connelly KL, Wolsh CC, Barr JL, Bauder M, Hausch F, Unterwald EM. Sex differences in the effect of the FKBP5 inhibitor SAFit2 on anxiety and stress-induced reinstatement following cocaine self-administration. *Neurobiol Stress*. 2020;13:100232.
501. Fornasari D. Pharmacotherapy for Neuropathic Pain: A Review. *Pain Ther*. 2017;6(Suppl 1):25-33.
502. Baischew A, Engel S, Geiger TM, Taubert MC, Hausch F. Structural and biochemical insights into FKBP51 as a Hsp90 co-chaperone. *J Cell Biochem*. 2023.
503. Rotoli D, Diaz-Flores L, Gutierrez R, Morales M, Avila J, Martin-Vasallo P. AmotL2, IQGAP1, and FKBP51 Scaffold Proteins in Glioblastoma Stem Cell Niches. *J Histochem Cytochem*. 2022;70(1):9-16.
504. Tufano M, Cesaro E, Martinelli R, Pacelli R, Romano S, Romano MF. FKBP51 Affects TNF-Related Apoptosis Inducing Ligand Response in Melanoma. *Front Cell Dev Biol*. 2021;9:718947.
505. Kim YS, Kim YJ, Lee JM, Kim EK, Park YJ, Choe SK, et al. Functional changes in myeloid-derived suppressor cells (MDSCs) during tumor growth: FKBP51 contributes to the regulation of the immunosuppressive function of MDSCs. *J Immunol*. 2012;188(9):4226-34.
506. Kautio AL, Haanpaa M, Saarto T, Kalso E. Amitriptyline in the treatment of chemotherapy-induced neuropathic symptoms. *J Pain Symptom Manage*. 2008;35(1):31-9.
507. Finnerup NB, Attal N, Haroutounian S, McNicol E, Baron R, Dworkin RH, et al. Pharmacotherapy for neuropathic pain in adults: a systematic review and meta-analysis. *The Lancet Neurology*. 2015;14(2):162-73.
508. Alles SRA, Cain SM, Snutch TP. Pregabalin as a Pain Therapeutic: Beyond Calcium Channels. *Front Cell Neurosci*. 2020;14:83.



- 
509. Gahr M, Freudenmann RW, Hiemke C, Kollé MA, Schönfeldt-Lecuona C. Pregabalin abuse and dependence in Germany: results from a database query. *Eur J Clin Pharmacol.* 2013;69(6):1335-42.
  510. Grosshans M, Lemenager T, Vollmert C, Kaemmerer N, Schreiner R, Mutschler J, et al. Pregabalin abuse among opiate addicted patients. *Eur J Clin Pharmacol.* 2013;69(12):2021-5.
  511. Zgajnar N, Lagadari M, Gallo LI, Piwien-Pilipuk G, Galigniana MD. Mitochondrial-nuclear communication by FKBP51 shuttling. *J Cell Biochem.* 2023.
  512. Ingawale DK, Mandlik SK. New insights into the novel anti-inflammatory mode of action of glucocorticoids. *Immunopharmacology and Immunotoxicology.* 2020;42(2):59-73.

---

## List of figures

---

**Figure 1: Nociception in physiological pain.** Noxious stimuli (thermal, mechanical, or chemical) are recognized by nociceptors at terminal endings of sensory neurons. The respective nociceptors transduce high-threshold stimuli into electric signals via the influx of cationic ions such as calcium. Next, the electric signal is conveyed via the cell bodies of sensory neurons, located in the dorsal root ganglia (DRGs), to the dorsal horn of the spinal cord. In the spinal cord, the signal reaches the first synaptic transmission and is processed. Afterwards, the signal is further transduced via ascending fibers into the brain to the somatosensory cortex. In the somatosensory cortex, the signal is finally processed and converted into a protective response which is then send via descending pathways to the executing organ. The illustration was created with images from motifolio.....2

**Figure 2: Pain transmission in pathological nociceptive pain.** Upon tissue damage, sensitization processes such as peripheral sensitization are established to prevent the body from further tissue damage and to enable a successful wound healing. Therefore, resident immune cells like mast cells and macrophages release pro-inflammatory mediators. These in turn recruit immune cells which release further mediators such as cytokines, chemokines, and nerve growth factors. Beside immune cells, sensory neurons additionally release mediators such as lipids and neuropeptides that contribute to the inflammatory soup and mediate a crosstalk between neurons and immune cells. The inflammatory soup leads to the sensitization of nociceptors and an increased calcium response upon stimuli, resulting in an enhanced action potential firing and a pathologically increased pain response. The illustration was created with images from motifolio.....4

**Figure 3: Structure of the TRPV1 channel.** The TRPV1 channel is composed of four subunits building a tetramer as all members of the TRP channel family (bottom left). One subunit of the homotetramer consists of six transmembrane domains from which domains five and six build up the conducting pore with the respective domains of the other subunits (top right). Both the amino and carboxy terminal of the channel are located intracellularly and comprise six ankyrin repeat domains and a TRP box domain,

---

respectively. Furthermore, several phosphorylation sites, consisting of serine and threonine, are located along both terminal ends that can in turn be phosphorylated by protein kinase A and C or CaMKII. In addition, each terminal end provides a calmodulin (CaM) binding site. The TRPV1 channel can be activated by noxious heat stimuli, protons that act on glutamic acid residues (indicated at the extracellular loops) and capsaicin that was proposed to bind close to the fourth transmembrane domain. The illustration was created with images from motifolio. .... 7

**Figure 4: Structure of the murine TRPA1 channel.** The TRPA1 channel is composed of four subunits that build a tetramer (bottom left). One subunit comprises six transmembrane domains from which domains five and six build up the conducting pore with the respective domains of the other subunits (top right). The amino terminal of the murine TRPA1 channel consists of 14 ankyrin repeat domains and several phosphorylation sites. Furthermore, the amino terminal comprises a suggested binding region for electrophilic agonists. In contrast menthol was predicted to bind near the fifth transmembrane domain. The carboxy terminal comprises predominantly a large voltage sensitive domain and provides a calmodulin (CaM) binding site. The illustration was created with images from motifolio..... 9

**Figure 5: PUFA release by the phospholipase A<sub>2</sub> from cellular membrane.** Polyunsaturated fatty acids (PUFAs) can be released by the phospholipase A<sub>2</sub> from the cellular membrane. Thereby, phospholipase A<sub>2</sub> hydrolyses the second ester bond of glycerophospholipids, liberating a lysophospholipid and a PUFA. Furthermore, PUFAs can be converted into other PUFAs upon elongation and desaturation processes. However, the depicted direction of PUFA conversion serves only for explanatory purposes and does not implicate that e.g. arachidonic and docosahexaenoic acid cannot be incorporated into cell membranes. The molecular structures were drawn with ChemSketch and the lipid bilayer was modified and originates from motifolio..... 14

**Figure 6: Enzymatic reactions catalyzed by LOX, CYP and COX enzymes.** The iron containing lipoxygenases (LOX enzymes) generate hydroperoxyl fatty acids under incorporation of one oxygen molecule. Cytochrome-P<sub>450</sub>-epoxygenases (CYP enzymes) catalyze epoxygenase and hydroxylase activities in dependency of iron ions, attaching either an epoxide group, preferentially to the double bond closest to the amino group,

---

or a terminal hydroxyl group, respectively. Cyclooxygenases (COX enzymes) catalyze the generation of predominantly bicyclic hydroperoxides under the incorporation of two oxygen molecules. The oxidized metabolites generated from the respective PUFA are depicted per enzyme. The molecular structures were drawn with ChemSketch..... 18

**Figure 7: Structure of FKBP51.** FKBP51 comprises a FK1 domain at the amino terminal (brown), an FK2 domain at the center (yellow) and a TRP domain at the carboxy terminal (green). The crystallographic structure was taken from the RSCB database (PDB-ID: 1KT0) and colored as well as labeled individually (306)..... 29

**Figure 8: Structure of SAFit2 and SAFit2 bound to FK1 of FKBP51. (A)** Molecular structure of SAFit2 with indicated C $\alpha$  which facilitates the conformational change in FKBP51. **(B)** Crystallographic structure of the FK1 domain of FKBP51 bound to SAFit2. The FK1 domain is colored in brown and SAFit2 in blue. The arrow indicates the displacement of phenylalanine 67 (green) due to the binding of SAFit2. The molecular structure was drawn with ChemSketch and the crystallographic structure was taken from the RSCB database (PDB-ID: 6txx) (372)..... 32

**Figure 9: Illustration of aims scheduled within this thesis.** To address the central question whether SAFit2 constitutes as potential novel treatment option for nerve injury- and paclitaxel-induced neuropathic pain, we firstly measured the mechanical hypersensitivity of mice as neuropathic pain behavior in both neuropathic pain models after SAFit2 treatment. Furthermore, lipid levels, cytokine and chemokine levels, the number of invading immune cells and the activation of glial cells was analyzed in dorsal root ganglia and spinal cord samples. In addition, we investigated the sensitization state of different pain-mediating TRP channels after SAFit2 treatment via calcium transients in primary sensory neurons and assessed related underlying mechanisms. The illustration was created with images from motifolio. .... 33

**Figure 10: Summary of SAFit2-mediated effects in nerve injury- and paclitaxel-induced neuropathic pain models.** SAFit2 significantly reduced mechanical hypersensitivity, a symptom of persistent pain, in both models. Furthermore, it significantly reduced levels of pro-inflammatory cytokines and pain-mediating chemokines in DRGs and spinal cord of nerve-injured mice. In contrast, paclitaxel-treated mice showed an increase of anti-

inflammatory cytokines and a decrease of pain-mediating chemokines in DRGs and spinal cord after SAFit2 treatment. Nevertheless, SAFit2 leads to changes in the number of activated immune cells in both models. Whereas SAFit2 decreases the invasion of immune cells into DRGs and spinal cord in the nerve injury model, SAFit2 reduces the activation of glial cells in the paclitaxel model. Notably, SAFit2 did not alter the number of immune cells at the site of injury, the sciatic nerve, in the nerve injury model. Moreover, SAFit2 counteracted an enhanced NF- $\kappa$ B pathway activation in DRGs and spinal cord of nerve-injured mice. Besides this, SAFit2 seems to increase the levels of free fatty acids as well as ceramides in both models. Furthermore, it restored the levels of an analgesic ceramide, dihydroceramide C16, after nerve injury and of anti-inflammatory oxylipins after paclitaxel treatment. In primary sensory neurons, SAFit2 lead to the desensitization of the ion channel TRPV1 and a reduced release of the neuropeptide CGRP. Orange arrows represent changes in the nerve injury model, whereas blue arrows display changes in the paclitaxel model. In addition, light orange boxes display either *in vivo* or *ex vivo* data, whereas the grey box illustrates results from primary sensory neuron cultures. SAFit2-mediated effects that are similar in the nerve injury- and the chemotherapy-induced neuropathic pain are printed in bold. The illustration was created with images from motifolio..... 159

**Figure 11: The SAFit2-FKBP51 network depicted as influencing factors of calcineurin and TRPV1 desensitization.** The influence of FKBP51 on the activity of the phosphatase calcineurin is controversially discussed in literature. However, both the complex of FKBP51 and FK506 as well as FK506 alone have been shown to inhibit the activity of calcineurin, whereas SAFit2 or analogues either have no effect on the activity of calcineurin or increased the calcineurin-mediated phosphate release. Furthermore, calcineurin was shown to mediate the dephosphorylation and subsequent desensitization of TRPV1 in primary sensory neurons. In line with this, SAFit2 and analogues also showed a desensitization of TRPV1 in sensory neurons. However, unspecific FKBP51 inhibitors as well as ddSAFit2, a chiral and biological inactive analogue, did not. Blocking lines indicate an inhibitory effect, arrows an inducing effect and straight lines illustrate neither an induction nor inhibition. Black lines indicate results from literature, whereas orange lines indicate insights from this work. .... 163

---

## Abbreviation list

---

AA	arachidonic acid
AMPA	amino-3-hydroxy-5-methylisoxazole-4-propionic acid
AP-1	activator protein 1
AR	androgen receptor
AS160	AKT substrate of 160 kDa
Ask1	apoptosis signal-regulating kinase 1
ATP	adenosine triphosphate
BDNF	bone derived neurotrophic factor
CaM	calmodulin
cAMP	cyclic adenosine monophosphate
CCL	C-C motif ligand
CCR	C-C motif chemokine receptor
CGRP	calcitonin gene-related peptide
CICR	calcium-induced calcium release
CIPN	chemotherapy-induced peripheral neuropathy
CNS	central nervous system
COX	cyclooxygenase
cPLA <sub>2</sub>	cytosolic PLA <sub>2</sub>
CREB	cAMP response element-binding protein
CSF1	colony-stimulating factor 1
CXCL	chemokine C-X-C motif ligand
CYP	cytochrome-P <sub>450</sub> -epoxygenases
DGLA	dihomo-gamma-linolenic acid
DHA	docosahexaenoic acid
DiHDPAs	dihydroxydocosapentaenoic acids
DiHOME	dihydroxy-octadecenoic acid
DRG	dorsal root ganglia
EDPs	epoxydocosapentaenoic acids
EEQs	epoxyeicosatetraenoic acids
EETs	epoxyeicosatrienoic acids
EPA	eicosapentaenoic acid
EpOMEs	epoxyoctadecenoid acids
ER	estrogen receptor

ER $\alpha$	estrogen receptor alpha
FKBP51	FK506 binding protein 51
GFAP	glial fibrillary acidic protein
GLUT4	glucose transporter 4
GPCRs	G protein coupled receptors
GR	glucocorticoid receptor
HEPEs	hydroxyeicosapentaenoic acids
HETE	hydroxyeicosatetraenoic acids
HETrEs	hydroxyeicosatrienoic acids
HODEs	hydroxyoctadecadienoic acids
HOTrEs	hydroxyoctadecatrienoic acids
HPA	hypothalamic–pituitary–adrenal
HpEPEs	hydroperoxyeicosapentaenoic acids
HpETE <sub>s</sub>	hydroperoxyeicosatetraenoic acids
HSP90	heat shock protein 90
HTT	huntingtin gene
IASP	international association for the study of pain
IBA1	ionized calcium-binding adaptor molecule-1
IL	interleukin
iPLA <sub>2</sub>	calcium-independent PLA <sub>2</sub>
LA	linoleic acid
LOX	lipoxygenase
Lys	lysine
MAPK	mitogen-activated protein kinase
mHTT	mutant huntingtin gene
mPTP	mitochondrial permeability transition pore
MR	mineralcorticoid receptor
mTOR	mammalian target of rapamycin
MyD88	myeloid differentiation primary response 88
NF- $\kappa$ B	nuclear factor 'kappa-light-chain-enhancer' of activated B-cells
NGF	nerve growth factor
NMDA	N-methyl-D-aspartate
NNT	number needed to treat
NSAID	non-steroidal anti-inflammatory drug
PDK1	pyruvate dehydrogenase kinase 1

PD-L1	programmed cell death ligand-1
Phe	phenylalanine
PHLPP	PH domain leucine-rich repeat phosphatase
PI3K	phosphoinositide 3-kinase
PKA	protein kinase A
PKC	protein kinase C
PLA <sub>2</sub>	phospholipase A II
PNS	peripheral nervous system
PP2B	serine/threonine-protein phosphatase 2B
PPAR $\gamma$	peroxisome-activated receptor $\gamma$
PPIase	prolyl-peptidyl-isomerase
PR	progesterone receptor
PUFA	polyunsaturated fatty acids
ROS	reactive oxygen species
S1P	sphingosine-1-phosphate
SAFit	selective antagonist for FKBP51 by induced fit
SC	spinal cord
sEH	soluble epoxide hydrolase
SHR	steroid hormone receptors
SNP	single nucleotide polymorphism
SNRIs	serotonin-noradrenaline reuptake inhibitors
sPLA <sub>2</sub>	secretory PLA <sub>2</sub>
SPM	specialized pro-resolving mediator
TLR4	toll like receptor 4
TNF $\alpha$	tumor necrosis factor $\alpha$
TRIF	TIR domain-containing adaptor inducing IFN- $\beta$
TRP	transient receptor potential
TRP domain	tetratricopeptide repeat domain
TRPA	transient receptor potential ankyrin
TRPM	transient receptor potential melastin
TRPML	transient receptor potential mucolipin
TRPP	transient receptor potential polycystin
TRPV	transient receptor potential vanilloid
$\alpha$ -LA	alpha linoleic acid



---

## Declaration - Ehrenwörtliche Erklärung

---

Ich erkläre hiermit ehrenwörtlich, dass ich die vorliegende Arbeit entsprechend den Regeln guter wissenschaftlicher Praxis selbstständig und ohne unzulässige Hilfe Dritter angefertigt habe.

Sämtliche aus fremden Quellen direkt oder indirekt übernommenen Gedanken sowie sämtliche von Anderen direkt oder indirekt übernommenen Daten, Techniken und Materialien sind als solche kenntlich gemacht. Die Arbeit wurde bisher bei keiner anderen Hochschule zu Prüfungszwecken eingereicht. Die eingereichte elektronische Version stimmt mit der schriftlichen Version überein.

Darmstadt, den .....

.....  
Saskia Wedel

---

## Acknowledgement

---

An dieser Stelle möchte ich mich bei allen Personen herzlich bedanken, die mich in den letzten Jahren unterstützt und bei meiner Doktorarbeit begleitet haben.

Ganz besonders möchte ich mich bei PD Dr. Marco Sisignano für die Möglichkeit bedanken, meine Doktorarbeit am Institut für Klinische Pharmakologie und im Besonderen in seiner Arbeitsgruppe durchführen zu dürfen. Darüber hinaus möchte ich mich für die tolle Betreuung, die vielen konstruktiven Anregungen sowie die fachliche und menschliche sehr gute Zusammenarbeit bedanken.

Zudem möchte ich mich auch bei Prof. Dr. Gerhard Thiel für die Möglichkeit bedanken in Kooperation mit Frankfurt promovieren zu können. Weiterhin bedanke ich mich für die tolle Unterstützung, die stetigen Ermutigungen und vor allem für die wertvollen Ratschläge.

Ich bedanke mich bei Prof. Dr. Dr. Gerd Geisslinger als Institutsleiter für die Möglichkeit, meine Doktorarbeit am Institut durchführen zu dürfen und die Weitsicht, die mir in Gesprächen gezeigt wurde.

Bei Dr. Natasja de Bruin, Prof. Dr. Felix Hausch, PD Dr. Mathias Schmidt sowie Prof. Dr. Sandrine Gérardon möchte ich mich für die gute Zusammenarbeit bedanken und freue mich auf weitere tolle Kooperationen.

Mein Dank gilt außerdem meinen Kollegen im Institut, die mir mit Rat und Tat zur Seite gestanden haben. Im Besonderen möchte ich mich bei Christian Müller und Nadine Merz für die vielen hilfreichen Gespräche, die Unterstützung, den Beistand in stressigen Zeiten und die daraus entstandenen tollen Freundschaften bedanken. Auch möchte ich mich bei Esther Schickel für ihre wertvolle Unterstützung bedanken.

Besonders herzlich möchte ich mich bei meinem Freund Niklas Götzl bedanken. Danke für deine Unterstützung, deine Aufmunterungen und dein Verständnis in den ganzen Jahren.

Darüber hinaus möchte ich mich auch bei meiner Familie für die stetige Unterstützung ganz herzlich bedanken.

# Curriculum Vitae

## Personal Information

---

### Saskia Wedel

📍 Frankfurt am Main  
📅 24.12.1997



## Professional Experience

---

April 2021 –  
October 2023

**PhD candidate** at the Institute of Clinical Pharmacology

- **Research topic:** “Investigation of SAFit2 as a potential treatment option for nerve injury- and chemotherapy-induced neuropathic pain”

February 2021 –  
March 2021

**Research Assistant** at the department of R&D at R-Biopharm AG

- Production and management of in-process controls
- Planning, implementation, and evaluation of stability and release tests

December 2020 –  
January 2021

**Tutor** at the Technical University of Darmstadt

- Conducting seminars for students

September 2017 –  
January 2020

**Student employee** at R-Biopharm AG

- Generation and distribution as well as quality and stability testing of in-process controls

## Education

---

October 2018 –  
January 2021

**Master Technical Biology** at the Technical University of Darmstadt

- Course of specialization: stem cell biology, neurobiology, radiation biology and immunology

**Research internship** at the Paul-Ehrlich-Institute (12 weeks)

- **Research topic:** “Investigation of the immune metabolic phenotype of dendritic cells stimulated with the allergen product Pollinex Quattro®”

**Master thesis** at the research group Neurophysiology and Neurosensory Systems headed by Prof. Dr. Laube

- **Research topic:** “Investigating low dose irradiation promoted differentiation of murine neural stem cells including a characterization of respective regulatory signaling pathways”

---

October 2015 –  
October 2018

**Bachelor Biology** at the Technical University of Darmstadt

- Course of specialization: developmental biology, microbiology, animal physiology and radiation biology

**Research internship** at R-Biopharm AG (6 weeks)

- Generation and testing of in-process controls

**Bachelor thesis** at the at the research group Stem Cell and Developmental Biology headed by Prof. Dr. Nuber

- **Research topic:** “Generation of neural cell type-specific lentiviral cre expression vectors for controlled gene inactivation”

## Trainings

---

April 2021 –  
October 2023

**Graduate school** (SFB 1039)

- PhD speaker of the graduate school, archived poster price 2021
- Poster an programming workshops

May 2021 –  
October 2023

**GRADE program** at the Goethe University

- GxP workshops
- Presentation and scientific writing workshops

July 2021 –  
October 2023

**Ingenium program** at the Technical University of Darmstadt

- Leadership workshops
- Project management workshops
- Agile project management workshops (certified scrum master)

## Grants

---

2023 – 2024

**e-Fellows scholarship**

2022 – 2023

**Mentee** in Mentoring Hessen

2019 – 2020

**Deutschlandstipendium**

## Conferences

---

September 2023

**International symposium on lipid signaling** in Frankfurt, Germany

- Poster presentation

September 2023

**International congress on neuropathic pain (NeuPSIG)** in Lisbon, Portugal

- Poster presentation

---

## Publication list

---

**WEDEL, S.**, HAHNEFELD, L., SCHREIBER, Y., NAMENDORF, C., HEYMAN, T., UHR, M., SCHMIDT, M. V., DE BRUIN, N., HAUSCH, F., GEISLINGER, G. & SISIGNANO, M. 2023. SAFit2 ameliorates paclitaxel-induced neuropathic pain by reducing spinal gliosis and elevating pro-resolving lipid mediators. *Journal of Neuroinflammation*, 20, 149; <https://doi.org/10.1186/s12974-023-02835-5>

KAUP, F.H., MEYNER, C., SUGIARTO, W.O., **WEDEL, S.**, SPRINGER, M., WALZ, C., GEIGER, T.M., SCHMIDT, M., SISIGNANO, M. & HAUSCH, F. 2023. Structure-Based Discovery of a New Selectivity-Enabling Motif for the FK506-Binding Protein 51. *J. Med. Chem.*, 66, 5965-5980; <https://doi.org/10.1021/acs.jmedchem.3c00249>

**WEDEL, S.**, HAHNEFELD, L., ALNOURI, M. W., OFFERMANN, S., HAUSCH, F., GEISLINGER, G. & SISIGNANO, M. 2022a. The FKBP51 Inhibitor SAFit2 Restores the Pain-Relieving C16 Dihydroceramide after Nerve Injury. *Int J Mol Sci*, 23, 14274; <https://doi.org/10.3390/ijms232214274>

**WEDEL, S.**, MATHOOR, P., RAUH, O., HEYMAN, T., CIOTU, C. I., FUHRMANN, D. C., FISCHER, M. J. M., WEIGERT, A., DE BRUIN, N., HAUSCH, F., GEISLINGER, G. & SISIGNANO, M. 2022b. SAFit2 reduces neuroinflammation and ameliorates nerve injury-induced neuropathic pain. *Journal of Neuroinflammation*, 19, 254; <https://doi.org/10.1186/s12974-022-02615-7>

**WEDEL, S.**, OSTHUES, T., ZIMMER, B., ANGIANI, C., GEISLINGER, G. & SISIGNANO, M. 2022c. Oxidized linoleic acid metabolites maintain mechanical and thermal hypersensitivity during sub-chronic inflammatory pain. *Biochem Pharmacol*, 198, 114953; <https://doi.org/10.1016/j.bcp.2022.114953>

ZIMMERMANN, J., GORETZKI, A., MEIER, C., WOLFHEIMER, S., LIN, Y. J., RAINER, H., KRAUSE, M., **WEDEL, S.**, SPIES, G., FÜHRER, F., VIETHS, S., SCHEURER, S. & SCHÜLKE, S. 2022. Modulation of dendritic cell metabolism by an MPLA-adjuvanted allergen product for specific immunotherapy. *Front Immunol*, 13, 916491; <https://doi.org/10.3389/fimmu.2022.916491>

